High Radiation Dosimetry: Methodology Development

A Thesis

Submitted in partial fulfillment of the requirements for the award of the degree of

Doctor of Philosophy

by

Malika Singhal

(Roll No. 20330011)

Under the supervision of

Dr. Naveen Chauhan

Associate Professor

Atomic Molecular and Optical Physics Division

Physical Research Laboratory, Ahmedabad, India

DISCIPLINE OF PHYSICS

INDIAN INSTITUTE OF TECHNOLOGY GANDHINAGAR

2025

Dedicated to

my

Mom and Dad

Declaration

I declare that this thesis report represents my own ideas in my own words and I have included others ideas with appropriate citations of original sources. I also declare that I have followed all principles of academic honesty and integrity and have not misrepresented or fabricated or falsified any idea/fact/source/data in my submission. I understand that any violation of the above can cause disciplinary action by the Institute and can also evoke penal action from the sources which have thus not been properly cited or from whom proper permission has not been taken when needed.

Malika Singhal

Roll No.: 20330011

Date: 21-04-2025

INDIAN INSTITUTE OF TECHNOLOGY GANDHINAGAR

CERTIFICATE

It is certified that the work contained in the thesis titled "**High Radiation Dosimetry: Methodology Development"** by **Ms. Malika Singhal** (Roll no: 20330011) has been carried out under my supervision and that this work has not been submitted elsewhere for a degree.

21-04-2025

Dr. Naveen Chauhan
(Thesis Supervisor)
Associate Professor,
Atomic Molecular and Optical Physics Division,
Physical Research Laboratory,
Ahmedabad 380009,
India.

Date: 21-04-2025

Acknowledgments

Completion of a journey cannot be marked without thanking and paying gratitude to the persons involved. I am grateful that I had the opportunity to collaborate with so many outstanding scholars along the way, who have shaped who I am now and increased my wisdom.

“The best teachers bring out the best in their students.” With deep respect and heartfelt appreciation, I extend my profound gratitude to my supervisor, **Dr. Naveen Chauhan**, Associate Professor, Atomic Molecular and Optical Physics Division, PRL, for his unwavering support, insightful guidance, and constant encouragement throughout my research journey. His generous sharing of knowledge and the academic freedom he offered me have been truly empowering and beyond words. It has been a great honor and privilege to work under his mentorship in the Luminescence Physics and Application Lab.

I am also deeply thankful to **Prof. Ashok Kumar Singhvi** for his invaluable guidance, regular engagement, and thought-provoking discussions that have profoundly enriched my scientific perspective. His dedication to scientific excellence and his inspiring approach to research have continuously motivated me to strive for the highest standards. I feel truly fortunate to be part of this exceptional research group and will always cherish the opportunity to have learned from such distinguished mentors. Special thanks to Anita Ma’am for joyous and heartfelt interactions over delicious food and for always making us feel at home.

I would like to express my sincere gratitude to Dr. Anna O. Lakshmi, Prof. Saibal Gupta, Prof. Devender Kumar, Dr. Linto Allapat, Dr. Munish Kumar, Prof. Parth Chauhan, Dr. Mahesh Thakur, Dr. Saptarshi Dey, and Dr. Anil Chavan for their valuable support in the form of experimental assistance, sample collection, and insightful discussions. Their contributions have been instrumental in the successful execution of various aspects of this research work. I am especially thankful to Ms. Madhusmita for her dedicated guidance during experimental work. Her consistent support and willingness to help are deeply appreciated throughout the course of this study.

I would like to give special thanks to my doctoral student committee members: Prof. B. Sivaraman, Prof. D. Banerjee and Dr. S. Vijayan for their insightful comments, enthusiasm,

encouragement and for the meaningful questions which motivated me to widen my research from various perspectives. A special thanks to Prof. R. P. Singh and Prof. Bijaya Sahoo, former Head and Head of the Division for their support and for providing all the necessary facilities in the department. I express my gratitude to all the faculty members and staff of PRL.

“Best research is produced when researchers and communities work together.” I am grateful and thankful to my lab members, Dr. Rahul Kumar Kaushal, Dr. Sukumar Parida, Dr. Kartika Goswami, Dr. Monika Devi, Santunu Kumar Panda, Sachin and Vinayak Sir. Thank you for sparing time and guiding me in the journey. Discussions with them were enlightening and motivating. I am thankful to you all for stimulating discussions, believing and exploring the research subject together.

I would like to thank Lakhan sir and J.K. Meka for helping with the machines. Special thanks to my friends, Aditya Das for helping in XRD measurements and Ranjan Kumar Mohanty for helping in QGIS.

I am deeply grateful to the Physical Research Laboratory (PRL), Ahmedabad, for providing excellent research facilities and a highly supportive environment, which have been pivotal in the smooth and successful completion of my Ph.D. work. I sincerely acknowledge the support of SERB-DST and PRL for sponsoring my participation in conferences, workshops, and experimental visits, which greatly enriched my academic experience. My heartfelt thanks to the Purchase and Stores Division at PRL for their constant cooperation, especially in addressing urgent requirements related to laboratory supplies and infrastructure. I am also thankful to the Accounts Department for their assistance with administrative and logistical matters, ensuring seamless coordination throughout. My sincere thanks goes to the Workshop at PRL, whose enthusiasm and craftsmanship helped bring technical drawings and ideas to life. I am equally thankful to the Central Maintenance Division (CMD) for their timely support in resolving maintenance-related issues, which was crucial for the uninterrupted functioning of the laboratory. Lastly, I would like to express my gratitude to the Medical Facilities at PRL for their continuous support in maintaining our health, especially during the pandemic period. Their dedication and reliability have been immensely reassuring during challenging times.

I would like to extend heartfelt thanks to my friends for making the Ph.D. journey joyful and for creating memories along the way. I am thankful to my friends Chahat, Kiran, Sanjay,

Trinesh, Arup C., Ankita, Akaash, Shivam, Aishwarya, Akanksha, Chandrima, Aditya, Arup M., Ananya, Mansi, Debasish, Gurucharan, Dharmendra, Kamran, Wafikul, Sandeep, Gaurav, Bijoy, Komal, Mudita, Neha, Arijit Maity, Varsha, Vaishnavi, Shreya, Goldy, Sahil, Nitin, J T. I would like to thank my seniors, Meghna, Namita, Shivani, Ritu, Akanksha, Sarika, Alka, Ria, Saumapushpa, Ruchita, Jalaja, Anju, Anshika, Tanya, Saumaya, Birendera, Vineet, Kshitiz, Vardaan, Sunil, Naval, Sandeep, Yash, Ankit, Abhay, Yogesh, Arijit, Arvind, Deepak, Deepak Raja, Harish, Priyank for their guidance and friendship.

“Together is indeed the best place to be.” I am thankful for the blessings of my elders particularly, my grandparents. I would like to express the heartiest gratitude to my parents, Mumma and Papa for the love, care, guidance and support. Without their constant will, efforts and endless love, I would not be anywhere near today. I thank my dearest sister, Meenal Singhal and Jijaji for always being my guide and for their companionship in every aspect of life. Special thanks to my dearest nephew Vivansh, for his occasional visit and warming my heart with love.

Malika Singhal

Abstract

Radiation dosimetry is the measurement of absorbed radiation dose (Gy = J/kg). Estimation of dose in natural minerals using luminescence emissions is an integral part of luminescence dating, which is a chronological technique to estimate the time of occurrence of various earth surface and archaeological events. In luminescence dating, the dose divided by the dose rate, estimates the time since radiation is absorbed and can be linked to the last burial or formation age of the sediments/minerals. The upper limit of luminescence dating is limited to ~ 0.5 Ma. This limit is because of saturation of luminescence intensity with dose and depends on the capacity of the traps (defect sites) inside the crystal to accumulate charges produced during irradiation. The saturation is mineral-dependent and found to differ for different minerals. Quartz and feldspar are two ubiquitous minerals that are widely used in luminescence dating. The quest to increase the datable range of luminescence dating has been long, and many new traps (and their corresponding luminescence signals) in the quartz and feldspar have been identified and probed to increase the datable range. However, the probed signals still face challenges in bridging the gap between laboratory calibrations and naturally acquired doses.

The present thesis attempts to develop a method to estimate high radiation doses (HRDs ~>1 kGy) by exploring new minerals for high dose estimates and developing a better understanding of the luminescence mechanism in conventional minerals (quartz and feldspar) in the high dose regime. This thesis, for the first time, explores the luminescence characteristics of jarosite, a hydroxyl sulphate of metal and iron, because of its importance as a direct indicator of paleo-aridity (hence climate change) and its abundance and occurrence on Mars. Essential dosimetry properties like identification of traps, their thermal stability, bleaching, dose saturation, and athermal fading are studied. Jarosite exhibits promising luminescence properties for radiation dose estimation, responding to both thermal and optical stimulation (blue and infrared). Thermoluminescence (TL) glow peaks appear around 100°C, 150°C, 300°C, and 350°C, with emissions recorded across a wide spectral range (325–700 nm). The signals are found stable and reproducible, with TL showing <6% variability and blue/infrared stimulated luminescence (BSL/IRSL) exhibiting <14% variability over repeated cycles. Heating to 450°C alters luminescence sensitivity without affecting the shape of glow curves, a finding supported by FTIR and CL-EDXS analyses. The 300°C TL peak has thermal stability over geological time periods, with a lifetime of ~0.3 million years (Ma) at 30°C and ~3 Ma at 10°C ambient temperature, indicating suitability for dating older events in

colder environments. Dose-response curves show saturation doses ranges from 590 to 1600 Gy for various traps probed by BSL, IRSL, pIRIR225 and TL. The pIRIR225 signal and the 350°C TL peak—recorded in both UV and blue detection windows—exhibit negligible athermal fading. Based on a terrestrial dose rate of ~2 mGy/year, jarosite has the potential to date events up to ~800 ka (constrained by the thermal stability to colder areas), while on Mars, where the dose rate is ~65 mGy/year, the dating limit is approximately ~25 ka.

The multi-spectral studies are conducted to understand the trapping, storage and recombination of charges in the conventional minerals (quartz and feldspar) at HRDs. Experiments are conducted in the broad spectral window from 325- 700 nm and are consequently narrowed down. Results show that quartz TL saturates in 10−18 kGy, whereas feldspar TL saturates around 1−5 kGy, the range being sample dependent. Since quartz provides a significant scope for estimating HRD, it is studied in detail in this thesis. The dose-response and saturation characteristics in quartz are found to be primarily controlled by the trapping centres rather than the recombination centres, with saturation doses showing minimal spectral dependence. Bleachability is found to be wavelength-dependent; longer-wavelength emissions exhibit reduced bleaching efficiency. Standard normalization protocols, such as the zero or second glow normalization, become unreliable beyond ~1 kGy, leading to inconsistent sensitivity correction. Instead, normalization approaches based on sample mass/ weight should be used. Additionally, the luminescence sensitivity is influenced by the prior regeneration doses, and only the 110°C TL in blue emissions remains largely unchanged. These findings highlight the need for revised protocols at HRD. The thesis further re-investigates the Blue Stimulated luminescence (BSL) from quartz at HRDs, which is known to saturate ~ 250 Gy, which is approximately 40 times less than the observed TL saturation. Results show that BSL measured on multiple aliquot of the same sample and compared by mass normalization does not saturate as early as seen in Single Aliquot Regeneration (SAR) protocol. Thus, suggesting that laboratory methodology is resulting in early saturation. Results show that as regeneration doses increase, charge carry-over to the test dose leads to an artificial increase in test signals, causing early saturation in dose response curves (DRCs). HRD is better measured using Multiple Aliquot Additive Dose (MAAD) protocols in combination with alternative normalization. Signals like zero-glow peak, annealed BSL, and annealed TL (blue emission) show reduced/negligible dependence on regeneration dose for the test signal, making them more suitable for constructing DRCs in the high-dose regime. Dose response curves generated using these normalization methods

show saturation around ~5800 Gy. Laboratory-administered doses of ~1000 Gy are accurately recovered using this approach, with dose recovery ratios typically ranging between 0.9 and 1.2, but with an error of 50% corresponding to scatter in data.

The thesis further uses the proposed methodology for two natural old geological settings: the Upper Shivaliks (~0.5- 5 Ma) and the Charavathur formation (> 2.5 Ma). In natural high-dose contexts, such as Shivalik sediments, where SAR-based curves show early saturation, the MAAD method proves particularly effective and could estimate higher radiation doses. In samples like those from Charavathur, where a low dose rate was estimated, the samples acquired an equilibrium between the trapping and detrapping due to thermal effects. MAAD accounts more appropriately for natural dose equilibrium, which cannot be explained by the SAR. These findings highlight the limitations of SAR at high doses and suggests the use of MAAD protocols appropriately normalized for accurate dose estimation in old geological settings. However, the estimated doses are accompanied by large errors which need further investigation in the future.

Keywords: Quartz, feldspar, jarosite, high dose dosimetry, luminescence dating, multi-spectral studies, single aliquot regeneration, multiple aliquot additive dose, thermoluminescence, optically stimulated luminescence, thermal effects, equilibrium.

Table of Contents

LIST OF FIGURES

List of Tables

Chapter 1: Introduction

1.1. Motivation and purpose

Radiations are present everywhere. These are present as cosmic rays originating from extraterrestrial sources and as alpha, beta and gamma radiation from radionuclides (Th-232, U-238, U-235, K-40, Rb-87 and their daughters) in soil, air and water. Airplane crew members, astronauts and satellite receive a huge amount of radiation. Radiations are part of numerous activities in day-to-day life. Today, radioactive sources are also used widely in many health and manufacturing industries. Foremost in the nuclear energy industry for power production (U-238, U235, Th-232). In detectors, it is used to detect smoke, leakages (Am-241). Food processing industries uses high radiation from Co-60 to preserve food by killing allergens and bacteria. Manufacturers of jewellery use it to enhance the properties of gems and jewels. The medical industry uses several radionuclides for diagnostic purpose (PET-scan), in devices like pacemakers (Pu-238) and for the treatment of ailments like cancer, tumour (Ga-67, H+, C-12, X-ray beams) etc. Exposure to radiation levels above the defined thresholds leads to fatal health effects. With such wide use, it becomes very important to quantify the radiation dose intake by people working near such area. Luminescence is a very effect tool to quantify radiation doses (energy deposited by the radiation source per unit mass of absorber, measured in Gray (Gy) 1 Gy = 1 Joule/kg). Over the time several artificial phosphors (e.g. Al_2O_3:C, Al_2O_3:Mg, LiF:(Mg,Ti), LiF:(Mg,Cu,P), $CaSO_4$:Tm, CaF_2:Dy, BeO, $Li_2B_4O_7$:Cu, Ca_3WO_6:Ho, Ca_2CeVO_6:Eu etc.; Degda et al., 2024a, 2024b, 2023; Yukihara et al., 2022) tailored for specific requirements are synthesized for dose estimation or dosimetry along with existing natural minerals (e.g. quartz, feldspar, gypsum, calcite etc.; Murray et al., 2021).

Further dosimetry with natural minerals has led to development of new techniques aiding the study of many geological processes such as earth surface dynamics, tectonics, paleo-climate, human evolution. Dose measurements (luminescence dosimetry) coupled with the knowledge of the annual rate of dose deposition (dose rate) can help in the estimation of the time since the start of radiation exposure. This has led to establishment of luminescence dating technique as

a chronological tool to time stamp various earth surface processes and archaeological events. By tracking the luminescence of natural minerals (present as sedimentary record), time of last sun/heat exposure can be estimated (Aitken, 1985). This time can be directly linked to phenomenon like floods, tsunami, earthquake, glacier movement, formation and shifting of sand dune, terrace formation, river channel migration, mountain formation, lacustrine deposition, forest fires etc (Aitken, 1998, 1985; Herman et al., 2010; Morthekai et al., 2025; Singhvi et al., 2022, 1982; Smith et al., 1990). As such, luminescence chronology plays an important part in understanding of shifting climate trends and its repercussions. It has become increasingly important over last three decades as it provides a robust chronological framework to understand the late Pleistocene climatic changes and associated patterns of human evolution. An understanding of paleo-records (10^2–10^5 years) of this kind are very helpful to national policymakers and climate-model simulations. Currently luminescence can be used to date events upto ~0.5 Million years (Thiel et al., 2011) and efforts are underway to extend dating limits of luminescence (Chauhan et al., 2009; Jain, 2009; Thiel et al., 2011; Wang et al., 2006). This thesis attempts to build an understanding of luminescence mechanism of natural minerals for high radiation doses so that we can make systematic efforts for contributing in this direction. In this introduction chapter, a brief introduction of luminescence, its mechanism, in view of its production form ionizing radiation is discussed followed by an overview on thermoluminescence (TL) and optically stimulated luminescence (OSL) which are generally used for dosimetry and dating. The chapter also introduces some popularly used natural minerals used for luminescence dating.

1.2. **Luminescence**

Luminescence is the emission of light (visible, UV and infrared) from an insulator, when the electrons occupying higher energy states are de-excited to lower energy state at ambient temperatures. Luminescence emission is also called a cold emission, unlike the hot emissions (called incandescent) from sunlight, candle etc. wherein heat energy is used to excite the electrons to higher energy states with conversion of heat into light energy. In luminescence prior stored energy in form of trapped electrons is probed. It is a three-step process, which includes excitation (input of energy), storage and emission (return to lower energy state emitting luminescence). Luminescence is a broad term and considering its wide range of

applications, it is categorized in many types based on de-excitation time, excitation source or emission stimulation source.

Luminescence is a spontaneous emission. On the basis of the time between the excitation of charges and the emission of light, luminescence is categorized as fluorescence (emission occurring within $\sim 10^{-8}$ sec) and phosphorescence (if emission occurs $\geq 10^{-5}$ sec). In phosphorescence, the lifetime may vary by orders of $\sim 10^{20}$, i.e., as high as 10^{8} years (Curie and Garlick, 1963).

Further luminescence is also categorized by the type of excitation source used, for example radioluminescence (radiation used as excitation), photoluminescence (photons used as excitation), cathodoluminescence (electrons used as excitation), chemi-luminescence (chemical reactions act as excitation), triboluminescence (mechanical force as excitation), electroluminescence (electric field as excitation).

Considering the enormous applications of luminescence to study the surroundings many a times the spontaneous luminescence process can be stimulated for early de-excitation of electrons and hence some luminescence phenomenon are named after the stimulation source used like thermoluminescence (heat used as stimulation), optically stimulated luminescence (light used as stimulation). This thesis majorly uses thermoluminescence and optically stimulated luminescence.

Luminescence is observed in crystalline insulators and semi-conductors with some impurities. For phosphorescence to occur, presence of metastable is required which acts as centres to trap or hold excited electrons for times longer than electronic dipole transitions. Pure crystal cannot produce phosphorescence. Generally, no natural crystal is pure as many impurities are present in matrix when it is crystallized in earth's crust. Even artificial manufacturing of pure crystal is very difficult as due to ambient temperature which is greater than absolute zero (zero Kelvin), diffusion of electrons occurs and thermodynamic equilibrium always creates some defects in crystals.

1.2.1. Defects in crystals

Any disruption from the periodic repetition of the basic unit of the crystal is called defect. It may be caused by inclusion of foreign impurity or the displacement of atoms in the crystal from their allocated site. Based on dimension, defects can be of three types. Zero-dimensional or point defects, that majorly effect the luminescence, mechanical, electrical properties. One

dimensional line defect that have major effect on the mechanical property of the crystal. Two dimensional defect that is the external surface itself and the grain boundaries in the crystal effect the crystallinity of the crystals (Kelly and Knowles, 2020). As luminescence properties are mainly influenced by point defects, these are discussed below. In a crystal point defects are further categorized into two kinds.

1.2.1.1. Intrinsic defects

If the periodicity of the crystal breaks due to imperfection in its constituent atoms like absence of an atom from its site (vacancy defect), or presence into the interstitial site (interstitial defect), it is called Intrinsic defects. In ionic crystal, such impurities are called Frenkel and Schotty defect respectively. Any crystal at room temperature will have such impurities and the probability of such defect is governed by the thermodynamics and is proportional to Gibbs free energy of defect formation given as,

$$c_D \propto \exp(\frac{-\Delta G_D}{kT}) \tag{1.1}$$

where c_D is the defect concentration, ΔG_D is Gibbs free energy for defect formation, k is Boltzmann constant and T is ambient temperature (Preusser et al., 2009). The proportion of such impurities changes when the crystals are heated and cooled again. Leading to large variation in luminescence properties.

1.2.1.2. Extrinsic defects

Inclusion of foreign impurity atoms into the crystal leads to extrinsic defects. The foreign impurity atom may replace a host site (substitutional defect) or may occupy an interstitial site. Atoms of similar size to the host atom replace them from the host sites. Additionally, atoms of size that is compatible to fit in the void space, have high probability to occupy interstitial sites. The concentration of defects also plays a major role in the luminescence properties. It is seldom observed that luminescence characteristics are enhanced by increase in concentration of impurities to a certain threshold after which with further increase in impurity concentration, the luminescence properties are quenched (Wang et al., 2024).

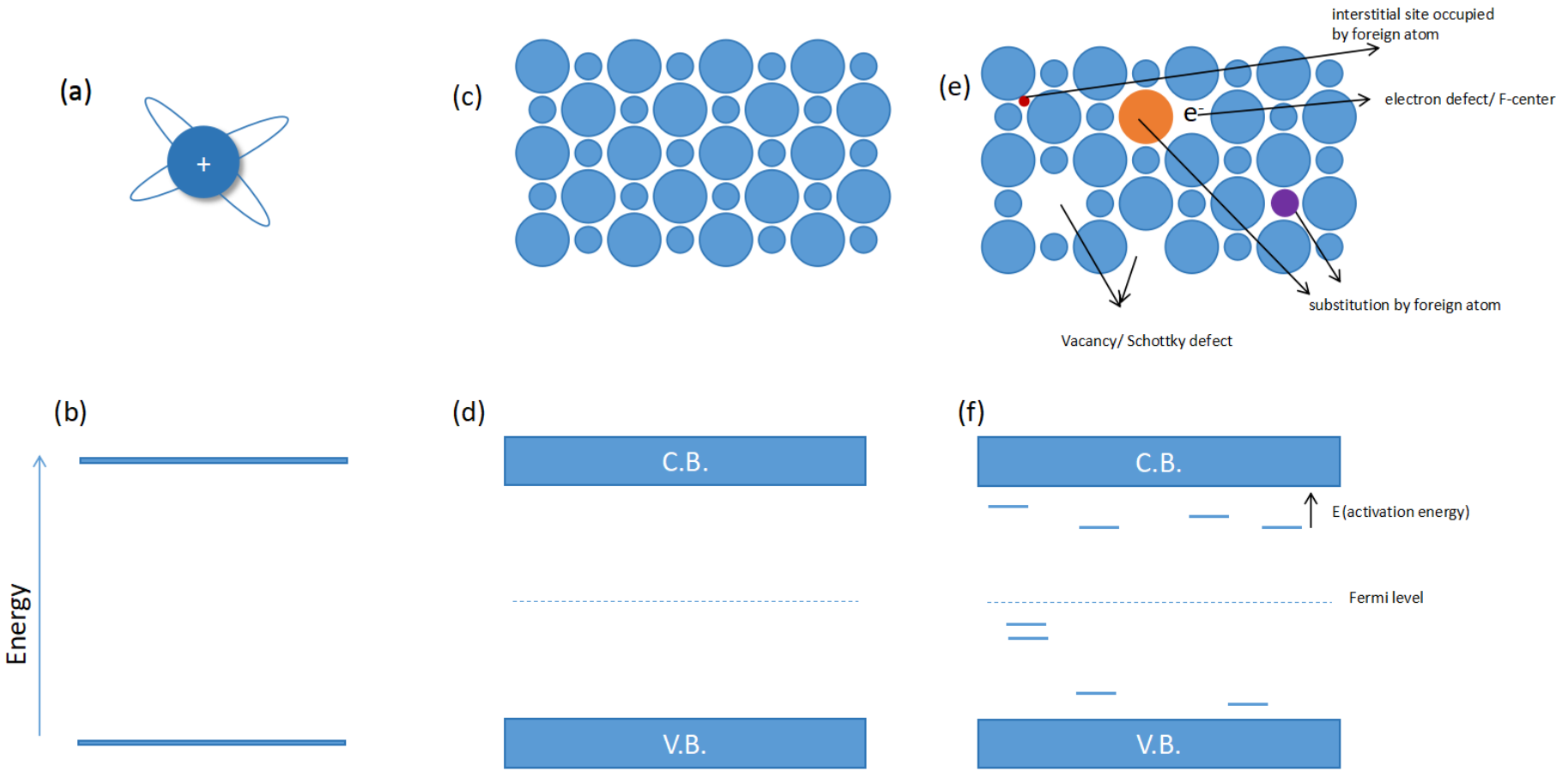

Figure 1-1 Pictorial representation of atom and cluster of atoms and their corresponding energy level diagram. (a) an atom and (b) shows its energy levels, (c) a crystal with periodic arrangement of atoms and (d) its energy band forming conduction and valence band, (e) a crystal with impurities and (f) its energy bands with introduction of metastable states in the forbidden band gap.

1.2.1. Effect of impurities/ defects in the crystal

The presence of these defects modulates the crystal field around defect sites thus effecting the energy band diagram (Figure 1.1). Individual atom in vacuum have energy levels. When atoms/molecules come together to form crystal, there periodic arrangement leads to the formation of conduction and valence bands with a forbidden gap between them. The introduction of defects breaks the periodicity of the crystal and creates localized energy levels in the forbidden band gap of the crystal. These levels are called metastable states/traps as they can hold charges (electrons/holes) temporarily and have life-time higher compared to the conduction band. These act as traps and stores electrons and holes generated in the crystal due to excitation source (Nambi, 1977). If the trap has higher probability to capture an electron from the conduction band, than a hole from valence band, then it is called electron ***trapping centre*** and thus metastable states near to the conduction band are electron trapping centres. Similarly, a trap having a higher probability of capturing a hole from the valence band is called a ***hole centre***. If a trap is significantly stable and has a low probability of losing the trapped charges and has a higher probability for electron-hole pair recombination, it is called a ***recombination centre***. The lifetime (τ) of charge in a trap is given as

$$\tau = s^{-1} \exp(\frac{E}{kT}) \tag{1.2}$$

where s is the escape frequency at a given ambient temperature T. E is the activation energy required by the electron to go to the conduction band and k is the Boltzmann constant. The lifetime of charges in traps can range from a few milli seconds to 10^8 years, as observed in natural minerals like Quartz and Feldspar (Aitken, 1985).

1.2.2. Luminescence Mechanism

Luminescence mechanism can be understood by the band theory of solids and is pictorially shown in Figure 1.2. An exposure to high-energy radiations such as UV, X-ray, alpha, beta, gamma, or cosmic rays produces a large number of electron-hole pairs in the crystal. Depending on the band gap of the crystal, and the energy gained by electrons, electrons are excited to the conduction band. Most of these electrons recombine immediately with the holes within 10^{-8} seconds to give fluorescence (Curie and Garlick, 1963). However, a small fraction proportional to the incident excitation source is captured by the metastable states present in the forbidden band gap. Similarly, holes present in valence band get trapped in hole trapping centres.

The electrons/holes are evicted from the metastable traps depending on the lifetime of the traps. The evicted electrons (holes) get excited to conduction (valence) band and move freely and recombine with opposite charges present in recombination centres producing phosphorescence. The intensity (I) of phosphorescence is given as

$$I = -\frac{dn}{dt} \propto np \tag{1.3}$$

where n is the concentration of electrons in the trap and p is the probability of eviction of electron which is inversely related to the lifetime.

$$p = \tau^{-1} = s\exp(\frac{-E}{kT}) \tag{1.4}$$

Upon eviction of the electrons, they may directly recombine with holes by radiative emission, or it may de-excite non-radiatively to reach a recombination centre where they combine with holes to give luminescence.

Electrons in the traps can be probed at any time by stimulating them with external energy such as heat or light resulting in emission of luminescence depending on nature of external stimulation.

1.3. **Thermoluminescence**

When heat is used as stimulation, the observed luminescence is called as thermoluminescence (TL). It is not to be confused with incandescence due to black body radiations, as in incandescent the maximum temperature involved is near to 2000℃ or greater, however in TL the maximum temperatures involved are ~500-600℃. As the temperature of the material increases, the vibrational motion of the trapped electrons increases, enabling them to escape to the conduction band from the trap. The thermal energy corresponding to 600℃ is 0.075 eV, whereas at 600℃, traps with a trap depth of ~3 eV can be probed owing to the Maxwell-Boltzmann distribution followed by trapped electrons due to their low concentration. The electrons non-radiatively de-excite to recombination centre and recombine with holes to give light output. The output energy is difference between the excited and ground state energy of the recombination centre. If the crystal is heated at a constant heating rates such that temperature increases linearly, electrons are evicted from electron traps in increasing order of their activation energy.

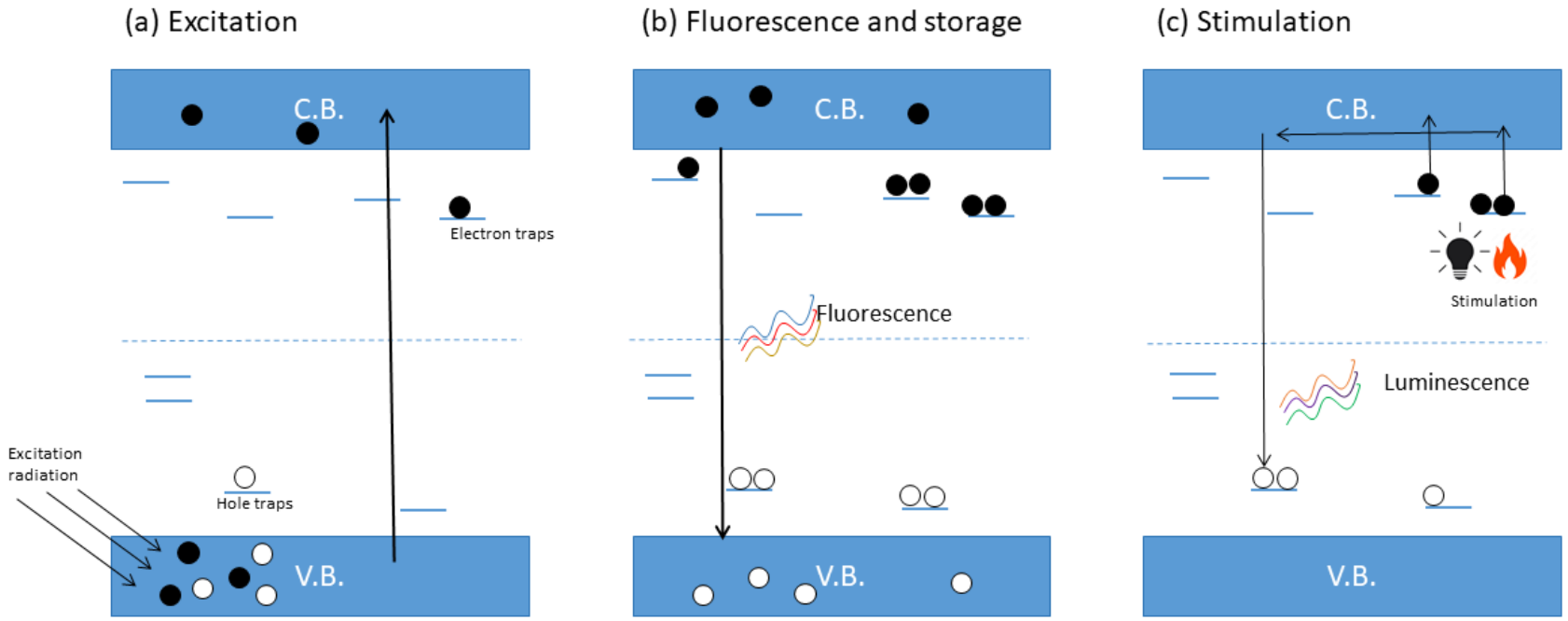

Figure 1-2 Diagram showing luminescence mechanism. (a) the process of excitation following absorption of energy from outside. (b) fluorescence (within 10^{-8} sec) and electrons in metastable states are stored depending on the lifetime of the state. (c) stimulation with heat or light to produce luminescence.

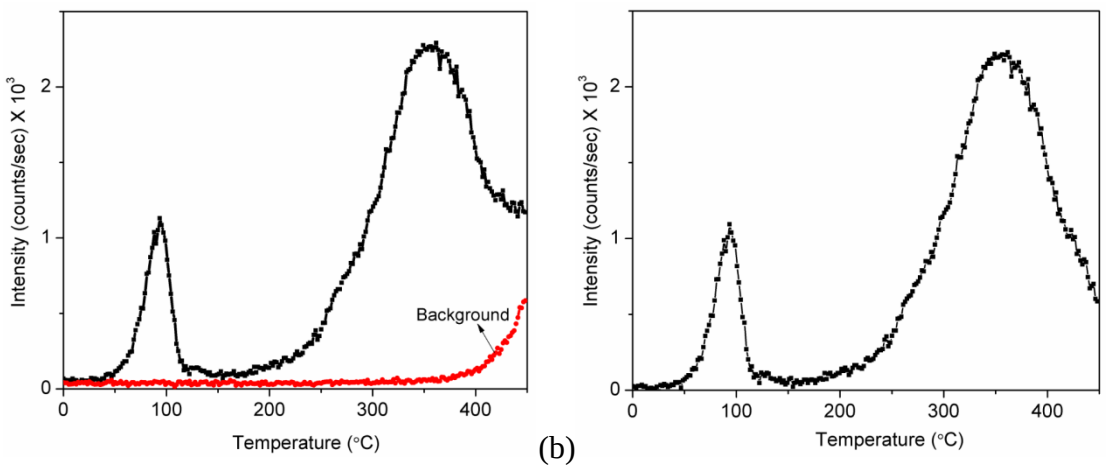

Figure 1-3 (a) Thermoluminescence glow curve with two glowpeaks and background (b)Thermoluminescence glow curve after background subtraction.

At temperatures higher than 300℃, thermal vibration between the lattice sites increases, leading to an emission of black body radiations in form of infrared light, which need to be subtracted from the TL. This resultant output TL intensity curve is called *glow curve* consisting of several glow peaks corresponding to different traps present in crystal (Figure 1.3).

The probability of eviction of electrons is given as

$$p = s.exp^{\frac{-E}{kT}} \tag{1.5}$$

The intensity of the glowpeak can be estimated taking following assumptions. The crystal has only one electron trap, one recombination centre and there is no retrapping of electron by trap centres (known as first order kinetics). The concentration of recombination centre is considered greater than electron traps. The non-radiative transitions involving luminescence are negligible, intensity can be calculated from equation 1.3 using equation 1.5

$$I = -\frac{dn}{dt} = n.s.exp^{\frac{-E}{kT}} \tag{1.6}$$

considering a precise and reproducible linear heating with a constant heating rate ß temperature at after time t can be written as

$$T = T_0 + \beta t \tag{1.7}$$

with T_0 being the initial temperature, equation 1.6 can be solved to give

$$I = n_0.s.exp^{\frac{-E}{kT}}.exp^{\int_0^{T}\frac{s}{\beta}e^{\frac{-E}{kT'}}dt} \tag{1.8}$$

This equation is called *Randall- Wilkins equation* and is of first order kinetics (Nambi, 1977). Equation 1.8 shows that the **intensity is proportional to the concentration of electrons in the trap.**

The peak temperature can be estimated by differentiating equation 1.8 and substituting $T=T_m$ (i.e., the peak temperature) when dI/dt = 0 and is given as

$$\frac{\beta.E}{k.T_m^2} = s.e^{\frac{-E}{k.T_m}} \tag{1.9}$$

TL gives useful information about the defects dynamics. And can be used to estimate activation energy, frequency factor. Equation 1.9 shows that that the peak temperature depends on heating rate and it shifts with the heating rate. This is also shown in Figure 1.4. Hence, measurement of a glow peak at multiple heating rate can be used to estimate the activation energy and frequency factor using equation 1.9.

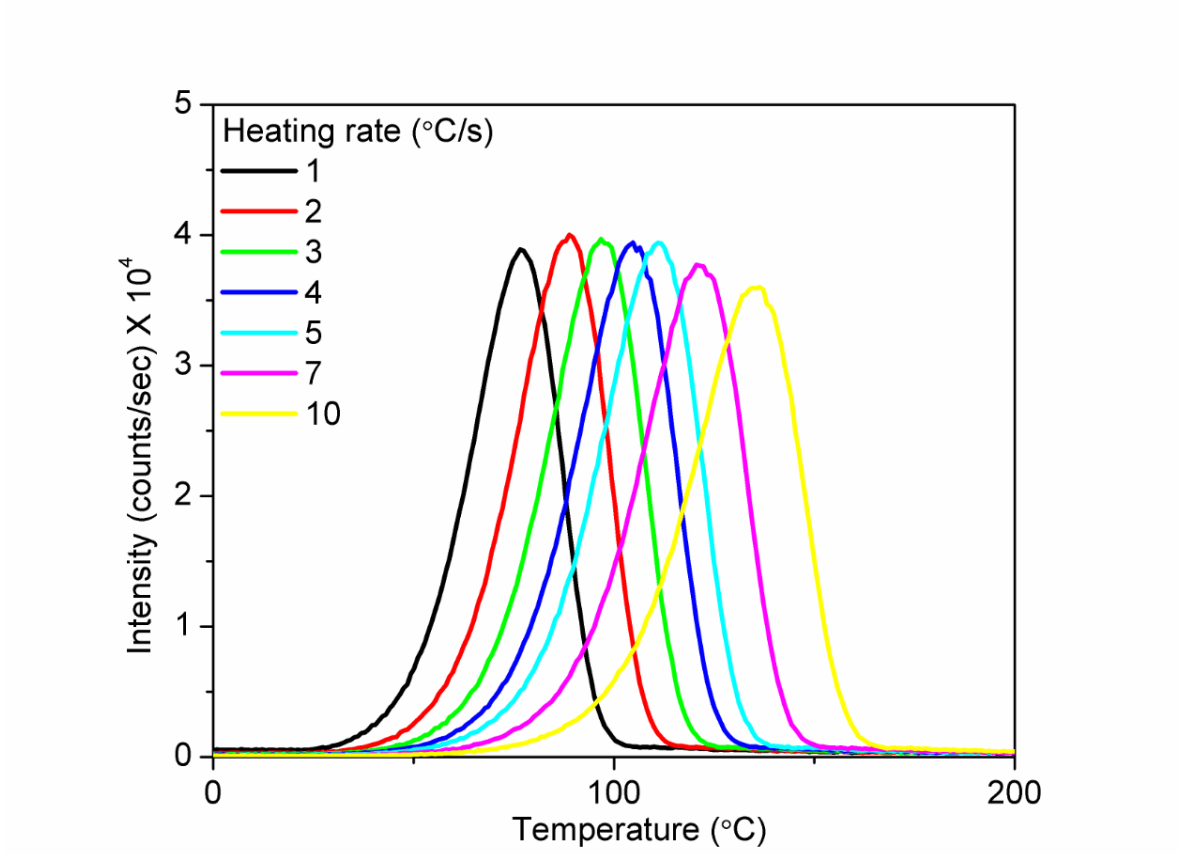

Figure 1-4 110°C peak of quartz at different heating rates.

Further considering the retrapping of electrons, the kinetics can be given by,

Garlick- Gibson equation (Garlick and Gibson, 1948; Pagonis et al., 2006) (known as second order kinetics)

$$I = -\frac{dn}{dt} = \frac{n^2}{N}.s.exp^{\frac{-E}{kT}} \tag{1.10}$$

and *May- Patrick equation* (May and Partridge, 1964) considering intermediate retrapping between first and second order (general order kinetics), with b the order of kinetics is given as

$$I = -\frac{dn}{dt} = n^b . s' . exp^{\frac{-E}{kT}} \quad (1.11)$$

1.3.1. Optically stimulated luminescence

If light is used as a stimulation source, the output emission is called optically stimulated luminescence (OSL). The stimulation sources can be modulated in different ways and consequently there are different kinds of OSL (Figure 1.5). For a continuous wavelength OSL (CW-OSL), the light output depends on the electron population (n), stimulation flux (ϕ), and photo-ionization cross-section (σ) (wavelength dependent) of the trap and is given as in equation 1.12.

$$I \propto n_o \sigma \phi exp^{(-\sigma \phi t)} \quad (1.12)$$

The output intensity is a decay function of σ and ϕ. The output curve is called the shine down curve. The OSL curve is composed of several exponential decay curves if several traps are contributing to luminescence. The CWOSL curve can be deconvoluted into different exponential decaying components using curve fitting methods. This aids in finding number of traps and their cross-section contributing to the output (Yukihara and McKeever, 2011).

In Pulsed OSL (POSL), the stimulation light is given as pulses of fixed width with a constant on and off times. The corresponding output can be gated to record either during on time or off time or can be counted during both on or off time.

In Linearly Modulated OSL (LM-OSL), the incident photon flux is increased linearly with time from zero to a maximum value. The benefits of using LM-OSL helps in distinguishing the traps having different photoionization cross-section as it sequentially removes traps from higher cross-section to lower cross-sections. This further enables determination of photoionization cross-section (σ)

Normally light emitting diodes (LEDs) and lasers are used as stimulation sources. These sources emit $10^{16} cm^{-2} s^{-1}$ photons or more, while the OSL output varies from 100 to 10^5 photons per second. Hence, it is necessary to use filters so that output can be distinguished from the stimulation source.

TL and OSL are both powerful techniques with their own advantages, as stated below.

Advantages of TL:

1. Calculation of activation energy "E" and escape frequency "s" is possible.
2. Complete removal of charges in metastable state by previous irradiation, provided the sample is heated above the maximum glow peak temperature.
3. TL is good for bleaching the sample completely, which cannot be done by OSL.
4. As all OSL sensitive traps are TL sensitive also, but the vice-versa is not true, therefore TL is mainly used to study the traps characteristics.

Advantages of OSL:

1. Multiple readout possible.
2. Does not have thermal quenching problem, which is the reduction in luminescence intensity at higher temperature.
3. High temperature heating in case of TL can change the structure of defects and hence the properties of phosphors, which is less probable in OSL.
4. In TL, we cannot probe deeper traps without interference from blackbody radiation, this is possible with OSL.
5. Estimation of photo-ionization cross section of trap is possible.
6. Information about the lifetime of recombination centre possible.
7. Since no heat is involved, it is possible to analyze materials that undergo phase transition while heating (example gypsum).
8. Zeroing of signal in OSL is much faster than TL.

The luminescence output (photons/sec) from TL/OSL is proportional to the number of charges trapped, which is proportional to the amount of dose received by the crystal as input. For a constant irradiation environment, the luminescence intensity is proportional to the time of dose accumulation. This is the principle used in luminescence dosimetry and dating.

1.4. **Luminescence Dosimetry and Dating**

Dosimetry is the measurement of dose. It is useful to estimate the amount of radiation energy given to materials.

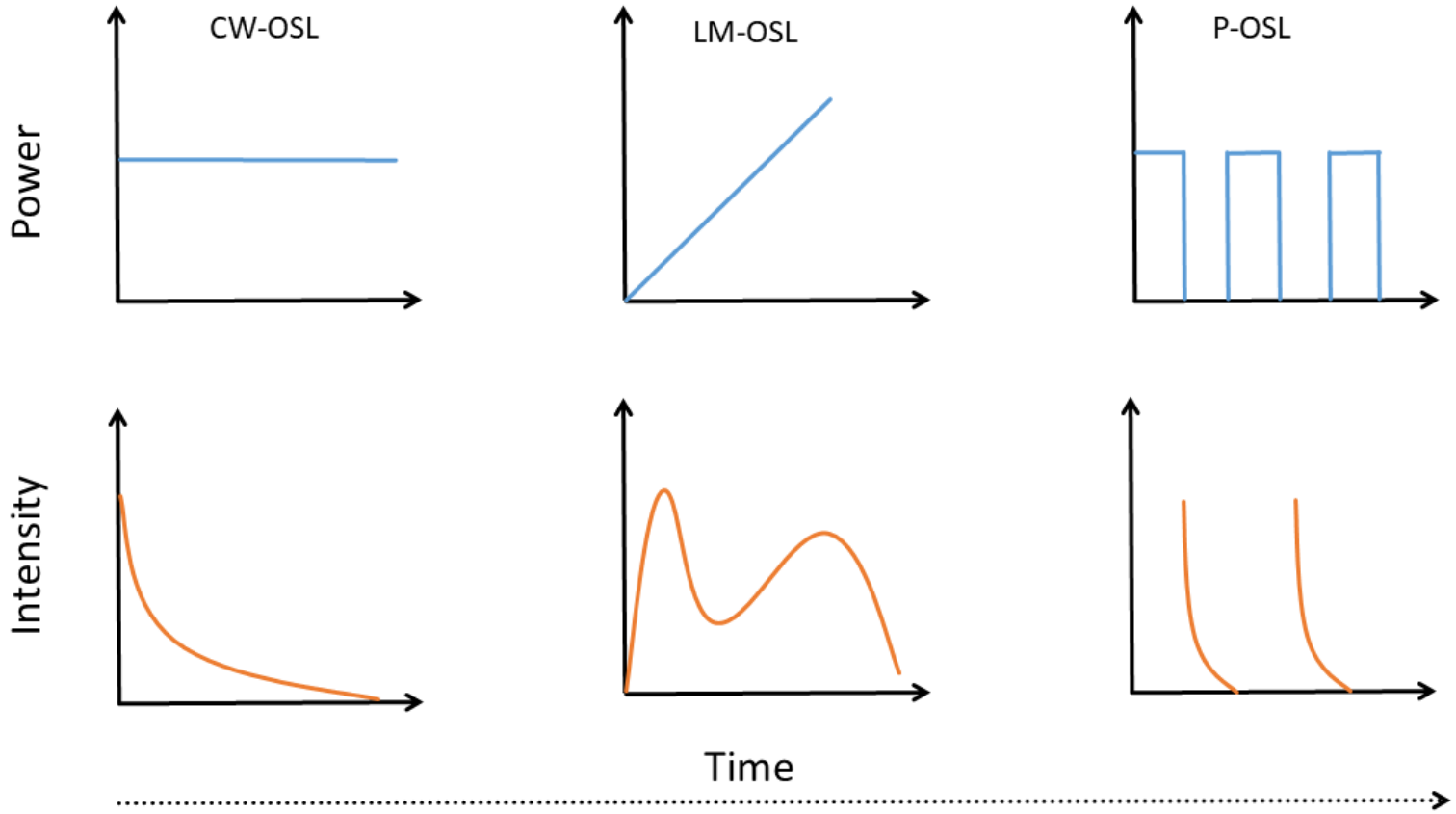

Figure 1-5 Optically stimulated luminescence shine down curve.

Dose is measured in terms of equivalent dose (D_e), which is the amount of laboratory dose that will produce the same amount of luminescence intensity as produced by the natural irradiation. There are many artificial and natural phosphors available to estimate the dose. BeO, Al_2O_3, CaF_2, $CaSO_4$ are widely used as artificial TL and OSL dosimeters. They have the advantage over natural minerals that the luminescence sensitivity (luminescence signal per unit dose per unit weight) is high, response is linear in the desired region of interest, have excellent reproducibility and no fading. Thus, the dose can be easily estimated by comparing area under the TL/OSL curves for unknown dose with known dose to get the D_e.

In the nature, minerals are present as natural dosimeters. The complexity in estimation of dose accumulated in natural minerals is that they undergo a large sensitivity change during the measurements due to presence of intrinsic defects. For the same dose the TL/OSL intensity is different in every repeated measurement. The D_e calculation is a bit complicated for natural phosphors due to their varying dose response during measurement procedures due to which direct comparison between the natural and laboratory dose is not possible. Several protocols are proposed to estimate the equivalent dose (D_e) reliably and are discussed in next chapter in detail. Dosimetry is an essential part of luminescence dating.

Luminescence dating is the estimation of time of irradiation of rocks and sediments by measuring the total stored luminescence, luminescence dose response and the rate of dose accumulation. The age can be calculated as in equation 1.13,

$$Age = \frac{Equivalent dose(D_e)}{Dose\, rate(DR)} \qquad (1.13)$$

In nature rocks and sediments receive radiation dose from decay of natural radioactive elements present in ambient surroundings matrix. These include U, Th, K, Rb and cosmic rays. The dose accumulated by cosmic rays is 2 order smaller than radioactive nuclides. Since the natural radioactive atoms have very high half-life, ^{238}U half-life = 4.8 billion years, ^{232}Th half-life= 14 billion years, ^{40}K half-life = 12.5 billion years, their decay rate is constant over million-year time and thus dose rate of irradiation of crystal is constant. When a crystal is formed in earth crust and is shielded from light, it starts to accumulate luminescence signal with time, hence the sample taken just after crystallization will give the crystallization age. If rock withers and get transported by wind or water, it is exposed to sunlight followed by deposition and burial. Sometimes during their antiquity, they may also face heat either due to forest fire or some other sources. These events reset luminescence signal to zero. After getting buried the signal again starts to build because of ambient radioactivity as depicted in Figure 1.6. A crystal may undergo

multiple cycles of burial and exposure, which can be because of various natural processes. These cycles of burial and exposure are due to fluvial, aeolian, other activities, which can directly be linked to floods, glacier movement, sand dune movement, earthquakes, human settlements etc. When the crystal (sediment) is excavated (taking into account that it is not exposed to light on excavation), the luminescence signal present depicts the last burial age. Heat resets all the traps completely that are probed below the heating temperature, whereas light resetting always leaves some residue. This residue can be estimated in lab and subtracted from the estimated luminescence while estimating the age.

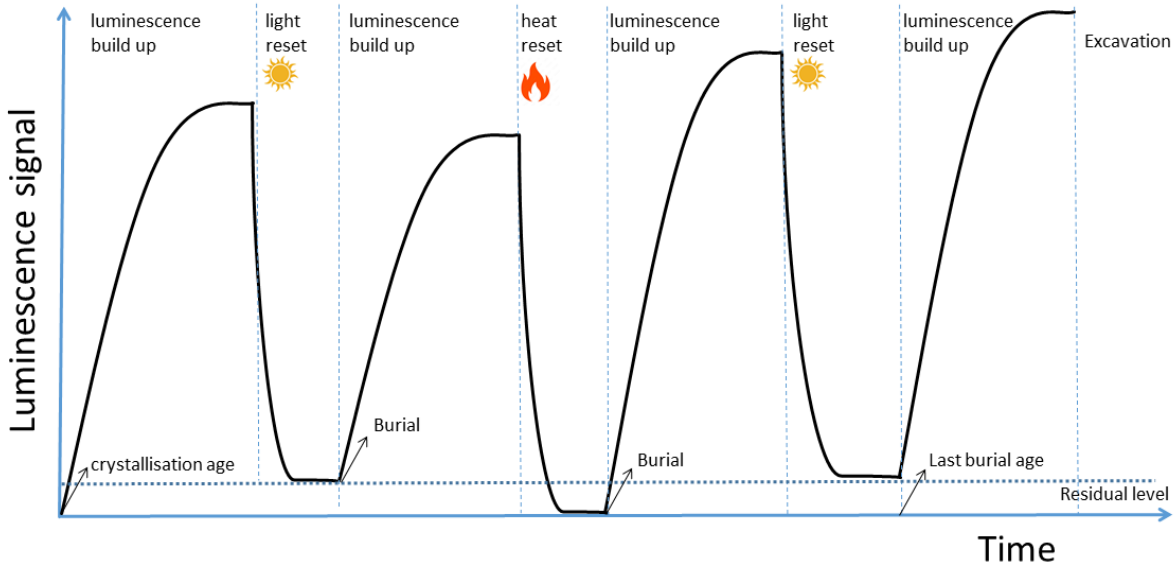

Figure 1-6 Buildup of luminescence in nature. The figure depicts multiple cycles of buildup and resetting over the geological time period.

1.5. Natural dosimeters

Many natural minerals are used for luminescence dosimetry. Quartz, feldspar, zircon, gypsum, basalts, calcite etc. are explored for luminescence properties. Among this quartz and feldspar are widely used because of their ubiquitous nature and well-established luminescence properties.

1.5.1. Quartz

Quartz is silicon dioxide (SiO_2). Its abundance in earth's crust is 12.6% of weight. It is a diamagnetic mineral, with a density of 2.65g/cc. It is quite resistant to physical and chemical weathering and is found in almost all sedimentary settings. It has tetrahedral structure and a bandgap of ~9 eV (Garvie et al., 1998). This huge band gap allows for the existence of many

impurity state with very long lifetime. Large number of defects are found in quartz. As intrinsic defects, it has both silicon and oxygen vacancies. Silicon vacancies are usually accompanied by oxygen atoms bonded with hydrogen atoms, thus forming H_3O_4 and H_4O_4 sites (Preusser et al., 2009). Depending on, if the oxygen atom causing the vacancy takes the electron pair with it or not, many oxygen vacancy defects are present termed as E' centres. E1' is formed when the oxygen takes one electron from silicon and hence the two silicon form a bond, E2' and E4' are formed when oxygen vacancy is accompanied by presence of one hydrogen atom bonding with a silicon, leaving the other silicon with one electron. Additionally, excess of oxygen is also observed and leads to formation of proxy linkage. When quartz is formed from the melt a lot of foreign impurities are captured in the crystal structure. Mostly, these are the atoms having size similar to silicon like Al, Ge, Ti, P, and monovalent impurities such as H, Na, Li etc. (Krbetschek et al., 1997; Preusser et al., 2009).

Several TL peaks are reported in quartz such as 110, 190, 230, 240, 310, 325, and 375°C at a heating rate of 5°C/s. Corresponding thermal stability of the peaks are 8 hrs, 700 years, 130 ka, 340 ka, 450 Ma, 100 Ma and greater than 100 Ma respectively (Aitken, 1985). The TL of quartz is shown in Figure 1.7 (a). Quartz is known to emit luminescence in several emission bands. The most popular of these are the UV, blue and red (Krbetschek et al., 1997).

UV emission is widely used for OSL dating purpose. Blue emission is also used for TL dating. Red luminescence from quartz is used for analysis of volcanic quartz. Quartz is optically stimulated with blue/green light and the emission in UV is widely studied, as shown in Figure 1.7(b). No athermal fading (leakage of stored electrons due to effects such as quantum mechanical tunnelling) of quartz signal is observed and its signal bleaches fast, the best amongst all natural minerals, thus it is often preferred for dating fluvial settings.

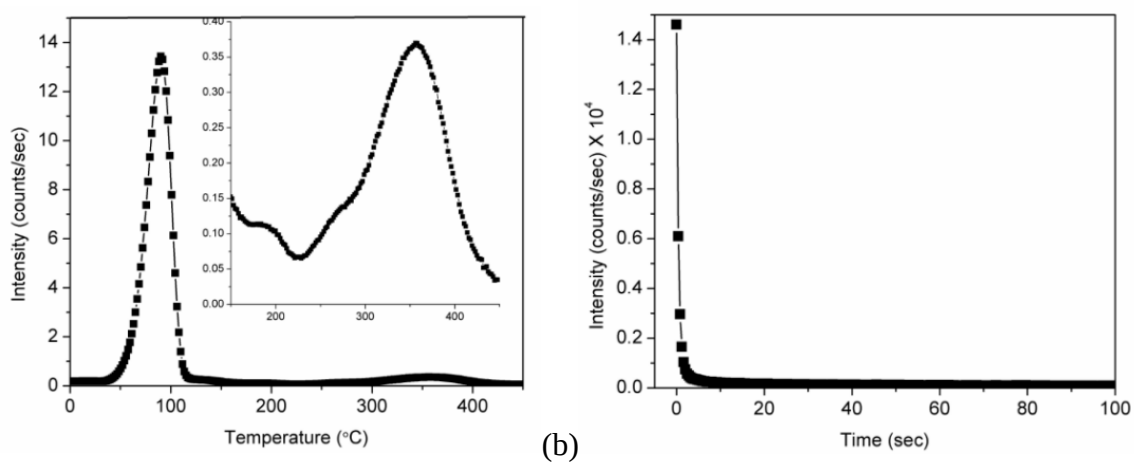

(a) (b)

Figure 1-7 (a) TL of Quartz in emission range 325-700 nm at a heating rate of 2°C/s. (b) OSL of quartz stimulated by blue light (470±20 nm) and observed in UV (340±40 nm).

1.5.2. **Feldspar**

The most abundant mineral in the earth crust with about 41% to the weight is feldspar, however it is prone to weathering and many times is not found in very old sediments. Feldspar belongs to a solid solution series of aluminosilicate with K, Na and Ca being its end members. Commonly known feldspar are; K feldspar ($KAlSi_3O_8$), albite ($NaAlSi_3O_8$), and anorthite ($CaAl_2Si_2O_8$). Its density varies from 2.56- 2.76 g/cc.

Its crystal structure consists of AlO_4 and SiO_4 tetrahedron with large compensating ions like Ca^{2+}, K^+ etc. occupying irregular cavities in tetrahedral framework. Numerous defects are possible in feldspar because many atoms such as Ga, Ge, Li, B, Ba, Be, Cs, Fe, Mg, Mn, P, Pb, Rb, Sn, Sr, Ti can substitute the host atoms (Krbetschek et al., 1997). Feldspar has a continuous TL glow curve, with no well-defined peaks (Figure 1.8(a)). This is attributed to its complex structure consisting of a lot of defects. The calculation of activation energy of these traps results in a continuum, with lifetime of traps > 300°C to be greater than 10^9 years. A principle trap in feldspar has energy matching with the infrared 1.44 eV and hence can be stimulated with infrared light. A shine down curve of feldspar stimulated with infrared light is shown in Figure 1.8(b). Notice that compared to quartz OSL (Figure 1.7(b)), feldspar OSL decays much slowly.

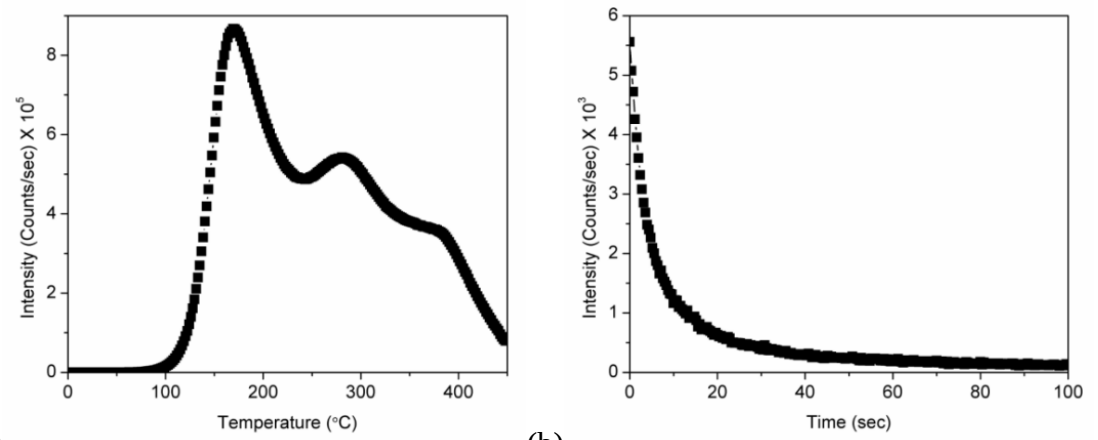

(a) (b)

Figure 1-8 (a): TL of Feldspar in emission range 325-700 nm. (b) OSL of feldspar stimulated by blue light (850±30 nm) and observed in blue (440±40 nm).

1.6. Chronology limits: comparison and possibilities

Chronology is an important tool to understand the past. There are several interesting scientific challenges which require chronology to extend beyond the present limits (Anil et al., 2022; Biswas, 2014; Biswas et al., 2011; King et al., 2016).

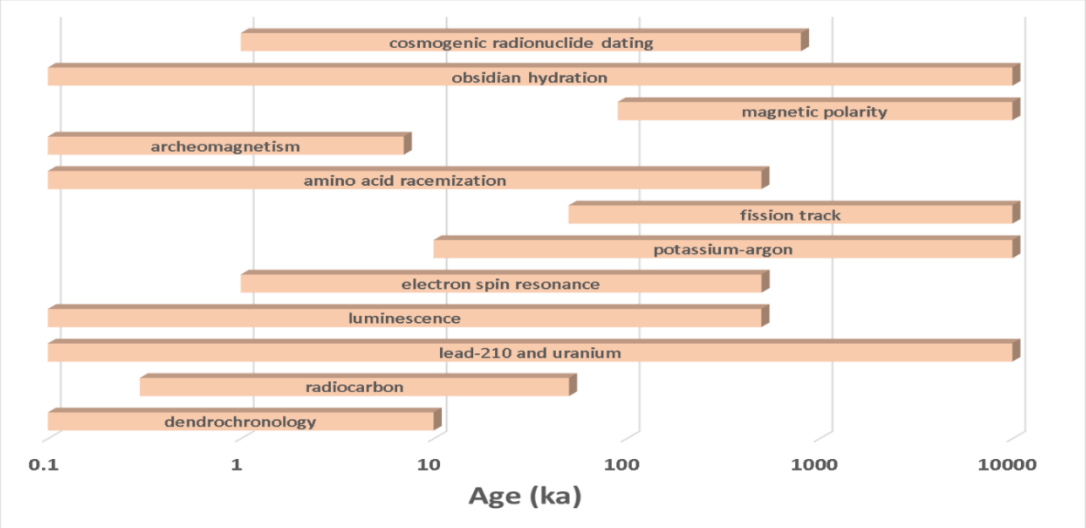

Figure 1-9 Various chronology techniques and their workable dating range.

In the quaternary period (present to 2.5Ma back), beyond the extent of luminescence dating (~0.5Ma) many chronometers are available like paleomagnetic dating, obsidian hydration, fission track dating and radiometric dating (Mahaney, 1984), as shown in Figure 1.9. However, they are limited in use and not applicable in every scenario. Depending on the scientific question in hand, the chronology technique is chosen. For e.g., potassium argon and fission track give formation age of the rocks. Obsidian hydration is a relative dating method and works on obsidian (volcanic glass) limiting its applicability. Magnetic polarity is yet again a relative dating method and gives formation of rocks and deposition of fine sediments based on the polarity of magnetic domains with respect to earth's magnetic polarity with a resolution, that corresponds with changes in earth's magnetic field. Cosmogenic dating can be used to estimate time of burial/exposure of rocks but can be complicated by the presence of inheritance of signal. Luminescence dating have the advantage that, it uses ubiquitous minerals, quartz and feldspar and hence is applicable everywhere. Further it gives depositional ages of sediments which can be used to directly study large number of geological processes as shown in Figure 1.10.

The quest to increase the luminescence dating limit has been since long. Many approaches have been taken in this regard.

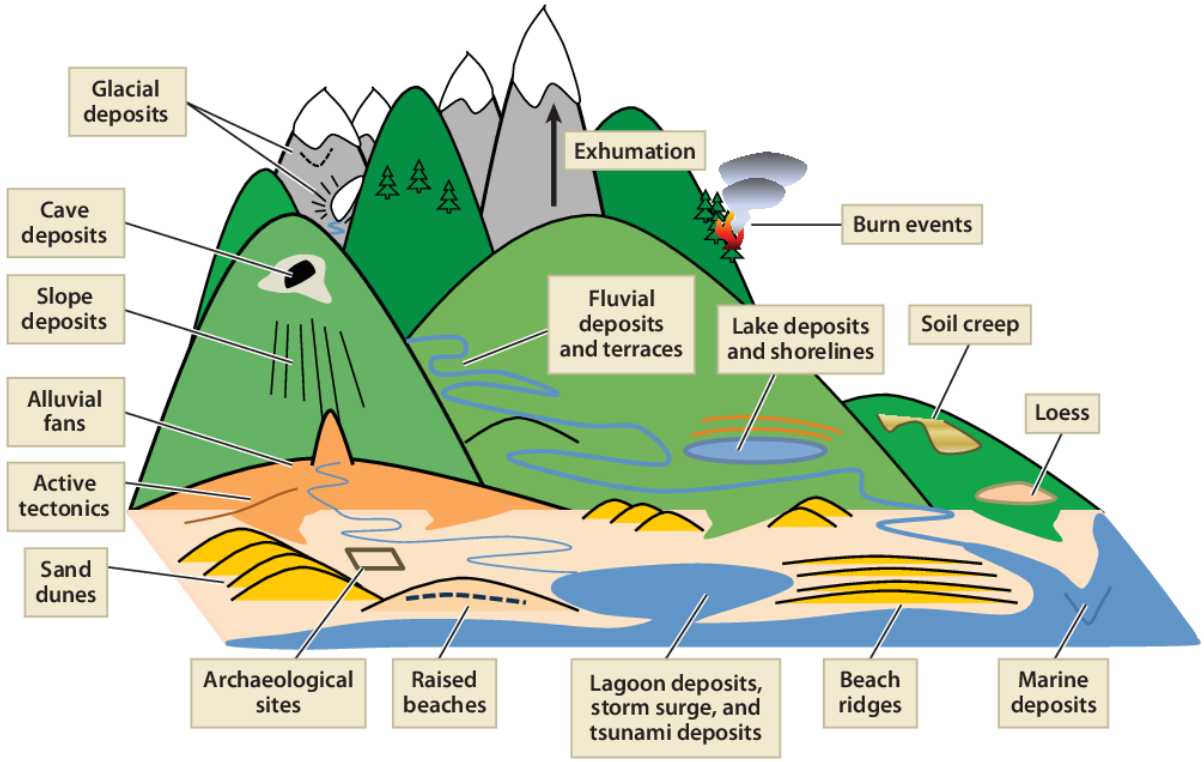

Figure 1-10 The picture indicates the sites where luminescence dating is applicable. Taken from Rhodes, (199

.

Exploring new minerals: Quartz is widely used mineral in luminescence dating. Its optical stimulation with green/blue light was discovered by Huntley (Huntley et al., 1985). The maximum datable range is limited by the saturation of luminescence signal for doses ~ 250 Gy (Chawla et al., 1998; Duller, 2008; Wintle, 2008; Wintle and Murray, 2006). Detection of IRSL in feldspar opened up another major domain in luminescence dating (Hütt et al., 1988). However, anomalous fading of the signal was a major concern (Wintle, 1973). Even with feldspar, the dating range is limited to dose estimates up to 2000 Gy (Thiel et al., 2011). Many new minerals are being studied for luminescence dating, with a saturation dose higher than the conventional (quartz and feldspar) minerals. Zircon is one such explored mineral. It is $ZrSiO_4$, a silicate mineral with high resistance to weathering and is thus found in many geological settings. It has a high amount of rare earth elements present inside the crystal matrix along with radioactive atoms such as uranium (U) and thorium (Th). The presence of U and Th inside the crystal makes a significant amount of internal radioactivity which overpowers the external dose rate, water content and beta inhomogeneity. However, U and Th content varies from grain to

grain of zircon and hence makes it challenging to use for dating. Several methods like auto regeneration techniques are applied on zircon for dating which are time consuming (Smith, 1988). Further, zircon also suffers from athermal fading (Krbetschek et al., 1997; Schmidt et al., 2024). Calcite and gypsum are two other minerals explored for luminescence dating. These are formed in arid conditions. Hence these have special application in studying arid paleoclimate. Impurities like Mn^{2+} are considered responsible for luminescence. Main emission peak of calcite is around 600nm. Gypsum is $CaSO_4.2H_2O$, various defects are associated with it for example SO^{3-}, SO^{4-}, CO^{2-}, SO^{2-}. On heating above 200 ℃ it losses water and its TL characteristics changes. However, it also show OSL which has scope for using it for dating (Nagar, 2007). The saturation dose for gypsum is reported to be > 6kGy (Jain et al., 2006). Further many basalts are also explored for its luminescence properties for example olivine, pyroxene with a saturation dose of 2.5 kGy or higher.The main limitation with them is the high fading which cannot be corrected by conventional methods (Jain et al., 2006; Morthekai et al., 2008). Since luminescence is well observed by crystalline solids, other minerals present in nature should be probed for its potential to be used a dosimeter for luminescence dating.

Probing new signals in conventional minerals: In the conventional minerals (quartz and feldspar) new signals with higher saturation are hunted over the years.

For quartz, blue stimulated luminescence, single aliquot regeneration (BSL-SAR) is the most widely used signal for dating till today. The traps are stimulated by 470 ± 30 nm wavelength and detected in 330 ± 50 nm UV wavelength. The maximum dose that can be estimated is ~250 Gy (Chawla et al., 1998; Duller, 2008; Wintle, 2008; Wintle and Murray, 2006). At high doses, near to SAR-BSL saturation, some paleodoses are reported to be underestimated by SAR (Dreimanis et al., 1978; Lowick et al., 2010a; Lowick and Preusser, 2011; Lu et al., 2007; Murray et al., 2007; Prescott and Robertson, 1997; Qin and Zhou, 2009; Timar-Gabor and Wintle, 2013; Wang et al., 2021). In this regard, many factors are explored such as, anomalous fading, thermal instability, saturation of natural signal, stepped irradiation (Bonde et al., 2001; Li and Li, 2006; Qin and Zhou, 2009; Ashok K Singhvi et al., 2011; Yoshida et al., 2000). Still deviations from the expected ages are not resolved. Further several methodologies are developed for quartz to extend and improve the dating protocols. These are discussed below.

The potential of using the slow component of the BSL for dating was proposed by (Singarayer et al., 2000) and has a saturation value ~ 4000 Gy. However, the bleachability of the signal is an issue (Biswas, 2014).

Isothermal Thermoluminescence (ITL) from quartz at 310°C and 320° allows to probe the slow component that we see in BSL (Jain et al., 2007b, 2005). It can be used to extend the dose till 1.4 kGy. Since, it is originated from slow component, the signal is limited by poor bleachability (Biswas, 2014). Further, it has been reported that dose estimated by ITL starts to diverge above 200 Gy (~70 ka) (Rahimzadeh et al., 2023b) and the dose is not recovered in most cases (Buylaert et al., 2006).

Violet stimulated luminescence (VSL) is another proposed signal for dating by Jain, (2009) and probes deep traps that are not accessible by BSL. The traps are stimulated by 405 nm (3.06 eV) compared to blue light 2.6 eV. Various studies have tested the applicability of VSL signal for dose estimates and have found that due to large sensitivity changes, SAR (single aliquot regeneration) may not be a suitable methodology and hence additive methods like SARA, MAAD and MAR methods should be used (Ankjærgaard, 2019; Ankjærgaard et al., 2016; Rahimzadeh et al., 2023a). Further bleachability of the deep traps is also an issue (Biswas, 2014). The maximum dose that can be estimated is the atleast up to 1000 Gy governed by the saturation of the electrons in the traps in laboratory growth curves. However, when applied to natural systems, divergence from the expected doses occur after 250 Gy (Rahimzadeh et al., 2021).

Thermally Transferred OSL (TT-OSL) is yet another signal proposed for quartz dating. First reported by Aitken as recuperation (Aitken and Smith, 1988), but its dating potential was identified by Wang et al., (2006). It was initially believed that some charge is transferred from 325°C peak to 110°C peak on measurement of OSL in SAR and back to 325°C peak during preheat (Biswas, 2014). This mechanism is called the double charge transfer mechanism. But since, the growth curve of TT-OSL saturates at higher dose than the signal of 325°C peak, this explanation is discarded. It is now believed that the signal in TT-OSL is obtained from deeper traps. It can date events upto 1Ma (Duller and Wintle, 2012). Though Wang et al., (2006) have shown that TT-OSL can estimate consistent ages atleast up to 0.8 Ma, however many studies suggest that above 100 ka the expected ages and TT-OSL ages diverge, thus questioning the reliability of the technique (Biswas, 2014; Chapot et al., 2016; Duller and Wintle, 2012; Rajapara, 2014). Further, the poor bleachability and low sensitivity, limits the use of this technique and its non-applicability to estimate very young ages are also an issue.

Yet another way of extending the dating limits is to probe the signal in the interior of quartz grain (Chauhan et al., 2009; Singhvi et al., 2010). For large quartz grains, the interior of grain will have contribution from gamma only and will therefore saturate late. This can enable us to date 3-4 times older samples. The initial grain size needed to employ this method will be around

cm size, thus limiting its applicability. This proposed method has not been yet tested for dose estimates.

Thermally Assisted OSL (TA-OSL) is another studied signal to probe very deep traps (peak maximum > 500°C) in quartz (Kitis et al., 2010; Polymeris, 2016; Polymeris et al., 2015). By a combination of light stimulation (470 nm) and heat stimulation (most effective at 180°C), these traps can be probed, with maximum limit till ~2500 Gy. However, the usability of this signal for dating older sample is still ambiguous given the limited studies done on this some suggesting suitable TA-OSL-SAR protocol to date old sample and some not (Polymeris et al., 2018; Şahiner et al., 2017).

Thermally Modulated OSL (TM-OSL) is another studied signal which can probe deep traps by using a combination of stimulation and temperature modulation from 0-300°C, thus limiting sensitivity changes (Palczewski et al., 2025). However, the oldest samples dated by this method is ~150 Gy and the validity for dating older samples and possible saturation dose is yet to be tested (Chruścińska et al., 2021).

Apart from OSL, TL is also studied for extending the current dating limit. In the initial days, when TL dating was done using UV and blue emissions, underestimation in ages above 100 ka was reported (Debenham, 1985; Prescott and Robertson, 1997). Further red TL is also explored for dating (Fattahi and Stokes, 2003; M. Fattahi and Stokes, 2000). Observed around 590-700 nm, the red luminescence signal in quartz is highly reproducible, thus SAR protocol can be used. Two major peaks are found; one low temperature peak centred around 100°C and one high temperature peak around 375°C. Atleast 50Gy dose is required to separate the signal from background (minimum detectable dose) (Miallier et al., 1991). Low temperature peak saturates at about 500Gy, whereas high temperature peak increases upto 20kGy. The characteristics dose was found to be around 6300Gy (M Fattahi and Stokes, 2000). This can depict ages of the order of 3.6Ma for a dose rate of 1-2Gy/ka. Although the bleachability is a problem in RTL. The intensity reduces to about 82% in 3 days (M Fattahi and Stokes, 2000). However, no age estimate as high as Ma are reported using red TL. Additionally, Electron spin resonance (ESR) and Exo-electron emissions are also used to extend the dating limits (Ankjærgaard et al., 2006; Duval, 2022; Kabacińska et al., 2022 and ref within), but these techniques are not discussed here, as this thesis focusses on OSL and TL methods.

In feldspar, in comparison to quartz, higher OSL (or Infrared stimulated luminescence (IRSL)) saturation dose is reported, and hence can date samples from a few decades to a few millions

of years. However, it suffers from athermal fading that leads to an underestimation of the age (Wintle, 1973).

Feldspar dating is done using infrared stimulated luminescence (IRSL). The stimulation is done using infrared stimulation (850 ± 30nm) and detection is done in blue (440 ± 40nm). But, the issue of anomalous fading (Wintle and Murray, 2006) holds back the use of feldspar in dating. There are two methods to circumvent the issue of anomalous fading: 1) to estimate for the amount of fading, 2) to probe non-fading traps.

Huntley and Lamothe, (2001) prescribed the age correction model considering fading rates. But the correction model assumes linearity in the dose response curve and which is applicable for samples with age less than 50ka. Another age correction for athermal fading is proposed by Huntley, (2006) and implemented by Kars et al., (2008) and can be applied to the non-linear region of dose response curve.

The second approach to probe non-fading traps has been explored using p-IR-IRSL and MET-IRSL(Buylaert et al., 2009, 2012; Li et al., 2014) . In the p-IR-IRSL or MET-IRSL technique, luminescence with IR stimulation at elevated temperatures (150 to 290℃) are measured after suitable preheat and IR 50℃ stimulation. The preheat and IR at 50℃ consumes the proximal electron and hole pairs which are more prone to fading and thus IR at 290°C probes distant electron and hole pairs, hence yields minimal fading, because the tunnelling probability is inversely proportional to the exponent of distance between the distant pairs (Huntley, 2006). However, we still need to calculate the fading.Further estimated doses and accepted doses are compared for IRSL and pIRIRSL and deviations in the two are observed after 200-300 ka (Li et al., 2018).

In feldspar, red TL is unaffected by anomalous fading (Fattahi and Stokes, 2000) and is optically bleachable. After 2-hour exposure to sunlight, the signal reduces by 70%. This signal has good dating scope, provided the overlapping of black body radiation with the output spectrum can be solved. The blue and red isothermal thermoluminescence (ITL) signal from feldspar do not show dose underestimation (Jain et al., 2005). Both blue and red ITL are thought to be originated from the same traps. These do not saturate till ~600 Gy. Age estimated by IRSL is about 34% lower than blue ITL and 70% lower than Red ITL. Thus ITL from feldspar can be used to extend dating limits. However, its application is limited by the sensitivity fluctuations in red ITL that are not tracked by the test dose signal.

Thermally Assisted OSL (TA-OSL) from feldspar is also studied to probe very deep traps. Use of both blue (470 nm) and infrared (870 nm) stimulation at a temperature of 300℃ can probe

charges, otherwise not possible because of thermal quenching and blackbody background. The maximum dose is ~2000 Gy found by investigation on polymineral (Şahiner et al., 2017) but suffers from high fading (Kalita and Chithambo, 2022).

Infra-Red Photo-Luminescence (IRPL) is a newly proposed technique which suggest, infrared stokes shifted photoluminescence emission at 885nm and 930nm when stimulated by 855 nm IR light has a dose response up to 1.5kGy. The signal is non-destructive and hence can be used for dating older sediments (Prasad et al., 2017). The methodology is still under development and need to be refined. Further post Violet infrared stimulated luminescence (pVIRSL) is another newly developed method for dating near zero fading traps (Devi et al., 2024). It also provides the possibility to date polymineral samples. A saturation of ~1000 Gy is reported. However, still more studies are required on IRPL and pVIRSL.

Following major points are observed for various signals reported above in quartz and feldspar,

1. The laboratory saturation of all signals is way higher than natural saturation. Although the methods are able to recover high radiation doses~1 kGy in the lab, but this is not possible in natural irradiated samples (Colarossi et al., 2015; Rahimzadeh et al., 2023a, 2023b, 2021 and ref within).
2. There are studies that show the role of laboratory procedures in paleodose underestimation. For example, Wang et al., (2021) have shown that Multiple Aliquot Regenerative (MAR) protocol can be used to increase the dating limits for quartz. Similarly, Zhang and Tsukamoto, (2022) have shown on feldspar, that protocol used for estimation of D_e affects the upper range to which the date can be estimated. Since, different signals (VSL, TT-OSL, etc.) originate from different traps inside the crystal, the consecutive maximum dose that can be estimated with them can vary. However, for the same signal the dependency of the laboratory protocol on the maximum dose or the paleodose should not exist and is not understood.
3. There is a need to develop more fundamental understanding of the luminescence mechanism at high radiation doses and to re-verify the role of laboratory methods in governing the saturation.

Limited studies exist which probes the luminescence properties of minerals at very high doses > 1000Gy. Some studies suggest that there can be shift of emission wavelength (Schmidt and Woda, 2019), creation of defects and radiation damage to the mineral with dose at high irradiation, leading to variation in luminescence properties but experimental data is limited

(Chawla et al., 1998). So far, the studies done to extend the dating limits have measured the output in limited spectral ranges. For quartz these are blue emission, UV emission and red emission. For feldspar, these are blue, infrared and red. Whereas, spectral studies of quartz and feldspar indicate the output in other spectral windows (Krbetschek et al., 1997). The quartz emissions are found at 175, 290, 330-340, 380-390, 420, 450, 470-500, 510-570, 580, 620-650, 700nm. Feldspar emission is found at 280, 300, 320-340, 355, 415-425, 450-480, 490, 500, 540-570, 690-780, 860nm. This could be potential candidates for extending the dating range and providing us with new tools for chronology or other related studies. There is a need to explore these possible spectral emissions to gain further understanding about the process and new possibilities.

1.7. **Challenges**

In the research related with luminescence on natural minerals, difficulties arise due to the sensitivity changes. Sensitivity changes are the changes in luminescence counts per unit mass for the same amount of dose given in multiple repeated measurements (Aitken, 1985). Sensitivity changes in the 110°C glow peak of quartz are shown in Figure 1.10. Therefore, in the early times of development in luminescence dating, various Multiple Aliquot Additive Dose (MAAD) methods were established to find the paleodose (D_e) (Singhvi and Mejdahl, 1985; Wintle, 1997) such as R-Γ method (Wintle and Huntley, 1979), total bleach method (Singhvi et al., 1982), Australian slide method (Prescott et al., 1993). To find the paleodose, a dose response curve was constructed for which each data point was a measurement on fresh aliquot and a large amount of sample was required (Aitken, 1985; Fleming, 1979; Mejdahl and Wintle, 2020). Efforts were aimed to track for these sensitivity changes and it was reported that TL and OSL sensitivity changes are correlated (Stokes, 1994), and hence TL can be used for tracking sensitivity changes making measurements possible on single aliquot. Hence, single aliquot regenerative (SAR) protocols were established (Murray and Mejdahl, 1999; Murray and Roberts, 1998). Later Murray and Wintle (2000) showed that a small test dose is suitable for tracking of sensitivity changes and consequently proposed BSL test dose normalized SAR (Wintle and Murray, 2006). SAR further provided a scope to study the bleachability of the depositional environment. The validity of the sensitivity correction by SAR was tested against the radiocarbon ages (Murray and Olley, 2002) and other independent chronology available

(Huntley, 1994; Huntley et al., 1993; Prescott and Robertson, 1997). Since the development of SAR, most of the research done on natural minerals is using SAR methodology. This methodology is well tested for low radiation dose < 1000 Gy, but at higher radiation doses, it becomes essential to validate this methodology. Most of the work done towards extending the dating range above 1000 Gy have been within the SAR methodology, however there have been underestimation and field saturation reported when these methods are tested on old natural samples (Colarossi et al., 2015; Rahimzadeh et al., 2023a, 2023b, 2021 and ref within).

1.8. **Scope of the Thesis**

The present thesis examines three minerals, quartz, feldspar and a new mineral jarosite for their potential in estimating high radiation doses. Quartz and feldspar are investigated for their luminescence mechanism above 1 kGy as characteristics below 1kGy are well studied. For this analysis, multiple aliquot approach normalized by mass was used. Such methodology minimizes the sensitivity changes. Fruitful results were obtained for quartz and hence it was carried forward for further investigation. Role of laboratory protocols is investigated in causing the saturation of luminescence signals and understanding is applied to natural samples.
Further, for jarosite, no data on luminescence exists till date. However, as it is formed when climate gets arid, it is a direct indicator of paleo aridity and hence paleoclimate (Bhattacharya et al., 2016a). Hence in this thesis, its luminescence characteristic were established. A brief introduction of jarosite is given below.

Jarosite: Jarosite is an anhydrous sulphate of "alunite super group" with a general composition, $AFe_3(SO_4)_2(OH,H_2O)$, where A is a metal (such as Ag, 1/2Pb, Na, K Rb Tl, 1/2Hg or hydronium). For Jarosite, A is potassium. In natural jarosite, five kinds of metal substitutions can occur forming sodium (natrojarosite), hydronium (hydronium jarosite), lead (plumbojarosite), silver (argentojarosite) and ammonium (ammoniojarosite) (Roca, 2022).
Spectroscopic measurements from Mars orbital missions viz., *Curiosity*, *Mars Pathfinder* and others, suggest the presence of Jarosite on the Mars surface. In the Pathfinder mission, Morris et al., (2000) used optical and Mossbauer spectroscopic data to confirm the presence of jarosite. *Opportunity* (MER-B) and the *Curiosity* rovers (Klingelhöfer et al., 2004) confirmed the presence of jarosite using Mossbauer spectroscopy. Formation of jarosite requires wet and acidic environment and therefore its presence implies existence of water.

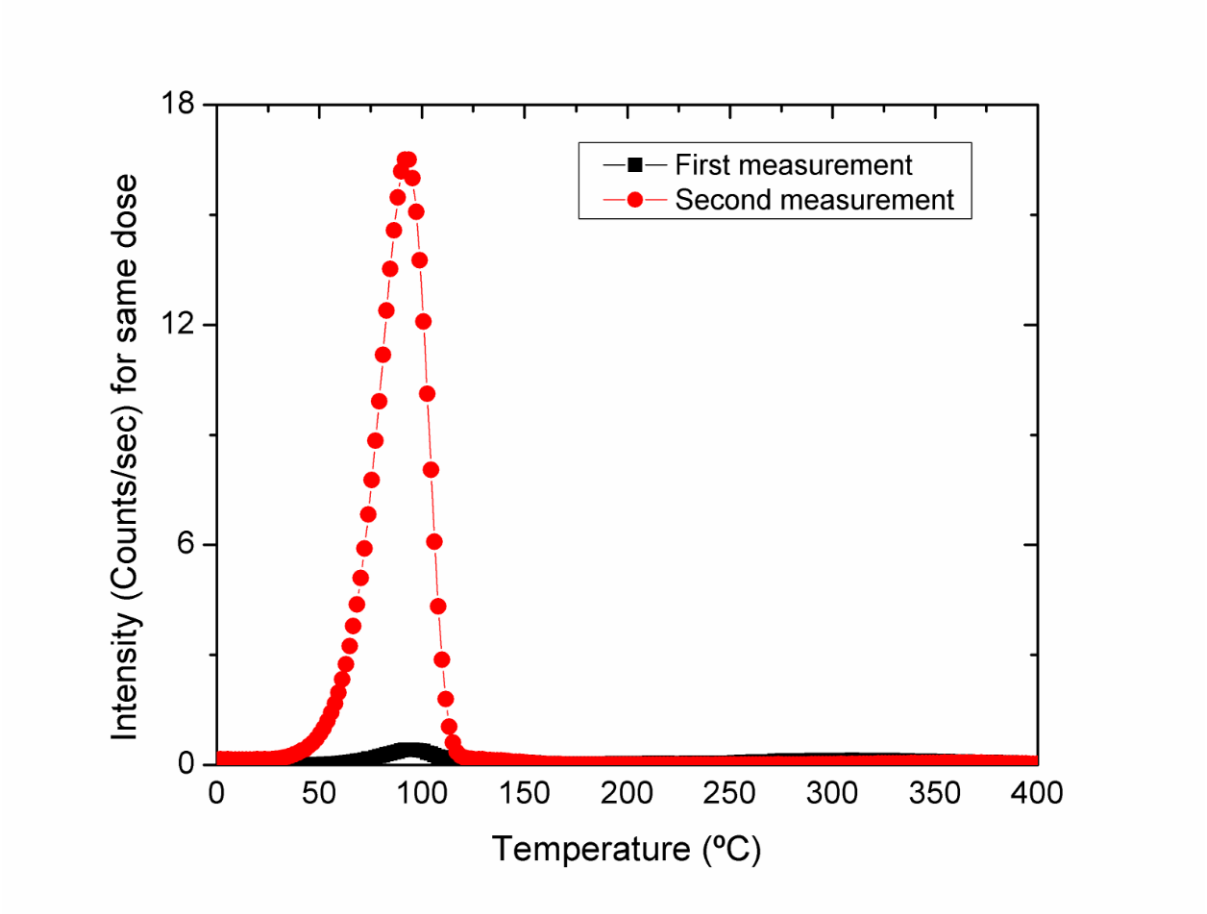

Figure 1-11 Sensitivity changes in the natural mineral (here quartz). The thermoluminescence intensity changes drastically for the same dose after heating to 450℃ in the first measurement step.

Jarosite has the ability to incorporate foreign molecules to its structure. For e.g. in natural jarosite on earth, Glycine has been detected (Kotler et al., 2008). This adds value to the mineral in detecting biological activity on Mars. On earth Jarosite occurrences have been reported from USA, Brazil, Canada, Iran, Romania, Greece and India (Bhattacharya et al., 2016b, 1955; Klingelhöfer et al., 2004; Marescotti et al., 2010; Reynolds, 2007; Velasco et al., 2013; Viñals et al., 2003, 1995), where it occurs in four contexts viz., a) in the sulphide ore deposits due to oxidation or in arid pyrite rocks; b) as nodules in clays; c) as segments of acid soils and; d) as hypogene minerals (Dutrizac and Jambor, 2000).

Jarosite forms from the weathering of sulphide ores, in acidic sulphate soils or through oxidation of iron by microorganisms and bioleach environment (Roca, 2022). Synthesized jarosite can be prepared by heating the metal sulphate and sulphuric acid solution at ~100°C, (Dutrizac and Kaiman, 1976; Fairchild, 1933) that leads to its precipitation .

Jarosite structure comprises alternative tetrahedral and octahedral sheets. The $[Fe(O,OH)_6]$ occupy octahedral sites connected by four hydroxyl group with neighbouring octahedral sheet and with two oxygen atom of $[SO_4]$ tetrahedral site (Xu et al., 2010). Metals (Ag, Pb, Na, K Rb Tl, Hg etc) are present on a 12-fold coordinated site, linked to 6 atoms of O from neighbouring $[SO_4]$ and 6 atoms from OH in $[Fe(O,OH)_6]$.

Several studies on the stability of Jarosite at elevated temperature exists. For e.g. neutron diffraction studies on deuterated jarosite shows that jarosite is thermally stable up to 277°C, beyond which it decomposes into yavapaiite, hematite and D_2O vapour (Xu et al., 2010). At 302°C, the diffraction peaks of yavapaiite and hematite appear and at 327°C the jarosite gets completely decomposed as follows,

$$KFe_3(SO_4)_2(OD)_6 \rightarrow KFe_3(SO_4)_2 + Fe_2O_3 + 3D_2O \quad (14)$$

Higher temperature increases the lattice parameters. Frost et al., (2005) report that jarosite decomposition depends on the cation such that between 130 - 330°C, loss of water occurs and at 500°C sulphur dioxide is lost leaving behind iron oxide and cation sulphate with a change in the structure from trigonal to monoclinic. Na-jarosite, decomposes at 215 - 230°C, then at 352°C and 555°C. For Pb-jarosite the decomposition is at 390°C and 418°C. Presence of Fe^{3+} in jarosite provides its magnetic properties (Inami et al., 2000; Wills et al., 2000). Its noteworthy that jarosite decomposes in alkaline and acidic medium, however it does not dissolve in water (Cruells and Roca, 2022).

1.9. **Objective of the Thesis**

The major objective of the thesis are as follows:

1. To explore the luminescence properties of conventional minerals and identify new minerals that can be used for high radiation and high radiation environment dosimetry.
2. To understand the luminescence characteristics of quartz at high doses (>1 kGy).
3. To test the validity of conventional methods at high radiation doses.
4. To apply the developed methods for dating older natural samples.

1.10. Chapters wise details

Chapter 1: Introduction

This chapter explains the fundamentals needed in the thesis. The basics of luminescence production in crystal and its mechanism is discussed. This is followed by the principle of luminescence dosimetry and dating. Then a literature survey of the natural dosimeters is given. Further study gap and challenges related to it are discussed. In the end, the thesis objectives are defined.

Chapter 2: Instrumentation and Methodology

This chapter explains the instrumentation used in the thesis work. This includes instruments for luminescence measurements and dose rate measurements. Sample collectionand mineral extraction techniques are explained. Further the methods to estimate the dose and dose rate are described. A brief introduction is given about the various protocols, normalization methods and signals used in luminescence dating.

Chapter 3: Natural Minerals for High Radiation Dosimetry

In this chapter the thermoluminescence characteristics of quartz, feldspar and jarosite are investigated. Further, detailed investigation on quartz is carried in the subsequent chapters. In this chapter luminescence characteristics of jarosite are established. Thermoluminescence, blue stimulated luminescence and infrared stimulated luminescence are investigated. Trap kinetics, reproducibility, sensitivity changes on heating, bleachibility, thermal and athermal fading is estimated. Further dose response for various signals and their saturation dose is estimated. Internal dose rate and its implication to dating arid environment on Earth and Mars is discussed with their possible workable dating range.

Chapter 4: Characterizing High Radiation Dose Response of Quartz

This chapter discusses the luminescence characteristics of quartz at radiation doses > 1 kGy. It further focusses on understanding the trapping mechanism, associated storing and detrapping mechanism in various spectral windows. Investigate the properties like bleachibility,

normalization methods and predose -dose effects in various spectral regions spanning from UV to red. This study provides enhanced insights into the role of recombination centres.

Chapter 5: Dosimetry using Blue Stimulated Luminescence of Quartz for High Radiation Doses

This chapter investigates the BSL from quartz by multiple aliquot additive approach. The chapter re-investigate existing methods and protocols to estimate dose using BSL (in particular the single aliquot regeneration method, SAR), and their applications at HRDs, and identify their limitations for HRD estimations. Applicability of test dose correction at high radiation doses is tested. The work also explores the possibilities of improvement in existing methods for increasing dose limits.

Chapter 6: Application to old geological settings

In this chapter, the methodology developed in the previous chapters is applied to natural old geological samples. For this, samples are taken from two different sites in India. The Upper Shivaliks from Northern India and the Charavathur Formation from Southern India. Ages are estimated using SAR and newly proposed methods in Chapter 5. Efforts are made to understand the reason for the underestimation of ages. This includes the study of kinetics of luminescence trapping and storage. Results indicate that the dose-response curve obtained in nature is different from that obtained in the lab due to thermal effects, which are dominant in nature.

Chapter 7: Summary and future prospects

This chapter summaries the present thesis, highlighting the potential applications of the work. It further outlines the future work that needs to done.

Chapter 2: Instrumentation and Methodology

2.1. Introduction

This chapter provides the experimental and analytical procedures involved in luminescence dating and covers the methods of sample collection, laboratory processing, measurements and analysis. It discusses a brief working principle of the major instruments used. The chapter discusses the various steps involved from sample collection to geochronology. Various dose measurement protocols including the intricacies of normalization techniques and thermal and athermal fading is described.

Geochronology as such comprises following main components:

1. Sample collection
2. Chemical processing
3. Instrumentation
4. Measurements
5. Data Analysis

2.2. Sample collection

Sample collection is one of the most important step for luminescence dating. Several precautions need to be considered for deciding sampling site as well as during sample collection. As luminescence signal is light sensitive, special caution should be taken while sample collection and it should not be exposed to sunlight. Hence, the samples are collected in metal pipes (steel/ iron/ aluminium) (Chandel et al., 2006). The sampling pipes (Figure 2.1 (a)) are either airtight to preserve water content or it can be measured at the site. Further, the sample should be collected such that it is surrounded by sediments ~30 cm (range of gamma radiation) around it, so that the infinite matrix assumption is followed. In unavoidable situations the distance from the surface should be measured and corrections should be made for it. The sample should not be taken from the sediment layer that has signatures of mixing or bioturbation. The

section should first be cleaned to remove light exposed surface and the sample should either be taken in dark, or the first 2 cm of sample in the pipe, should be not be considered for dose estimation. Further, the latitude, longitude, altitude, depth from surface should be noted at the site of sample collection.

(a)  (b) 

Figure 2-1 (a) Galvanised iron sampling pipe, with airtight seal O-ring used in the study. (b) Sample collection from the site.

2.3. **Sample preparation**

The samples are chemically and physically treated under subdued red light (> 630 nm). Sequential chemical and physical processes are carried out to separate the minerals from the samples. The upper and lower 3 cm part of the sample in the sampling pipe is taken for the measurement of the dose rate and water content. Rest of the portion is used for the dose estimation. For dose estimation, minerals such as quartz and feldspar are separated. The sample is first treated with 1 N HCl to remove the carbonates for atleast 30 minutes or until the reaction stops. Next it is treated with 30% H_2O_2 for atleast 24 hours to eliminate organic contaminants and dried. Grain size plays an important role in the calculations as with change in the grain size the dose rate the grains in nature and laboratory changes. Two grain categories used are fine grain (4-11 µm) and coarse grain (90-150 or 180-210µm). The choice of grain size categories defines the sample preparation method and dose estimation the procedure to be followed.

Coarse grain sample preparation: A grain size fraction of 90-150 µm is separated by sieving. Next, to separate heavy minerals, quartz and feldspar, a magnetic separator is used (Frantz magnetic separator (Model LB-1)) at ~0.5 and 1.5 ampere current values (Porat, 2006). After cleaning, quartz is subjected to 40-80 minutes of 40% HF treatment to eliminate the ~ 20 µm

alpha skin and 30 minutes of 37% HCl treatment to eliminate fluorides. Feldspar is subjected to 10% of HF for 40 minutes to remove ~20 µm alpha effected skin, followed by 37% HCl treatment to remove fluorides. The sample is sieved again to eliminate grain size smaller than 90 µm. A schematic of procedure is depicted in Figure 2.2. The samples are mounted on stainless steel discs as a monolayer using Silicon Spray oil and further used for measurements.

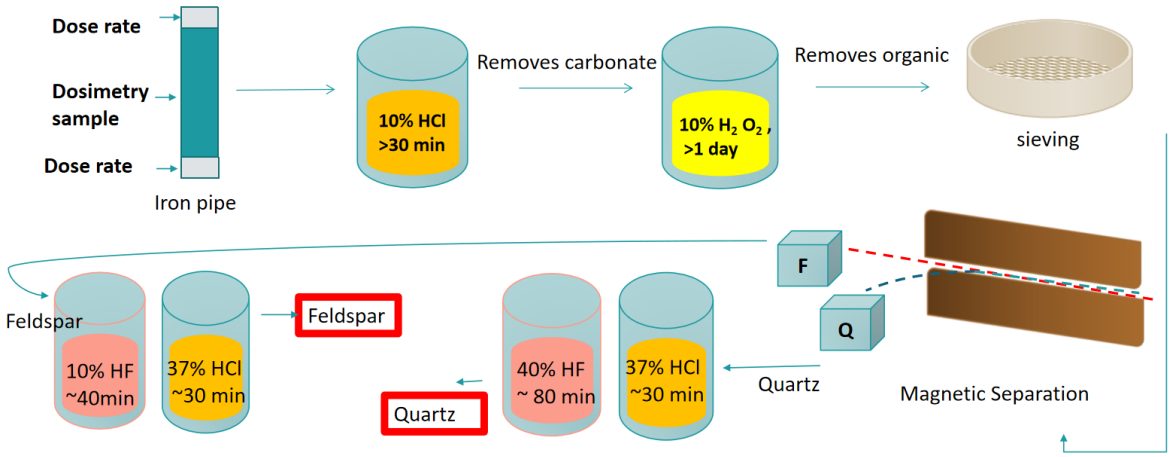

Figure 2-2 Flow diagram of sample preparation involved in coarse grain dating.

Fine grain sample preparation: After H_2O_2 treatment, the sample is dissolved in 0.01 N sodium oxalate ($Na_2C_2O_4$) solution for ~12 hours. $Na_2C_2O_4$ deflocculates the sample and neutralize static charges from clay particles and then separate them out. A grain size of 4-11 µm is separated by stokes settling (Frechen et al., 1996; Zimmerman, 1971). The sample solution is poured in a test tube, marked with a 2 cm mark. The grains > 11 µm are discarded by taking the suspended portion (above 2 cm) of the test tube after vigorous shaking and keeping for 90 sec. This procedure is repeated throughout the sample. The sample portion < 11 µm is filled in the test tube. Next grains less than 4 µm are discarded by taking the lower 2cm portion of the test after vigorous shaking and keeping for 15 minutes. The desired grain size 4-11 µm is diluted with alcohol to a level that it slightly scatters light. The solutions are poured in test tube kept with Al discs and dried at 45°C, till the solution evaporates and leaves a thin layer of the sample.

For pottery samples, upper 2 mm light exposed surface layer of pottery is removed. The sample is then gently crushed by providing slight pressure such that the original grain size is not altered, before treating with HCl. The prepared sample is studied using following instrumentation.

2.4. Instrumentation

2.4.1. Luminescence measurements: TL/OSL reader

A TL/OSL reader consists of automated setup, which can irradiate and stimulate the thermoluminescence (TL) and optically stimulated luminescence (OSL) and measure the emitted photons. It mainly consists of following functional units to execute specific purposes.

1. Irradiation unit
2. Stimulation unit
3. Detection unit

Risø TL/OSL reader model DA-20 is one such instrument which consists of parts of the above units and designed specially to study luminescence properties of material and geological and archaeological dating. The schematics of the setup are as shown in Figure 2.3 and experimental setup in Figure 2.4.

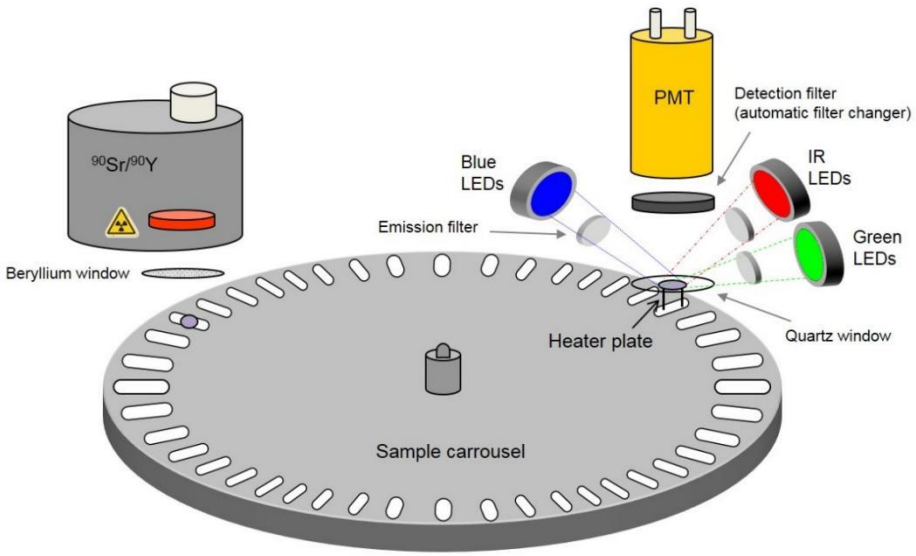

Figure 2-3 The Risø TL/OSL reader schematic diagram. Source: Risø manual.

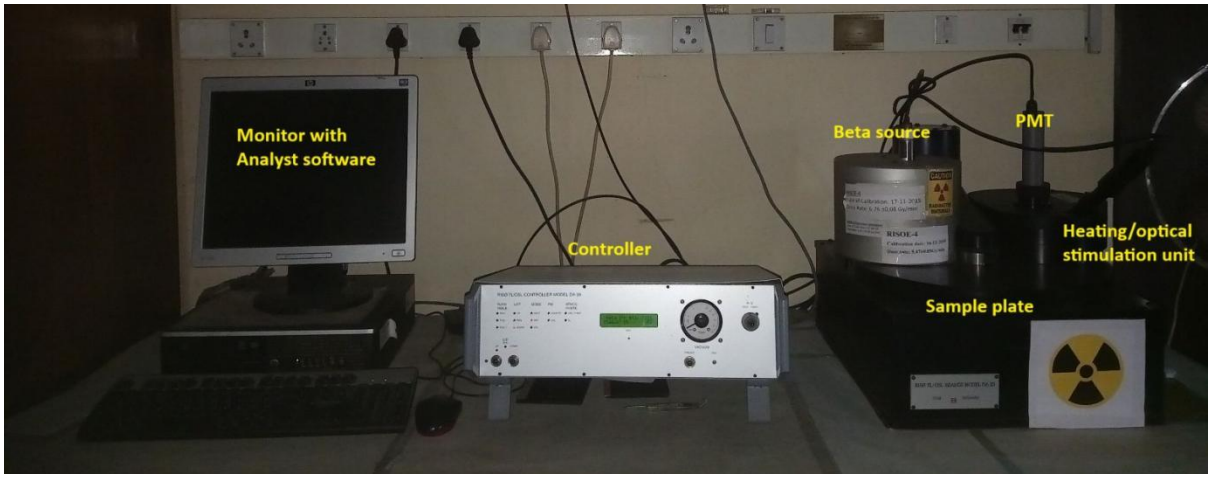

Figure 2-4 Experimental setup of Risø TL/OSL reader.

2.4.1.1. Irradiation unit

The irradiation unit is used to artificially irradiate the samples in laboratory. Three radioactive sources which are generally used are Strontium-90 (^{90}Sr) a beta source, Cobalt-60 (^{60}Co) a gamma source and Americium-241 (^{241}Am) an alpha source.

Beta source ^{90}Sr, has a half-life of 28.8 years. ^{90}Sr decays into ^{90}Y with the emission of beta rays of energy 0.546 MeV, which further decays into ^{90}Zr (stable) with a half-life of 64 hours emitting 2.28MeV beta rays. It is an almost pure beta source with negligible gamma < 0.001MeV having an activity of ~1.48 GBq. Its long lifetime makes it suitable to use for laboratory purpose. The source is shielded with lead from top and sides. The bottom consists of beryllium window which attenuates the 0.546 MeV beta rays but allows 2.28 MeV beta rays to pass through. The salt of ^{90}Sr is placed on a rotating aluminium wheel, so that it faces upwards towards carbon absorber, away from beryllium window, when not in use. Routine TL/OSL readers are equipped with ^{90}Sr beta source, because of its intermediate range (~cm) compared to gamma and alpha, which can be easily shielded, integrated with a compact reader and can irradiate the grains (~200 μm) throughout.

Americium-241(^{241}Am) source has a half-life of 432.2 years. It decays to Neptunium-237 by emitting alpha and gamma. The alpha decay energy is approximately 5.486 MeV. The gamma decay energy is 0.059 MeV. Due to high ionization capabilities and small range of

alpha particles the samples kept at small distances are irradiated in the vacuum to minimize the energy absorption of alpha particles in air.

Cobalt-60 (^{60}Co) is a gamma source with major emissions of 1.17 and 1.33 MeV. It has a half- life of 5.27 years. ^{60}Co 0 undergoes beta decay 99.88% by emitting beta particles with an endpoint energy of 0.31 MeV, which further undergo gamma decay to Nickel-60 (stable) by emitting 1.17 and 1.33 MeV gamma. Alternatively, Cobalt 60 decays to Nickel 60 by first emitting 1.48 MeV beta particles followed by 1.33 MeV gamma with a probability of 0.12 %. For present thesis, Cobalt 60 source at Indira Gandhi Centre of Atomic Research, Kalpakkam, India is used for bulk irradiation of the samples.

2.4.1.2. Stimulation unit

The stimulation unit is provides external energy to the phosphor to excite trapped electrons /holes resulting in emission of luminescence when they combine at recombination centers. Standard automated TL/OSL readers are equipped with two kind of stimulations viz. thermal and optical.

The heating unit consists of a strip of low mass, high resistivity kanthal (an alloy of iron, chromium and aluminium). The temperature is measured with K-type (Cromel- Alumel) thermocouple using Seebeck effect. The heating rate is digitally controlled and can be set at any value from 0.1°*C* to 10°*C*. In Risoe TL/OSL reader used for the studies, the sample can be heated up to 700 °*C* at mentioned variable rates. During the analysis, the sample containing chamber is evacuated and is filled with nitrogen gas for high temperatures (>200°C) to protect the disc and heating plate from oxidation and provide convective heating to the sample.

The optical stimulation unit consists of blue, green, infrared LEDs and violet laser with the specifications given in Table 2.1 for sample stimulation. Various filters are used in front the LED's and lasers to ensure stimulation of samples with narrowly defined wavelength band. The power of the light sources can be varied with time and ramped to measure Linearly modulated OSL (LM-OSL).

Table 2-1: Specifications of the optically stimulating system used.(Source: Risø manual)

Source	Wavelength(nm)	Power density/ Power
Blue LED	470±20	~80(mW/cm^2)
Infrared LED	850±33	~300 (mW/cm^2)
Green LED	525±40	~30(mW/cm^2)
Violet laser	402±2	~100 mW

2.4.1.3. Detection unit

It consists of two main part a) Detector and b) Detection filters

Detector: Detection of luminescence primarily involves measurement of low photons counts ranging from ~ 100 to 10^5 photon counts per second. Thus, a detector which can convert extremely weak output and amplify it without adding large amount of noise is required. A photomultiplier tube (PMT) just suits the application as it covers this vast dynamic range with sufficient amplified signal and low noise incorporation. PMT has a photocathode with low or negative ionization potential and emits, electrons after absorbing luminescence photons. The electrons are accelerated and multiplied by various dynodes. PMT are used because of their high amplification power and very less dead time ($30\mu m$). The PMT used in Riso TL/OSL reader is EMI 9235QB as it has good quantum efficiency (Figure 2.5) for the detection range 160-630 nm which is of interest for luminescence measurements. This PMT has a bialkali photocathode enabling high efficiency in blue region and very less thermionic emission. It can be operated from -30 to 60 °*C*. The dark noise is <50 cps. It has a high dynamic range with a count rate of 20 Mcps. Besides this, some modern systems use other type of detectors such as EMCCD, Imaging photon detectors and other solid state detectors.

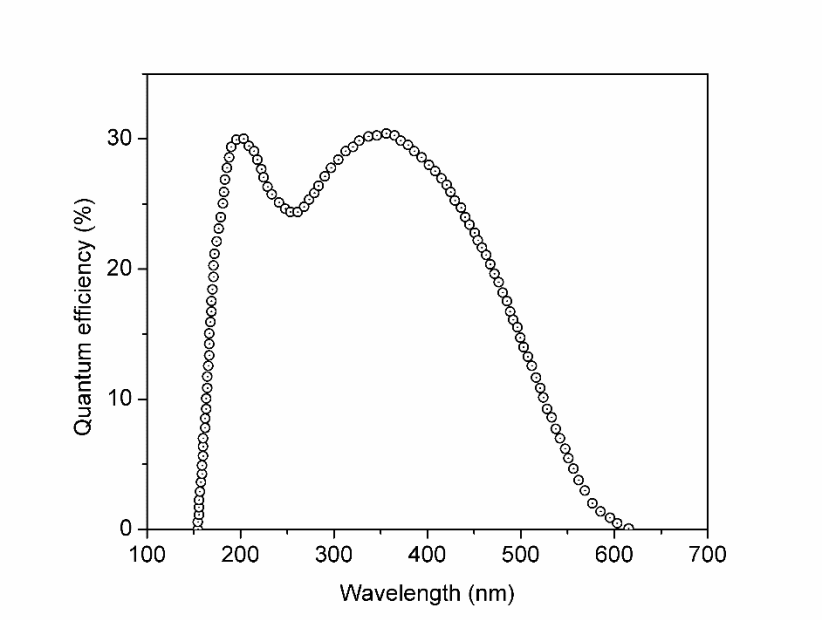

Figure 2-5 Quantum efficiency of bi-alkali PMT EMI 9235QB used in the study. (Data obtained from official website of the ET-Enterprises;https://et-enterprises.com/images/data_sheets/9235B.pdf).

Detection filters: Since the stimulating sources (LED's and lasers) have a photon intensity of 10^{18} photons, while the luminescence emission have maximum 10^{5}order of photons it is essential to prevent stimulation light from reaching detector and is normally achieved by means of a set of detection filters. The filters allow only a specific band of wavelength to pass through them. A proper choice of detection filters and stimulation light is made to prevent damage of system. For multi-spectral luminescence studies, an EMCCD-based high-sensitivity spectrometer is often required. However, due to the high cost and unavailability of the required instrument, measurements for present studies were done using variable transmission interference filters as done by many previous studies (Caicedo et al., 2021; Monti et al., 2019; N. A. Spooner and Questiaux, 2000). Optical filters used for present study are listed in Table 2.2 and their spectral transmissions are shown in Figure 2.6. These are colored glass with high transitivity for specific wavelength band. These filters are used in combination with BG39 filter (output from 325 - 700 nm) to reduce IR blackbody background. In addition, suitable neutral density (ND) filters are also used wherever the counts are significantly high and can lead PMT to non-linear region.

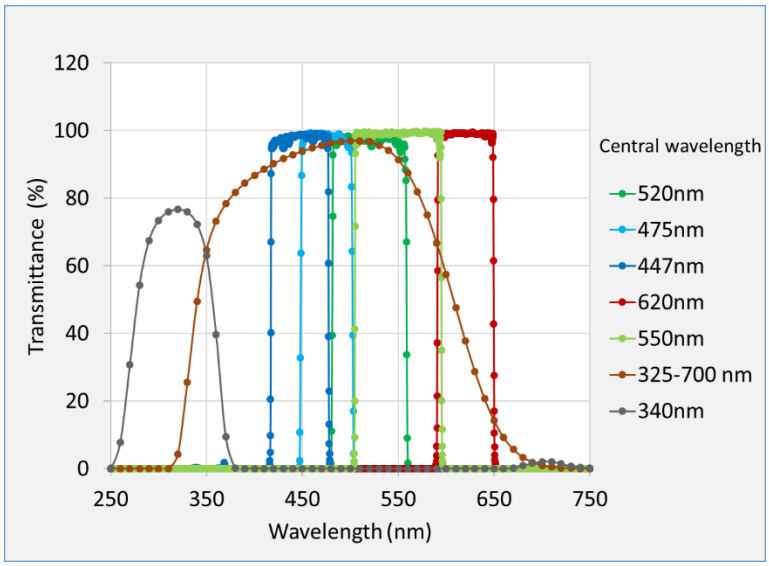

Figure 2-6 The intensity transmittance of various optical band pass filters used in the study. (Data obtained from official website of the filter supplying companies, i.e., www.schott.com, https://hoyafilter.com/, www.edmundoptics.in)

2.4.2. Alpha, beta, gamma counting

Alpha, beta and gamma counting is used to measure the activity (disintegration/sec) or concentration of the radionuclides present in the samples that create electron hole pairs in the crystal. Majorly two methods are used to measure the activity/concentration, these are coincidence counting and comparison of peaks counts. On these principles many instruments are manufactured. Additionally, mass spectrometers and XRF are also used to measure the concentration of radionuclides. Here, the instruments used in this thesis work are discussed below and are shown in Figure 2.7.

Table 2-2 Specification of different optical filters used in the study.

Filter Name	Central wavelength (nm)	Bandwidth (nm)
UV_{340}	340	100
$Blue_{447}$	447	60
$Blue_{475}$	475	50
$Green_{520}$	520	70
$Yellow_{550}$	550	100
Red_{620}	620	60

2.4.2.1. NaI (Tl) Scintillation counter

In scintillation counting a sodium iodide crystal doped with thallium is used to convert the gamma rays from the radionuclide to visible photons which are further counted by the photomultiplier tube. The pulses are counted and based on their energy are categorised into channels of different energy using a multi-channel analyser. Thus, an intensity versus energy graph can be obtained. Gamma rays interact with the crystal by compton effect, photoelectric and pair production. The photoelectric peaks are used for analysis as they are the well distinguished for each radioisotope. For potassium a peak at 1.48MeV is observed. The concentration is estimated by comparison of the sample's potassium peak against a known concentration standard. For the analysis an AR grade KCl standard with a ^{40}K activity of 52.5% is used. The Compton counts and background subtracted peaks are compared.

2.4.2.2. Thick source alpha counting (TSAC)

Thick source alpha counting measures the concentration of U and Th radionuclides based on the alpha particles emitted by them. Finely grinded sample (<10 μm) is spread on a zinc sulphide (ZnS:Ag) screen of 42 mm diameter. The thickness of the sample layer is kept greater

than the range of alpha particles (> 25 μm for density 2.6 g/cc). Hence about 1g of the sample is used. The alpha emitted from the U and Th series are converted into photons using the ZnS screen which fall on the photo-multiplier tube to produce a signal. Further the coincidence counting is used to distinguish the counts from uranium and thorium. In the uranium series, ^{219}Rn undergoes alpha decay to ^{215}Po which further undergoes alpha decay. The half-life of ^{215}Po is 0.002 sec. Hence any two alpha counts found within ~0.002 sec interval are counted as to be from uranium. Such a pair is called fast pair. Similarly, in the thorium series, ^{220}Rn undergoes alpha decay to ^{216}Po, which further undergoes alpha decay. The half-life of ^{216}Po is 0.145 sec. Hence any two alpha counts found within ~0.145 sec interval are counted as to be from thorium. Such a pair is called slow pair. Further the count rate can be converted into concentration and the calculations are given in (Aitken, 1985).

Figure 2-7 Various dose rate estimation instruments. Scintillation counter (left), Thick source alpha counter (middle) and μ-dose (right).

2.4.2.3. μ-dose

μ-dose is a compact instrument which can estimate the activity/concentration of U, Th, K by beta and alpha counting. It has a dual scintillation screen consisting of ZnS:Ag coated on plastic scintillator. When alpha or beta strike the dual scintillator, they produce photons which further falls on photomultiplier tube to produce a pulse. The pulse shape and height are noted. Alpha produces more narrow pulses than beta rays. With a pulse shape analyser, the system measures the amplitude of the pulse, shape of pulse and the time of arrival of the pulse. Just like thick source alpha counting the, ^{214}Bi/^{214}Po (half-life of 299 ns), ^{220}Rn/^{216}Po, ^{212}Bi/^{212}Po (half-life of 164 μs) and ^{219}Rn/^{215}Po pairs are counted here (Kolb et al., 2022; Tudyka et al., 2018). In addition to the pairs counted in TSAC, here two additional ß/α pairs are counted. The net count rate of four pairs along with the net count rate of alpha and beta can be used to estimate the U, Th and K activity/concentration.

2.4.3. Fourier transformed infrared spectrometer

Fourier transformed infrared (FTIR) spectrometer is an instrument used to measure the infrared absorption of the samples. The vibrational and rotational transitions of the samples have energy in the infrared and can absorb or emit infrared which can be used to characterise the samples as the transition wavelengths are unique and fingerprints of the material. The incident infrared beam contains a range of wavelength, which interact with the sample and thus processing of the output wavelength is required to get meaningful information. Fourier transformation algorithm is required to separate each wavelength in the output, hence the name Fourier transformed infrared (FTIR) spectrometry. FTIR operates in two modes, transmittance or reflectance. Transmittance mode is used to study the bulk properties of the sample. Attenuated total reflectance (ATR) is used to study surface properties or samples which are around 1 or 2 micrometres thick. The spectral range of 4000–400 cm^{-1} at the spectral resolution of 4 cm^{-1} using a NICOLET 6700 (Thermo Fisher Scientific Instruments, USA) FTIR spectrometer is used in the present work. Figure 2.8 shows the experimental setup of the FTIR spectrometer.

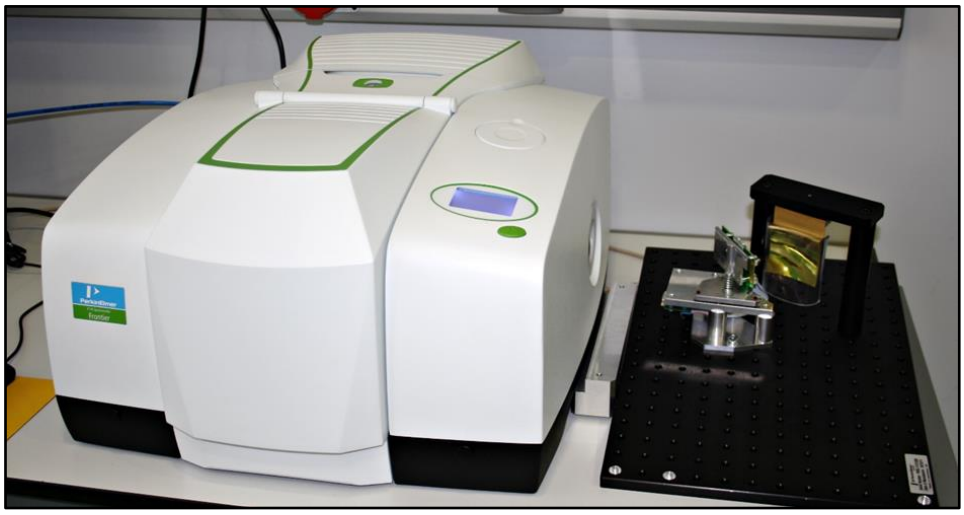

Figure 2-8 Experimental setup for FTIR.

2.4.4. CL-SEM-EDXS

Scanning electron microscopy (SEM) coupled with cathodoluminescence (CL) and electron dispersive X-ray spectroscopy (EDXS) can provide the elemental composition of the samples with a sub-micrometer scale resolution. SEM is an electron microscope in which a narrow electron beam is guided by magnetic field to the sample and the reflected, backscattered electrons are used to generate a high-resolution image of the sample. Further when electrons interact with the samples, characteristics X-ray are released which are detected and analysed

to estimate the elemental composition. For CL imagining, a SEM unit (Hitachi S-3400 N) is utilized at an electron beam (emitted from a Tungsten filament) of 15kV. The Energy Dispersive X ray Spectroscopy (EDXS; Model: Oxford Ultim max 40) is used as shown in Figure 2.9. The sample preparation involves mounting the sample on a thin double-sided carbon tape to adhere the sample grains onto 15 x 4 mm stubs, the sample is carbon-coated using a Hitachi E-1010 Ion Sputter carbon coating unit, operating under a vacuum of 1 Pascal with a current of approximately 14 amperes to prevent charging of the sample while interaction with the electron beam. With CL, we can focus on the bright spots, giving high luminescence sensitivity and can selectively analyze the spectrum there.

Figure 2-9 Experimental setup of SEM-CL-EDXS.

2.5. **Measurements**

2.5.1. **Equivalent dose estimation**

Quartz and feldspar undergo a large sensitivity change during the measurements due to presence of intrinsic defects. The D_e calculation is not so straightforward as in case of artificial materials as direct comparison between the natural and laboratory dose is not possible. Various protocols are proposed to estimate the equivalent dose (D_e). The protocols are either based on additive or regeneration methods. In additive methods, measurements are done on multiple aliquots in which laboratory dose is given in addition to natural dose. Several methods like multiple aliquot additive dose (MAAD), multiple aliquot regeneration (MAR) are formulated (Aitken, 1998, 1985; Singhvi and Mejdahl, 1985; Wintle, 1997). In regeneration methods, the same aliquot is used first to measure the natural luminescence signal, and then incremental regeneration laboratory doses are given to plot the growth curve, from where the equivalent

dose is estimated. This includes methods like single aliquot regeneration (SAR), single aliquot additive dose (SAAD) and single aliquot regeneration added (SARA) (Duller, 1994, 1991; Mejdahl and Bøtter-Jensen, 1997). Usually all the protocol/methods include a preheat followed by OSL measurement. The preheat step is important to eliminate signals from shallow traps, which are not stable in geological time scale of the event being studied. The time, temperature of OSL measurement is also optimized for the measurement. In the additive measurements protocol MAAD is most commonly used. In regeneration protocols the most commonly used is SAR. Both types of protocols have their benefits and utility. These protocols are discussed below:

Multiple Aliquot Additive Dose (MAAD): This protocol is one of the oldest protocol and is today used for the samples where luminescence characteristics are significantly affected by the measurement protocol. In this, multiple aliquots made from a sample are given increasing doses in addition to the natural dose (N+β1), (N+β2), (N+β3), (N+β4), etc. (Aitken, 1985). Signals from different aliquots are compared and are used to plot the dose response curve. Since, there will be variations in the amount of grains that produce the signal from aliquot to aliquot, it is very important to normalize the signal. Normalization is done by many methods available such as weight normalization, short shine method, test dose, zero glow etc. These are discussed in the next section. The normalized signal is then plotted with respect to the additive doses as shown in Figure 2.10. The natural dose is extrapolated from the curve on the "Dose-axis".

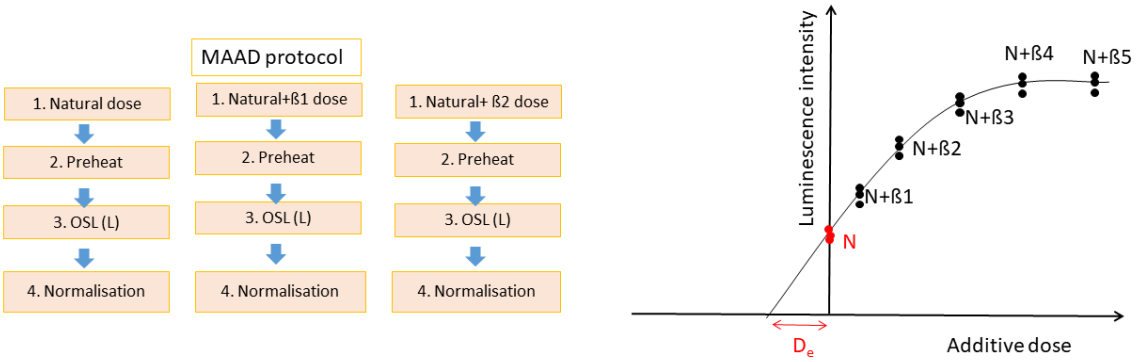

Figure 2-10 MAAD protocol (left), MAAD growth curve (right).

Single Aliquot Regeneration Protocol (SAR): In SAR one equivalent dose is estimated from one aliquot. Thus, measurements from a number of aliquots gives multiple equivalent doses and thus distribution in data can be used to study the bleachability and dose heterogeneity

condition of the depositional environment. It is routinely used protocol for most of the natural samples and is shown in Figure 2.11. It corrects the sensitivity changes during the measurement via response to a test dose (Murray and Wintle, 2000a; Wintle and Murray, 2006). The changes in the luminescence sensitivity proportional to the main signal are observed in the test dose signal measured just after the actual signal measurement. Thus, the ratio of the two signals will cancel out the proportional sensitivity variation and the signal is called sensitivity corrected signal (L/T). The sensitivity corrected signal is first measured on the natural sample followed by measurement on incremental beta doses given in lab. The regeneration dose signal normalized test dose signals are used to plot dose response curves and the equivalent dose is estimated by interpolating signals on these growth curves (Figure 2.11).

The protocol consists of several checks to evaluate the reliability of estimated doses. These include the recuperation, recycling ratio and preheat and dose recovery test.

Recuperation: Recuperation may arise due to the thermal or optical excitation of charge from deeper, light-insensitive traps to light-sensitive traps, which are not completely bleached. Recuperation is estimated by investigating the signal without giving any laboratory dose. Recuperation less than 5% of the natural signal is acceptable (Wintle and Murray, 2006).

Recycling ratio: In this test a measurement is repeated by irradiating the sample by giving one of the previous dose. The ratio of signal from both the measurements if less than 10% is acceptable.

Dose Recovery: In this test, a known laboratory dose is recovered using the protocol. The protocol is then used to calculate the dose. This test is the ultimate reliability test for a protocol.

Additionally, to find the suitable preheat temperature, preheat plateau test is conducted. The preheat temperature is specific to the mineral. It is estimated experimentally by performing plateau test (Wintle and Murray, 2006). In the plateau test, the variation of preheat temperature is studied with the D_e. The plateau region in the graph signifies that the D_e is independent of the variation in this preheat temperature range and can be chosen for the analysis.

As each signal has different stability and coming from different traps so stimulation parameters and protocols are optimized for particular signal. Based on the type of signal various protocols are proposed. Table 2.3 provides two basic protocol for quartz and feldspar.

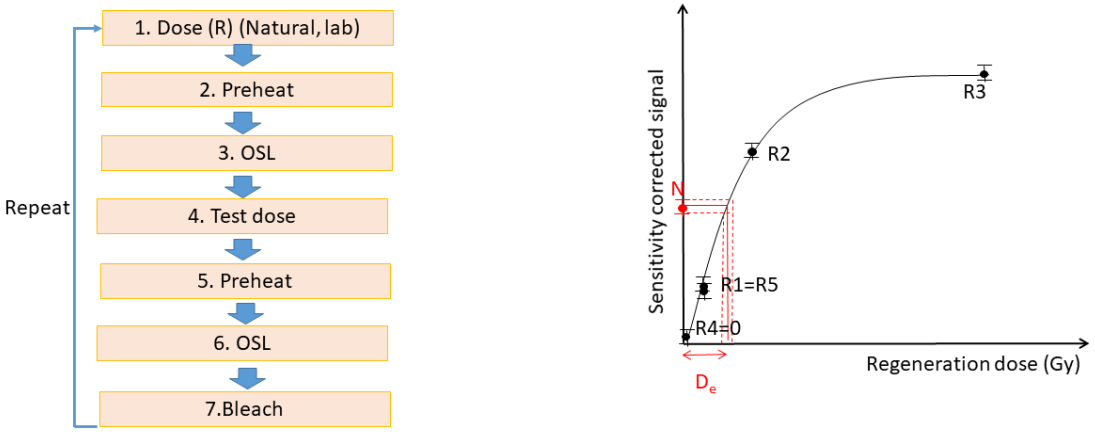

Figure 2-11 SAR protocol (left), SAR growth curve (right).

Table 2-3 BSL-SAR and IRSL-SAR protocol for quartz and feldspar.

	For Quartz	For Feldspar	
Step. No.	**BSL**$_{UV}$ (Murray and Wintle, 2000a)	**IR50**$_{blue}$ (Wallinga et al., 2000)	**Remarks**
1	Natural dose/ Regeneration dose	Natural/ Regeneration dose	
2	Preheat (200-260) °C for 10 s	Preheat 250 °C for 60 s	
3	BSL at 125°C for 40 s	IRSL at 50°C for 100 s	Lx
4	Test dose	Test dose	
5	Preheat (200-260) °C for 10 s	Preheat 250 °C for 60 s	
6	BSL at 125°C for 40 s	IRSL at 50°C for 100 s	Tx
7	BSL at 200°C for 100 s		
8	Go to step 1	Go to step 1	
Emission under investigation (nm)	300-380	400-480	

2.5.2. Normalization Methods

For making inter-aliquot comparison or for making multiple measurements on the same aliquot, normalization of the signals is required. Several methods are used till date and are discussed below.

Mass/weight normalization: In this method multiple aliquots are compared by dividing the signal of interest with the weight of the sample on the aliquot (Aitken, 1985). It has been seen that only a minor percentage of grains in the aliquot give significant luminescence signal, these

are called the bright grains. This method assumes that the bright grains are homogenously distributed in the sample. It does not include any other sensitivity changes that are due to sensitivity changes of other signal used in normalization. In some cases, it has been observed that mass/weight normalization leads to large scatter such that it becomes impossible to make correlation between the data (Jain et al., 2003).

Zero glow normalization: Normalization in which any signal used for normalization is measured before the main signal is called the zero glow normalization. In general, low temperature peak (110°C in quartz) which is thermally unstable in geological time scale is used for zero glow normalization (Aitken et al., 1979). A small test dose is given in this method and counts of the zero glow peak are measured, followed by the measurement of the main signal. Next the counts of the main signal are divided by the counts 110°C peak counts.

Second glow normalization: In this method the signal used for normalization (OSL/TL) is measured after the main signal measurement. A small test dose is given and consequently the signal is measured. This normalization is widely used in SAR protocol (Murray and Wintle, 2000a).

Short shine normalization: In this method, OSL response is measured from the sample for a very small interval of time (0.1 sec), compared to the main measurement. Negligible amount of signal is depleted from such a measurement (~0.5%) (Roberts et al., 1994), however the sensitivity can be recorded which can be used for normalization.

2.5.3. Thermal and Athermal Fading

The dose estimates are further limited by the thermal and athermal fading. In dose estimation, one needs to probe the traps that have negligible thermal fading over the geological period of interest. Further estimation and correction of athermal fading is required if it is observed. These two fading's are explained below:

Thermal fading: At any ambient temperature above zero kelvin, electrons have some probability of escaping the trap over a period of time from their trapping sites. This results in thermal fading of the signal which can be explained by the mean lifetime of the electrons in the trap given by the equation 1.2 of chapter 1, given as

$$\tau = s^{-1} e^{\frac{E}{kT}} \qquad (2.1)$$

It can be seen from equation 2.1, that traps with higher activation energy or lower frequency f actor will have higher lifetime. Thus, there is a definite nonzero probability of escape of charg es from traps at temperature above absolute zero. Many experimental methods are proposed a

nd used widely to estimate the lifetime of the traps and to identify the geologically stable trap s such as

1. Initial rise method (Randall and Wilkins, 1945)
2. Isothermal decay method (Bailey, 1999)
3. Fractional glow curve analysis method (Gobrecht and Hofmann, 1966)
4. Variable heating rate method (Bohun and Öas, 1954; Chen et al., 2022)
5. Deconvolution of glow curves (Dosimetry, 1996; Peng et al., 2015)

Athermal fading: The escape of electrons from the traps, even at zero kelvin is called atherm al fading. It was discovered by Wintle, (1973) in feldpsar. It is because of quantum mechanica l tunnelling of electrons. Initially, the cause of such a fading was not understood and hence it was also termed as "anomalous fading". As feldspar suffers from anomalous fading, a correct ion for fading has to be made. Quartz does not show athermal fading, except for volcanic quar tz (Tsukamoto et al., 2007). The extent of athermal fading at any temperature can be measure d by estimating the g value (%/decade). g-value can be estimated by giving radiation dose to t he sample and holding the sample for various time delay before measurement. As athermal fa ding is dose dependent, the measurements of g-value should be done near to its equivalent do se. Methods used for correcting the athermal fading.

1. Huntley, (2006)- when the equivalent dose is in the linear region of DRC,
2. Kars et al., (2008) -when the equivalent dose is in the linear or non-linear region of DRC.

2.5.4. Data Analysis and Statistics

Since the SAR protocol estimates dose on a single aliquot, measurement on multiple aliquots provides a distribution of the equivalent dose. The data is then used to obtain various information about the site and is modelled to get the true representation of equivalent dose. There may exist various reasons for the scatter in the data. Such as

1. Inherent statistical nature of dose absorption (Knoll, 2000)
2. Poor bleachability (Roberts et al., 1999)
3. Beta heterogeneity (Mayya et al., 2006)
4. Pedoturbation (Bateman et al., 2003) etc.

Plots like histogram, radial plot are used to view the spread in the data as shown in Figure 2.12. Such a visualization is helpful in deciding the model to be used. For example for the data corresponding to Figure. 2.12(a,c), central age and common age models can be applied whereas for Figure. 2.12(b,d), the distribution suggests that the majority of data is from the lower dose range and hence minimum age can be taken.

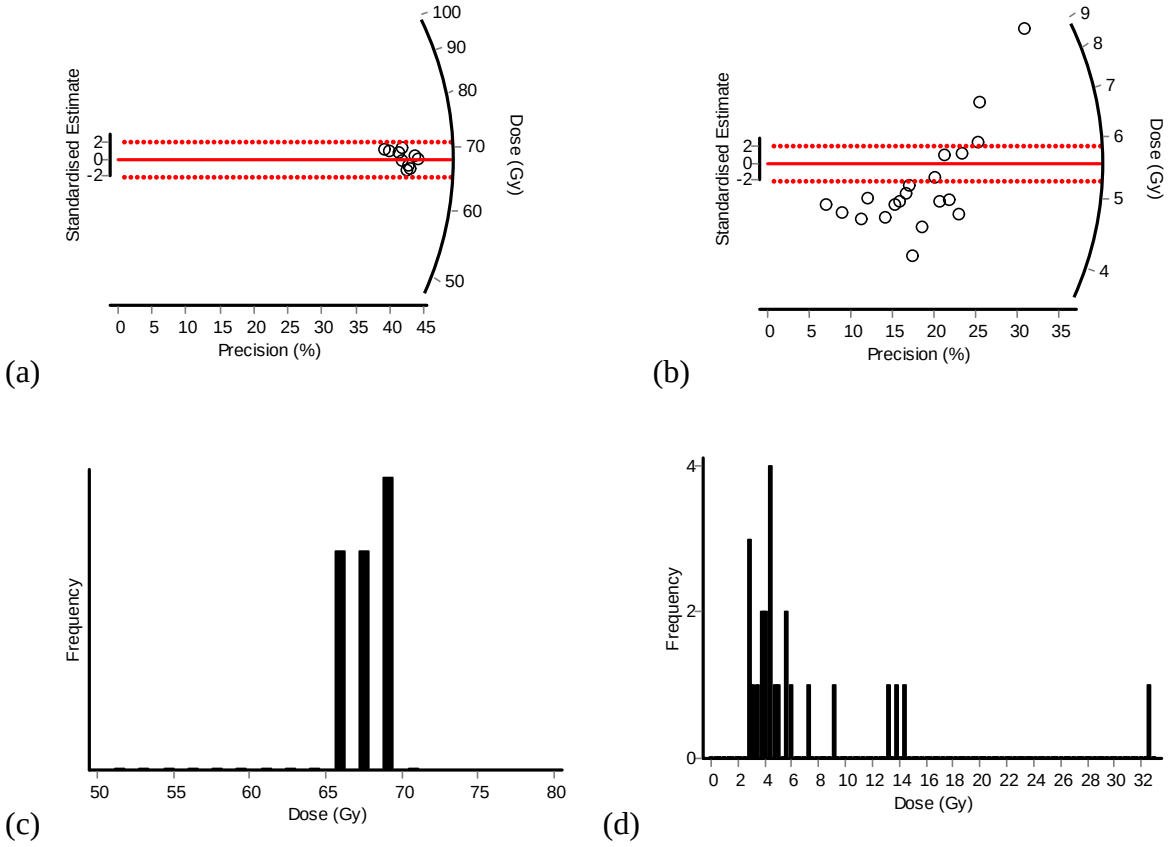

Figure 2-12 Radial plots and histogram for BSL-SAR of two samples with different depositional environment (a, c) less scattered data, (b, d) more scattered data.

Further there are criteria's that help in deciding the model to be used such as

1. Bailey and Arnold, (2006) – based on the skewness, kurtosis and overdispersion of the equivalent doses.
2. Chauhan and Singhvi, (2011)- based on the ratio of minimum to maximum beta dose due to K-40.

Based on this suitable model is chosen such as

1. Common age model (Galbraith et al., 1999)
2. Central age model (Galbraith et al., 1999)
3. Minimum age model (Galbraith et al., 1999)
4. Leading edge model (Lepper and WS McKeever, 2002)
5. Finite mixture model (Galbraith, 1990)
6. Bayesian model (Li et al., 2022)

2.5.5. **Dose rate**

Dose rate is contributed by the radiation environment. The radionuclides present in the sediment matrix and the cosmic ray contribute to the dose received by the sample. Various other factors are to be considered for the annual dose rate calculation of the samples. The water present in the sediment matrix and the alpha efficiency needs to be included. Including all the factors the dose rate is given as:

$$\dot{D} = a\,\dot{D}_{\alpha} + \dot{D}_{\beta} + \dot{D}_{\gamma} + \dot{D}_{CR} \tag{2.2}$$

where $\dot{D}$ is the total dose rate, a is the alpha efficiency, $\dot{D}_{\alpha}$, $\dot{D}_{\beta}$, $\dot{D}_{\gamma}$ is the alpha beta and gamma dose rate and $\dot{D}_{CR}$ is the cosmic ray dose rate. These factors are discussed below.

Presence of radionuclides: Radionuclides such as U^{235}, U^{238}, Th^{232}, K^{40}, Rb^{87} are present in sediment matrix decay and emit alpha, beta and gamma radiation. The radiation deposit energy in the minerals. The energy deposited in each decay can be calculated summing the energy of all daughter decay in the radioactive chain. This energy can be converted into dose (dose=energy deposited per unit mass). Further, the total dose deposited can then be estimated by measuring the activity/ concentration of radionuclides in the sample. This can be calculated by the techniques described in instrumentation section. The conversion factors are given in many studies (Adamiec and Aitken, 1998; Guérin et al., 2011; Stamoulis et al., 2012).

Cosmic ray contribution: The cosmic ray radiation originating from extra-terrestrial sources also deposits the dose. For terrestrial samples the contribution of the cosmic ray to dose rate is a magnitude order less than that due to radionuclides. This contribution can be calculated by noting the altitude, latitude, longitude and depth of the samples and using the equations given by (Prescott and Hutton, 1994).

$$\dot{D}_0 = 0.21 \exp(-0.070x + 0.0005x^2) \tag{2.3}$$

where x is the depth of the samples below the surface; $\dot{D}_0$ is the dose rate (Gy/ka) for a geomagnetic latitude of 55°. For calculation of dose rate at the site, the geomagnetic latitude can be calculated by geographic latitude θ and geographic longitude φ as follows,

$$sin\lambda = 0.203\ cos\theta \cos(\varphi - 291) + 0.979\ sin\theta \tag{2.4}$$

The conversion factors can be read from the Figure 2.13

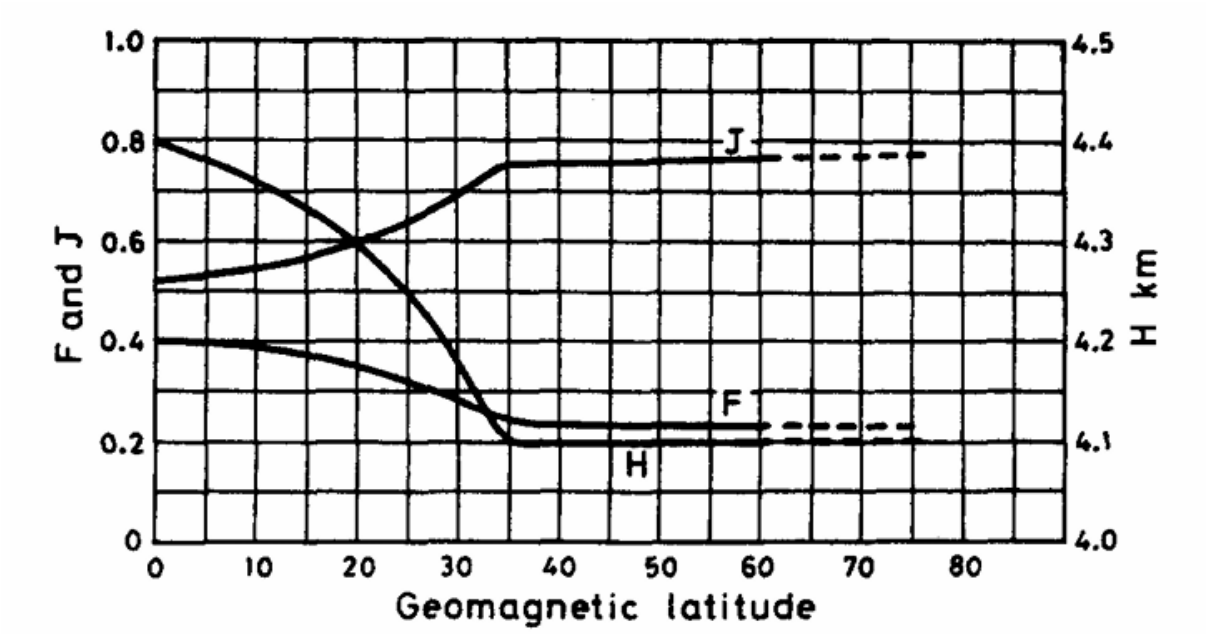

Figure 2-13 Parameters for finding cosmic ray dose rate. Taken from Prescott and Hutton, (1994)

and the cosmic ray dose rate at the sample site can be calculated using the following equation

$$D = \dot{D}0[F + J \exp(h/H)] \quad (2.5)$$

Effect of water content in soil: The water present in the soil also absorbs some proportion of the incoming radiation in the sediment. This leads to overestimation of dose rate received by the sample. A correction for the dose rate is done by estimating the amount of water present in the sample and correcting for it (Aitken, 1985; Murray et al., 2021). The factors W and F are calculated as follows,

$$W = \frac{weight\ of\ water}{dry\ weight\ of\ sample} \quad (2.6)$$

$$F = \frac{average\ water\ content}{saturation\ water\ content} \quad (2.7)$$

These are used to correct the dose rate; the corrections are given as below.

$$\dot{D}_\alpha = \frac{\dot{D}_{\alpha\, dry}}{1+1.5WF} \quad (2.8)$$

$$\dot{D}_\beta = \frac{\dot{D}_{\beta\, dry}}{1+1.25WF} \quad (2.9)$$

$$\dot{D}_\gamma = \frac{\dot{D}_{\gamma\, dry}}{1+1.14WF} \tag{2.10}$$

Alpha Efficiency: Alpha, beta and gamma interact differently with matter. Beta particles interact with orbital electrons via coulomb interactions. They are light particles and thus undergo large deflections inside the material. They homogeneously irradiate the material. Gamma rays and cosmic rays interact via photoelectric effect, compton scattering and pair production and homogeneously irradiate the material. Alpha particles are heavy and are not deflected much inside the material. With a charge of +2 units, the linear energy transfer (LET) is high and number of electron-hole pairs generated is very high in small track length. The material is not homogeneously irradiated with alpha radiation, but only locally, near the emission of alpha. Most charges produced recombine back and rest are stored in traps. Thus, the luminescence efficiency of alpha is less than beta and gamma and this fact is incorporated in the dose rate equation by the factor "a", which is the alpha efficiency of material as given in equation 2.11 and is given as below:

$$a = \frac{D_\beta}{13\ s\ T_\alpha} \tag{2.11}$$

where D_β is the equivalent beta dose, for an alpha irradiation of time T_α (minutes) by a source of strength s.

2.5.6. Age Estimation

The age can be calculated as

$$Age = \frac{Equivalent\ dose\ (D_e)}{Dose\ rate\ (\dot{D})} \tag{2.12}$$

This age can then be related to various processes related to the deposition/formation of the sediments in the strata layer from which the sediments are sampled. The estimated age is used with other proxies like isotopic ratios, provenance studies etc. to study paleoclimate, tectonics or human evolution.

Chapter 3: Natural Minerals for High Radiation Dosimetry

3.1. Introduction

This chapter explores the luminescence characteristics of three natural minerals; quartz, feldspar and jarosite for high radiation doses (HRD) with aim of extending the datable limit of luminescence dating. For terrestrial studies, quartz and feldspar are preferred minerals as they are ubiquitous in nature. There luminescence characteristics are well studied for low doses (< 1 kGy) (Franklin et al., 1995; McKeever, 1984; Medlin, 1963; Visocekas et al., 1994) and equivalent dose estimates up to 250 Gy for quartz and up to 2000 Gy for feldspar are suggested (Murray and Wintle, 2000b; Thiel et al., 2011) till now. For quartz, few thermoluminescence (TL) studies show a linear increase in intensity with dose above 10 kGy (Durrani et al., 1977; Sawakuchi and Okuno, 2004; Schmidt and Woda, 2019). Durrani et al. in 1977 showed that quartz TL increases up to 10 kGy. However, even after ~ 50 years such high dose estimates are not possible, despite enormous amount of studies over the years continued till date to extend the luminescence dating limit (Jain, 2009; Schmidt and Woda, 2019; Stevens et al., 2009). This suggests that there is need to explore the luminescence mechanism in quartz, especially at high radiation doses. Further, not much is known about the luminescence characteristics of feldspar at doses > 1 kGy. In the recent years, researchers are interested in feldspar TL for thermochronolology (Biswas et al., 2020; Brown et al., 2017; Niyonzima et al., 2024). So, a systematic study is done to understand the luminescence characteristics of the sample at high radiation doses and comparing the results against the conventional methods.

Besides this the luminescence potential of new mineral for high radiation dosimetry, which could also contribute for space research program of India was explored. One such mineral is jarosite which is an extra-terrestrial analogue abundant on Mars. Accessibility of Mars by many satellite/ rover mission, stability of temperature condition in comparison to moon, its solid crust unlike Venus and possibility to understand the extinction of life that once existed on Mars makes it very interesting to study. In this regards, considerable efforts are being made to

understand surface processes that would have governed the change, largely through remote sensing methods (Howari et al., 2021; Lancaster and Greeley, 1990; Rangarajan et al., 2018). Till date, the chronological information on surface processes has been based on crater counting, which has a poor resolution and needs calibration (Doran et al., 2004). With the anticipation of sample return and onsite measurements, instrumentation has been developed and modelling efforts are undertaken to evaluate the properties of rocks on Martian surface (Jain et al., 2006; Lepper and McKeever, 2000; Morthekai et al., 2007; 2008, McKeever et al., 2003; Tsukamoto et al., 2011). Abundance of quartz on Mars is negligible (Smith and Bandfield, 2012). Feldspar in Martian surface is of basaltic origin and is prone to athermal fading (loss of signal through quantum mechanical tunnelling (Wintle, 1973)). Morthekai et al., 2008 show that for the basalts the athermal fading cannot be adequately corrected. Presently available methods do not enable a proper corrections (Huntley and Lamothe, Kars Gliganic et al., 2012, Haresh 2020), and to an extent, limits their use as a geochronometer. Jarosite is reported in many locations of Mars, thus can be a preferred mineral for sediment dating on Mars and is yet not explored for its luminescence properties. Thus, in this chapter the luminescence characteristics of this new mineral is studied for high radiation doses for extending the dating limit.

3.2. **Samples**

The samples are used from varying provenances and deposition history in order to capture variability in the luminescence characteristics from different types of samples in high dose regime, given in Table 3-1. Three quartz, samples are chosen from Northern India (Himalayan river sediment sample YS-5), Northwestern India (Aravalli's range quartzite rock (RQ-1) and sediment (SR-23) samples). Two feldspar samples are used from Southeastern India (NaFKVR, a rock feldspar sample from Kaveri basin) and from Southwestern India (BPOT4, a sediment feldspar sample from Bharathpuzha basin). The samples from rock and sediment from same provenance are generally known to have varied characteristics (Sawakuchi et al., 2011). The mineralogy of quartzite rock sample RQ-1 and NaFKVR was confirmed using XRD. The XRD spectrum is shown in Figure 3.1 and 3.2.

Six natrojarosite samples collected from Kachchh, India, for this study. The samples were from different stratigraphic units in sediment successions at Kachchh. Samples 57D2 and 56B2 are from the Guneri member of the Mesozoic Bhuj Formation. Samples 65B2, 66B2 and 67F2 are from the Upper Palaeocene to Lower Eocene Naredi Formation, and sample 68B2 is from the Middle Eocene Harudi Formation. The relevant part of the Mesozoic succession is described by Desai and Saklani (2012), and the Tertiary stratigraphy is documented in Biswas (1992). The host rocks are predominantly shales, with natrojarosite occurring in veins that cut across and are also parallel to the layering. Bhattacharya et al. (2016) established the presence of jarosite in the Matanumadh Formation of Kachchh using X-ray diffraction and FTIR methods, and the mode of occurrence was used by them to present the locality as a mineralogical Martian analogue. The present study includes jarosites from a location near to the Matanumadh Formation given in Table 3-1. For luminescence studies, the samples in powder form (fine grain < 11μm) were treated with 1N HCl for 2 minutes. This increased the luminescence yield possibly due to removal of surface gley. Sample were mounted on stainless steel. A Sr^{90}/Y^{90} beta source, calibrated for fine grain quartz (4-11 μm grains), was used. The dose rate for quartz was 0.33 and 0.056 Gy/s. The corresponding absorbed dose for fine grain jarosite calculated using the stopping power was 0.038 and 0.066 Gy/s respectively.

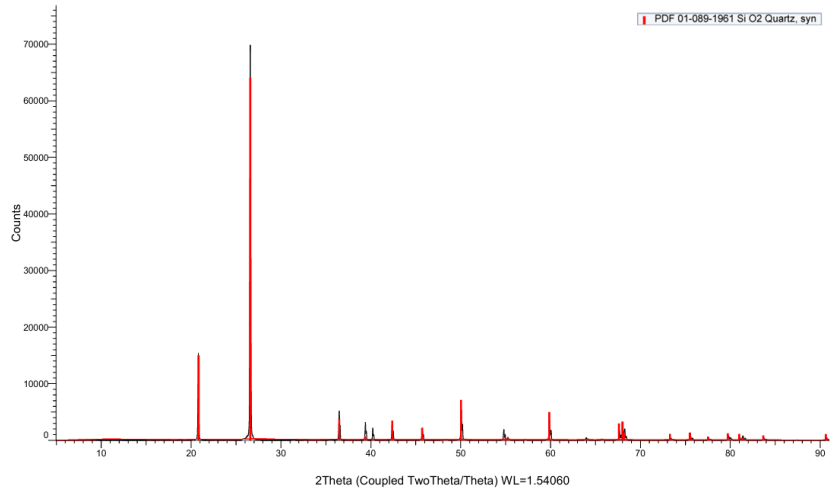

Figure 3-1 XRD spectrum of RQ-1, spectrum confirms that it is a quartz sample.

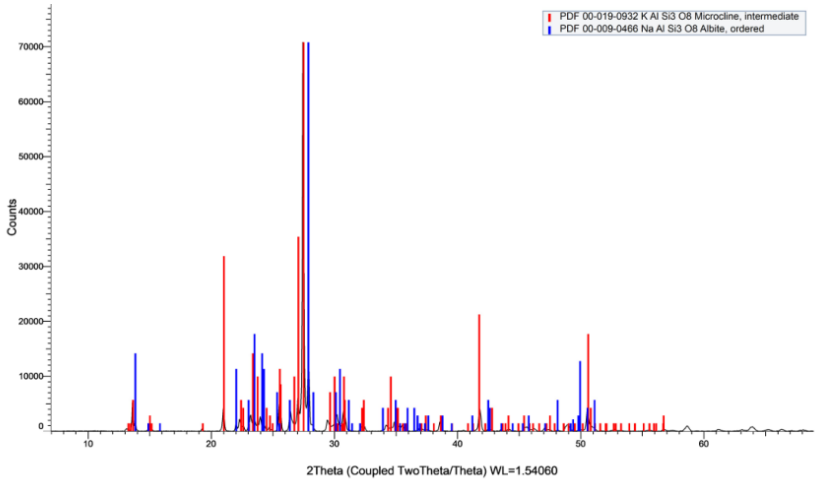

Figure 3-2 XRD spectrum of NaFKVR, spectrum indicates that it is 68% K-feldspar and 32% Na-feldspar.

Table 3-1 Sample details

Sl. No.	Sample Name	Latitude	Longitude	Remarks
Quartz				
1	YS-5	29°45'47.80 "N	77° 8' 29.20"E	Himalayan river sediment, Northern India
2	SR-23	24°29'12.00 "N	73°13' 18.00"E	Sediment sample from Aravalli range, Northwestern India
3	RQ-1	24°29'12.00 "N	73°13'18.00" E	Quartzite rock sample from Aravalli range, Northwestern India
Feldspar				
4	NaFKVR	12° 33' 15.0732" N	76° 28' 57.7092" E	Rock sample from Kaveri basin, Southeastern India 68% K-feldspar, 32% Na-feldspar
5	BPOT4	10°45’59.77 ” N	76°22’10.85” E	Sediment sample from Bharathpuzha basin, Southwestern India
Jarosite				

6	56B2	23º47′07′′ N	68º50′22′′E	Guneri formation, Shale, Sandstone, Laterite
7	57D2	23º47′01′′ N	68º50′22′′E	Guneri formation, Shale, Sandstone, Laterite
8	65B2	23º34′47′′ N	68º38′52′′E	Naredi formation, Shale, Limestone
9	66B2	23º34′43′′ N	68º38′38′′E	Naredi formation, Shale, Limestone
10	67F2	23º34′31′′ N	68º38′36′′E	Naredi formation,Shale, Limestone
11	68B2	23º31′28′′ N	68º41′08′′E	Harudi formation, Shale, Limestone

3.3. Luminescence characteristics of natural minerals for high doses

Initially, luminescence characteristics for HRDs (> 1kGy) were investigated for known natural minerals such as quartz and feldspar. The TL glow curves of all the samples were measured for variable doses in the range 1-21 kGy in spectrum range (325-700 nm) using a BG39 filter. A preheat of 260°C for 10 s was used to remove the contribution from shallow traps, which generally overpowers the signal from higher temperature peaks (>300°C) (N. A. Spooner and Questiaux, 2000). Multiple aliquot additive dose (MAAD) response curves were obtained using mass normalized integrated TL intensity in 340-380°C temperature range. The MAAD protocol ensures the measurement of samples at similar sensitivity. The measurement protocol is provided in Table 3-2. Three aliquots were measured for each dose point. For samples SR-23, YS-5 and NaFKVR, a test dose of 21 Gy was added to measure low-temperature peak 80-100°C TL peak for using it to monitor zero glow sensitivity. The saturation dose was found by fitting a single saturating exponential equation, where I_0 is the saturation intensity and D_0 is the

characteristics dose (Murray and Wintle, 2000). The maximum dose (saturation dose) that can be estimated is $2D_0$ which corresponds to 86% of the maximum intensity is calculated (Wintle and Murray, 2006). The results for quartz and feldspar are discussed below separately.

Table 3-2 Protocol to measure the dose response curve (DRC)

Sl. No.	Operation	Remarks
1.	Dose (1-21kGy)	Laboratory doses for DRC
2.	Preheat 260 ℃ for 10 sec	Removal of shallow traps
3.	Test Dose (21 Gy)	Dose for zero glow normalization
4.	TL 450 ℃ (@ 2℃/s)	Luminescence intensity
5.	Mass normalization	

3.3.1. Quartz

Figure 3.3(a), 3.4(a) and 3.5(a) represent the TL glow curves of the quartz samples (YS-5, RQ-1 and SR-23) for increasing HRDs. The TL peak intensity increases with HRD maintaining the glow curve shapes throughout the temperature range. Insets of Figure 3.3(a) and 3.5(a) show the 110°C zero glow peak response to a dose of 21 Gy, appearing around 90°C in these experiments. Such a shift in the peak has previously been reported (theoretically and experimentally) and is due to changes in heating rate (Pagonis et al., 2006). At a heating rate of 2°C/s, it appears at 90°C, but at 5°C/s, it is at 110°C (Figure 3.6). For the sample YS-5, dose quenching (Bailiff, 1994; Oniya, 2014) in the low-temperature (80-100°C) peak is observed with the increase in the HRD Figure 3.3(a), inset. However, no quenching is observed for the sample SR-23, Figure 3.5(a) inset. Figure 3.3(b), 3.4(b), and 3.5(b) show the DRC for 340-380°C peak. The estimated saturation dose ($2D_0$) is ~18 kGy in the annealed rock quartz sample (RQ-1), and 8.12 ± 1.8 kGy and 11 ± 1 kGy for the sedimentary samples, SR-23 and YS-5 respectively. In the initial part of the DRC of sample RQ-1, supralinearity is observed with an increase in dose. This changed to linear characteristics after 6 kGy, and to sublinearity after 15 kGy. A slight shift in peak maxima is observed in all the glow curves towards higher temperatures with an increase in dose. The extent of peak shift is measured from the TL glow curves by noting the temperature corresponding to maximum intensity in the >300°C temperature region. With increase in dose, the peak maximum shifts towards higher temperature by 35°C from 1 to 15 kGy for sample RQ-1, 25°C from 1 to 12 kGy dose for the sample YS-5, after which signal saturates and no further shift in peak maximum is observed. However, for the sample SR-23, peak temperature first decreases by 10°C from 1 to 3 kGy,

then it increases by 15 °C till 12 kGy. The DRCs measured in visible region using BG39 bandpass filter for HRDs indicate that saturation dose is about 50-100 times higher (~10-18 kGy) (Figure 3.3, 3.4 and 3.5) than conventional methods, which implicates potential to increase the dating limit by two order of magnitude. This result agrees with previous studies (Durrani et al., 1977; Kuhn et al., 2000; Ogundare et al., 2006; Sawakuchi and Okuno, 2004; Schmidt and Woda, 2019; Woda et al., 2002). This suggests that further the TL signals should be investigated for various properties crucial for TL dosimetry and dating, like bleachibility, normalization methods, peak shift and previous dose effect.

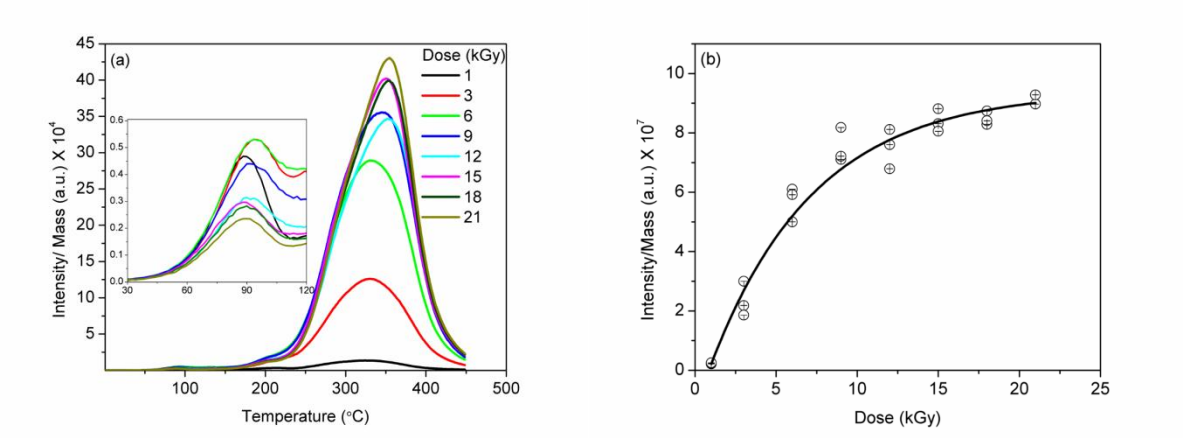

Figure 3-3 a) Thermoluminescence glow curves of sample YS-5 (sedimentary quartz sample) at various high doses in spectral range 325-700 nm. b) Dose response curve of peak from temperature 340-380°C, normalized by the mass. The $2D_0$ value is 11 ± 1 kGy. Each TL glow curve is obtained by pointwise averaging of three aliquots.

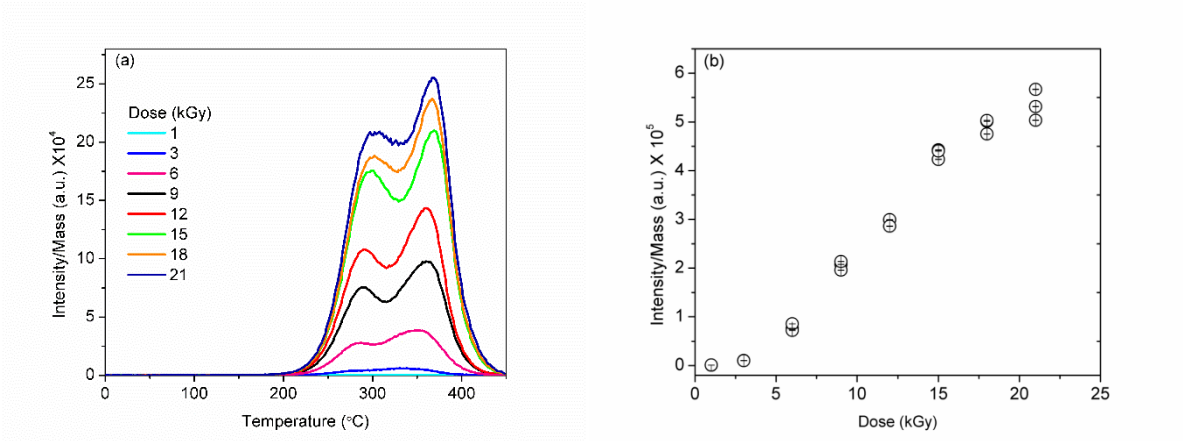

Figure 3-4 (a) Thermoluminescence glow curves of sample RQ-1 (rock quartz sample) at various high doses in spectral range 325-700 nm. b) Dose response curve of peak from temperature 340-380°C, normalized by the mass. Each TL glow curve for a given dose is obtained by pointwise averaging of three aliquots.

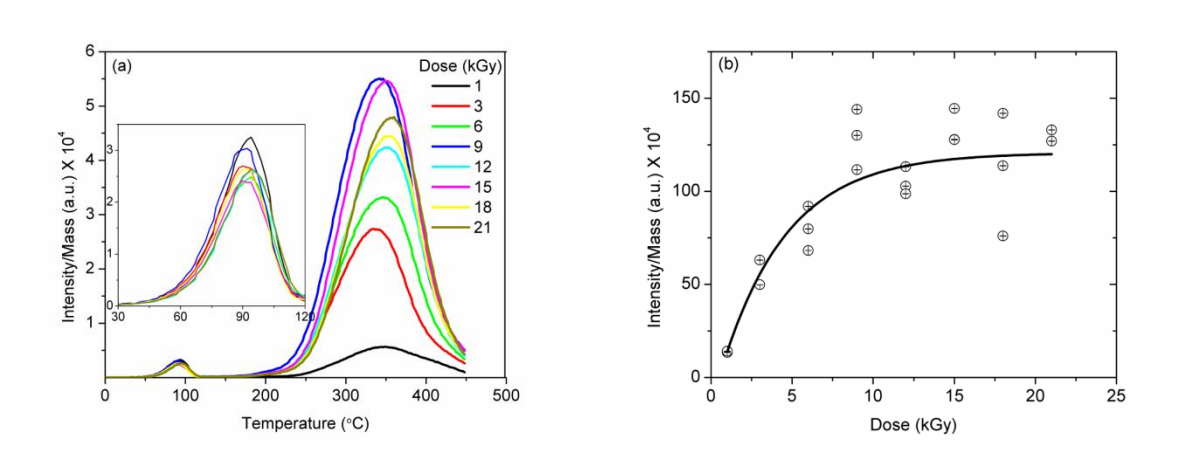

Figure 3-5 a) Thermoluminescence glow curves of sample SR-23 (sedimentary quartz sample) at various high doses in spectral range 325-700 nm. b) Dose response curve of peak from temperature 340-380°C, normalized by the mass. The $2D_0$ value is 8.12 ± 1.8 kGy. Each TL glow curve is obtained by pointwise averaging of three aliquots.

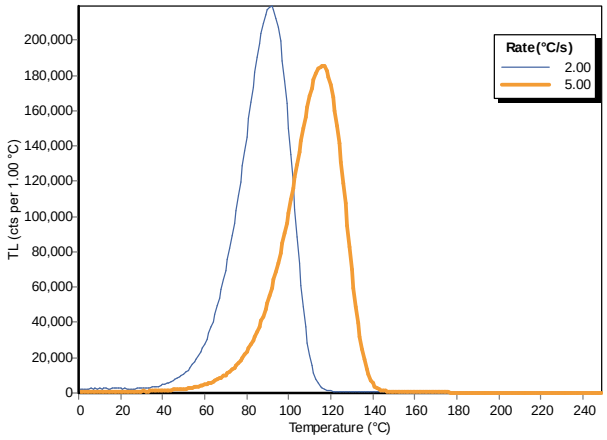

Figure 3-6 Shifting of 110°C peak of YS-5 quartz sample with change in heating rate.

3.3.2. Feldspar

Figure 3.7(a) and 3.8(a), shows the TL glow curves of feldspar samples. The graph shows that even at high doses the shapes of the glow curves are maintained. Figure 3.7 (b) and 3.8 (b) shows the dose response curve of the counts integrated from temperature 340-380°C and mass normalized. The $2D_0$ values for NaFKVR and BPOT4 are 1.56± 1.59 and 6.3 ±0.9 kGy. These values are very less than the quartz $2D_0$. Further the saturation values are near to the feldspar saturation observed in pIRIR protocols (Thiel et al., 2011) and hence feldspar samples were not analysed further in the thesis, as quartz showed much more promising results in comparison to feldspar.

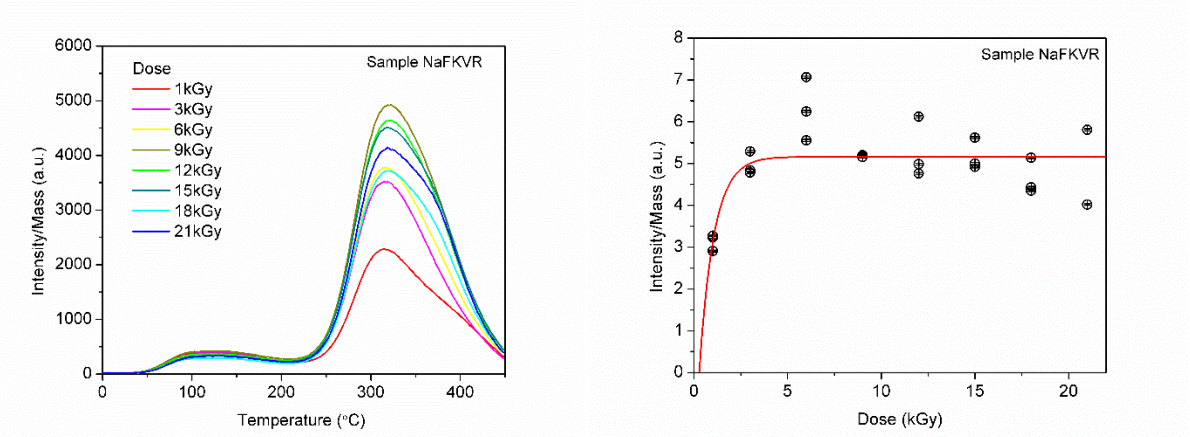

Figure 3-7 a) Thermoluminescence glow curves of sample NaFKVR (rock feldspar sample) at various high doses in spectral range 325-700 nm. b) Dose response curve of peak from temperature 340-380°C, normalized by the mass. The $2D_0$ value is 1.56± 1.59 kGy. Each TL glow curve is obtained by pointwise averaging of three aliquots.

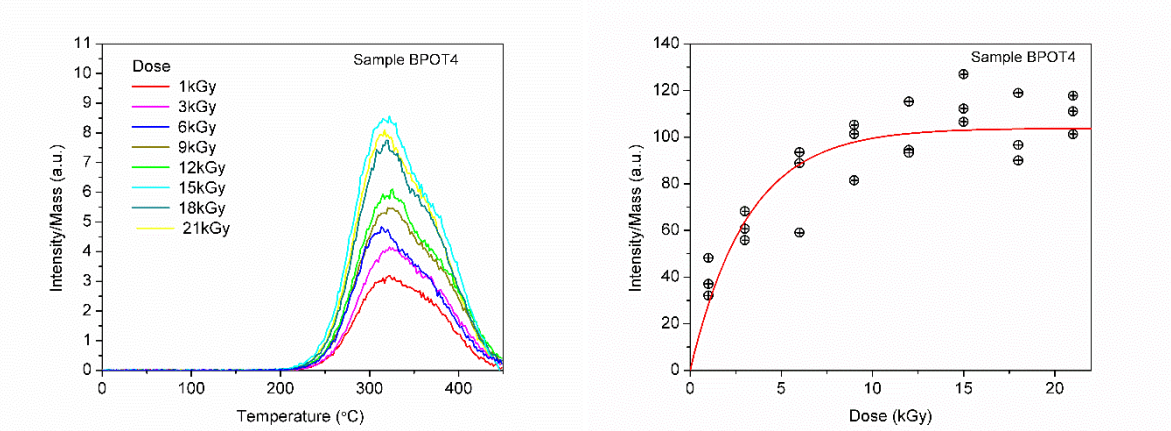

Figure 3-8 a) Thermoluminescence glow curves of sample BPOT4 (sedimentary feldspar sample) at various high doses in spectral range 325-700 nm. b) Dose response curve of peak from temperature 340-380°C, normalized by the mass. The $2D_0$ value is 6.3 ±0.9 kGy. Each TL glow curve is obtained by pointwise averaging of three aliquots.

3.3.3. **Jarosite**

The natural TL glow curves were recorded from room temperature to up to 450°C at a heating rate of 2°C/s without giving any laboratory dose. Figure 3.9 (a), shows the mass normalized TL glow curve of natural and irradiated jarosite. Natural jarosite comprises a broad glow peak from 200°C up to 450°C. Further on the same aliquots a beta dose of 19 Gy was given and TL glow curve is recorded. Figure 3.9(b) shows the glow curve, additional glow peaks at 100, 150°C is observed. Combining both the observations, the glow peaks present are 100, 150, 300 and 350°C. Given that jarosite shows TL characteristics, but since it decomposes on heating

above 300°C, it is important to understand the change in mineralogy with heating, hence petrology studies were carried out.

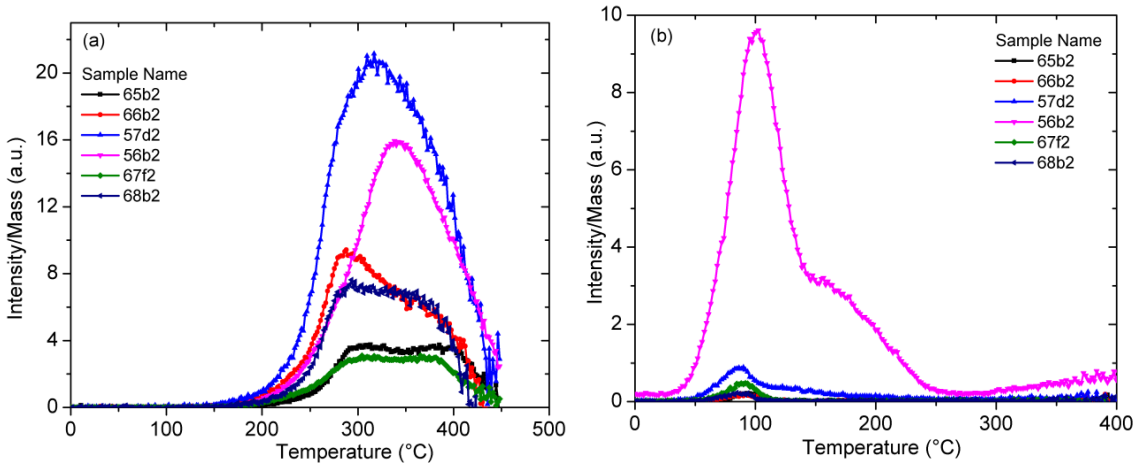

Figure 3-9 TL Glow Curves of jarosite samples in emission range 325-700 nm; a) Natural grains with HCl wash. (b) beta irradiated (19Gy) grain after a preheat of 450°C and given a dose of 19 Gy (taken from (Singhal et al., 2025a))

3.4. Jarosite: Petrology studies

Jarosite samples were annealed to 450°C in a muffle furnace in quartz test tubes. The samples cooled inside the furnace, which took about ~6hrs. The annealed and non-annealed samples were characterized using Cathodoluminescence- Energy Dispersive X-ray Spectroscopy (CL-EDXS) and Fourier Transfer Infrared Spectroscopy (FTIR). Key issues examined is the effect of heating on luminescence.

3.4.1. CL-EDXS studies

The samples are mounted on 15 x 4 mm stubs, after applying a thin double-sided tape to adhere. The sample was carbon-coated using a Hitachi E-1010 Ion Sputter carbon coating unit, operating under a vacuum of 1 Pascal with a current of ~14 amperes. CL imagining was performed using Hitachi S-3400 N at CSIR-National Geophysical Research Institute, Hyderabad at an electron beam (emitted from a Tungsten filament) of 15kV, and luminous portions were detected. The EDXS; (Model: Oxford Ultim max 40) was performed on the luminous spots to obtain the EDXS spectra for both natural and annealed samples.

The comparison of EDXS spectra for natural and annealed samples (Figure 3.10) indicated that in most samples, annealing leads to a relative decrease in oxygen and aluminium, and an increase in potassium and sulphur concentrations. The iron content for sample 66B2, 57D2

remained unchanged, after annealing and decreased for 65B2 and 68B2. The calcium concentration in 65B2 and 68B2 on annealing increased from 6.6% to 25.5% and 1.6% to 8.2% respectively. These variations indicate that annealing did alter elemental distribution to a limited extent, suggesting changes in crystal structure or elemental diffusion and were sample dependent.

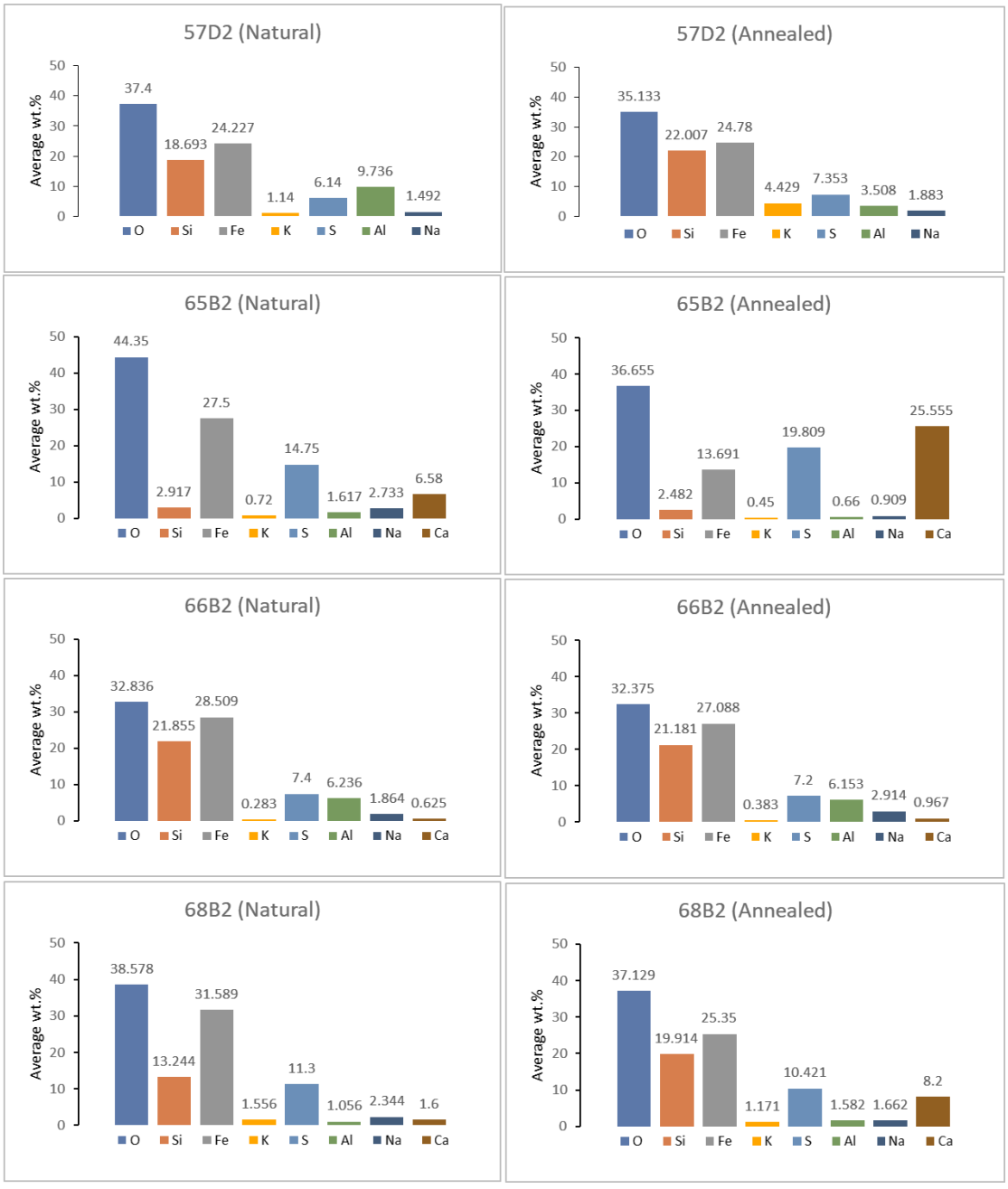

Figure 3-10 Elemental composition of phases luminescing under CL. natural and annealed jarosite samples. Annealing was at 450°C.

3.4.1. **FTIR studies**

For FTIR, finely powdered samples were pressed into pellets after mixing them with dehydrated KBr powder in weight ratio of 1:300. FTIR spectra of the powder samples were collected in a transmittance mode and both, the samples as received and their fractions annealed to 450°C were measured.

The mid-infrared spectra of samples 57D2 and 57D2 Annealed and 66B2 Annealed were typical of jarosite, Figure 3.11 (Bhattacharya et al., 2016c; Bishop and Murad, 2005; Cloutis et al., 2006; Farmer, 1974; Sarkar et al., 2022). Spectra of 57D2 and 66B2 were nearly identical. The difference between the spectra of the annealed and non-annealed samples is that the non-annealed sample spectrum shows a higher overall absorbance, indicating larger proportion of crystalline jarosite. The spectral absorptions attributed to jarosite used in this study are listed in Table 3-3.

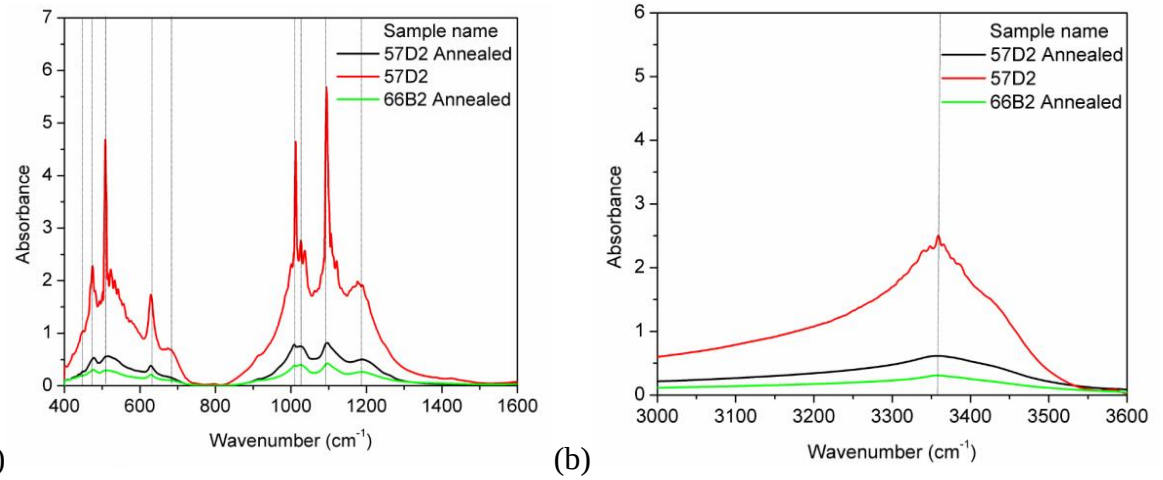

Figure 3-11 Mid-infrared spectra of jarosite samples 57D2, 57D2 Annealed and 66B2 Annealed from (a) 400-1600 cm^{-1} to study the fundamental absorptions and (b) from 3000-3600 cm^{-1} to study the absorptions due to the hydroxyl ion. These show that jarosite signatures are preserved after annealing to 450°C. The marked lines are discussed in Table 3-3.

Table 3-3 FTIR spectral absorption attributes of jarosite.

Wavenumber (cm^{-1})	**Molecular transition**	**Attribute**
449	ν2 (SO_4)-2	fundamental bending vibrations in sulphate ion
474	M-O(M:Al/Fe)	metal-oxygen vibrations
508	M-O(M:Al/Fe)	metal-oxygen vibrations
629	ν4 (SO_4)-2	fundamental stretching vibrations in sulphate ion
673	ν4 (SO_4)-2	fundamental stretching vibrations in sulphate ion
1012	δ(OH)	in-plane bending vibrations of hydroxyl ion
1025	δ(OH)	in-plane bending vibrations of hydroxyl ion
1094	ν3 (SO_4)-2	fundamental stretching vibrations in sulphate ion
1189	ν3 (SO_4)-2	fundamental stretching vibrations in sulphate ion
3358	ν (OH	fundamental stretching vibrations in hydroxyl ion

3.5. Jarosite- Luminescence measurements

3.5.1. TL studies: glow curves

To investigate the change in the TL of jarosite on heating, a dose of 260 Gy is given to natural sample and its TL up to 450°C is recorded. Again, a dose of 260 Gy is given and TL is recorded. The result is shown in Figure 312. It is evident that heating to 450°C, changes the sensitivity of the sample, however the glow curve shape does not change. Reproducibility of the TL curve is very crucial in deciding the protocols that can be used for dose estimation. Protocol in Figure 3.13 is used to analyse the effect of repeated heating. Figure 3.14 (a) show the results for multiple heating to 250°C i.e. below loss of stoichiometric water. Figure 3.14(b) plots the luminescence intensity with repeat measurement cycles of irradiation and readout. Figure 3.15a and 3.15b shows changes in glow curve shape and luminescence sensitivity after cut heating to 450°C.

In both the cases and for all the glow peaks in multiple cycles of heating to 250°C and 450°C, the reproducibility was within 1 % and 6% respectively. The similarity of glow curve shape also suggests that phase changes in jarosite ~277°C and at ~352°C did not interfere with luminescence.

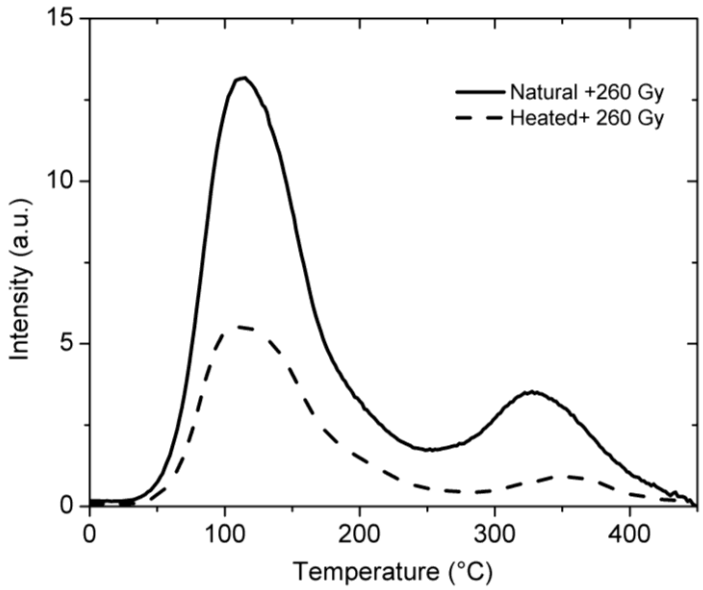

Figure 3-12 Jarosite sample 56B2. TL when the natural sample is given a dose of 260 Gy and when the same heated sample is given a dose of 260 Gy.

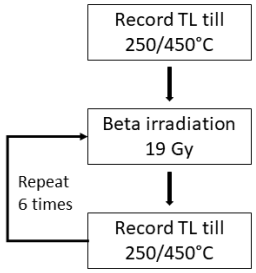

Figure *3-13 Protocol for reproducibility measurement, observation in emission range 325-700 nm.*

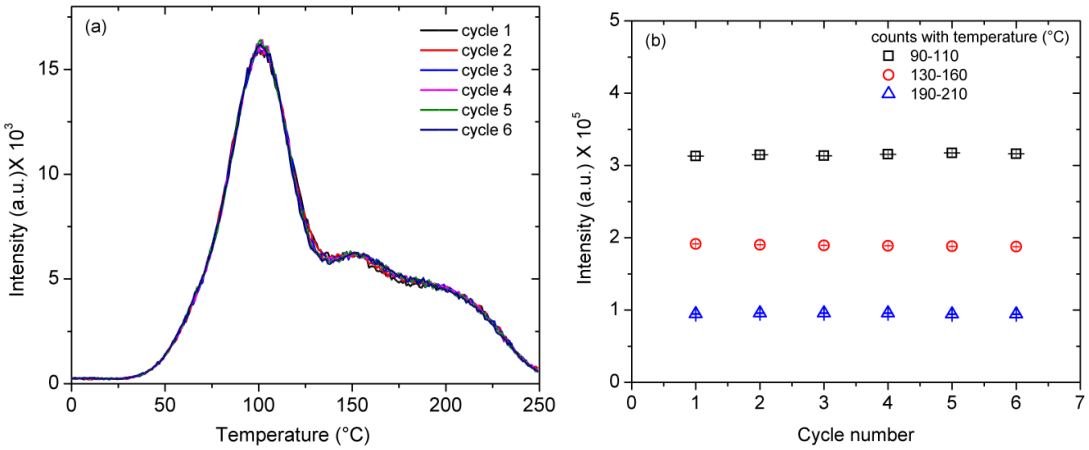

Figure 3-14 Jarosite sample 56B2. (a) Reproducibility of TL glow curve up to 250°C. (b) Photon counts with measurement cycles.

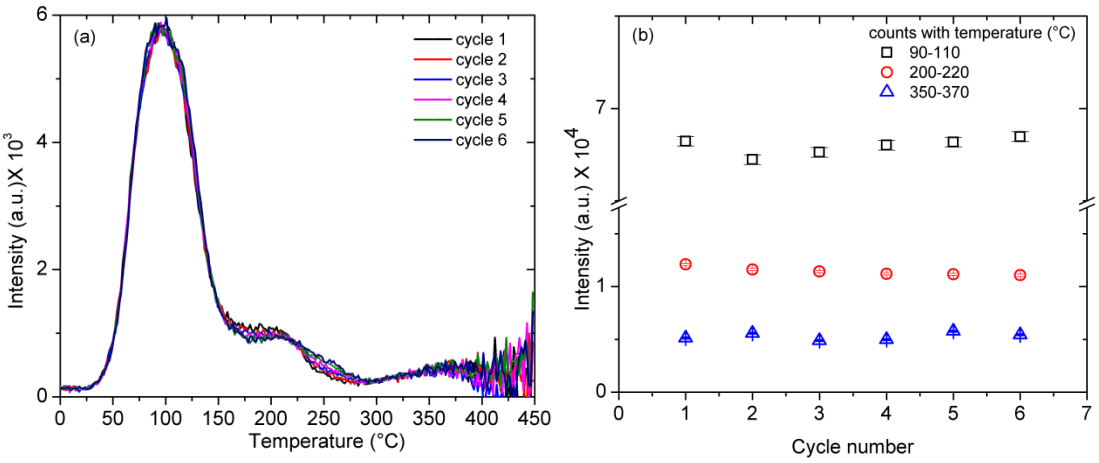

Figure 3-15 Jarosite sample 56B2. (a) Reproducibility of TL glow curves up to 450°C. (b) Photon counts with measurement cycles.

Luminescence sensitivity (luminescence per unit mass and per unit radiation dose (counts/(mg/Gy)) was also measured after heating to 250°C and 450°C and Figure 3.16 shows that the sensitivity is variable. Jarosite from Guneri formation has the highest sensitivity, indicating towards source variability. After heating the sensitivity for sample 66b2, 57d2, 56B2 decreased and for the other 3 samples it increases.

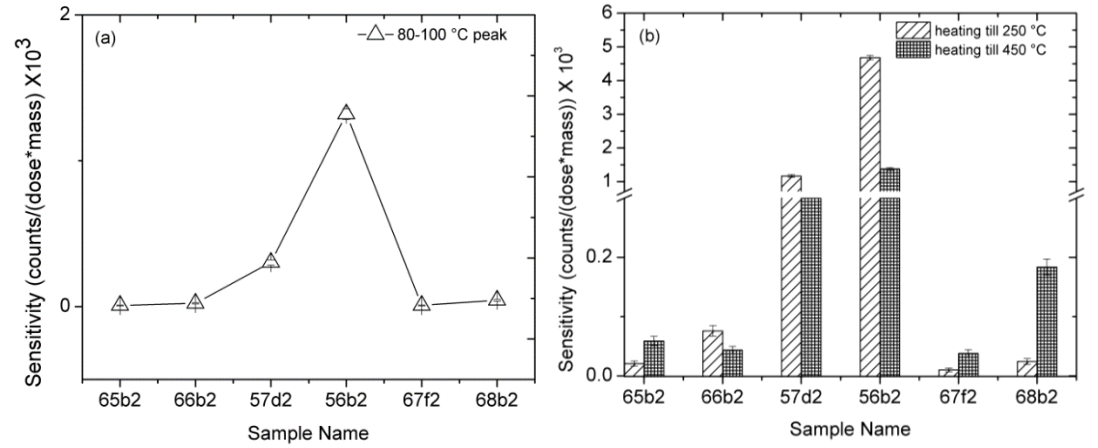

Figure 3-16 (a) Sensitivity of 80-100°C peak was measured for all jarosite sample by heating to 250°C then giving a dose of 19Gy. (b) Effect of heating of jarosite to 250°C and 450°C on the sensitivity of 50-200°C peak.

3.5.2. Stability: Kinetic Parameters:

Kinetic parameters are estimated to know the stability of the electron traps over geological time scales. Activation energy E(eV)), frequency factor (s(s^{-1})), lifetime of electrons in the trap (τ(s))

were estimated using fractional glow method. Considering the first order kinetics, the intensity (I) of the TL glow peak is given by

$$I = -\frac{dn}{dt} = nse^{-\frac{E}{kT}} \quad (3.1)$$

where n is the charge population in the trap, k is Boltzmann constant, T is the ambient temperature. For the measurement of activation energy, the aliquots are irradiated with beta dose, then heated sequentially to increasing temperature (starting from room temperature), cooled and heated again to temperature, higher than previous. Value of activation energy, corresponding to the maximum heating temperature in the cycle is calculated by fitting the following Arrhenius equation to the obtained data.

$$\ln(I) = constant - \frac{E}{kT} \quad (3.2)$$

Consequently, the frequency factor can be calculated from the Randall and Wilkins equation given as

$$s = \frac{\beta E}{kT_m{}^2} e^{-\frac{E}{kT_m}} \quad (3.3)$$

where, ß is the heating rate, T_m is the maximum temperature of heating and the lifetime of the electrons in the trap is given as

$$\tau = \frac{1}{s} e^{-\frac{E}{kT}} \quad (3.4)$$

Three aliquots of the 56B2 sample are irradiated with 325 Gy dose and consequently heated to temperature 40°C, cooled to room temperature and again heated to T_i+10°C. This cycle is repeated up to 450°C. The activation energy for each cycle is calculated from equation 3.2. The same procedure is repeated on 3 aliquots which have been annealed to 450°C for 10 sec. The activation energy and the maximum heating temperature for both annealed and not annealed case are plotted in Figure 3.17. The plateaus are marked with black line and indicate the presence of an electron trap. From the figure, it can be seen that the annealed and non-annealed sample have same trap structure till 300°C, after which deviation is observed. In the non-annealed sample three plateaus, hence three traps are visible, marked as A, B and C. Whereas, on annealing the traps above 300°C changes and two distinct trap centres are visible marked as D and E. Hence on heating above 300°C, jarosite changes its luminescence properties. The details of the calculated kinetic parameters are summarised in the Table 3.4. The traps with higher lifetime are present above 300°C. Assuming a first order kinetics, the life time at 27°C ambient temperature for the unannealed sample is ~0.3Ma for 350°C glow peak. For the annealed sample the highest lifetime is ~31Ma for glow peak at 360°C peak.

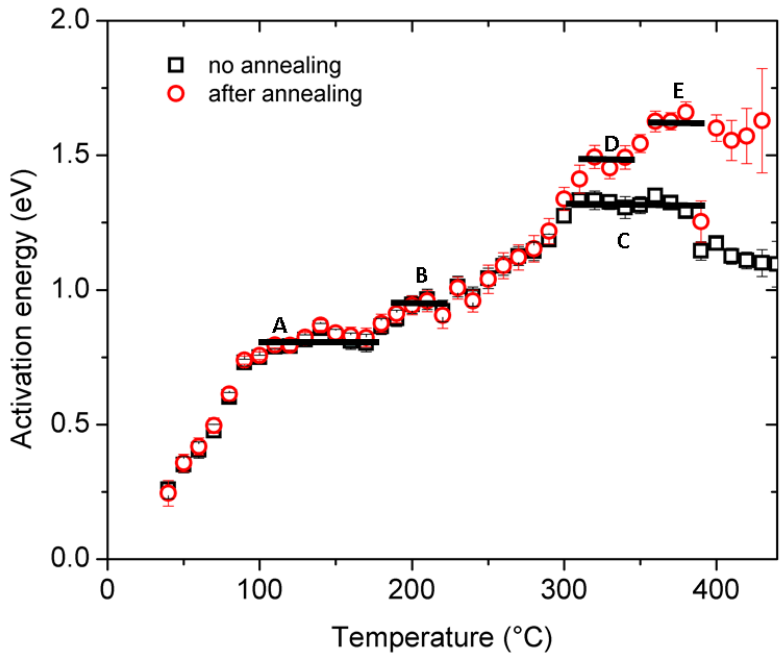

Figure 3-17 Activation energy versus maximum heating temperature graph for jarosite sample 56B2 obtained by Fractional glow curve method. Observation in emission range 325-700 nm.

Table 3-4 Kinetic parameters for jarosite sample 56B2, lifetime calculated at 27°C ambient temperature.

Peak	Sample as received followed by 325 Gy beta dose				Peak	Samples after heating to 450°C for 10 s followed by 325 Gy beta dose			
	Peak Temperature (°C)	Activation energy E (eV)	Frequency factor s (s^{-1})	Lifetime (s) at 27°C		Peak Temperature (°C)	Activation energy E (eV)	Frequency factor s (s^{-1})	Lifetime (s) at 27°C
A	150	0.82±0.04	(2±1) $\times 10^9$	(5.4±3.5) $\times 10^4$	A	150	0.83±0.04	(2.15±0.3) $\times 10^9$	(125±24) $\times 10^4$
B	210	0.94±0.04	(8.5±5.3) $\times 10^8$	(1.1±0.3) $\times 10^7$	B	210	0.93±0.04	(1.1±.1) $\times 10^9$	(3.5±3) $\times 10^7$
C	300	1.32±0.03	(9.4±10) $\times 10^9$	(4.8±3.6) $\times 10^{12}$	D	300	1.47±0.04	(2.75±2.25) $\times 10^{11}$	(13±13) $\times 10^{12}$
					E	360	1.63±0.04	(7.2±1.3) $\times 10^{11}$	(5±7) $\times 10^{15}$

3.5.3. TL Dose Response Curve and fading:

Since TL shows reproducibility within a maximum of 6%, we opted for a single aliquot regenerative (SAR) protocol approach with no sensitivity correction. Table 3.5 gives protocol used for TL-DRC. Figure 3.18 shows the DRC of sample 56B2, the dashed lines are the data of individual disc and solid line is the average. The photons count from 340-360℃ were integrated for the 350°C peak. Whereas the photons count from 200-220℃ were integrated to obtain the DRC for the 210°C peak. The growth curve here was fitted to a simple saturating exponential, with equal weightage to all data points. These peaks can measure a maximum dose of ~1600 and 2600 Gy, constrained by their thermal stability. The recycling (ratio of luminescence produced by same dose but at different cycles of the protocol (Table 3.6)) and recuperation (ratio of luminescence due to zero dose to natural dose) were within the error limits of 10 and 5% respectively, suggesting that the given protocol is suitable for estimating the doses. Athermal fading was estimated by irradiating the sample to a fixed (100 Gy) beta dose, followed by measurement after variable time delays. The protocol is given in Figure 3.19 (Huntley, 2006; Huntley and Lamothe, 2001; Kars et al., 2008). Athermal fading with a g-value of 4.27%/decade and near zero was observed for the 210 and 350°C peaks.

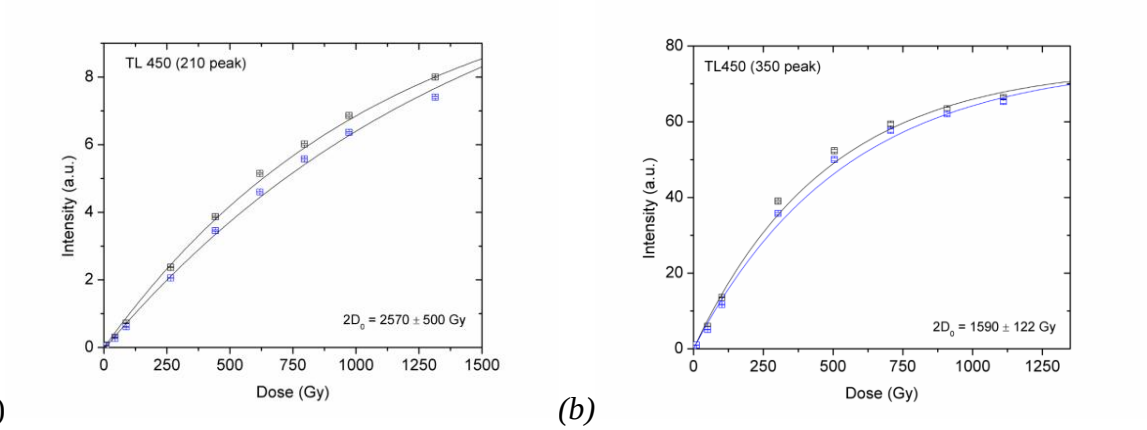

(a) *(b)*

Figure 3-18 Jarosite sample 56B2 TL dose response curve DRC. (a) The counts are integrated from 340- 360℃. (b) The counts are integrated from 200-220℃.

Table 3-5 Various protocol used to estimate the dose.

Step. No.	TL450	$BSL200_{UV}$ (modified after Wintle and Murray, (2006))	$IR50_{blue}$ (Wallinga et al. 2000)	$pIRIR225_{blue}$ (Buylaert et al. 2009)	$pIRIR225_{UV}$ (Buylaert et al. 2009)
1	Natural dose/ Regenerative dose	Natural dose/ Regenerative dose	Natural/ Regenerative dose	Natural/ Regenerative dose	Natural dose/ Regenerative dose
2	TL 250°C	Preheat 250 °C for 10 s	Preheat 250 °C for 60 s	Preheat 250 °C, 60 s	Preheat 250 °C, 60 s
3	TL 450°C	BSL at 200°C for 100 s	IRSL at 50°C for 100 s	IRSL at 50°C, 100 s	IRSL at 50°C, 100 s
4	Go to step 1	Test dose	Test dose	IRSL at 225°C, 200 s	IRSL at 225°C, 200 s
5		Preheat 250 °C for 10 s	Preheat 250 °C for 60 s	Test dose	Test dose
6		BSL at 200°C for 100 s	IRSL at 50°C for 100 s	Preheat 250 °C, 60 s	Preheat 250 °C, 60 s
7		Go to step 1	Go to step 1	IRSL at 50°C, 100 s	IRSL at 50°C, 100 s
8				IRSL at 225°C, 200 s	IRSL at 225°C, 200 s
9				Go to step 1	Go to step 1
Emission under investigation (nm)	325-700*	280-380#	400-480#	400-480#	280-380#

**325-700 nm is the transmission range when transmittance intensity < 0.01 and 330-625 nm is the transmission range when transmittance intensity <0.2.*

 # transmission range based on FWHM.

Table 3-6 Dose response parameters for jarosite sample 56B2.

Sr. No.	Protocol name	No. of disc	Saturation dose ($2D_0$)(Gy)	g-value (%/decade) (average of 10 aliquots)	Alpha efficiency	Recycling ratio (%)	Recuperation (%)
1	TL450 (210 peak)	2	2570±500	4.3 ±1	0.075±0.004	< 10	< 2
2	TL450 (350 peak)	2	1590 ±122	-1 ±0.7	0.051±0.004	< 10	< 1
3	$BSL200_{UV}$	3	867±85	7.6 ±0.6	0.093±0.01	< 10	< 2
4	$IR50_{Blue}$	3	1180± 181	7.4± 0.7	0.058±0.005	< 10	< 2
5	$pIRIR225_{UV}$	3	817±95	0.7±0.2	0.029±0.002	< 10	< 2
6	$pIRIR225_{blue}$	3	685±36	-0.5±0.4	0.041±0.004	< 10	< 2

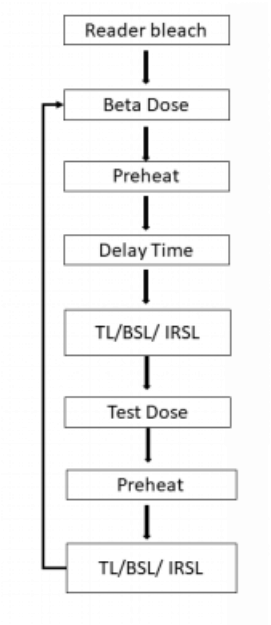

Figure 3-19 Protocol used to estimate fading.

3.5.4. **Signal Bleachability**

In luminescence dating, the resetting of luminescence clock on earth is due to daylight. In this study bleachability of various TL peaks under exposure to Solar lamp (Osram, Ultravitalux, 300 watts filtered through a window glass) was investigated. Aliquot of sample 56B2 each were annealed to 450°C, irradiated to 300 Gy were bleached under solar lamp for different time period varying from 0 to 1000 minutes. The photon counts of glow peaks 150, 210, 300 and 350°C were mass normalized and the results are plotted in Figure 3.20. Each data point is an average of three aliquots. TL intensity to 1/e of the

maximum intensity in 16, 20, 70 and 105 minutes of solar lamp exposure for 150, 210, 300 and 350°C.

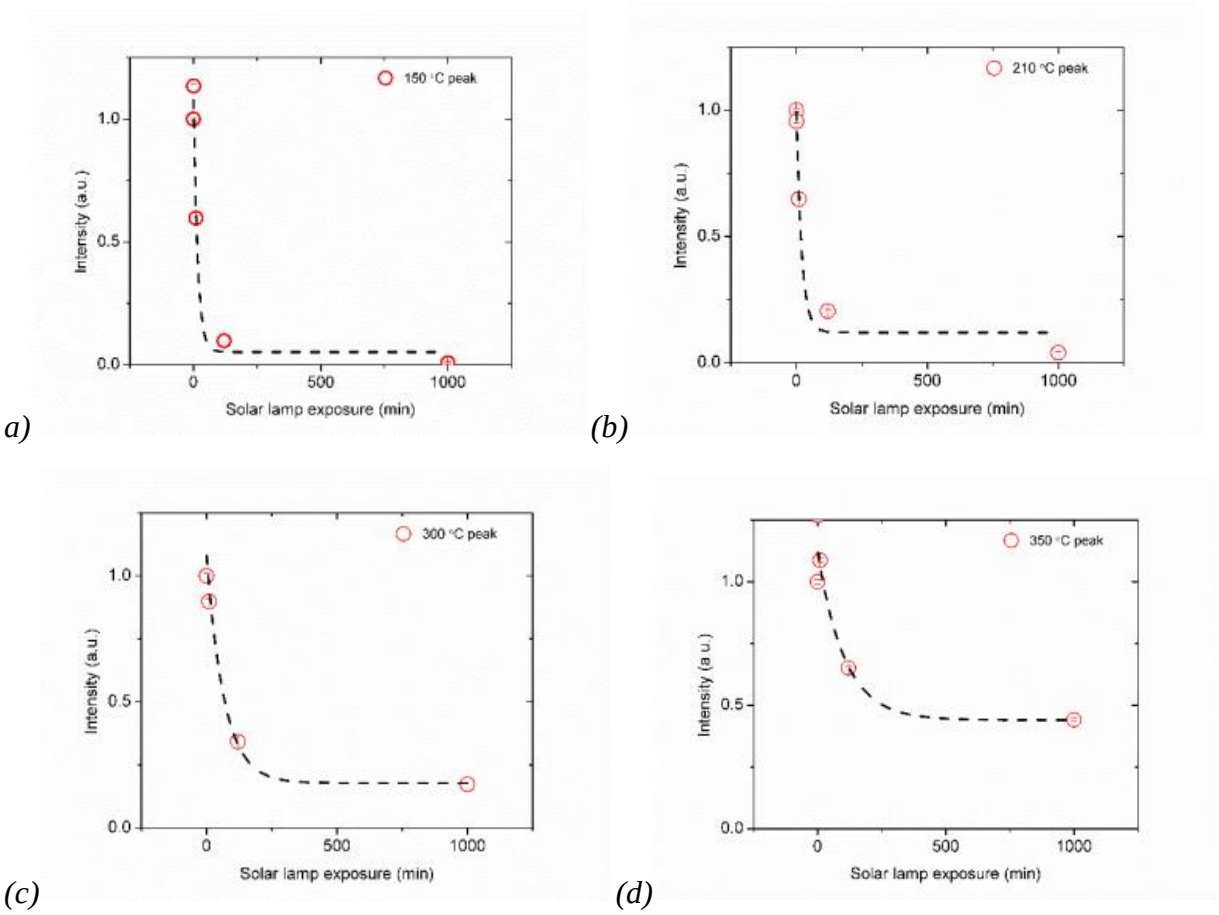

Figure 3-20 Solar lamp resetting of annealed jarosite sample 56B2 after a dose of 300 Gy for different TL peaks. Each data point is an average of three aliquots. The curves were fitted with $y=a.e^{-b.t}$.

3.5.5. Blue Stimulated Luminescence (BSL) - characteristics

Blue stimulated luminescence decay curve for sample 56B2 irradiated to 350 Gy (natural signal cleaned by BSL for 100s at 200°C) measured at room temperature is shown in Figure 3.21. The optical decay curves were deconvoluted using fit_cWCurve by (Kreutzer et al., 2024) using the equation

$$I = \sum_i I_i \sigma_i e^{-\sigma_i t} \quad (3.5)$$

Where, I_i is the initial concentration of charges of the i^{th} component, σ_i is the decay constant, and t is the time. The photoionization cross-section (cs) can be calculated from the knowledge of I_i, σ_i and the power, wavelength of the light stimulation used. From Figure 3.21, it is seen that the signal is composed of three components, c1(fast component), c2(medium component), c3(slow component). The parameters are summarised in Table

3.7. Further BSL, measured at 200°C, after a preheat of 250°C in the ultraviolet emission is shown in Figure 3.25(a).

Figure 3.22 shows the reproducibility of different components of the BSL shine down curve on repeated dosing (40 Gy) and stimulation with blue light. For the BSL measurements at room temperature the average deviation between repeated signals is 5, 3.38, 3% for the fast, medium and slow components and for the BSL at 200℃ is 8, 10, 8%. The reproducibity experiments suggest that a test dose correction is needed in the estimation of dose response curve of jarosite

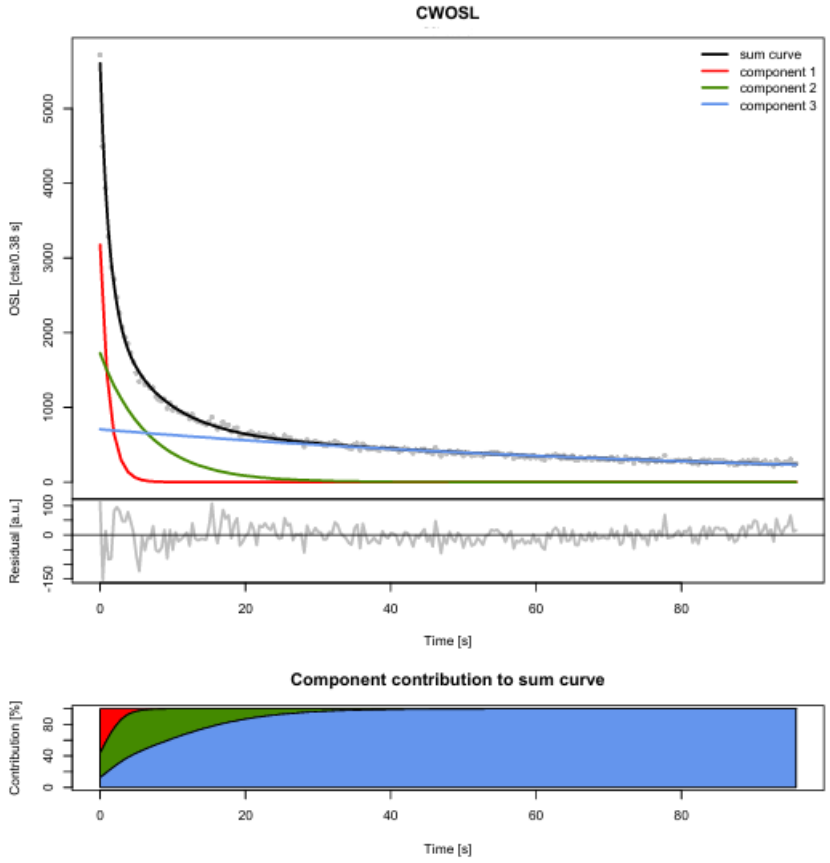

.

Figure 3-21 Jarosite sample 56B2, irradiated with 350 Gy, BSL at 25℃ component analysis.

Table 3-7 CW-OSL components of jarosite sample 56B2. The optical decay curves were deconvoluted using fit_cWCurve by (Kreutzer et al., 2024) using the equation $I = \sum_i I_i \sigma_i e^{-\sigma_i t}$ *where, Ii is the initial concentration of charges of the ith component,* σ_i *is the decay constant, t is the time and photoionization cross-section (cs) calculated from the* I_i, σ_i *and the power, wavelength of the light stimulation used.*

Signal	Components	Intensity (I_0) (arb. units)	Decay constant (σ) (s^{-1})	Photoionisation cross-section (cs) (cm^2)	R-squared
BSL at 25°C	c1 (slow)	3074±804	0.93±0.15	9.87E-18	0.9972
	c2 (medium)	10570±654	0.19±0.03	1.97E-18	
	c3 (fast)	56527±1519	0.01±0.001	1.49E-19	
IRSL 50°C	c1 (slow)	17538±6082	0.25±0.03	1.94E-19	0.9996
	c2 (medium)	62382±3129	0.09±0.01	6.99E-20	
	c3 (fast)	105514±1952	0.012±0.002	9.32E-21	

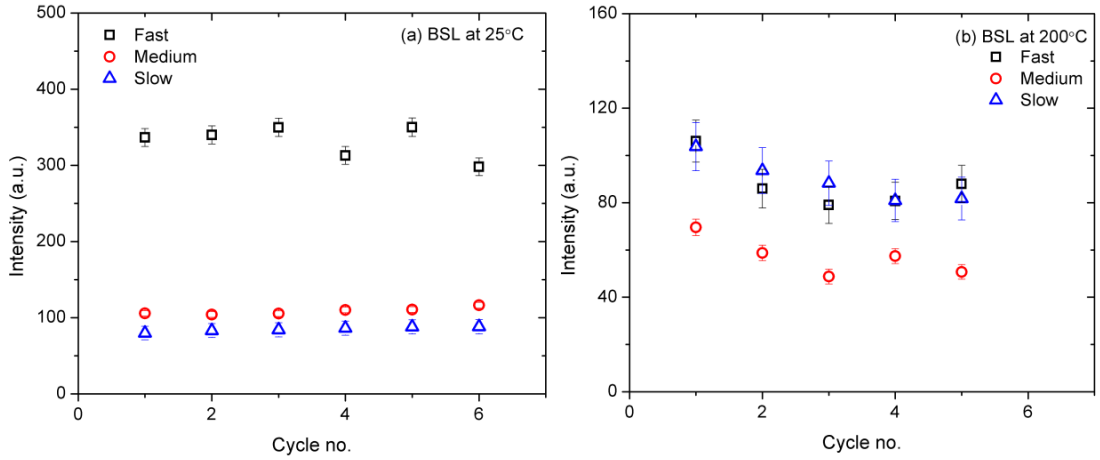

Figure 3-22 : Jarosite sample 56B2. (a)BSL signal at 25°C. Protocol → Dose (40 Gy) → BSL at 25°C for 100 s. Repeat the protocol.(b)BSL signal at 200°C. Protocol → Dose (40 Gy) →preheat 250°C for 10 sec → BSL at 200°C for 100 s. Repeat the protocol. For reproducibility test the fast component is calculated by integrating initial 1.92 sec counts and subtracting the background from the medium component, medium by integrating 10-15 sec counts and subtracting the slow component and slow by 60-100 sec counts.

To obtain the dose response curve, the BSL signals should be thermally stable over the time period of interest. The protocols used for BSL 200_{UV} DRC was modified after Wintle and Murray, (2006) to probe deeper trap and to minimise the contribution from shallower traps (Table 3.5) results are summarised in Table 3.6. Sensitivity correction by test dose normalisation was used. The DRC are fitted with following single saturating exponential equation

$$I = I_0 e^{(1-\frac{D}{D_0})} \quad (3.6)$$

where, I is the intensity at dose (D), and D_0 is the saturation dose defined as the dose where the intensity is 66% of maximum intensity (I_0). The maximum dose that can be estimated is till $2D_0$, after that error becomes extremely large. The graph is shown in Figure 3.25. The saturation dose is 867 ± 85 Gy. Athermal fading of BSL was measured using standard procedures of Huntley (protocol in Figure 3.7) (Huntley, 2006; Huntley and Lamothe, 2001; Kars et al., 2008). The results are an average of measurement on 15 aliquots. BSL signal shows a fading of 6.64 ± 0.82 %/decade.

3.5.6. Infrared Stimulated Luminescence (IRSL)-characteristics

The jarosite samples also showed infrared stimulated luminescence, observed in blue emission (400-480 nm). The optical decay curve of IRSL at 50℃ is shown in Figure 3.23 and 3.25. Compared to BSL, IRSL decay is slower. The component analysis (Figure 3.23) shows presence of three components. The estimated parameters are given in Table 3.7.
The Figure 3.24 shows the reproducibility of the sample. For the IRSL measurements at 50 ℃ the average deviation between repeated signals is 3, 3, 14% for the fast, medium and slow component.

To obtain the DRC of IRSL, measurements are made at 50°C in UV emission, the protocols used are listed in Table 3.4, results in Table 3.5 and Figure 3.25. The saturation dose for IRSL 50 is 1180 ± 181 Gy and the fading is 7.4 ±0.7 %/decade. The saturation is higher than BSL and fading in both IRSL50 and BSL is comparable. Recuperation and recycling were well within the limits. Further to circumvent the fading, IRSL at elevated temperature of 225°C is measured in UV and blue emissions after measurement of IR50. This enables measurement of luminescence from distant electron hole pairs. Near zero fading is obtained for both the signals, however a reduced saturation dose of 817±95 Gy (for pIRIR225 in UV emission) and 685±36 Gy (for pIRIR225 in blue emission) is obtained. This is contradictory to quartz and feldspar, wherein it is observed that at higher energy measurements the saturation dose increases.

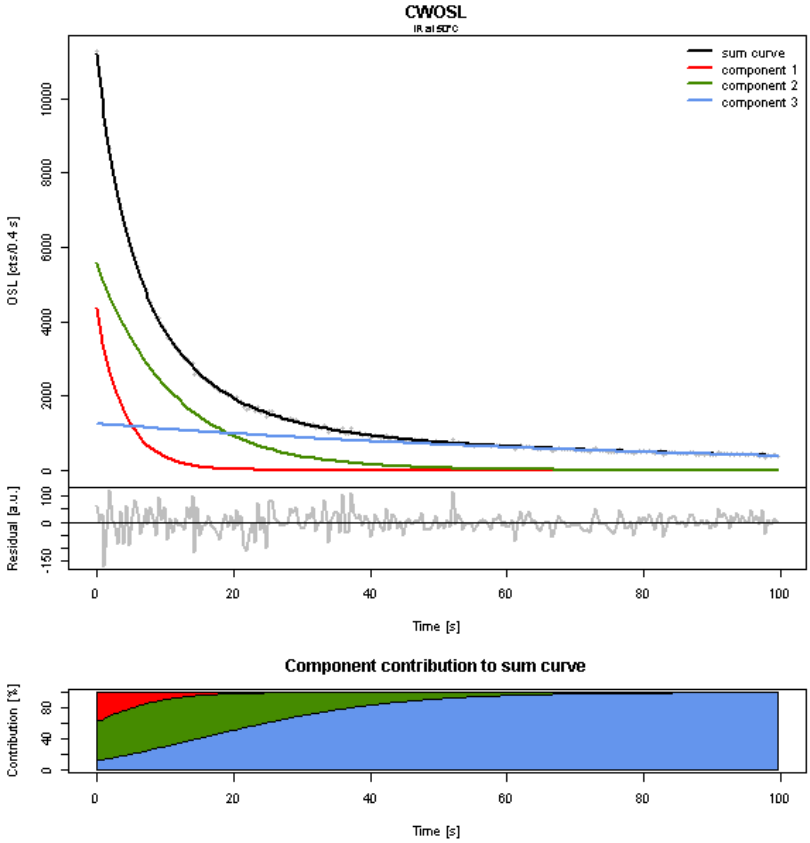

Figure 3-23 Jarosite sample 56B2, IRSL 50 in blue filter on a dose of 340 Gy.

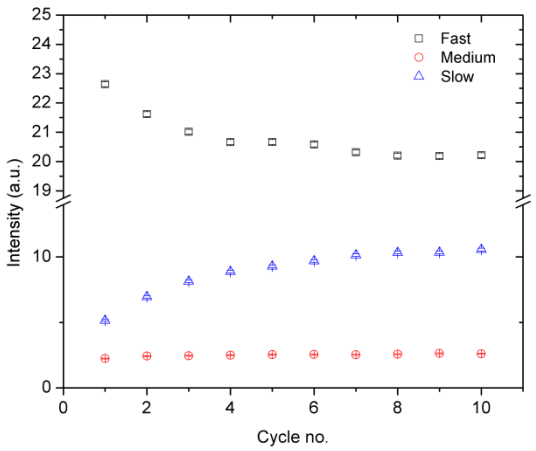

Figure 3-24 Jarosite sample 56B2, reproducibility of different components of the IRSL 50 signal. The fast component is calculated by integrating initial 2 sec counts and subtracting the background from the medium component, medium by integrating 35-40 sec counts and subtracting the slow component and slow by 90-100 sec counts. For more details refer to text.

TL-OSL correlation: To assess the origins of signals in BSL200 and IRSL50, their yield with the pre-heat temperature is examined. Sample is divided into groups of 3 aliquots, where each group of aliquots is given a dose of 150 Gy and heated to temperature of 100, 200, 300, 400°C followed by BSL200 or IRSL50 measurement.

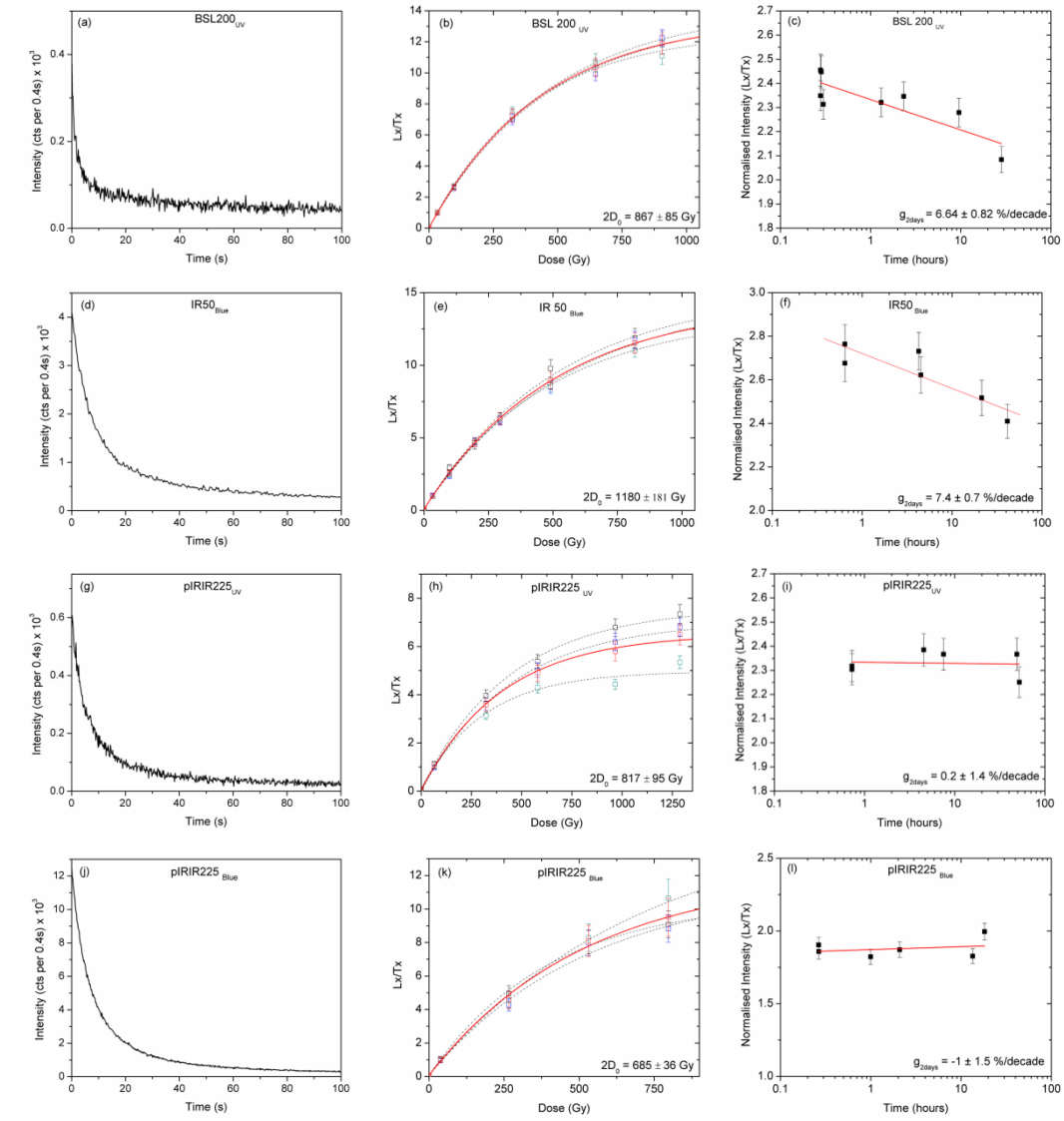

Figure 3-25Jarosite sample 56B2 optical decay curves (left); Dose response curves (middle), each dashed line is data on individual aliquot and solid line is average; Fading characteristics (right) of BSL200Uv, IR50Blue, pIRIR225UV, pIRIR225Blue respectively.

Figure 3.26 (a) shows the graph of weight normalised BSL200 signal after the preheat temperature. It can be seen that the signal first increases and then decreases. The increase indicates towards a possibility of thermal transfer of charges due to preheat. Also, the

graph indicates that the signal comes from a wide temperature range, even at a preheat of 400°C, the signal becomes feeble but still significant signal can be observed, showing the presence of BSL trap even after 400°C. Similarly, Figure 3.26 (b), shows the results for IRSL signal, the trend is similar to BSL, however, the thermal transfer percentage is less. The signal at a preheat of 400°C is very feeble but still exists. This shows that the major contribution of signal for both BSL and IRSL is below 400°C.

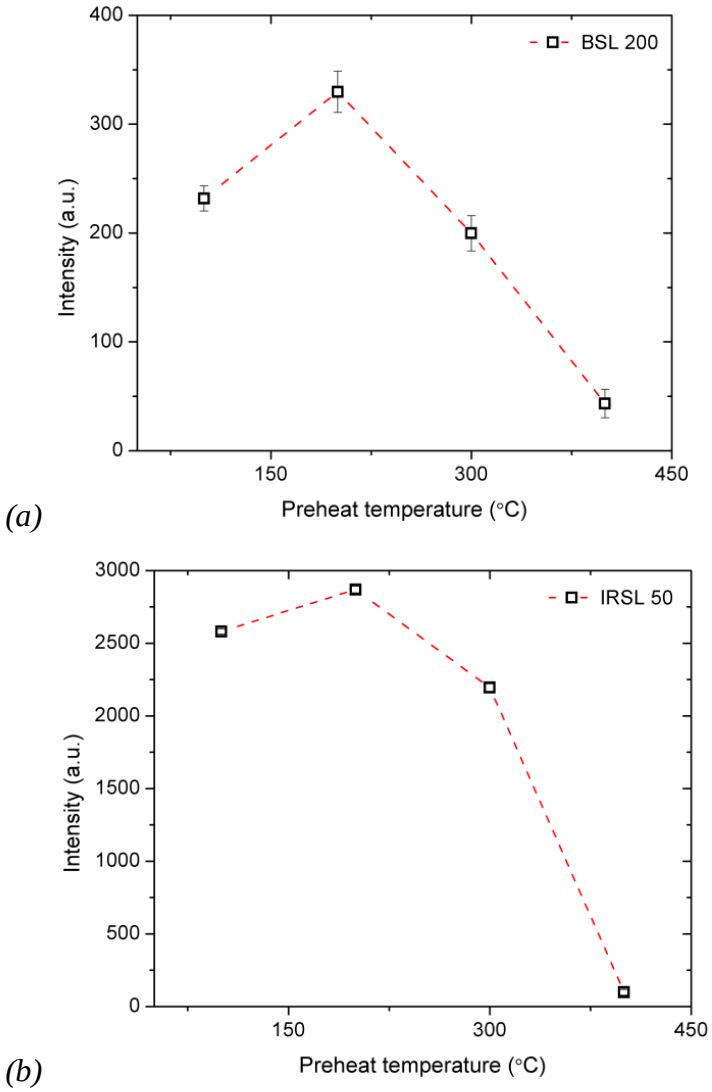

(a)

(b)

Figure 3-26 Jarosite sample 56B2 (a) BSL200 signal intensity variation with preheat temperature. (b) IRSL50 signal intensity variation with preheat temperature.

3.6. Jarosite -Dose rate and dating limits

The dose rate for terrestrial dating will comprise of radionuclides in jarosite sample and other sediments nearby which comes in 30 cm range (range of gamma rays) and cosmic ray dose rate. Whereas for Martian dating the dose rate contribution due to the cosmic ray flux overpowers the dose rate.

3.6.1. Radionuclide concentration estimation

To estimate U, Th concentration, thick source alpha counting, where an alpha thick layer (~2mm) of sample is mounted on perplex holder being in direct contact with ZnS:Ag scintillator and scintilations/unit area /unit time was used. NaI-scintillation counting was used to measure K concentration through the 1.46 MeV gamma ray from 40K, the sample was mounted in plastic vials, with same geometry as the standard (AR grade KCl) and background and the concentration is estimated by peak area comparison method. The estimation of dose rate requires the estimation of annual dose accumulation from both these factors and is given in Table 3.8. The measured value for 67F2 sample here is 1.62±0.6 mGy/year. For Martian surface, the cosmic ray external dose rate calculation as done by (Morthekai et al., 2007) using GEANT4 stimulation, gives a cosmic dose rate estimation of 63 mGy/ year for solar minimum. Summing with internal dose rate gives an average total dose rate of ~65 mGy/year. For terrestrial studies, typical dose rate of the sediments is ~3 mGy/year. Hence considering a terrestrial dose rate to be between 1-3 mGy/year.

Table 3-8 Summary of dose rate; Jarosite sample 67F2.

Internal Dose rate (mGy/yr)	Concentration of radionuclide		Dose rate estimation technique
	U^{238} (ppm)	1.87± 0.1	ZnS alpha counting
	Th^{232} (ppm)	1.06 ±0.35	ZnS alpha counting
	K (%)	0.78± 0.07	NaI Scintillator, gamma counting
	Total internal dose rate	1.62±0.6	
External dose rate (mGy/yr)	Cosmic Ray	63	Simulation; (Morthekai et al., 2007)
Total dose rate (mGy/yr)		65	

3.6.2. Efficiency factors

The track length of charge particles in a crystal matrix depends on their mass and energy. Thus, dose deposition by alpha particles with higher mass and charge, results in a short track length along which higher ionization density imply loss of charges being trapped and consequence reduction in luminescence production / unit dose of alpha as compared to weakly ionizing beta particles (Aitken, 1985; Zimmermans, 1972). For low energy alpha particles, as in the case of terrestrial sediments, a ratio of luminescence produced per unit dose of alpha to beta called as alpha efficiency (a-value), is measured, and is included in computation of annual dose rate. The a-value is measured by bleaching the samples for 5 hours and irradiating using ^{241}Am, in a vacuum alpha irradiator (Singhvi and Aitken, 1978), for 120 minutes. The protocols used to recover the dose are as per Table 3.5 were used to measure the "a-value". A-value for alpha particles was 0.075 and 0.051 for the 210 and 350℃ peak respectively. For BSL200, the a-value is is 0.093± 0.01. The 'a-values' are of 0.058 ± 0.005, 0.041±0.004 and 0.029 ± 0.002 for IR50 (blue), pIRIR225 (blue) and pIRIR225 (UV), respectively. The alpha efficiency of jarosite for a particular detection window (BG39, blue and UV) correlates with athermal fading g- value (Table 3.6). Lower g-value corresponds to lower alpha efficiency as suggested by Singhvi (1981) and this needs to be explored further. On the Martian surface the major source of ionizing radiation is largely high energy protons and limited studies so far (Jain et al., 2007a) suggest that the luminescence production efficiency would be in the range 0.5 to 1. Pending these measurements for the case of Jarosite, we used a luminescence production efficiency of 1 for integrated cosmic ray flux on Mars.

3.6.3. Jarosite- dating limit

1. *Earth surface processes:* The high temperature (>300℃) traps in jarosite can be used for dating and the relevant age can be calculated by the following classic equation

$$\text{Age} = \frac{\text{Total dose accumulated}}{\text{Annual accumulation of dose}} \tag{3.7}$$

From the above analysis, dividing the saturation dose (~1600 Gy) with annual terrestrial dose rate of ~2 mGy/year gives a dating range of ~0.8Ma. This will be constrained by the kinetic stability of the trap ~0.3Ma. At colder environment with an ambient temperature of 10°C, the lifetime of the same peak is 3Ma and hence in such environment it can be used for dating upto 0.8Ma. Jarosite formation is indication of start of aridity in the region and thus climate change. On Earth, various paleo-lakes have jarosite deposition. Since

this study shows the possibility of directly dating the jarosite formation age itself and not the minerals and organics found nearby, it can give more accurate understanding of the climate change in the late quaternary time.

2. *Martian surface process:* Using the Martian dose rate ~65mGy/ka, gives a dating range ~25 ka. This can be used to study and get the absolute time information of occurrence of aeolian events and wind storms which transport jarosite. Recently, many such events are recorded by Perseverance rover on Mars. Jarosite's luminescence can be a proxy for the absolute knowledge of such events in the past.

3.7. **Summary**

In this chapter, three minerals were studied and following are the major findings from this work. Quartz show an increase in intensity up to ~10 kGy and 18 kGy for sedimentary and rock samples. Taking a dose rate of ~3 mGy/year, this suggests the possibility to date events upto atleast 3Ma. The increase in intensity of feldspar with dose is less than that of quartz. In feldspar saturation is observed around 1.5 kGy in rock sample and 6 kGy in sedimentary sample. Further jarosite shows considerable luminescence properties which can be used for luminescence dating of Earth surface and Martian processes. The major findings of jarosite being:

1. HCl increases the luminescence yield, possibly due to the removal of gleying.
2. In the detection window of 325-700 nm TL glow peaks of Jarosite are at 100, 150, 300 and 350°C.
3. Jarosite luminescence can be stimulated by both blue and infrared light and detection in both blue (400-480 nm) and UV (280-380 nm) are observed.
4. The luminescence signals are reproducible under repeated cycles of irradiation and read out. Reproducibility of TL was <6 % and that of BSL/IRSL (<14 %).
5. Luminescence sensitivity (LS) of the samples was variable. Samples from the Guneri formation had highest sensitivity. Heating up to 450 °C, changed the LS but the glow curve shapes remained the same. This is also supported by FTIR and CL-EDXS.
6. Fractional glow curve analysis suggests that kinetic parameters of glow peaks below 300°C are similar for both the annealed and non-annealed sample. For higher temperature glow peaks deviation occur. The glow peak at 300°C has an estimated lifetimes of ~ 0.3 Ma and this is suitable for dating.

7. Both BSL and IRSL comprise 3 components.
8. Saturation doses of various luminescence signal range from 590Gy to 1600 Gy. Any or all of these could be used for dating.
9. Jarosite shows large fading of the BSL and IRSL, i.e., around 6.64 and 7.4 %/decade. In TL for glow peak at 210°C, a fading of 4.3 %/decade is observed. However, no fading is observed for the pIRIR225 in blue and UV detection window and for TL glow peak at 350°C.

With an average dose rate of ~2 mGy/year on Earth and ~65 mGy/year on the Martian surface, a dating range of ~800 ka and ~25ka is proposed with jarosite constrained by the thermal stability.

Chapter 4: Characterizing High Radiation Dose Response of Quartz

4.1. Introduction

It is already seen in Chapter 3 that the TL of quartz saturates ~10-18 kGy, which suggests that it should be possible to use it for dose estimation. Such high dose estimates will enable dating possibly up to the tertiary era (> 2.5 Ma). However, for such high doses, effects such as peak shift (as also observed in Chapter 3) and dominance of some spectral bands is observed (Schmidt and Woda, 2019). This is often linked with the defect creation. In chapter 3, we have made observations in visible emission covering 325-700 nm. However, quartz luminescence is observed in several emission bands viz. 175, 290, 330-340, 380-390, 420, 450, 470-500, 510-570, 580, 620-650 nm) as reported by previous research works (Krbetschek et al., 1997; Rink et al., 1993). These are mainly classified as UV, blue, green, and red emissions. Most of TL studies using blue and UV emission so far report luminescence mechanism in quartz up to 1 kGy (Adamiec, 2005; Chawla et al., 1998; Debenham, 1985; Hunter et al., 2018; Huntley, 1994; Huntley et al., 1985; Ogundare et al., 2006; Singhvi, 1985; Singhvi et al., 1982; Wintle, 1997) and only a few exists for higher doses in excess of 1 kGy (Durrani et al., 1977; Hashimoto et al., 1987; Hunter et al., 2018; Huntley and Prescott, 2001; Sawakuchi and Okuno, 2004; Schmidt and Woda, 2019). In UV TL (Chawla et al., 1998; Fleming, 1969; Huntley et al., 1996), saturation is observed around 200 Gy, however, few other studies (Dutkiewicz and Prescott, 1997; Huntley, 1994; Huntley et al., 1993) observed an increase in the TL response until 1 kGy, which was the maximum studied dose in their respective work. Apart from UV emissions, many signals such as blue, green, and red having signal strength stronger than UV are reported (Kuhn et al., 2000). Earlier works (Sawakuchi and Okuno, 2004) has shown that for Brazilian quartz, the blue TL 350°C peak saturates after 10 kGy while in case of granitic quartz the blue TL does not saturate till 47.9 kGy (Schmidt and Woda, 2019).

Further, several studies are done for volcanic quartz on the red TL emission, (Corpusculatre, 1991; Fattahi et al., 2004;Fattahi and Stokes, 2000; Hashimoto et al., 1987; Schmidt and Woda, 2019) and the saturation is found to be ~ 6 kGy. Different spectral studies are carried on different samples and a simultaneous cohesive study in all emissions still not done. The saturation characteristics for quartz are still not well understood, and role of electron traps and recombination centers in saturation is not yet exactly known (Ankjærgaard et al., 2006; Sally E. Lowick et al., 2010b).

Besides this, some physical processes are reported which are not yet completely explained. The increase in the sensitivity of quartz is reported with the increase in laboratory dose (Chawla et al., 1998) and is attributed to the creation of defects. Further, it is observed that the luminescence sensitivity for doses in excess of 1 kGy changes in blue and UV TL emissions but not in red (M. Fattahi and Stokes, 2000; Sally E. Lowick et al., 2010b). If the process of creation of electron traps is linked with increase in dose, then red TL should show change in sensitivity for the same electron trap that shows sensitivity change in UV and blue TL emissions. The shift in TL peak maxima with dose is reported by Ogundare et al., (2006) and shift in maximum emission wavelength by Schmidt and Woda, (2019) at high doses. One explanation given for these shifts is that the TL glow curve is a complex convolution of multiple glow peaks responding to dose in different ways, which is not well understood.

For investigating the effects stated above, it is necessary to follow either of the two approaches; multiple aliquot measurement or single aliquot measurement. To avoid the incorporation of sensitivity changes due to measurement methodology, it is important to use the multiple aliquot approach. Further, some normalization procedure is required to make inter-aliquot comparisons for conclusions. Various normalization procedures have been reported in literature (Aitken, 1983; Jain et al., 2003) and are discussed in chapter-2. Some of these are weight normalization, zero glow normalization, second glow normalization, test dose normalization, short shine normalization, etc. The weight normalization procedure is considered to be universal as it is not affected by any of the laboratory measurement procedures such as bleaching, heating or dosing (Aitken, 1985) . However, statistical fluctuations due to number of bright grains in weight normalization may result in scatter and hence other methods of normalization evolved. In zero glow, second glow, test dose, and short shine normalization methods it is assumed that, sensitivity changes in the test signal or the corresponding 110°C TL signal used for normalization are the same. These normalization procedures are best suited for doses

below 1 kGy and needs to be verified for higher doses. The fundamental understanding about the processes of dose/charge accumulation, storage and luminescence response of minerals at high radiation doses is still lacking. Since the luminescence dating and retrospective dosimetry applications are limited by the saturation in the signal, it is very important to understand the factors that govern the saturation. A systematic study of the luminescence characteristics of minerals at high radiation dose values will help in understanding the crystal and defect dynamics for such doses and thus will enable exploring of possibility for dosimetry and dating applications.

Therefore, this chapter aims to understand the charge storage in stable electron traps at high doses and the role of recombination centers in Dose Response Curve (DRC) and saturation. Further, this work investigates the dose-response, signal bleachablity and sensitivity normalization at doses >1 kGy.

4.2. **Methodology**

In this chapter, four quartz samples are used. Three of the samples are described in Table 3.1 of Chapter 3. Additionally, a sample from western India, Deccan traps sediment sample, KG-1 (23° 15' 3.24" N, 69° 37' 48.72" E) is also included. The sample KG-1 is naturally high dosed and is in field saturation. It was used to study the bleaching effect and natural luminescence in different spectral windows. Of the four samples used in this study, detailed investigations are carried out on the sample YS-5, because of the less inter-aliquot scatter and clear observability of signal saturation as shown in Chapter 3. Optical filters used for present study are listed in Table 2.2 of chapter 2 and their spectral transmissions are shown in Figure 2.2 of chapter 2.

To study the luminescence characteristics for known dose, the signal due to prior dose was removed by bleaching the sediment samples YS-5 and SR-23 in solar lamp for 24 hours. This reduced the previous TL signals in the samples. As the sensitivity of rock sample (RQ-1) was low and it didn't yield a measurable S/N ratio, it was sensitized by annealing at 450°C for 30 minutes. This removed the previous TL signal and enhanced the dose sensitivity as well as stabilizing it. The residuals are shown in Figure 4.1. Following this, the samples were irradiated with known doses. Apart from KG-1, all samples were irradiated with gamma radiation from 1 to 21 kGy.

4.3. **Trap Characterization**

Quartz in general has several traps (Aitken, 1985; Khoury et al., 2008). To understand the effect of high dose on trap kinetics, a T_{max}-T_{stop} analysis was carried out at various doses (Garlick and Gibson, 1948; McKeever, 1985; Pagonis et al., 2006). The sample was irradiated with a dose of 50 Gy, and preheated till T_{stop} (from 30 to 450°C, in steps of 10°C) followed by a measurement of TL 450°C. To avoid irradiation of samples multiple times (as is done in T_{max}-T_{stop}), the activation energy (E_a) was estimated using the repeated initial rise method (fractional glow technique) (Gobrecht and Hofmann, 1966), thus enabling the study of trap characteristics at high radiation doses. This method enables the determination of E_a of trap of any order. The initial part which is known to follow first-order kinetics of the glow curve was analysed. The method here was applied on 50 Gy, 3000 Gy and 18000 Gy dosed samples.

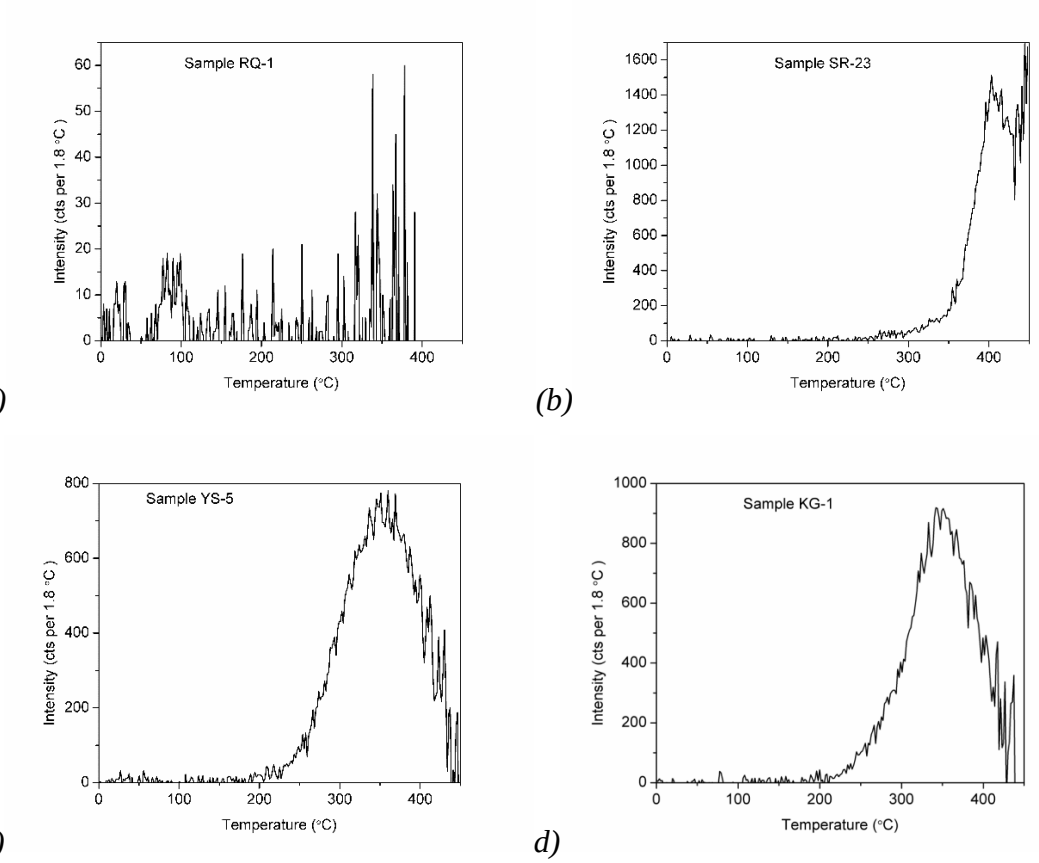

Figure 4-1 Residual TL (a)RQ-1 after annealing, (b)SR-23, (c)YS-5, (d)KG-1 after 24 hour bleaching under sun lamp.

The irradiated samples were heated till T_{stop} (from 30 to 450°C, in steps of 5°C), cooled and heated again. The blackbody subtracted intensity was used to compute the activation energy using Arrhenius relation between intensity and temperature (Pagonis et al., 2006). Additionally, to observe the effect of high radiation dose on trap characteristics after annealing, a dose of 50 Gy was administered and activation energy was re-estimated.

The TL glow curves of sample YS-5 measured following varying preheat temperatures are shown in Figure 4.2. Several traps are observed and are marked with black arrows. It shows that at least three traps are present beyond 300°C. Further, Figure 4.3 shows the T_{max}- T_{stop} graph for the sample YS-5. Multiple traps are visible for temperatures <200°C and a continuum in T_{stop} is observed for temperatures > 200°C and T_{max} is found to increase towards end. The activation energy estimated at various doses is shown in Figure 4.4(a), the curve for 50 Gy shows multiple plateaus, in agreement with the multiple traps observed in TL glow curve (Figure 4.2). Towards the end the errors increase, because of poor signal to noise (S/N) ratio. However, at 3 kGy and 18 kGy significant differences in the activation energy of the quartz system are observed at low (< 200°C) temperatures and small variations at high (> 350°C) temperatures. The 110°C peak has a low lifetime (~8 hrs) (Aitken, 1985). The time of gamma irradiation of samples with 3 kGy and 18 kGy and time of transportation of samples is significantly higher than lifetime of low-temperature peak leading to thermal fading, hence activation energy for this peak for high radiation doses could not be calculated. Further, for high radiation doses, the activation energy distribution for higher temperatures becomes like a continuum, rather than plateaus that are observed at 50 Gy. Further Figure 4.4(b) shows the comparison of activation energies for 50 Gy doses before and after different high radiation dose treatment of samples. Results shows that the crystal tries to restore E_a once the high doses are removed. Trap kinetic parameters such as τ, E_a and s also gives insights into the trap structure with the changing high radiation doses. The activation energy (Ea) estimated for different radiation doses, Figure 4.4 shows that low-temperature traps (< 200°C) are majorly affected during high radiation doses as their activation energy increases. This signifies that the potential energy at the site of these electronic states is modified due to accumulation of large trapped charges. Higher activation energy indicates towards lesser probability of eviction at room temperature and strongly bound charges, which are difficult to evict. However, the deeper traps at temperatures > 200°C are much more stable in terms of changes in activation energy, with high radiation doses. This agrees with study by Hunter et al., (2018) on the blue emission for 210°C and 350°C peaks, which show that

the kinetic parameters remain unaltered at high radiation doses. Annealing samples by heating to 450°C reduces the activation energy of the low-temperature traps (Figure 4.4(b)). This again indicates that permanent defect creation does not occur due to high radiation doses and after removal of charges from trapping centre, crystal tries to restore the original configuration of traps in crystal. Kinetic parameters are previously derived by Spooner and Questiaux, (2000) for the 3 major emissions in quartz, UV, blue and red. These authors show that kinetic parameters are same for different emissions. This further suggests that trap structure does not change with irradiation.

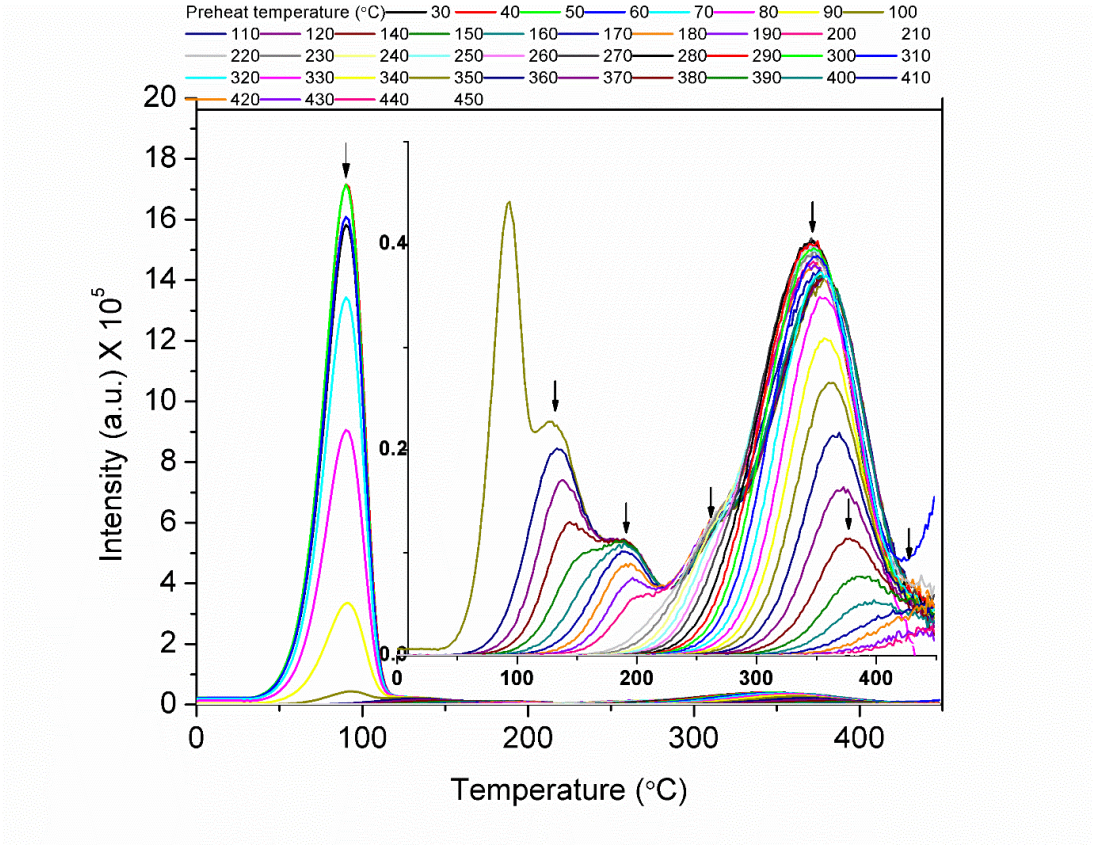

Figure 4-2 TL glow curves of sample YS-5 recorded after various preheat temperatures. A dose of 50 Gy is given in each cycle. The visibly distinct peaks are marked by black arrow, measured in visible using BG39 Filter (325-700 nm).

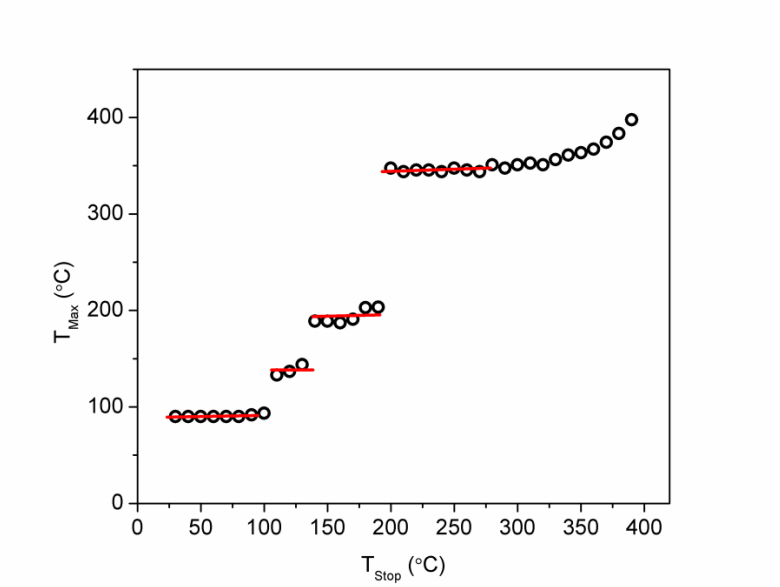

Figure 4-3 Tmax-Tstop graph for sample YS-5, Dose 50 Gy, measured in visible using BG39 Filter (325-700 nm).

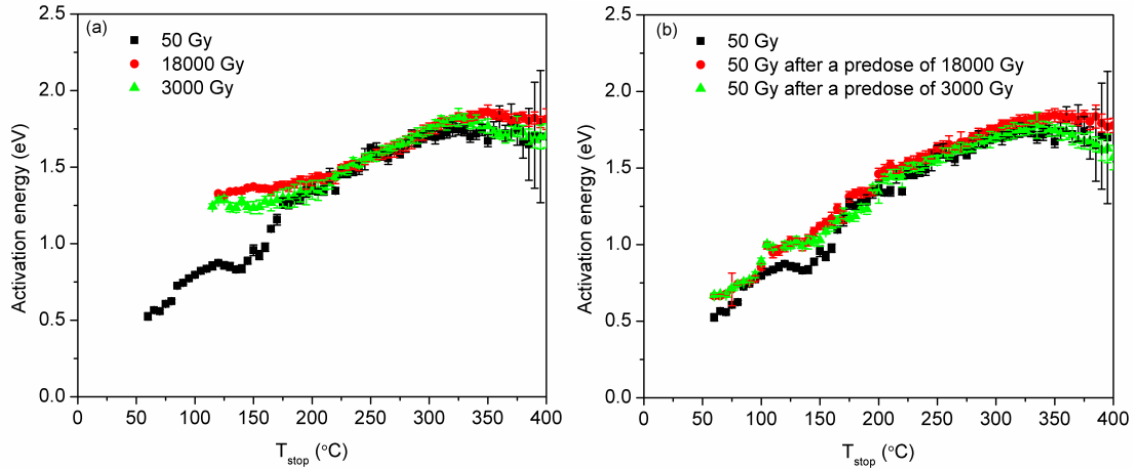

Figure 4-4 Activation energy of sample YS-5 (a) at different doses, (b) at 50 Gy dose but after different HRpD removed by heating upto 450°C, measured in visible using BG39 Filter (325-700 nm).

4.4. **Dose response curves with varying preheat temperature**

A peak shift is observed in TL glow curves (Figure 3.3-3.5, Chapter 3). McKeever, (1985) suggested that for non-first order kinetics TL glow peak temperature shifts to lower

temperatures with increase in dose. However, in Figure 3.3-3.5, Chapter 3, majorly the TL peak shifts to higher temperatures with dose. Such a shift can be explained based on the variable electron capture cross-sections of different traps, resulting in different saturation (suggested by Ogundare et al., (2006)). To study this, the TL dose response curve was measured for variable doses in the range 1-21 kGy in spectrum range (325-700 nm) using a BG39 filter. A preheat of 260°C for 10 s and a preheat of 350°C for 10 s was used based on T_{max}-T_{stop} analysis was used to remove the contribution from shallow traps, which generally overpowers the signal from higher temperature peaks (>300°C) (Spooner and Questiaux, 2000). Multiple aliquot additive dose (MAAD) response curves were obtained using mass normalized integrated TL intensity in 340-380°C temperature range. The MAAD protocol ensures the measurement of samples at similar sensitivity. The measurement protocol is provided in Table 4.1. Three aliquots were measured for each dose point. $2D_0$ was calculated. Figure 4.5 shows the DRC comparison for a preheat temperature of 260°C and 350°C and the $2D_0$ is 9.2 ± 1.3 and 13.3 ± 1 kGy respectively. The saturation dose is found to increase by 40% in the case when higher preheat is used. This suggests that there are multiple traps contributing to TL signal in quartz above 300°C. Traps beyond 200°C could not be distinguished in Figure 4.3 because of the overpowering intensity from 350°C peak. For deep traps having peak temperature > 350°C the saturation dose is significantly higher (Figure 4.5). Presence of multiple traps with different saturation characteristics, results in continuous increase in intensity of deeper traps even after comparatively shallow traps are saturated resulting in shift of peak maxima towards higher temperature.

Table 4-1 Protocol to measure the dose response curve (DRC)

Sl. No.	Operation	Remarks
1.	Dose (1-21kGy)	Laboratory doses for DRC
2.	Preheat 260 ℃ for 10 sec	Removal of shallow traps
3.	Test Dose (21 Gy)	Dose for zero glow normalization
4.	TL 450 ℃ (@ 2℃/s)	Luminescence intensity
5.	Mass normalization	

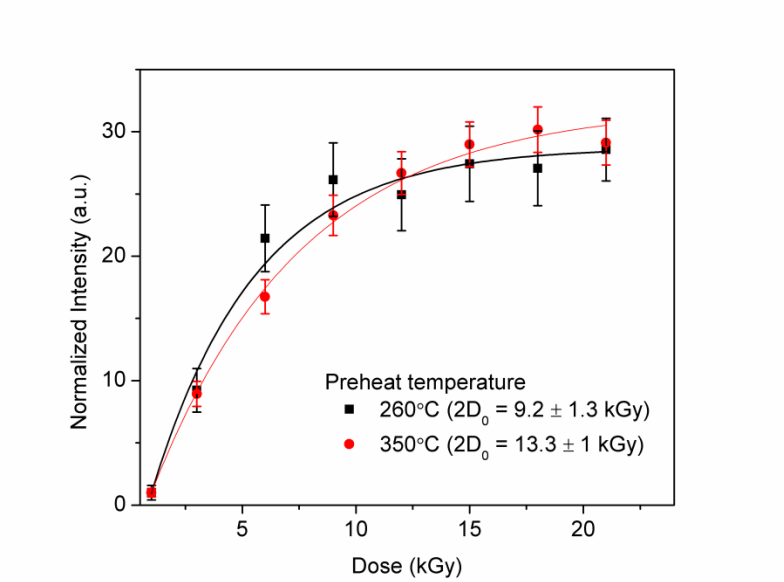

Figure 4-5 : DRC of sample YS-5 for different preheat. Intensity is integrated from 250°C-450°C and is normalized by mass and counts corresponding to 1kGy dose in both case. Each point in graph is an average of measurement on 3 aliquots. Measurements made in visible spectral range 325-700nm.

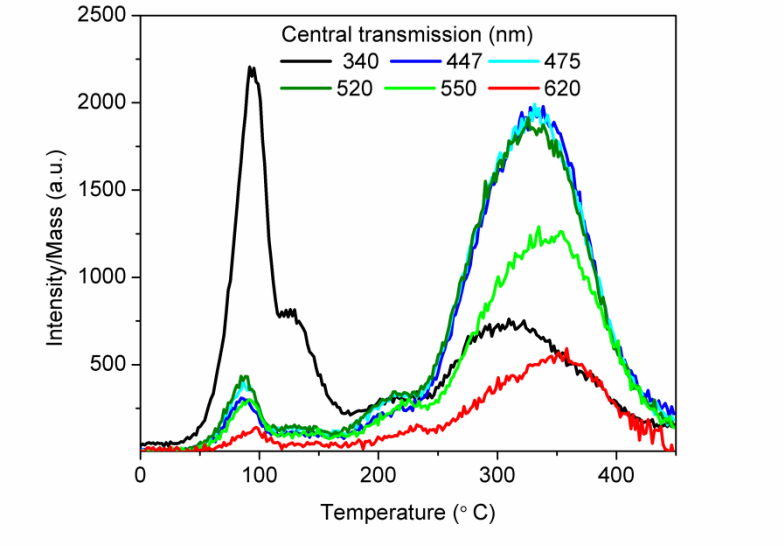

Figure 4-6 TL glow curves of sample YS-5 in different transmission bands. An irradiation of 1000 Gy is given and on measurement after a preheat of 260°C, 10 s, a small dose of 21 Gy is given for zero glow normalization. The intensity of the curves is not to be compared, because of differences in transmitivity, PMT efficiency and diameter of the filters.

4.5. Multi-Spectral studies

As quartz TL is of complex nature, consisting of several traps and recombination centre, it is essential to select and confine measurements for one emission and trap centre combination for dose estimations. This is needed unless it is established that all emissions behave in the same way with the dose. In this study, the luminescence spectral characteristics are measured using different filter combination spanning the full transmission range from UV to red (300-660 nm).

4.5.1. Thermoluminescence glow curves

Multi-spectral studies were carried out using various bandpass filters (details in Table 2.2). The variation of TL response in different transmission bands was studied for the sample YS-5 for an irradiation dose of 1 kGy and a test dose of 21 Gy (zero glow) by heating linearly up to 450°C at a rate of 2°C/s. Following this, the dose response curve (DRC) is obtained for high radiation dose as per section 4.4, in various spectral regions and $2D_0$ was estimated.

Figure 4.6 shows the glow curves for the sample YS-5 irradiated with 1 kGy dose in different transmission bands. The low-temperature peak is most prominent in UV emission for 21 Gy test dose and the ratio of low temperature peak (110℃) to high temperature peak (>300°C) decrease as the spectral emission wavelength increases. After a TL 450°C wash (Figure 4.7),t is observed that the high-temperature peak (>300°C) has emissions in all selected spectral bands. However, the relative intensity of low-temperature peak w.r.t. high-temperature peak varies. The ratio is lower for higher wavelengths and maximum for the UV emission (340± 40 nm).

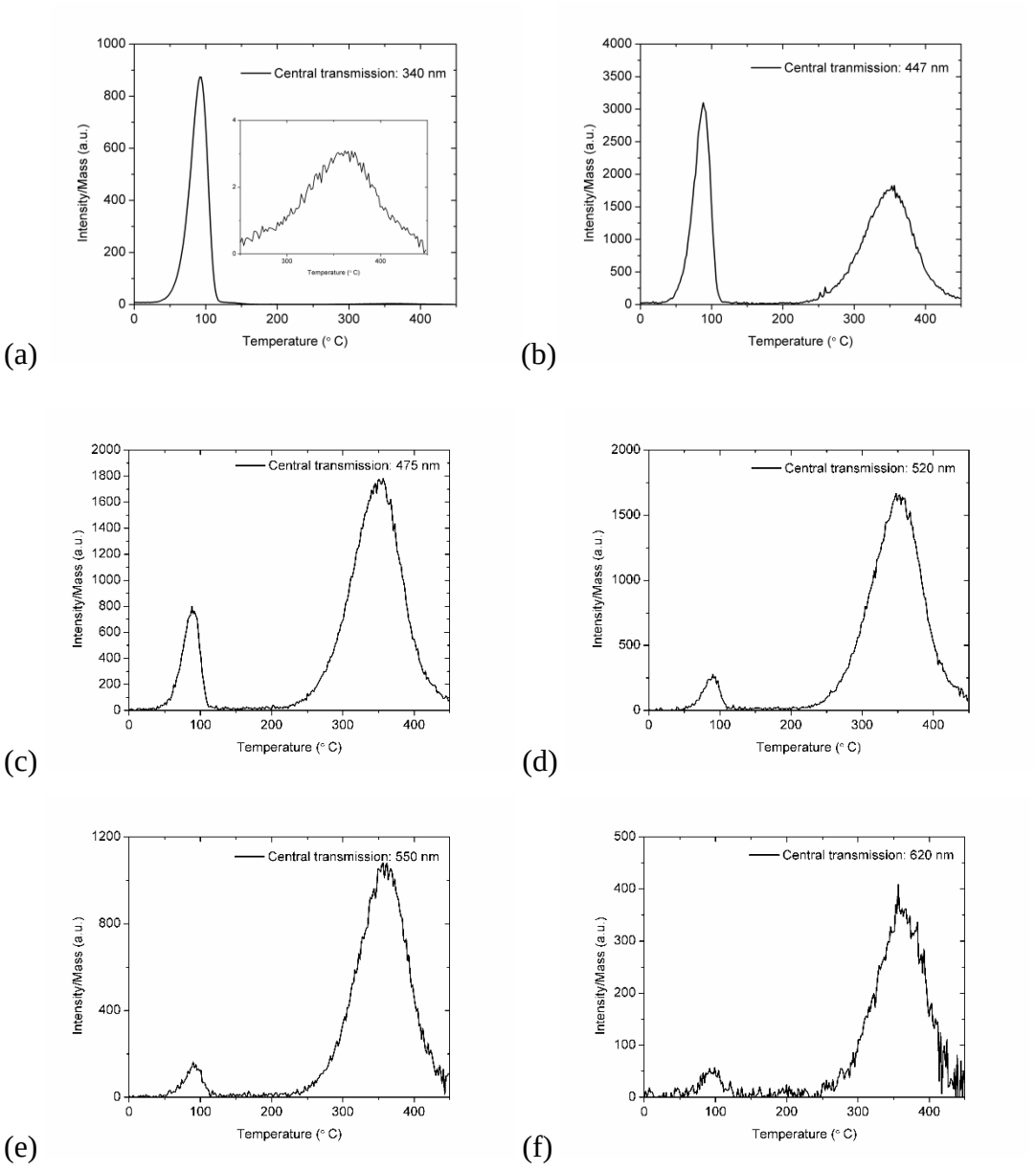

Figure 4-7 Thermoluminescence glow curves of sample YS-5 in different transmissions. An irradiation dose of 21 Gy is given to bleached aliquots (heated to 450°C) in each case and TL glow is measured at 2°C/s. The aliquots were previously irradiated with 1000 Gy. The central wavelength of filter transmissions is (a) 340 nm (b) 447 nm (c) 475 nm (d) 520 nm (e) 550 nm (f) 620 nm.

4.5.2. **Dose response curves**

The DRC in different spectral transmissions are shown in Figure 4.8 for sample YS-5. All the DRCs have $2D_0$ within 2σ (Grey Band) of the mean 11 kGy as shown in Figure 4.9. DRC for all emissions for annealed RQ-1 are shown in Figure 4.10. It shows a similar linear increase with dose in all emissions and no saturation is observed.

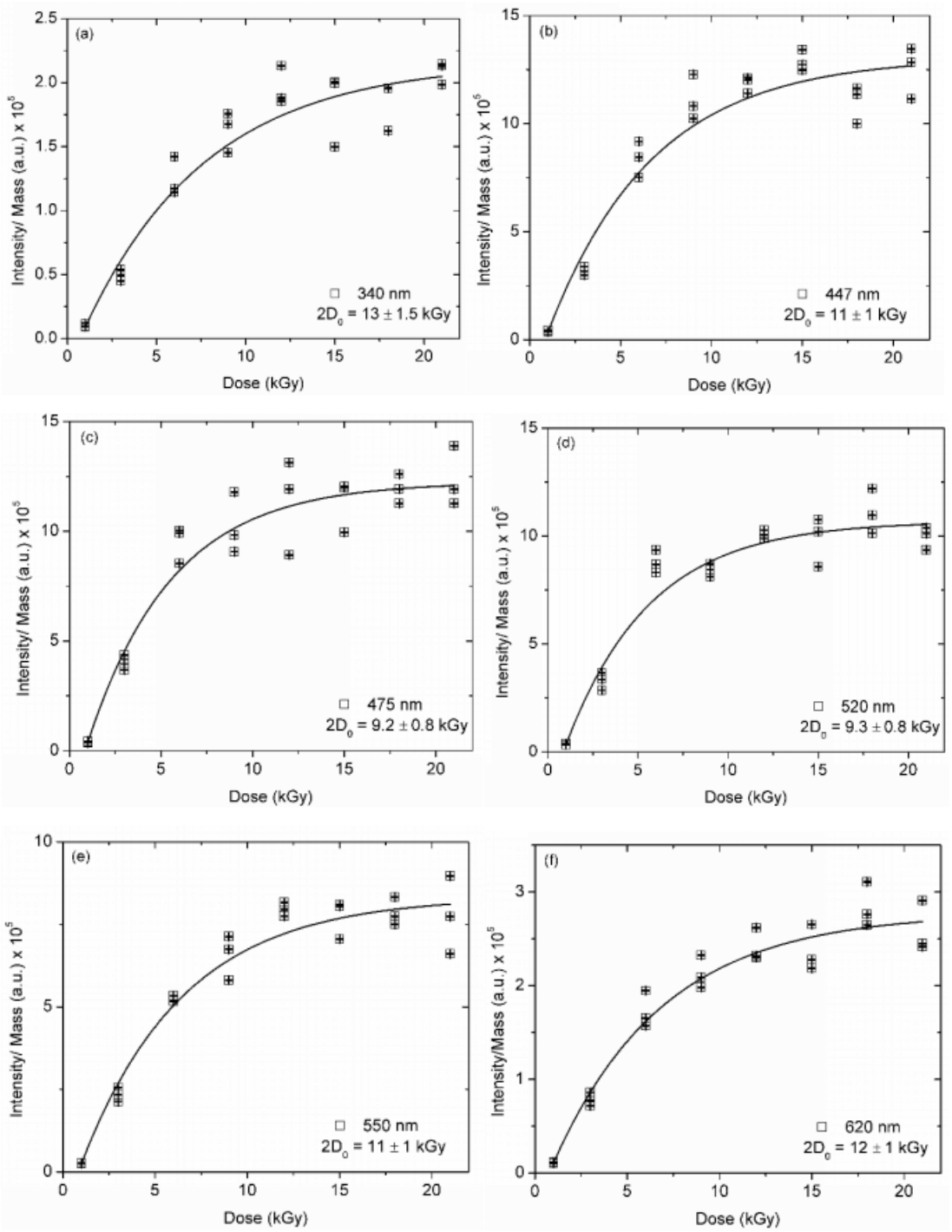

Figure 4-8 The dose response curves of sample YS-5 different spectral windows for 340-380°C peak, normalized by mass.

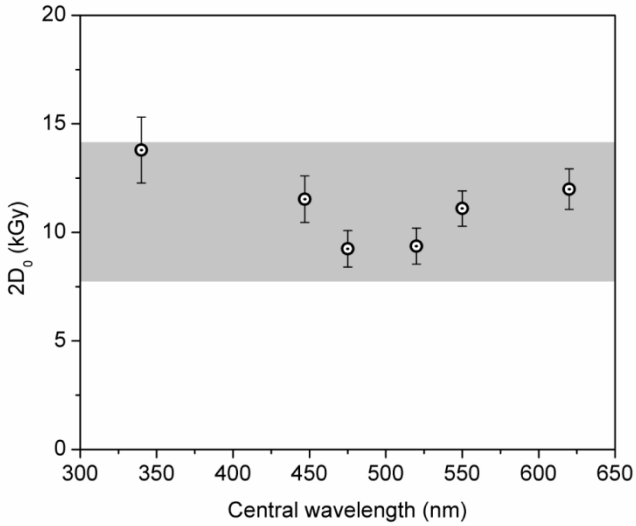

Figure 4-9 Plot of TL saturation dose ($2D_0$ (kGy)) for different emission wavelengths for the sample YS-5.

Figure 4.8 - 4.10 shows that the saturation dose ($2D_0$) is similar for all emissions within 2sigma of the mean. The similar saturation dose in all emissions suggests that for measured samples possibly recombination centres are not influencing dose saturation and it is mainly controlled by the charge population of trapping centre. Possibly, there is an excess of recombination centres, thus sufficient numbers are available for all the emission bands. The saturation dose previously reported for red TL agrees with our results (Westaway and Roberts, 2006). Some works also report an increase in TL intensity in blue and red up to doses of the order of 10 kGy (Corpusculatre, 1991; Hashimoto et al., 1987; Hunter et al., 2018; Schmidt and Woda, 2019). Besides this, study using the optically and thermally stimulated electrons (OSE and TSE) (Ankjærgaard et al., 2006) have shown that trapping centres in quartz do not saturate till 10 kGy and may even go beyond that. Study by Lowick et al., (2010) on TL also shows an increasing luminescence emission in both blue and UV until 1.2 kGy, which was the maximum dose studied. Some other studies using MAAD also suggest saturation in kGy (Durrani et al., 1977; Sawakuchi and Okuno, 2004). Hence, it can be concluded that MAAD TL signals have very high saturation ~ 10 kGy for the samples under study and are consistent with previous works.

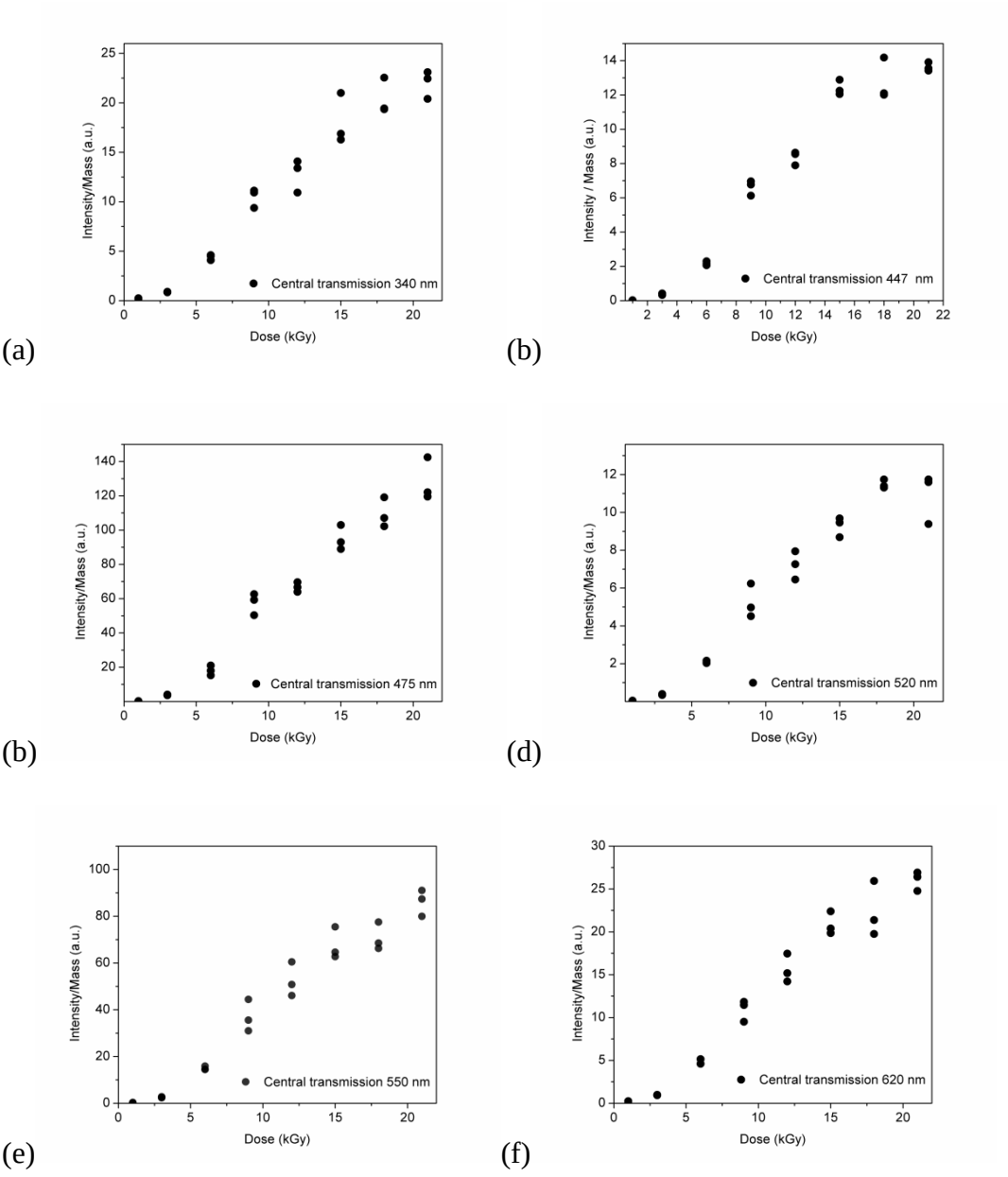

Figure 4-10 The dose response of sample RQ-1 in different spectral regions.

4.5.3. **Signal resetting by sunlight**

For dating applications, an important requirement for any signal is its resetting before burial by sunlight or heat or the reduction of signal to residual level before burial. The TL dating method can be applied to sunlight resettable events by subtracting the residual dose found by laboratory experiments (Singhvi and Mejdahl, 1985). Thus, bleachability of different TL spectral bands by sunlight and the magnitude of the residuals was investigated. The aliquots of naturally irradiated quartz sample KG-1 were exposed to

sunlight for different time periods of 30 s, 1 min, 10 min, 30 min, 1 hour, 2 hour and 3 hour. Their respective TL responses were measured following sunlight exposure.

Figure 4.11 shows the effect of sunlight exposure on TL intensity of the sample KG-1, in various spectral regions. The mass normalized TL signal of bleached aliquot is further normalized by the mass normalized counts of non-exposed aliquot. The counts in red emission in present setup are an order less than other emissions, thus has larger error. The high-temperature region is further divided into two regions with 320-330°C and 370-380°C, integrated mass normalized counts in these regions are plotted. The bleachability of the region 370-380°C is less than 320-330°C. This accord with earlier observations (Wintle, 1997). Further, it is found to decrease with increasing emission wavelength. The red signal is found to be the least bleachable for both regions. It is observed with decrease in the energy of output luminescence emission, the extent of resetting/bleachability decreases (Figure 4.11(a) and 4.11(b)) suggesting role of recombination centres in governing extend of bleachablity. Thus, UV emissions has the least residuals (most bleachable) and red has the maximum residual (least bleachable). Possibly, the charges in the recombination centres associated with higher wavelength emission (i.e., red emission) are tightly bound and are thus slow to bleach. The results are consistent with the previous findings on blue and UV TL (Singhvi et al., 1982), red TL (Lai and Murray, 2006; Miallier et al., 1994). It will be interesting to further explore the mechanism governing this trend. The results suggest that the role of recombination centre is undermine and needs more attention.

4.6. **Sensitivity normalization**

For inter-aliquot comparisons proper normalization of signal corresponding to a given dose is required. It may include normalization by mass, which assumes homogeneity in luminescence sensitivity of the grains throughout the sample, or by luminescence response of same or another peak, which assumes the signal to be proportional to mass or dosimetric signal being used and takes care of sensitivity fluctuations during measurements. These methods are well tested and characterized for low doses, but are yet not investigated for high radiation doses and needs to be verified for high radiation doses.

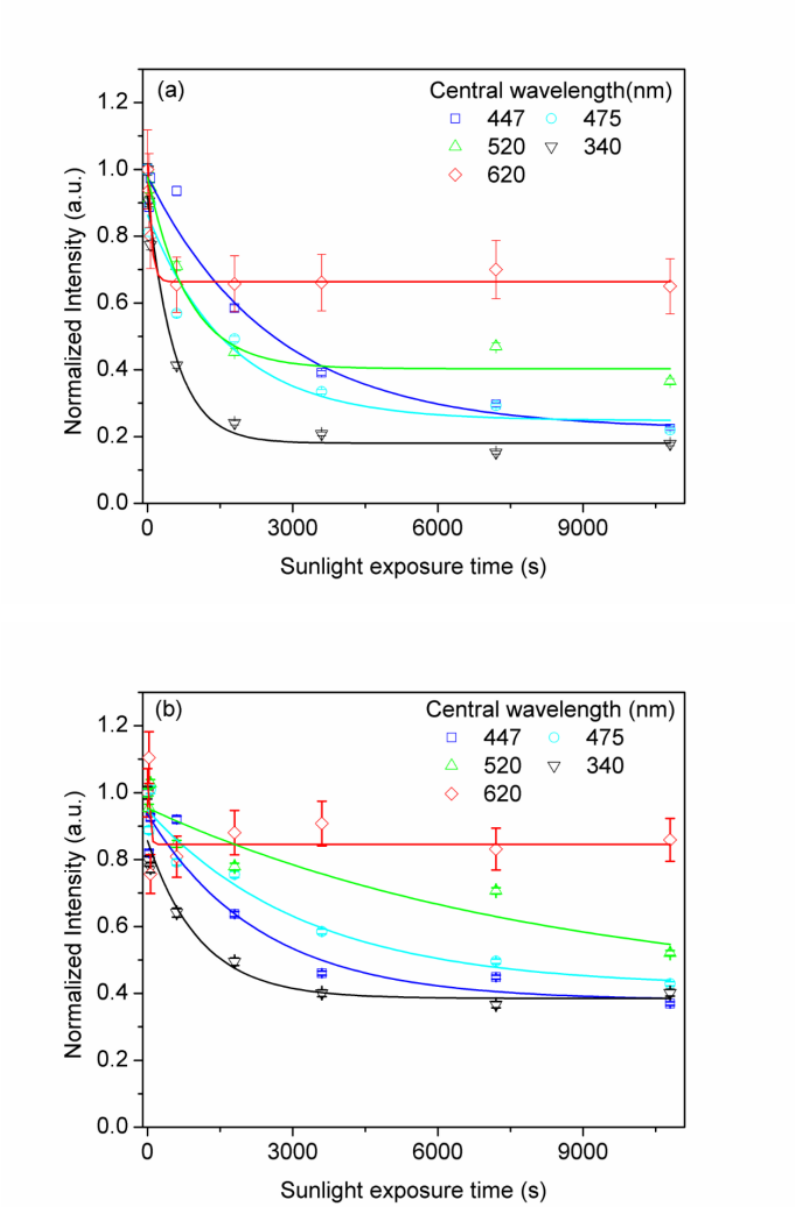

Figure 4-11 Signal bleachability of (a) 320-330°C region, (b) 370-380°C peak, of sample KG-1 exposed to sunlight for different time period.

Hence, the zero glow and second glow normalized signal corresponding to a test dose of 21Gy were compared with mass normalized signal as per protocol given in Table 4.2. The zero glow normalization was obtained by dividing the integrated TL1 signal intensity in the range 340-380°C with the integrated TL1 intensity in the range of 80-100°C. Similarly, in the second glow normalization the integrated TL1 intensity in range 340-380°C is normalized with the integrated TL2 intensity in range 80-100°C, obtained after test dose TD2.

Table 4-2 Protocol to study various normalization method.

Step no.	Operation	Remarks
1	Fresh sample	
2	Irradiation with variable high radiation doses to different batches in range 1 to 21 kGy	
3	Preheat 260°C (10s)	
4	Test dose (TD1) 21 Gy	
5	TL 450°C (@ 2°C/s)	TL1 (recording the zero glow 110°C and first glow 340-380°C peak signal)
6	Test dose (TD2) 21 Gy	
7	TL 450°C (@2°C/s)	TL2 (recording the second glow 110°C peak signal)

Figure 4.12 shows the comparison of DRC for signal normalized by mass, zero glow and second glow TL signals for the sample YS-5 in visible emission (325-700 nm). Normalization results for specific emission bands are shown in Figure 4.13. The $2D_0$ of 11 ± 1 kGy, 143 ± 55 kGy, 19.6 ± 2.6 kGy for mass normalization, zero glow normalization and second glow normalization are obtained respectively. Zero glow normalization shows linear increase with dose and no saturation is observed. Such huge differences implicate caution during normalization. The deviations from the expected trends suggest that 110°C and 340-380°C peak does not respond to dose in similar manner. The increase in the zero glow normalized intensity beyond weight normalized intensity in the Figure 4.12 & 4.13 is a consequence of decrease in the 110°C TL intensity with dose as shown in Figure 3.3(a). This is due to quenching of zero glow 110°C signal during high dose irradiation as predicted by some earlier works (Zimmerman, 1971) when a high dose is present in the high temperature (340-380°C) traps. The trap competition can significantly affect the normalization process. It is to be noted that during zero glow normalization irradiation fills charges in traps corresponding to 110°C peak when high temperature peaks (340-380°C) are filled. On the other hand, for second glow normalization, irradiation fills 110°C traps while high temperature traps are empty. Thus choice of normalization technique at high doses should be chosen with caution. In present case weight normalization is found to provide better results as shown in Figure 4.12 & 4.13. This is because mass normalization is not affected by the characteristics of any other trap.

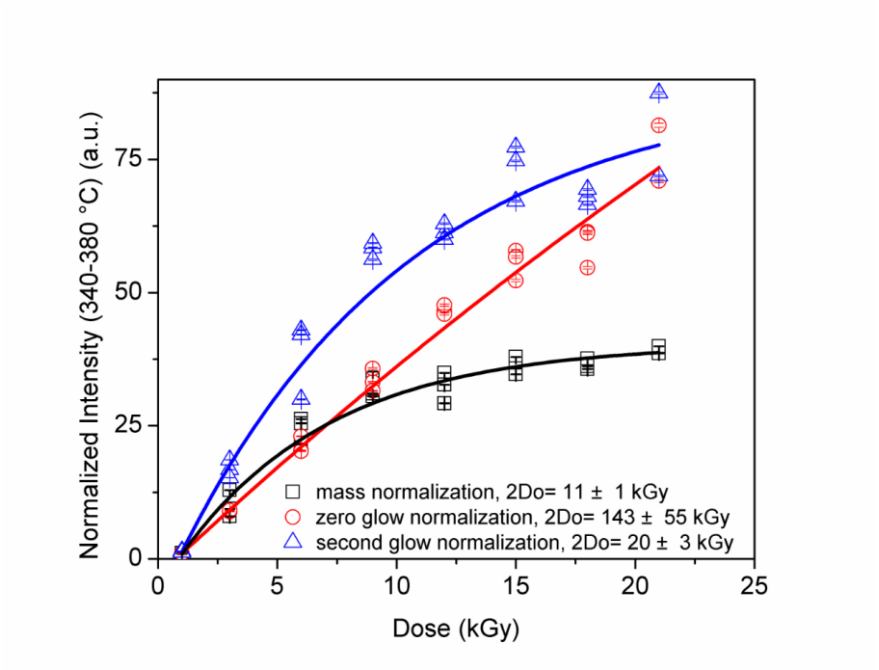

Figure 4-12 Dose response curve of sample YS-5 with different normalization technique. The counts are integrated from 340- 380°C temperature range. The graph has been normalized by the counts of 1 kGy dose. Measurements made in visible spectral range 325-700 nm.

(a)

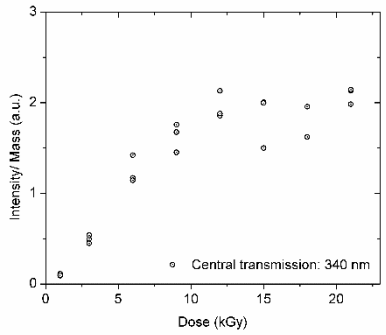

(b)

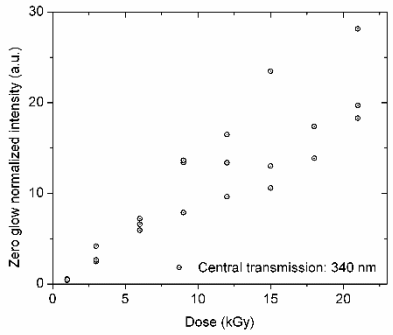

(c)

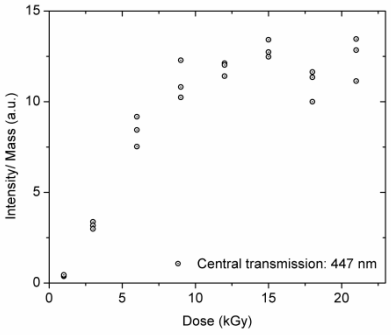

(d)

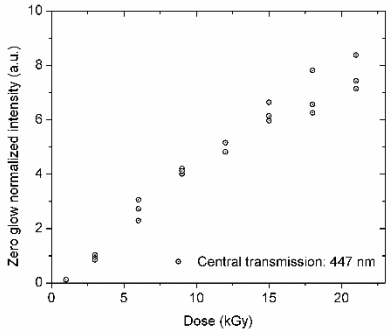

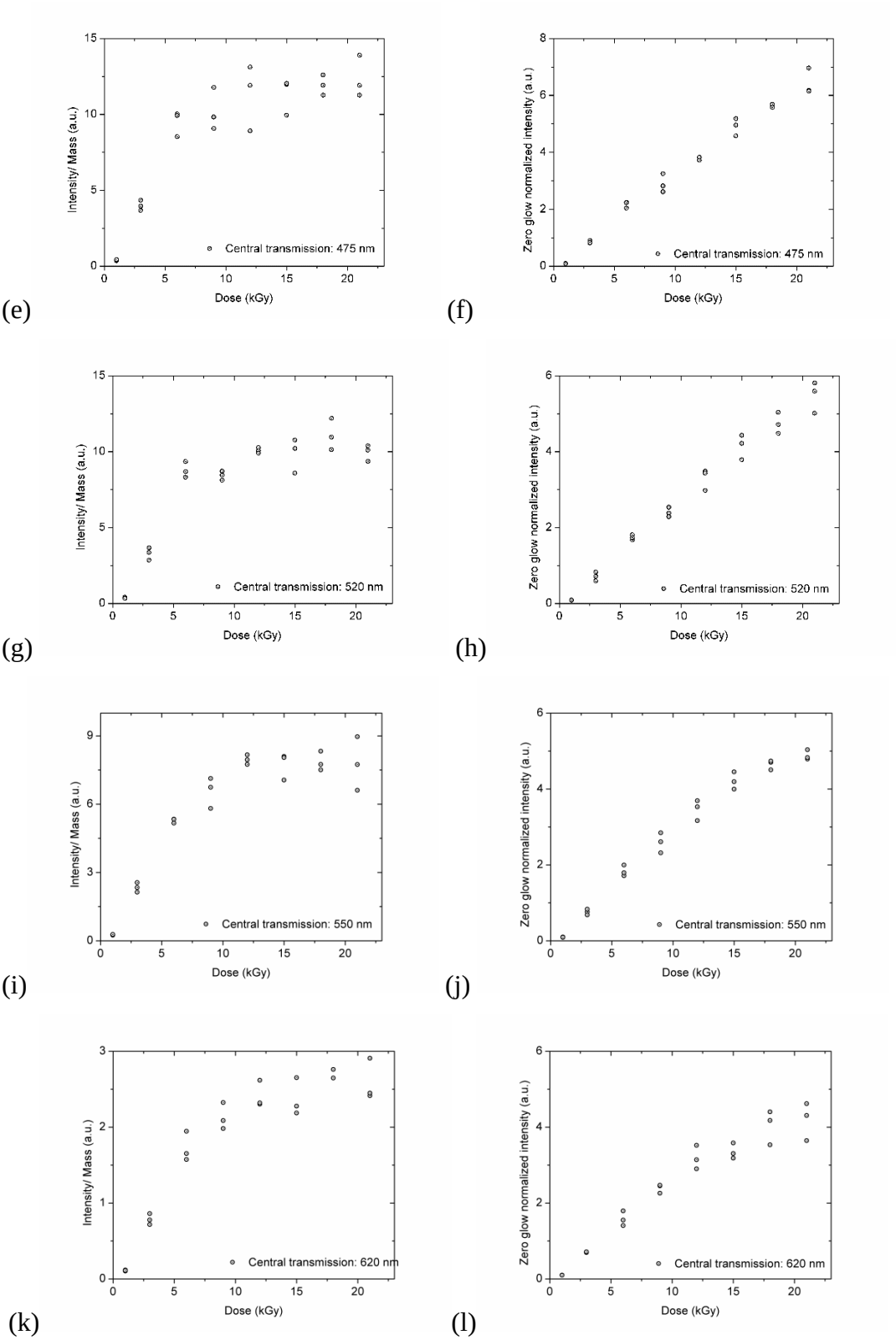

Figure 4-13 The dose response curve of sample YS-5 at high doses in different luminescence transmissions. The graphs a,c,e,g,i and k are mass normalized, whereas the graphs b,d,f,h, j and l are zero glow normalized.

4.7. **High radiation predose (HRpD) effect**

Here high radiation predose (HRpD) effect implies the effect of dose given in previous measurement cycle and is being propagated to its next measurements. Effect of HRpDs on the TL signals of the samples was studied by examining the TL intensity of various trapping and recombination centres. Fresh samples were divided into 8 batches and each batch was given a different dose in range 1-21 kGy followed by TL wash up to 450°C to remove signal stored due to this dose. Then an identical dose was given to all batches followed by TL measurement (Table 4.3). The measurements were made in various wavelength bands to see the characteristics of various recombination centres.

Table 4-3 Protocol to measure the HRpDs response of various peaks of quartz in different wavelength range.

Step no.	Operation	Remarks
1	Fresh sample (8 Batches)	
2	Irradiation with variable high radiation doses to different batches in range 1 to 21 kGy	(X-axis)
3	TL 450°C (@ 2°C/s)	
4	Same test dose 34 Gy to all aliquot	
5	TL 450°C (@ 2°C/s)	Y-axis (Observations using different detection filters)

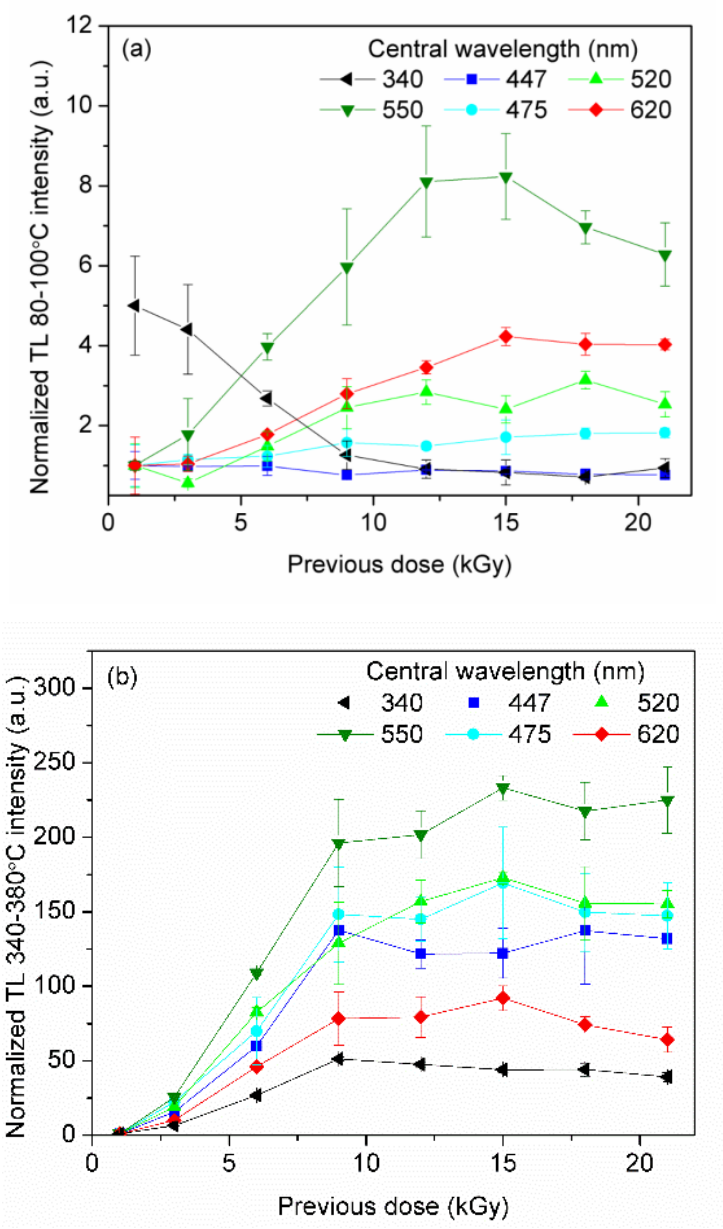

Figure 4-14 The response of sample RQ-1 (a) 80-100 °C peak counts (b) 340-380°C peak counts, to a test dose of 34 Gy after the previous high dose was followed by heating to 450 °C as per table 4.3. The legends give the transmission in different filters.

The results for HRpD experiment (Table 4.3) on sample RQ-1 are shown in Figure 4.14(a) and 4.14(b). The 340-380°C peak intensity for a 34 Gy test dose is dependent on the HRpD. This dependence is observed in all emission bands. For low doses, intensity first increases with previous dose and then saturates after 10 kGy dose. Similarly, for the low-temperature peak, the intensity for the same 34 Gy test dose is dependent on the previous dose except for the blue emission. The low-temperature UV emission, sensitivity decreases with increase in HRpD and around 10 kGy becomes constant. For low-

temperature 447 and 475 nm emission bands, sensitivity has negligible dependence on HRpD. However, for 520, 550 and 620 nm emission, low-temperature peak intensity increases with HRpD. Some centers like UV emissions are quenched by high dose, while blue is unaffected and further green and red are enhanced. Similarly, the 340-380°C TL sensitivity is also affected, but in similar manner.

4.8. **Conclusions**

Till date, the use of quartz for dosimetry and dating is limited to a dose of ~250 Gy (Chawla et al., 1998; Fleming, 1969; Huntley et al., 1996) using conventional UV emission. It is however observed by several researchers that the TL signals increases even further (Durrani et al., 1977; Sawakuchi and Okuno, 2004; Schmidt and Woda, 2019) and generally considered as new centre creation region, but dedicated studies are limited. The lack of understanding related to luminescence response of quartz for high doses limits the potential of using these signals in practice. Present work provides new insights for investigation of luminescence mechanism of quartz. Quartz has the potential to estimate doses 50-100 times the present limit. The work enhances on the role of recombination centers in the luminescence mechanism, which previously is not stressed upon. In particular, it is observed that all luminescence emissions from UV to red have high saturation and their signals reduce to constant residual levels during sun exposure. However, extend of residual is depend on luminescence emission and luminescence sensitivity of different emissions after predose changes. Further, due to effects such as dose quenching, normalization techniques should be used carefully. Mass/weight normalization appears to be best for normalization for doses in excess of 1 kGy. Several interesting results are observed as stated above and are discussed below.

This study leads to the following major conclusion

1. TL signal in 340-380°C temperature range of quartz is seen to increase with doses up to 18 kGy for rock quartz and around 10 kGy for sedimentary quartz in the spectral range of 325-700 nm.
2. The peak shift observed in 300-450°C range is a result of different saturation characteristics of traps present in 300-450°C range.

3. The spectral analysis of the luminescence emission signifies that the trapping centres are majorly responsible for saturation in the samples and the saturation dose is similar within error for the output wavelength from UV to red.
4. The bleachablity of signal is found to be anticorrelated with wavelength of luminescence emission and mechanism need to be further probed.
5. Zero glow and second glow normalization does not correct for sensitivity changes at high doses and weight normalization should be used.
6. Predose effect shows that high dose history enhances the sensitivity of all emissions in the 340-380°C temperature range and green and red 110°C emissions, while there is a quenching of the UV 110°C and blue 110°C is independent of predose effects.

Chapter 5: Dosimetry using BSL for High Radiation Doses

5.1. Introduction

Previous chapters investigated the high dose (>1kGy) TL characteristics of quartz. Therein, it was observed that the TL saturates at ~ 10-18 kGy (Figure 3.4-3.6). Further multi-spectral analysis showed that saturation is majorly dependent on the trapping centres and not on emission centres (Figure 4.8-4.10). Thus, the UV emission also showed a saturation around 10 kGy in TL emission. However, blue stimulated luminescence (BSL) from quartz saturates around 250 Gy (Chawla et al., 1998; Duller, 2008; Wintle, 2008; Wintle and Murray, 2006). This suggests that there exists a 40-80 times difference in the saturation of BSL and TL. It is expected that the BSL will saturate earlier than the TL, as all BSL traps are TL traps but vice-versa is not true. Still, it doesn't explain this huge difference in saturation doses.

BSL is the most widely used signal for luminescence dating. It has the best bleachability of all signals and no fading. The trapped electrons are stimulated by 470 ± 30 nm wavelength and detection is made in 340 ± 40 nm (UV) wavelength. The measured OSL signal is related to be coming from 325 °C TL trap (Murray and Wintle, 2000a) and have a thermal stability of $10^{7\text{-}8}$ years making it suitable for dating atleast upto million years (Biernacka et al., 2022a). The dose estimates are generally made using single aliquot regenerative (SAR) protocol which provides a scope to study the distribution in doses and hence understand the bleachability of the depositional environment (Roberts et al., 1999). Many research works report that at high radiation doses (~> 250Gy), paleodoses are underestimated by SAR (Dreimanis et al., 1978; Sally E Lowick et al., 2010; Lowick and Preusser, 2011; Y C㎡ Lu et al., 2007; Murray et al., 2007; Prescott and Robertson, 1997; Qin and Zhou, 2009; Timar-Gabor and Wintle, 2013; Wang et al., 2021). The SAR procedure provides reliable dose estimate for doses upto ~250-300 Gy for quartz, after which signal saturates and do not increase with further increase in dose. However, some

research works suggested that signal of quartz increase beyond ~250 Gy and the DRC is better fitted with single + saturating exponential (Chapot et al., 2012; Timar-Gabor et al., 2012). Further, our investigations on TL (Chapter 4) suggested that the normalization methods that work at low radiation doses, does not work at high radiations (>1 kGy) due to disproportionate variation of normalizing signals. Thus, it is important to investigate the validity of SAR protocol and normalization procedure adopted in SAR for higher radiation doses (HRDs).

In order to understand the cause of underestimation, previously many experiments were done to measure anomalous fading, thermal instability, saturation of natural signal, stepped irradiation (Bonde et al., 2001; Li and Li, 2006; Qin and Zhou, 2009; Singhvi et al., 2011; Yoshida et al., 2000) and other parameter and their correlation with underestimation was studied. Most of these factors are associated with the processes that occur in nature. However, there are studies that show the role of laboratory procedures could also result in paleodose underestimation. Previously, Wang et al., (2021) have shown that multiple aliquot regeneration (MAR) protocol can be used to extend the dating limits for quartz. Similarly, Zhang and Tsukamoto, (2022) have shown on feldspar, that protocol used for estimation of D_e affects the upper range to which the date can be estimated. Since, different signals (VSL, TT-OSL, etc.) originate from different traps inside the crystal, the consecutive maximum dose that can be estimated with them can vary. However, for the same signal the dependency of the laboratory protocol on the maximum dose or the paleodose should not exist and is not understood.

Hence, the present chapter investigates the saturation of BSL signal and its dependence on various experimental parameters and protocols is investigated, to answer some of these questions. BSL characteristics at doses greater than SAR saturation (~ 250 Gy) is studied and hence for clarity doses greater than 250 Gy are defined as DGSS (doses greater than SAR saturation) thoughout the chapter.

5.2. **Samples**

Five quartz samples were used in the study. Sample RQ-1 is described in earlier chapters. The sensitivity of RQ-1 is low. PRL-1 is a flood deposited sedimentary sample of high sensitivity from Bharathpuzha basin, Southern India (10° 46' 44.0292" N, 76° 34' 30.36"

E). A natural dose of 21.5 Gy was present in PRL-1. MS-BCFA (30° 48.200'N, 76° 55.707'E) and MS-BCFB (30° 48.290'N 76° 56.126'E), are sedimentary deposit in the boulder conglomerate formation of upper Shivaliks, in Northern India. MS-BCFA and MS-BCFB are found to be in dose saturation in SAR BSL. YS11 (28° 53' 52.90" N, 77° 13' 59.90" E) is a surface sedimentary samples of the Yamuna river basin, India and hence have a zero dose. IR depletion ratio was estimated for the samples to check for the feldspar contamination at various doses (Duller, 2003) and was found to be negligible.

Table 5-1Sample details

Sr. No.	Sample name	Latitude, Longitude	Provenance	Remarks
1.	RQ-1	24°29'12"N, 73°13'18"E	Sabarmati basin, Western India	Rock sample
2.	PRL-1	10° 46' 44.03" N, 76° 34' 30.36" E	Bharathpuzha basin, Southern India	Bright sedimentary sample; flood deposit; natural dose 21.5 Gy
3.	MS-BCFA	30° 48.200'N, 76° 55.707'E	Boulder Conglomerate Formation, Shivaliks, Northern India	Natural signal in saturation in SAR, independent age from paleomagnetic study
4.	MS-BCFB	30° 48.290'N, 76° 56.126'E	Boulder Conglomerate Formation, Shivaliks, Northern India	Natural signal in saturation in SAR, independent age from paleomagnetic study
5.	YS11	28° 53' 52.90" N, 77° 13' 59.90" E	Yamuna Basin, Indo-gangetic plain, India	Dull sedimentary sample

5.3. Measurements

Throughout the experiments, the fast component of the BSL signal is investigated using early background subtraction method. In this, 0.2 s to 1 s is used as signal and 2.88 s to 4 s is taken as background. Further, the dose response curve (DRC) is fitted with single saturating exponential equation, until mentioned otherwise i.e., $I = I_0(1 - e^{-(\frac{D}{D_0})})$, with I_0 as the saturation intensity and D_0 as the characteristics dose and $2D_0$ is the saturation dose.

5.3.1. Multiple Aliquot Additive Dose (MAAD) measurements

For the MAAD measurements, set of 5 aliquots (3, if inter-aliquot scatter is less) are taken for each dose point measurements. The mass of sample on each aliquot is carefully measured to a precision of 0.01mg. Each set is given a known dose. BSL measurements

are done at 125°C for 40 s after preheating to 220 or 240°C for 10 s. The luminescence emission measurements were done in ultraviolet (340 ± 40 nm) using Hoya U-340 filter. The measurement protocol steps are tabulated in Table 5.2. The saturation dose is estimated by fitting the dose response curve to observed signal.

Table 5-2 Protocol used in MAAD and SAR BSL DRC.

Step No.	**MAAD BSL**	**SAR BSL (Murray et al 2006)**
1	Natural sample + (additive doses)	Natural sample
2	Preheat (220-260 °C)	Preheat (220-260 °C)
3	OSL at 125 ºC (Li)	OSL at 125 ºC (Li)
4	Mass normalized	Test dose (Dt)
5		Preheat (220-260°C)
6		OSL at 125 ºC (Ti)
7		Blue bleach 200 ºC for 100 s
8		Regenerative dose (Ri)
9		Go to step 2

5.3.2. Single Aliquot Regeneration (SAR) measurements

The SAR (Murray and Wintle, 2000a) measurements are done on single aliquots using test dose sensitivity normalization as per protocol given in Table 5.2. BSL signal at 125°C for 40 sec is measured after preheating samples aliquots to 220-240°C for 10 sec. A test dose signal for a dose of 40 Gy is used to monitor and correct luminescence signal for the sensitivity changes during measurements. A hot bleach of BSL at 200°C for 40 sec is used to remove any signal in between the SAR cycles. A 0 Gy dose is used to measure the recuperation and a repetitive dose is used to measure the recycling. Any aliquot having recuperation > 5% or recycling ratio higher or lower than 10% of unity is discarded. Saturation dose is obtained after fitting the DRC with single saturating exponential. Following these, experiments were conducted to investigate the effect of test dose on saturation dose.

5.3.3. Effect of Regeneration Dose on Test Dose signal

In this, experiments to investigate the effect of regeneration dose on test dose signals were carried out. The details of experiments are given below.

1. The variation of test dose signal (T_X/T_N) for 2 constant alternately repetitive high and low regeneration doses during SAR cycle is investigated. The protocol used

is as per Table 5.3. All measurements are normalized w.r.t first test dose signal (T_X/T_N).

Table 5-3 Protocol used for TX/TN ratio variation.

Step No	**Measurement**
1	Regenerative dose 426 Gy
2	Preheat (220-260 °C)
3	OSL at 125 ºC (Li)
4	Test dose (8.5 Gy)
5	Preheat (220-260 °C)
6	OSL at 125 ºC (Ti)
7	Blue bleach 200 ºC for 100 s
8	Regenerative dose (8.5 Gy)
9	Preheat (220-260 °C)
10	OSL at 125ºC (Li)
11	Test dose (8.5 Gy)
12	Preheat (220-260 °C)
13	OSL at 125 ºC (Ti)
14	Blue bleach 200 ºC for 100 s
15	Go to step no. 1

2. The effect of variation in test dose on saturation dose is investigated. For this, the increasing test doses viz. 7, 70, 280 and 860 Gy are used in SAR protocol provided in Table 5.2 and respective DRC is constructed.
3. SAR procedures strongly relies on correlation of regeneration and test dose signal. A constant L_X/T_X ratio with SAR cycle for a fixed regeneration and test dose is one of the prerequisites for the use of any test dose correction. The L_X/T_X variation with SAR cycle is studied for high and low regeneration doses. Three sets of regeneration dose (R) and test dose (T) are chosen with R, T as (28, 7), (280, 7) and (860,70) Gy and repetitively measured using SAR procedures.
4. Murray and Roberts, (1998) suggested that 110 °C TL peak counts could also be used to correct for the sensitivity changes as it is correlated with OSL signal. Hence, the use of 110°C TL peak for normalization within the SAR methodology is tested and its effect on saturation is investigated. This DRC is obtained by normalizing the BSL signal (Step 3, Table 5.2) by 110°C peak intensity counts (Step 5, Table 5.2) (emission 340 ± 40 nm). Results of the saturation obtained by this normalization are compared with the standard SAR protocol (Table 5.2).

5. Additionally, experiments were conducted for investigating TL and BSL signals, with and without annealing of samples for identifying their potential for normalization of BSL signals at high radiation doses. It was seen in Chapter 4; (also published as Singhal et al., (2024)), that TL after annealing, blue emission 110°C peak is independent of the predose effect. Hence, BSL, TL in blue emission (400-480 nm), zero glow normalization, are investigated for its dependence on regeneration dose as per protocol given in Table 5.4.

Table 5-4 Protocol to study various signals for suitability as normalization.

Step No	**SAR BSL**	**Measurement**
1	Natural sample	
2	Test dose	
3	TL (220-260 °C)	Zero glow (TL, UV emission)
4	Additive dose	
5	Preheat (220-260 °C), 10 sec	
6	OSL at 125 ºC	L
7	Test dose	
8	TL blue (220-260°C)	TL blue emission
9	OSL at 125 ºC	BSL
10	Heat till 450 °C	
10	Test dose (Dt)	
11	TL Blue (220-260°C)	TL after annealing, blue emission
12	OSL at 125 ºC	BSL after annealing

5.3.4. Saturation and Dose recovery by different protocols

Multiple aliquot regeneration protocol, MAR is used to build the dose response curves and see the saturation of BSL signal. To construct the DRC from zero, the natural sample is bleached in solar lamp for 24 hrs to remove previous signal. Mass normalizations and the normalizations that pass the criteria of being independent of regeneration doses (in previous experiment) are used to construct dose response curve. Further a gamma dose of 1000 Gy given to sample YS11 in February 2023, is recovered using the above MAAD protocol and suitable normalizations in February 2025.

5.4. **Results**

5.4.1. **MAAD versus SAR dose response**

Figure 5.1 shows the BSL shine down curves normalized by mass. It is found that the intensity increases beyond 250 Gy, that is the saturation of SAR. An increase in the medium and slow component is also observed with dose. Figure 5.2 shows the comparison of SAR and MAAD DRC for RQ-1, PRL-1. Results show that the MAAD DRC has higher saturation than the SAR DRC. For RQ-1, the $2D_0$ in MAAD is 1080 ± 90 Gy and SAR is 260 ± 20 Gy. MAAD has a saturation of 4 times higher than SAR. For PRL-1, MAAD $2D_0$ is 2181± 1158 Gy and SAR $2D_0$ is 259 ± 27 Gy, which is also higher.

5.4.1. **Effect of regenerative dose on test dose**

Figure 5.3. show the T_X/T_N variation for RQ-1 and PRL-1. In both the graphs, two trends are visible. An overall linear increase in the sensitivity with the SAR cycle and a systematic change in T_X/T_N ratio in accordance with the regeneration dose alteration. For all high regeneration dose points, the T_X/T_N ratio is higher, than the T_X/T_N corresponding to previous low regeneration dose. Similarly, Figure 5.4 shows the variation of $2D_0$ with test doses. The graphs are normalized by the luminescence intensity corresponding to maximum dose. For the sample RQ-1, saturation dose increases from 120 ± 40 Gy to 408 ± 20 Gy with increasing test dose. Similarly, for the sample PRL-1, the saturation dose increases from 201 ± 8 Gy to 545 ± 27 Gy. Figure 5.5 shows the variation of L_X/T_X for same regeneration and test dose (R,T), with SAR cycle. The luminescence signals are normalized by first L_X/T_X signal. It is observed that when dose for R and T signals is less than DGSS, the L_X/T_X remains constant with constant regeneration dose in SAR cycle. However, for constant regeneration dose > DGSS given in SAR sequence (Table 5.2), L_X/T_X is not constant but decreases with the SAR cycle (Figure 5.5). The decrease is more for higher regeneration doses.

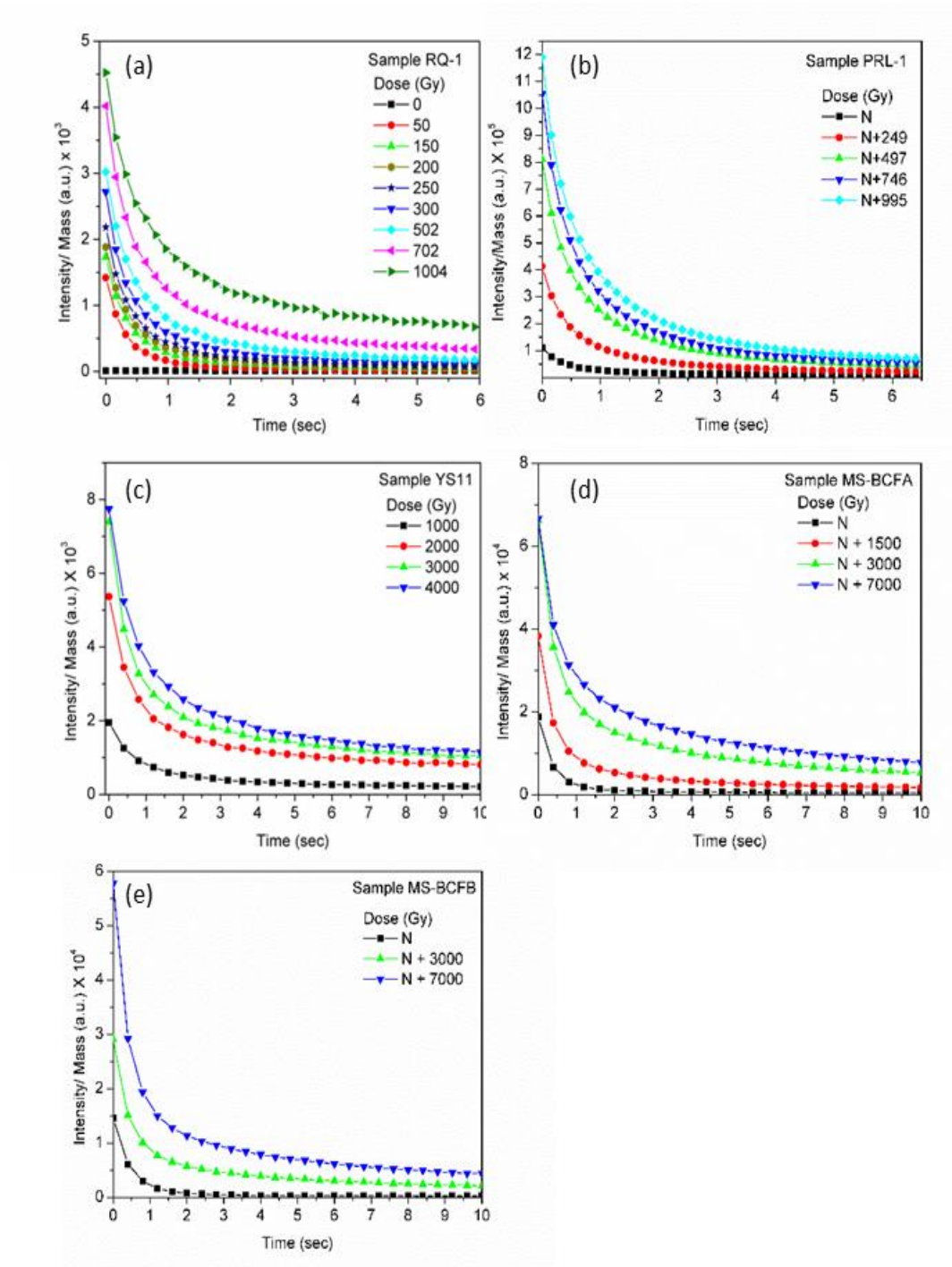

Figure 5-1 Shine down curve of sample (a) RQ-1 and (b) PRL-1 (c) YS11, (d) MS-BCFA, (e) MS-BCFB, normalized by mass and average of 5 aliquot data respectively. RQ-1 is average of 3 aliquots, as the scatter was less. 'N' stands for natural dose (Taken from (Singhal et al., 2025b)*).*

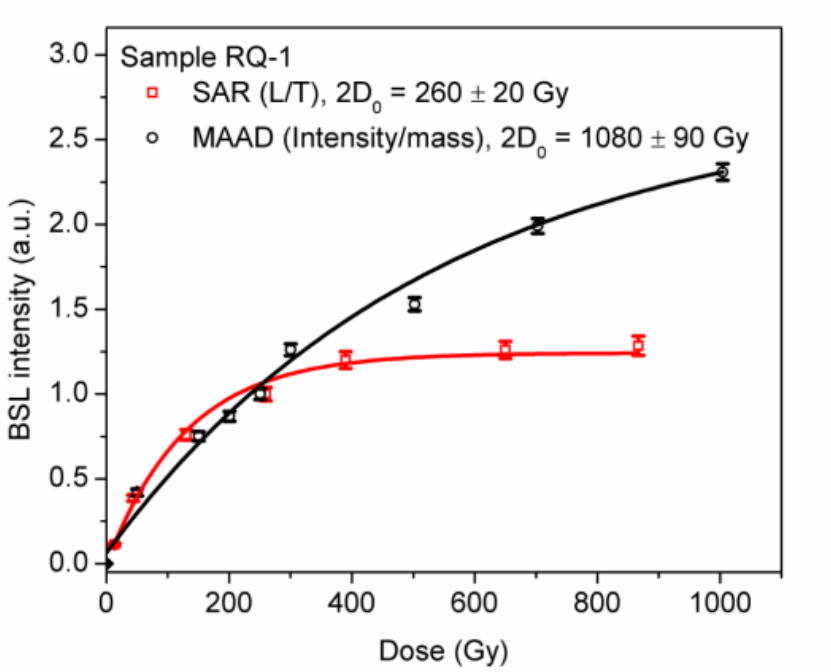

(a)

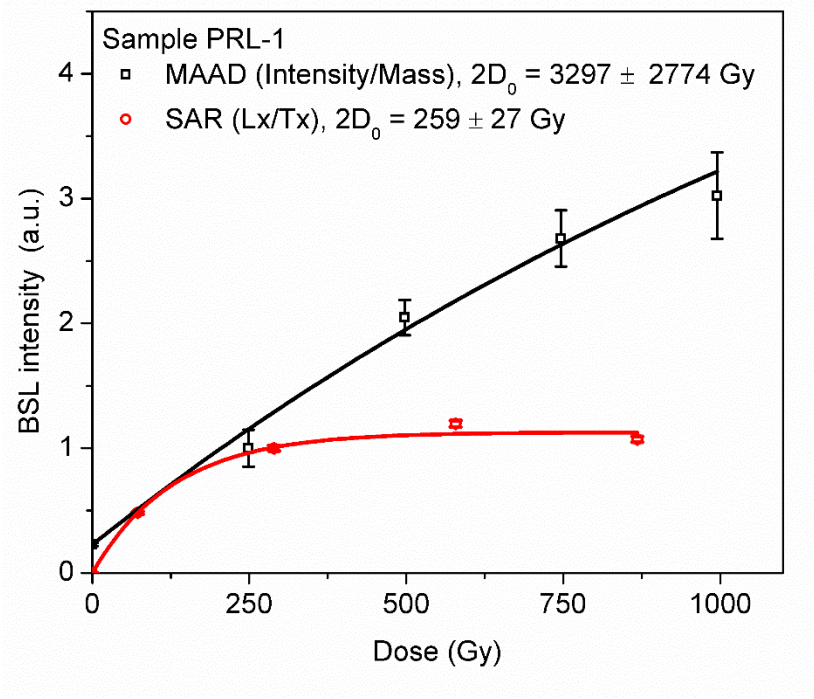

(b)

Figure 5-2 Comparison between MAAD and SAR BSL dose response of sample (a) RQ-1, (b) PRL-1. The saturation dose is obtained by fitting the single saturating exponential equation $I=I_0\,(1-\exp(-(x-x_c)/D_0))$.

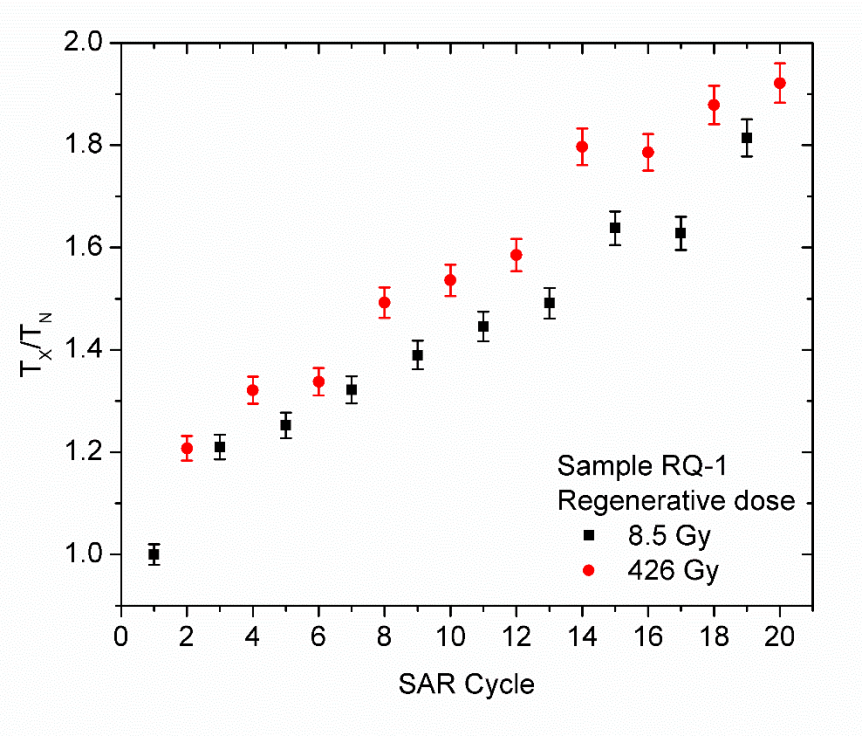

(a)

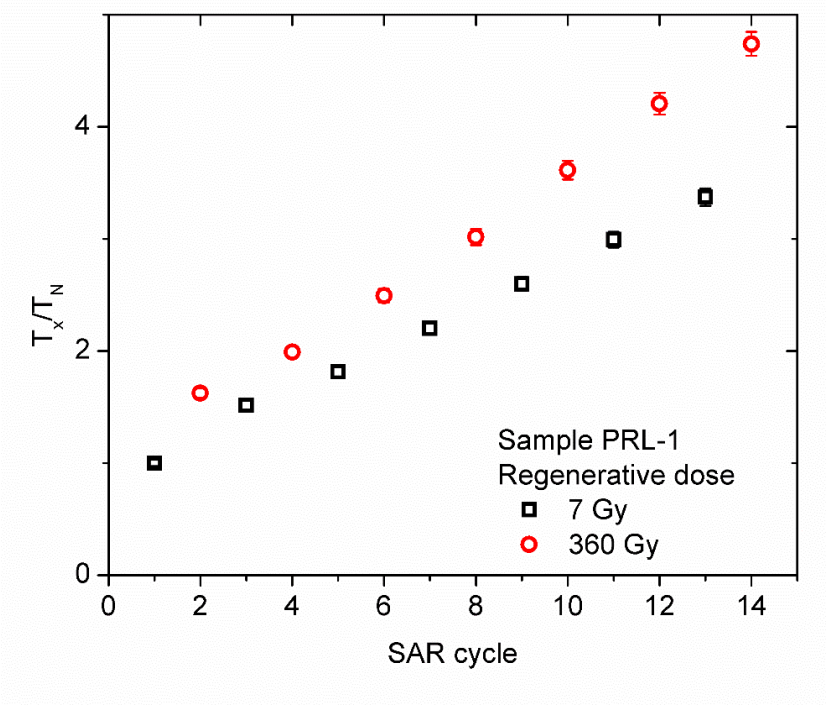

(b)

Figure 5-3 T_X/T_N ratio of sample (a) RQ-1 and (b) PRL-1, for alternative regenerative doses and fixed test dose.

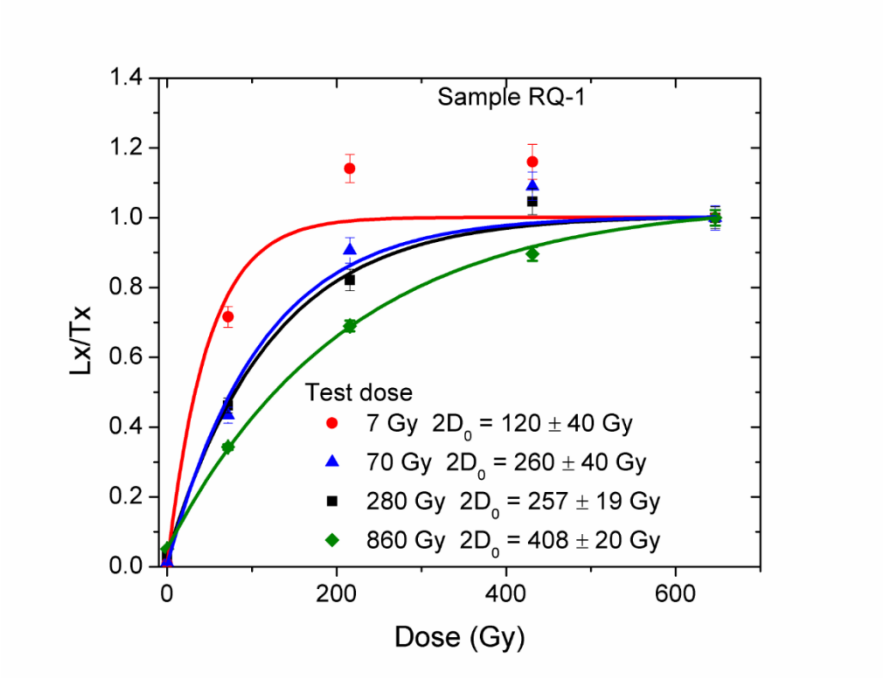

(a)

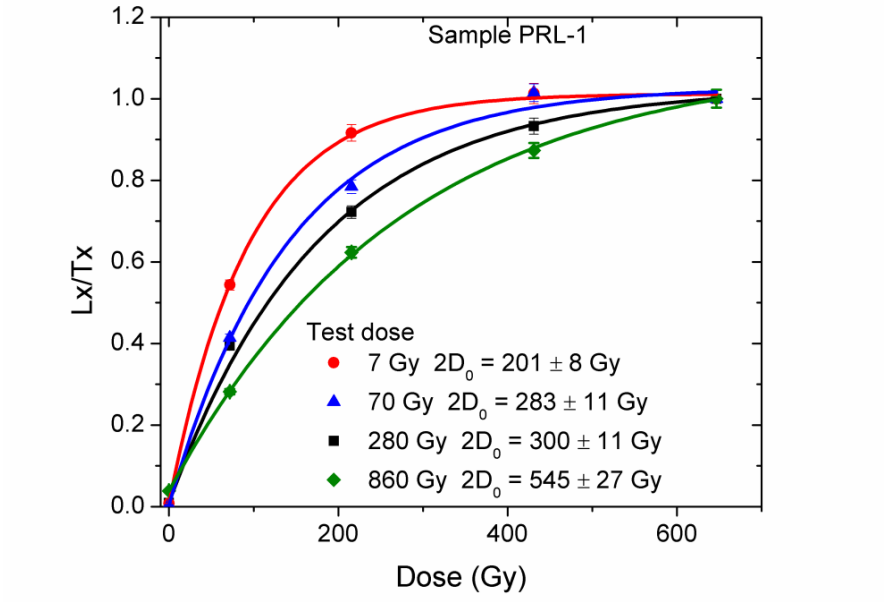

(b)

Figure 5-4 The DRC of sample (a) RQ-1 and (b) PRL-1, for 4 different test doses. The curves are fitted with single saturating exponential.

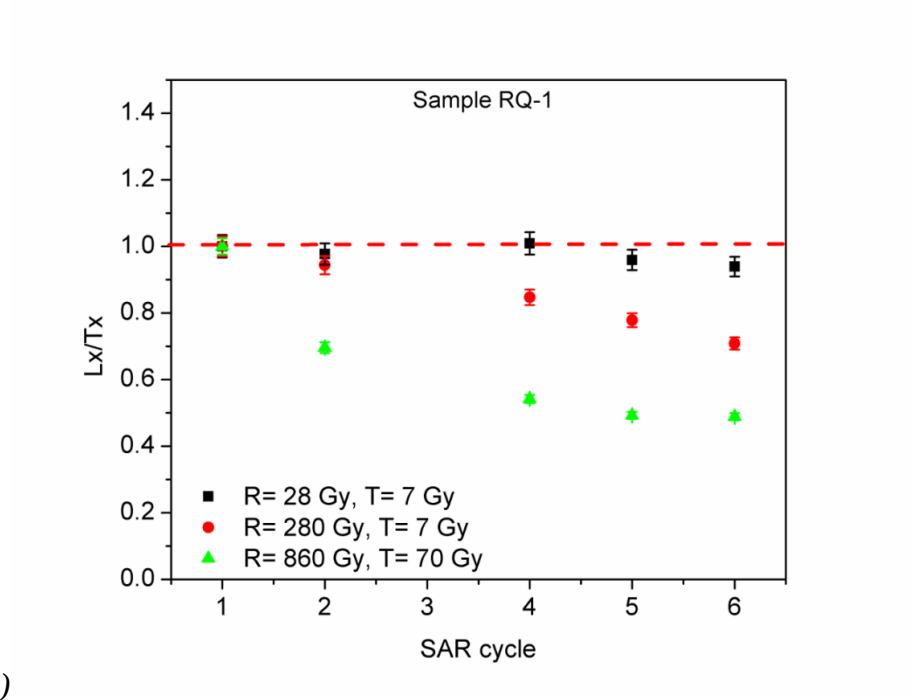

(a)

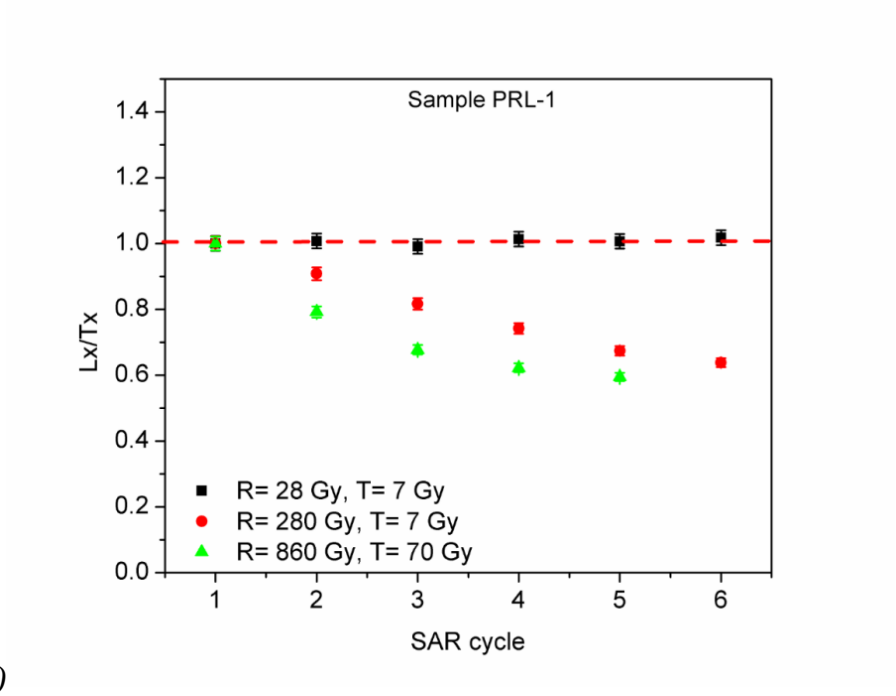

(b)

Figure 5-5 L_X/T_X variation with SAR cycle, for fixed regenerative and test dose. (a) RQ-1 and (b) PRL-1.

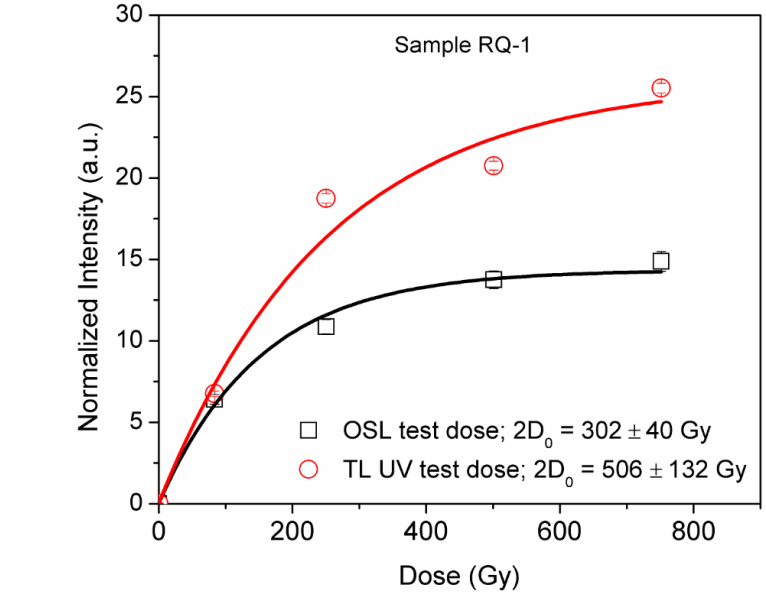

(a)

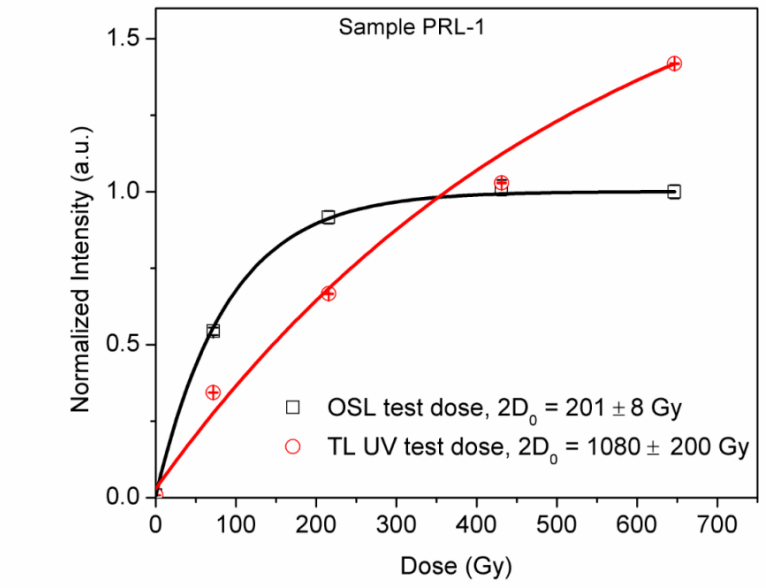

(b)

Figure 5-6 DRC of sample (a) RQ-1 and (b) PRL-1. The black curve is BSL-SAR normalized by SAR test dose as per given in Table 5.3. The red curve is OSL dose normalized by 110°C counts obtained from step 5 in the SAR protocol given in Table 5.3.

5.4.2. Alternative normalization method

Figure 5.6. show the comparison of SAR BSL test dose normalization and TL UV normalization. The saturation dose changes with the change in the normalization method. Both for RQ-1 and PRL-1, the saturation dose is higher for the TL UV normalization.

However, the recycling was not followed, which is an essential condition for the SAR validity. Figure 5.7 shows the results of various normalization on RQ-1. It can be seen that BSL test dose has a significant carry-over of charge from the regenerative dose (Figure 5.7a). However, after annealing of the sample to 450°C, the carry-over is significantly reduced (Figure 5.7c), still small increase in the test dose signal with regenerative dose is observed. The corresponding DRC of these BSL normalizations are shown in Figure 5.7b, d. For BSL test dose T1, the signal starts to saturate around 400 Gy, however for T2, signal increases up to 600 Gy, then starts to saturate. Figure 5.7e shows that the TL zero glow normalization is independent of the regenerative dose, as expected, as it is measured before any regenerative dose. Figure 5.7f shows the DRC. Additionally, Figure 5.7g, h shows that other TL blue normalization can also be used. The corresponding DRCs are shown in Figure 5.7h and j.

Figure 5.8 shows the results of the PRL-1 sample. The results are consistent for the BSL, zero glow and TL anneal normalization. However, for the TL blue there is an initial increase in the response of test dose with the regenerative dose, saturating latter after 200 Gy. Corresponding DRCs are shown. Results, clearly state that BSL normalization leads to early saturation, and other methods of normalization are useful.

5.4.1. Saturation and Dose Recovery of BSL signal

Figure 5.9, shows the DRC of multiple aliquot regenerative dose response curve of MS-BCFA and MS-BCFB samples. As in Figures 5.7 and 5.8, in the initial part of the DRC, a saturating exponential characteristic can be observed and after 500 Gy, the slope of the DRC changes. Hence, the DRC is fitted with double saturating exponential as shown in Figure 5.9, with equation $I = I_{01}\left(1 - \exp\left(-\frac{D}{D_{01}}\right)\right) + I_{02}\left(1 - \exp\left(-\frac{D}{D_{02}}\right)\right)$. Where, $2D_{01}$ and $2D_{02}$ are the characteristics dose indicating two trap system. The fitted value for the mass normalised MS-BCFA sample is with $2D_{01}$ is between 120±30 Gy and $2D_{02}$ is between 5800±800 Gy.

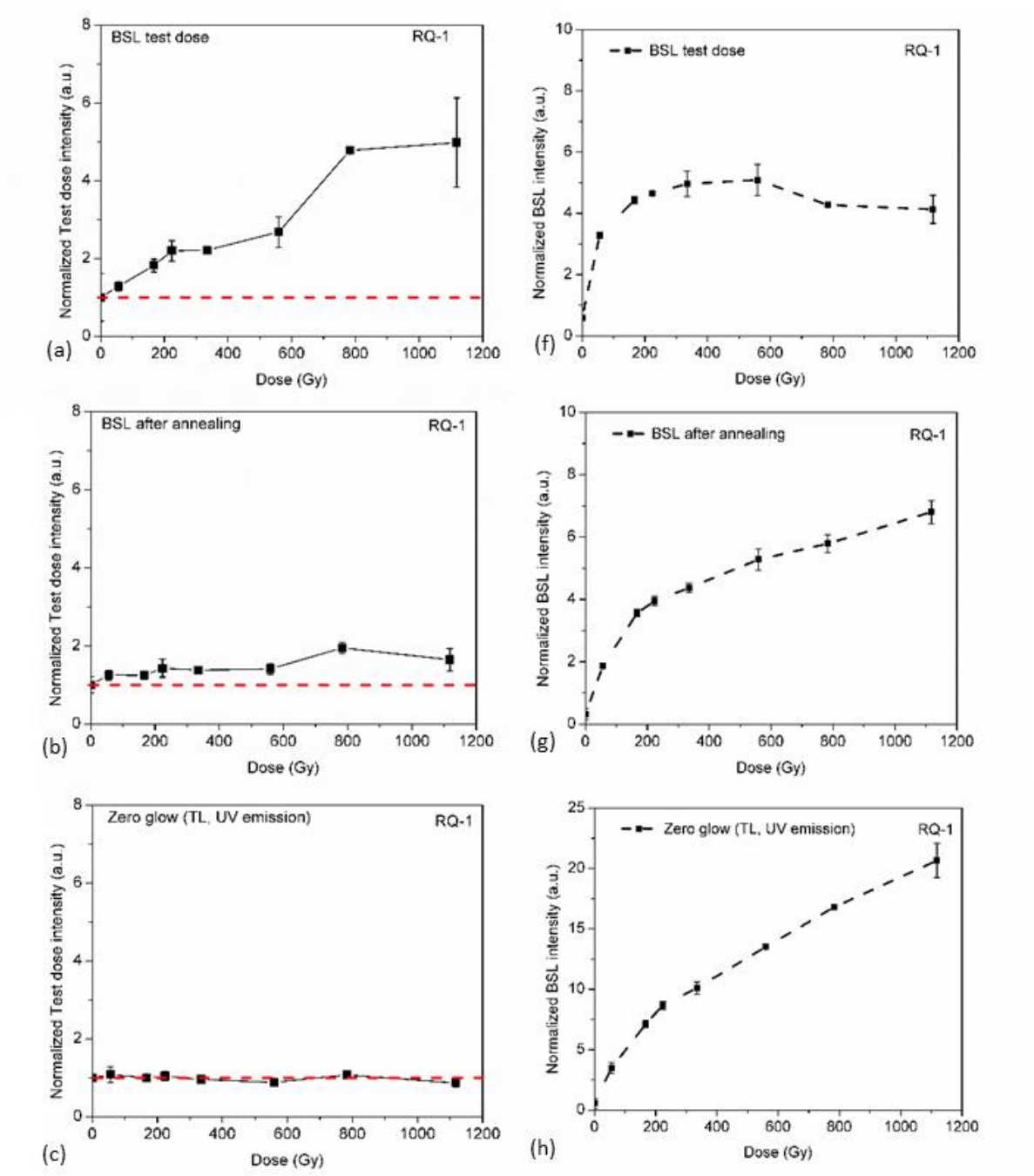
BSL test dose
RQ-1
Normalized Test dose intensity (a.u.)
Dose (Gy)
(a)
BSL test dose
RQ-1
Normalized BSL intensity (a.u.)
Dose (Gy)
(f)
BSL after annealing
RQ-1
Normalized Test dose intensity (a.u.)
Dose (Gy)
(b)
BSL after annealing
RQ-1
Normalized BSL intensity (a.u.)
Dose (Gy)
(g)
Zero glow (TL, UV emission)
RQ-1
Normalized Test dose intensity (a.u.)
Dose (Gy)
(c)
Zero glow (TL, UV emission)
RQ-1
Normalized BSL intensity (a.u.)
Dose (Gy)
(h)

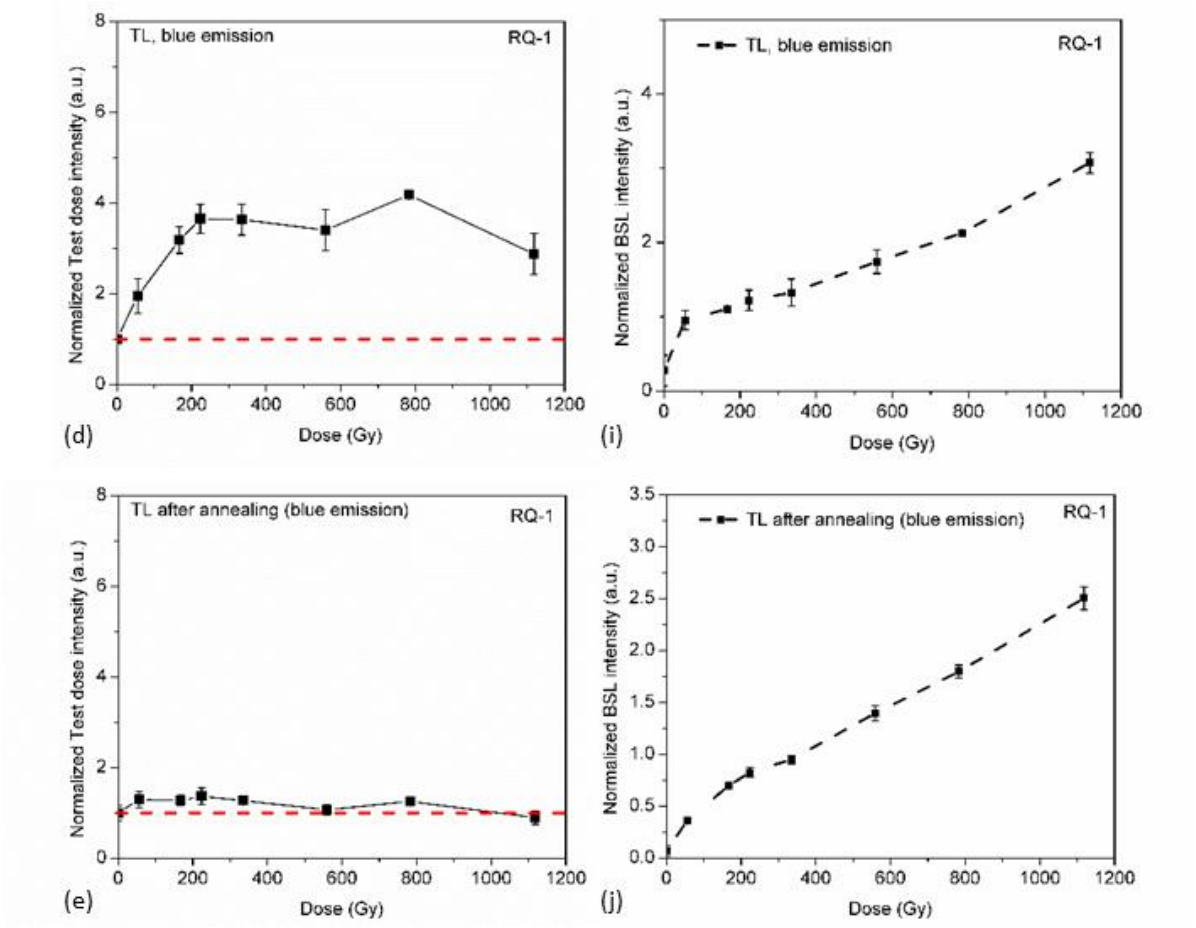

Figure 5-7 Sample RQ-1 data, with different normalization. (a-e) shows the variation of fixed test dose signal with regeneration doses, (f-,j) shows the dose response curve obtained by using the mentioned normalization in the graph.

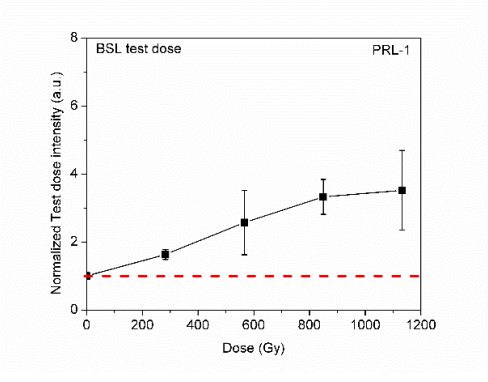
BSL test dose
PRL-1
Normalized Test dose intensity (a.u.)
Dose (Gy)

(a)

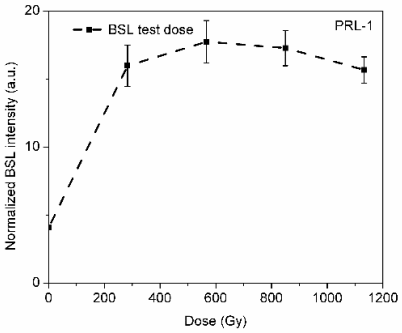
BSL test dose
PRL-1
Normalized BSL intensity (a.u.)
Dose (Gy)

(b)

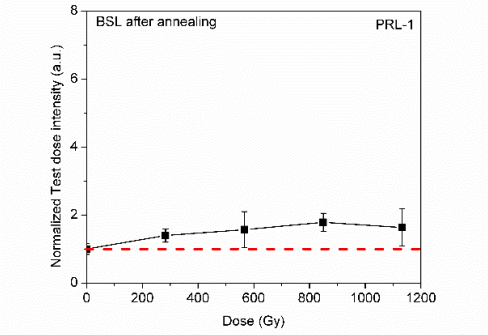
BSL after annealing
PRL-1
Normalized Test dose intensity (a.u.)
Dose (Gy)

(c)

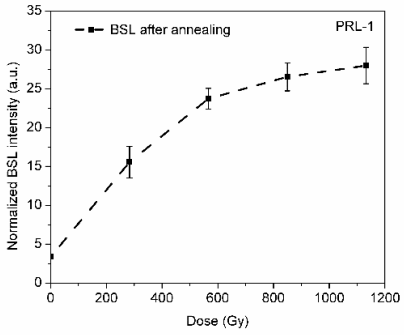
BSL after annealing
PRL-1
Normalized BSL intensity (a.u.)
Dose (Gy)

(d)

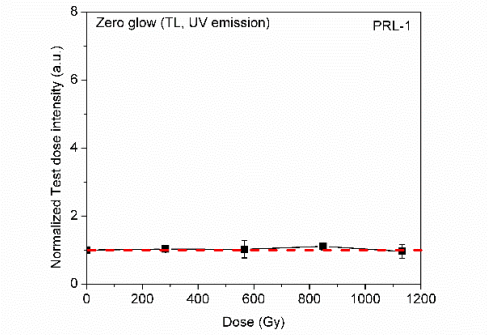
Zero glow (TL, UV emission)
PRL-1
Normalized Test dose intensity (a.u.)
Dose (Gy)

(e)

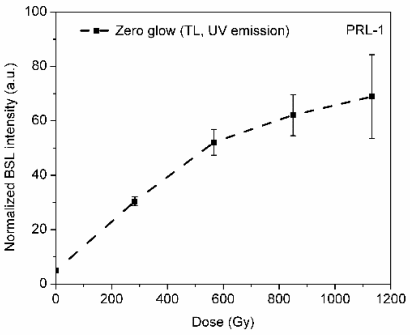
Zero glow (TL, UV emission)
PRL-1
Normalized BSL intensity (a.u.)
Dose (Gy)

(f)

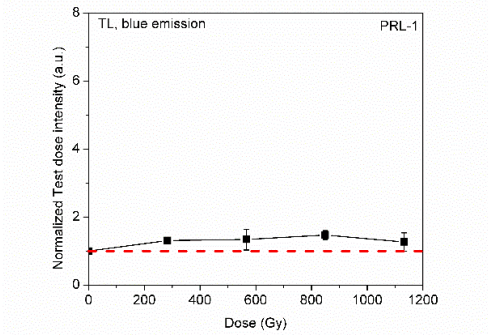
TL, blue emission
PRL-1
Normalized Test dose intensity (a.u.)
Dose (Gy)

(g)

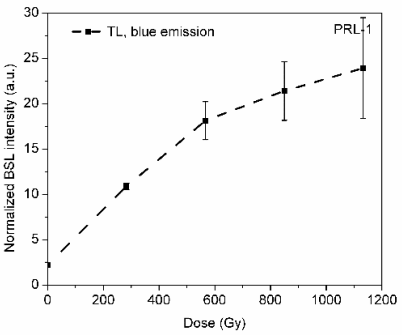
TL, blue emission
PRL-1
Normalized BSL intensity (a.u.)
Dose (Gy)

(h)

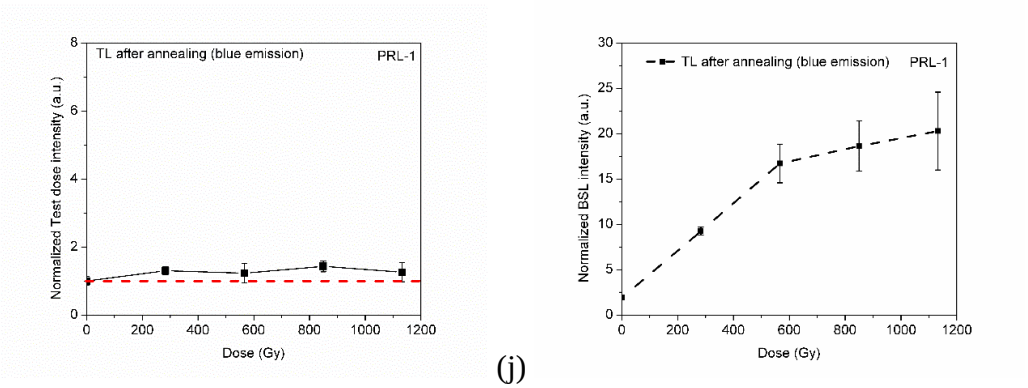

(i) (j)

Figure 5-8 Sample PRL-1 data, with different normalization. (a,c,e,g,i) shows the variation of fixed test dose signal with regeneration doses, (b,d,f,h,j) shows the dose response curve obtained by using the mentioned normalization in the graph.

Figure 5.10, shows the DRC of YS11 (previously given 1000 Gy gamma dose), the dose response curves are fitted with saturating exponential and given dose is recovered by extrapolation. Table 5.5, summaries the results. A dose recovery ratio from 0.9-1.2 is obtained. Although the errors in the dose estimates are around 50%.

Table 5-5 Dose recovery of sample YS11; given dose 1000 Gy.

Normalization used	**Recovered dose (Gy)**	**Recovery Ratio**
Mass	1219±520	1.2 ± 0.5
Anneal TL (Blue emission)	917±490	0.9 ± 0.5
Anneal BSL	1037±570	1 ± 0.5

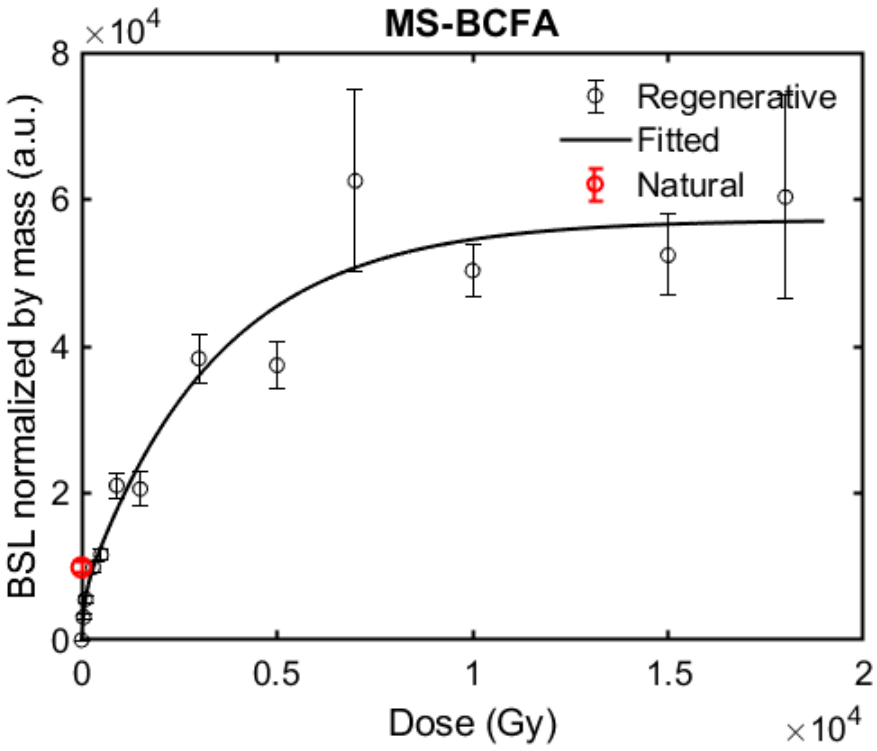
MS-BCFA
×10^4
8
6
4
2
0
BSL normalized by mass (a.u.)
Regenerative
Fitted
Natural
0
0.5
1
1.5
2
Dose (Gy)
×10^4

(a)

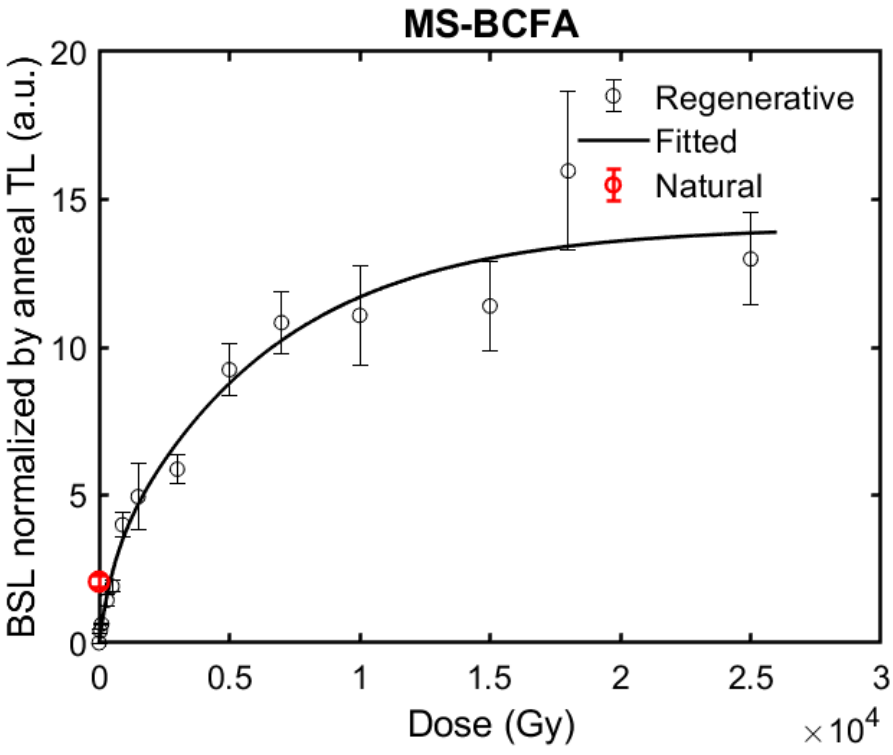
MS-BCFA
20
15
10
5
0
BSL normalized by anneal TL (a.u.)
Regenerative
Fitted
Natural
0
0.5
1
1.5
2
2.5
3
Dose (Gy)
×10^4

(b)

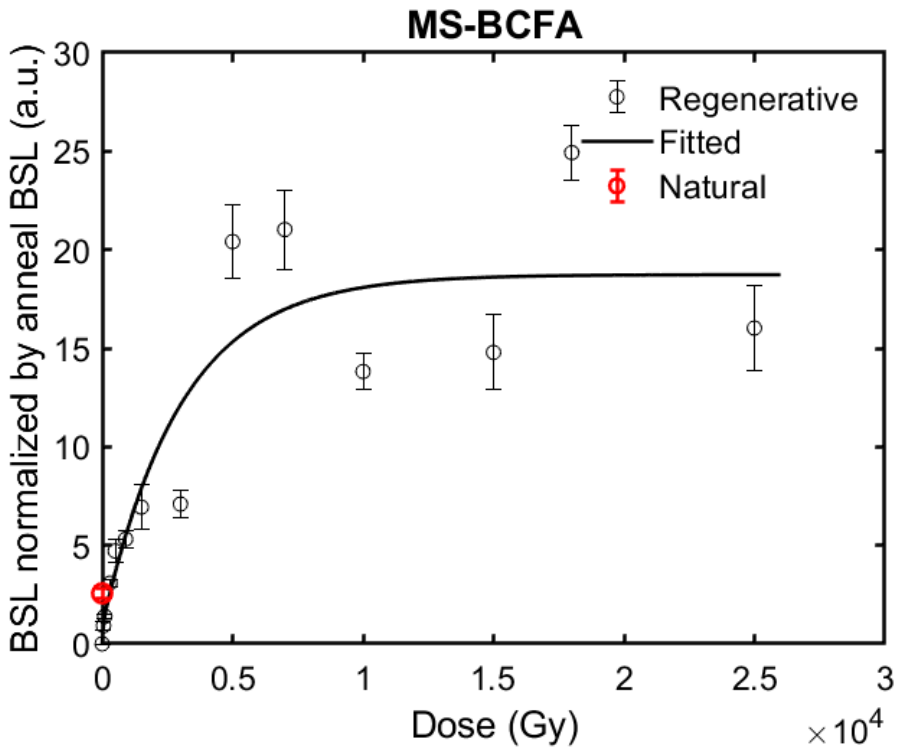
MS-BCFA
Regenerative
Fitted
Natural
BSL normalized by anneal BSL (a.u.)
Dose (Gy)
×10^4
0
5
10
15
20
25
30
0.5
1
1.5
2
2.5
3

(c)

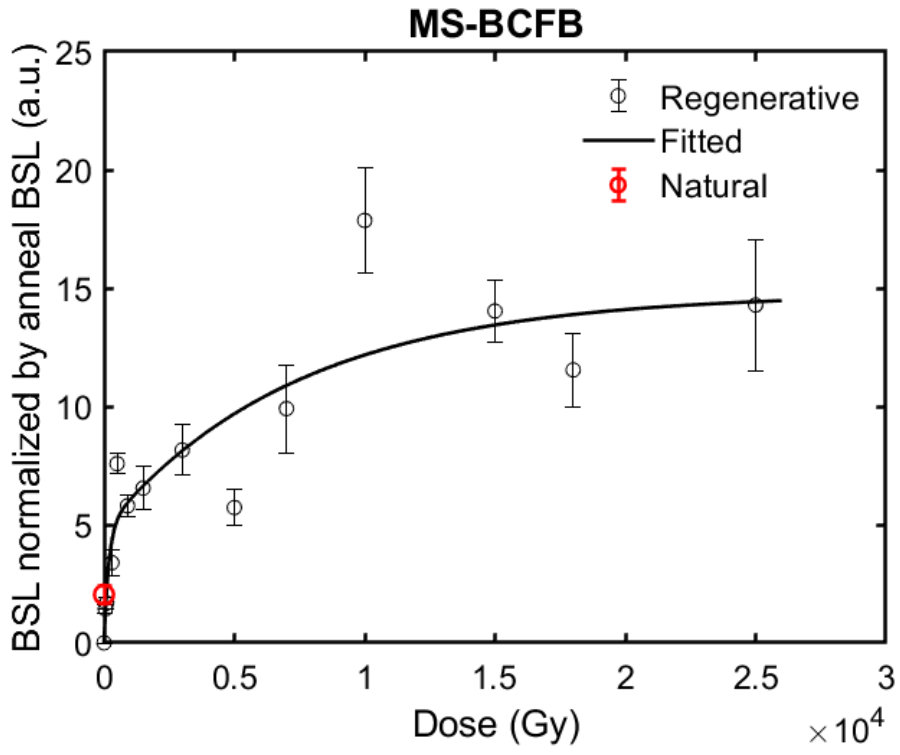
MS-BCFB
Regenerative
Fitted
Natural
BSL normalized by anneal BSL (a.u.)
Dose (Gy)
×10^4
0
5
10
15
20
25
0.5
1
1.5
2
2.5
3

(d)

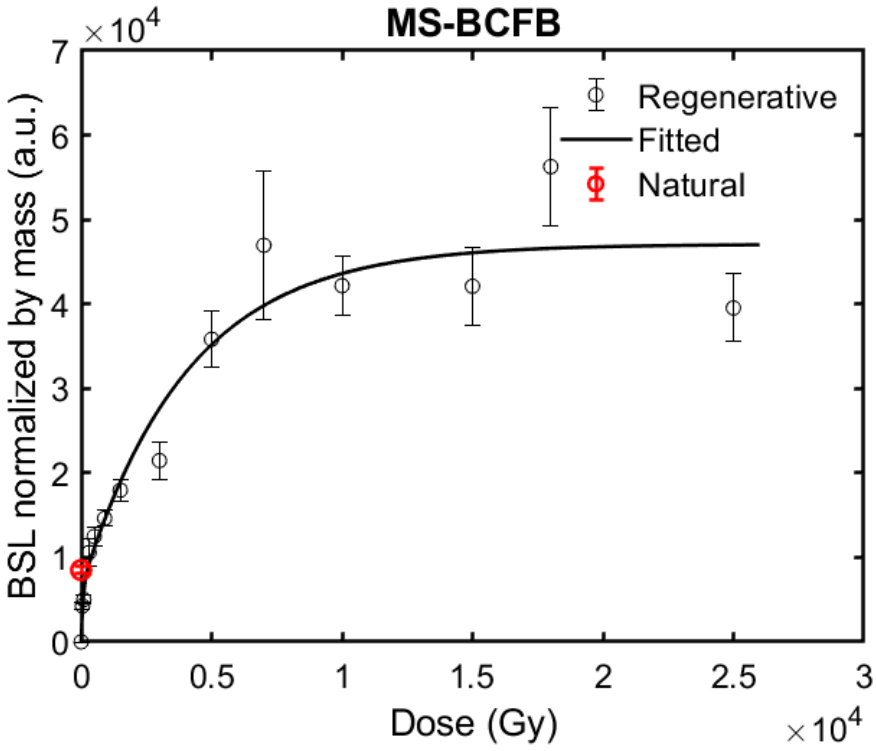

(e)

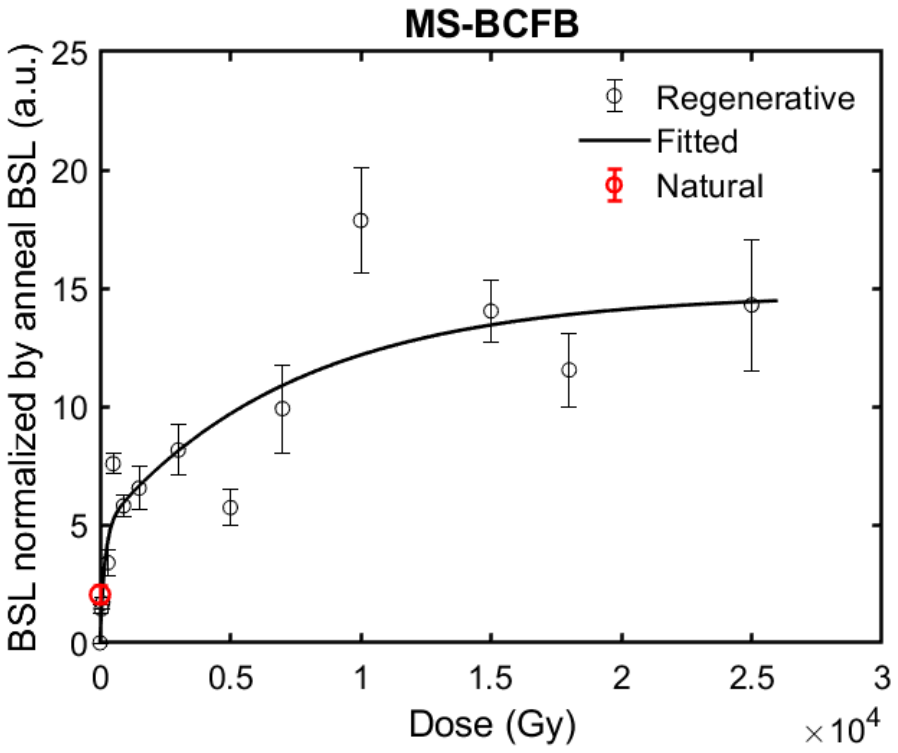

(f)

Figure 5-9 MS-BCFA and MS-BCFB saturation dose response curves with various normalizations.

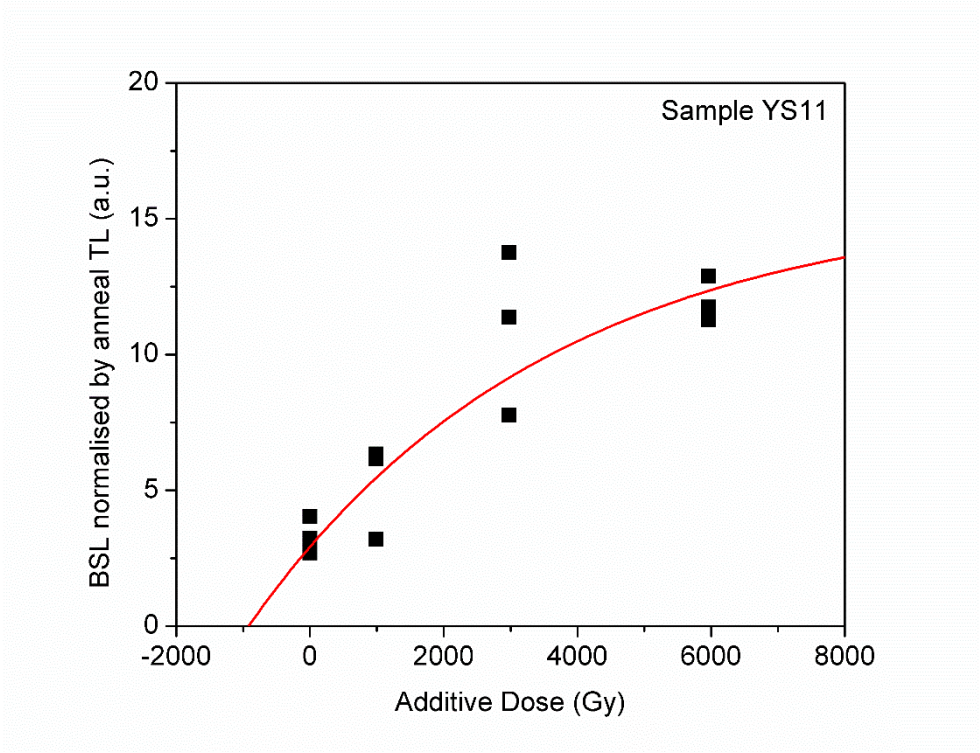
Sample YS11
BSL normalised by anneal TL (a.u.)
Additive Dose (Gy)
0
5
10
15
20
-2000
0
2000
4000
6000
8000

(a)

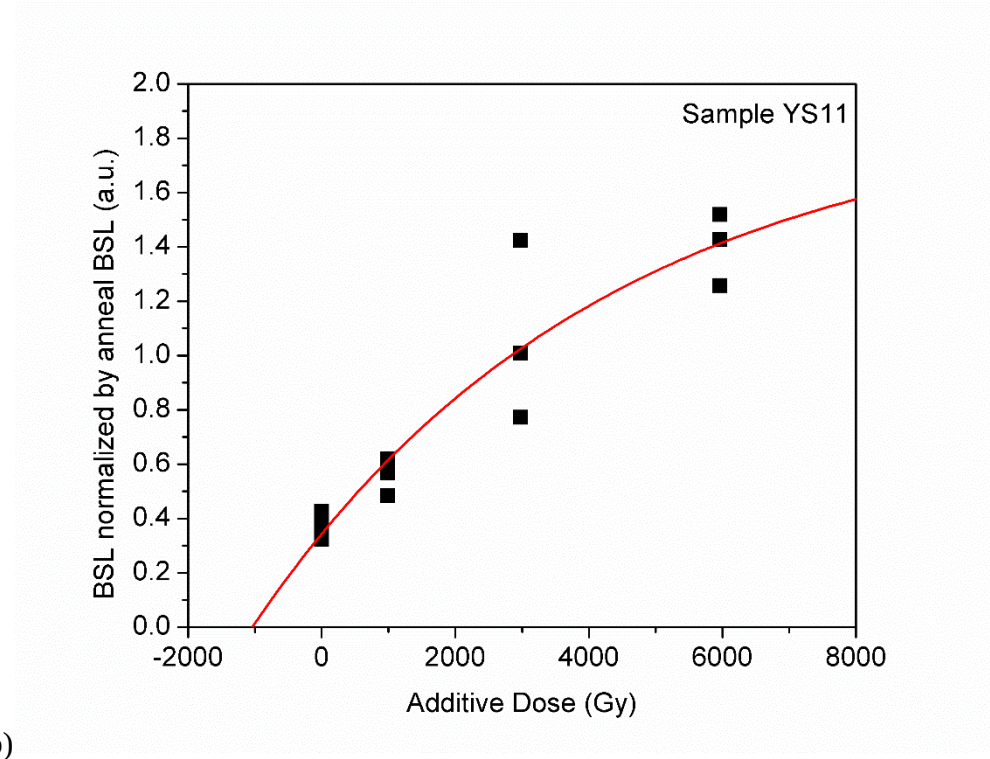
Sample YS11
BSL normalized by anneal BSL (a.u.)
Additive Dose (Gy)
0.0
0.2
0.4
0.6
0.8
1.0
1.2
1.4
1.6
1.8
2.0
-2000
0
2000
4000
6000
8000

(b)

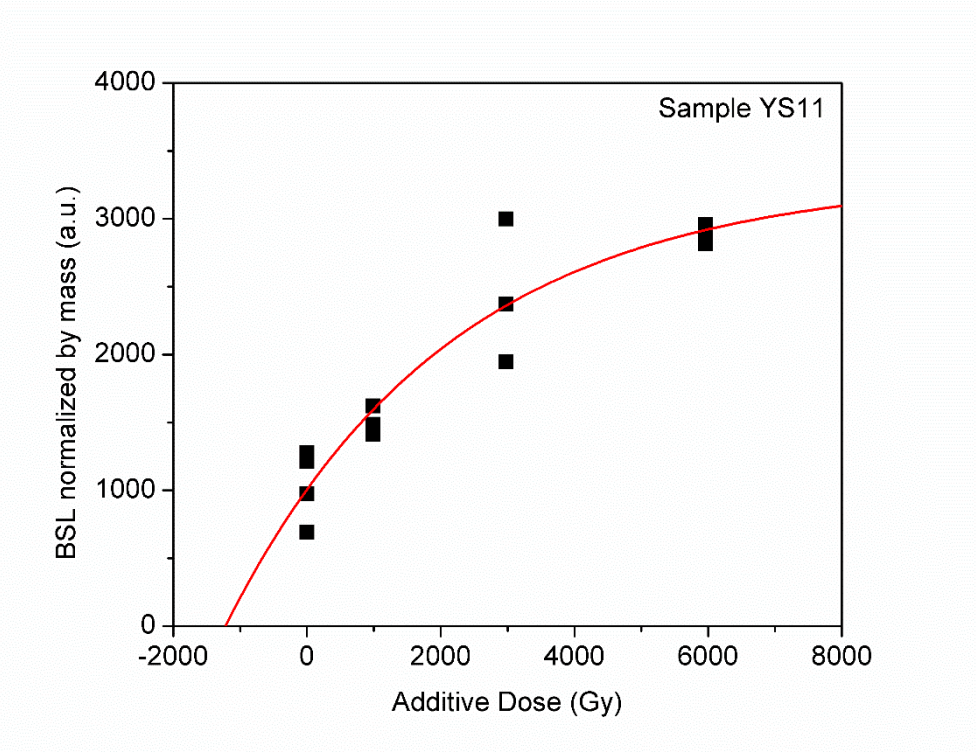

(c)

Figure 5-10 Dose recovery of YS11 with various normalizations. (a) BSL normalized anneal TL, (b) BSL normalized by anneal BSL. (c) BSL normalized mass.

5.5. **Discussion**

As of now, quartz BSL is known to saturate ~250 (±100) Gy as suggested by several earlier research (Chawla et al., 1998; Duller, 2008; Wintle, 2008; Wintle and Murray, 2006). However, it is also suggested that the saturation dose is protocol dependent (Murray et al., 2021; Wang et al., 2021; Zhang and Tsukamoto, 2022). Thus, it is crucial to identify the measurement variables that affect the luminescence saturation dose, as it influences the luminescence dating limit. This chapter investigated procedures, which can be used for estimating higher radiation doses for extending the dating limit by comparing DRCs for BSL measured at 125°C as it has the fastest resetting and no fading. The results suggest that BSL signals in general do not saturate as early as observed during SAR procedure (Figure 5.2) suggesting the need of improvement in laboratory measurement protocols. The protocols such as MAAD and MAR provide much higher saturation doses (Figure 5.2, 5.7, 5.8 and 5.9) compared to SAR and also supported by previous research works (Y. C. Lu et al., 2007; Murray et al., 2021; Wang et al., 2021). This indicates that

the saturation in SAR is somewhat protocol induced and cause needs to be probed. The SAR protocol is known to produce very reliable result for low doses (<D_0~250Gy), which is verified against other standard techniques and methodologies (Murray and Olley, 2002; Vandenberghe et al., 2004; Watanuki et al., 2005). However, SAR's early saturation compared to other luminescence protocols warrant careful investigation of its applicability for doses near and beyond saturation limit.

One of the important differences in the measurement techniques is in normalization methods. Therefore, the effect of normalization is investigated in SAR and other protocols. In SAR protocol, the luminescence signal is normalized by signal corresponding to an immediate test dose, expecting it to correlate with luminescence signal (Murray and Wintle, 2000). This is in-fact the case for doses less than saturation doses; however, more investigation for doses near and higher than saturation is required. For this, the variation in T_X/T_N for a fixed test dose is observed for multiple cycles of constant alternate low (~8 Gy) and high (~426 Gy) regeneration doses (Table 5.3). The periodic variation of T_X/T_N ratio correlating alternating regeneration doses (Figure 5.3) suggests a regeneration dose dependence of test dose signal for doses near or higher than saturation. This can influence the saturation limit. During L/T measurement, as the regeneration dose increases, the dividing factor i.e. test dose signal (T) also increases. This increase in the denominator of L/T will reduce the proportional increase in L/T with dose resulting in early saturation of SAR DRC. On comparison of SAR-BSL protocol (Table 5.2) with any TT-OSL protocol (Chapot et al., 2016; Duller and Wintle, 2012), it is evident that the test dose signal in SAR-BSL is the main signal (Lx) in TT-OSL, difference lies in the fact that in TT-OSL a dose between two OSL measurements is not given. Hence the test dose will show significant dependence on the regeneration dose. This contribution becomes even more significant at high doses. Some previous studies have also reported dependency of BSL test dose signal on regeneration dose (Jain et al., 2003; Rhodes, 1992). The regeneration dose dependency in the test dose can be minimised either by increasing the size of test dose such that the percentage contribution from the regeneration dose to the test dose is suppressed or adopt another normalization procedure. Results (Figure 5.4) show that growth curve modifies with increasing test dose and saturation doses are higher for high-test doses. Similar observations are made by Colarossi et al., (2018) for feldspars, Palczewski et al., (2022) for TM-OSL for quartz, however, a decrease in saturation is observed by Liu et al., (2022). Several authors (Chauhan and Singhvi, 2019; Murray and Mejdahl, 1999; Murray and Roberts, 1998; Singhvi et al., 2011) suggested that 110°C

peak is correlated with BSL signal, so it can also be used to track sensitivity changes similar to test dose BSL signal. The feasibility of using 110°C (UV emission) peak as normalization signal was investigated. The integrated counts within the maximum peak temperature ± 5°C is used for normalization of BSL signal and a DRC with higher saturation dose was observed (Figure 5.6). However, in this the estimated recycling ratio was below suggested limit of 10% of unity. The differences can again be attributed to the fact that 110°C TL peak and BSL sensitivity are not correlated at higher doses (Singhal et al., 2024). The experiment to monitor L/T above DGSS for a constant regeneration dose in SAR cycle suggested that the L/T is not constant but decreases with number of cycles (Figure 5.4). This implies that at higher doses (D>~DGSS), SAR test dose signal (TL or OSL) is inappropriate for correcting luminescence signal for the sensitivity changes occurring during measurement procedures and require a revisit of normalization methods. Further as regeneration dose signal is propagated to next OSL measurements, it is not possible to correct for this propagation of charge within SAR methodology.

It is important to identify alternative methods that can be used for estimating DGSS. Other methodologies such as MAAD and MAR are useful since in these aliquots are measured only once and sensitivity correction is not required. However, in these methods as well, normalization is required for removing inter-aliquot variability due to inhomogeneity in weight and sediment grains. Experiments done to identify best normalization procedure (Table 5.4) suggests that zero dose normalization is the best method (Figure 5.7 and 5.8). However, in cases, when the samples subsets are irradiated with different high radiation doses (>1kGy) then zero glow normalization is also not possible due to radiation quenching of 110°C peak (Schmidt and Woda, 2019; Singhal et al., 2024) which again depends on dose in dosimetric traps (> 300°C) (Singhal et al., 2024). In such cases, test dose BSL or TL (blue; Singhal et al., (2024)) signals after annealing can be used for normalizations, as they are found to be independent of the regeneration dose (Figure 5.7). Previous studies by Timar-Gabor et al., (2015) have also reported that the use of zero glow TL 110°C normalized MAAD DRCs have higher saturation doses than 2000 Gy in and supports the argument.

Normally BSL signal is considered to be arising from single trap corresponding to 325°C peak (Aitken, 1998; Wintle and Murray, 2006), so single saturating exponential is considered to explain the nature of fitting. Some of the works also uses linear fitting for very low doses (~10 Gy) as at low doses single saturating exponential approaches linear approximation. However, interestingly for doses near saturation of SAR signal, different

type of fitting procedures are reported as single saturating exponential is unable to explain the dose response. Some of the works uses a combination of linear and saturating exponential curves (Sally E. Lowick et al., 2010b; Rodrigues et al., 2022) while some others used double saturating exponentials as they are found to fit well (Ankjærgaard, 2019; Chapot et al., 2012; Timar-Gabor et al., 2012). But, the physical reason for such fittings is not explained. The results obtained in present study (Table 5.4 and Figure 5.7,5.8) indicates towards existence of two trap systems because a difference in slope for doses in range 0 to 300 Gy and 300 to 1000 Gy is observed. A similar change in slope is observed in many previous studies (Chawla et al., 1998; Rodrigues et al., 2022; Singhal et al., 2024) however, these studies either focus on the low dose range (from 0 to ~ 1000 Gy) or high dose range (> 1000 Gy) and provide limited picture of dose response curve. In the present study dose response is constructed from 0 Gy to till the second linear increase also results in saturation (Figure 5.9). A second saturation around 5800±800 Gy is observed. This suggests that it should be possible to estimate radiation doses above the current limit of 250 Gy. Additionally, an artificial lab dose of 1000 Gy is administered to the sample YS11 and recovered through the MAAD protocol using mass, annealed TL (blue emission) and annealed BSL test dose. A dose recovery varying from 0.9-1.2 is observed, making the proposed protocol suitable for dating beyond D_{GSS}.

5.6. **Conclusion**

The following conclusions can be obtained from this study,

1. Laboratory protocol being used influences the saturation dose that can be estimated using BSL signals.
2. SAR methods are widely used and works well at low radiation doses, however, as regeneration dose increases, the carry-over charge from regeneration dose cycle to the test dose cycle results in increased test dose signal (T). Thus, the increase in T, reduced proportional increase in L/T and results in early saturation of SAR DRCs. The normalization provides reliable result for doses less than D_{GSS} using SAR, however for paleodoses estimation near saturation or beyond, these normalization procedures are in appropriate as reported by any previous works.

3. The dependency of regeneration dose is reduced only after annealing, hence MAAD and MAR methods normalized by suitable normalizations are preferred for high dose estimations.
4. Zero glow, BSL after annealing and TL after annealing (blue emission) are observed to carry negligible regeneration dose dependence and can be used for normalization.
5. The DRCs constructed using these normalizations need to be fitted by double saturating exponential. Second saturation is observed ~5800 Gy in this study.
6. A laboratory dose of 1000 Gy could be successfully recovered with a dose recovery ratio of 0.9-1.2.

Chapter 6: Application to Old Geological Settings (of Million Years Timescale)

6.1. Introduction

In chapter 5, it was observed that BSL signals saturate at very high radiation doses ~5000 Gy, when using a multiple-aliquot protocol using signal normalization by mass or other suggested signals, as compared to a conventional test-dose normalization based single-aliquot regeneration protocol. Considering natural dose rate (1~3 Gy/ka), this should imply that it should be possible to estimate old ages ~ 1.6 - 5 Ma. Chapter 5 also illustrated that a laboratory dose of 1000 Gy could be recovered by the BSL, which is 4-5 times the dose recoverable by conventional methods using BSL (SAR-BSL). In chapter 6, the BSL signals are used establish the chronology of old geological sites (formed millions of years ago). The samples from two sites in India are investigated. The upper Shivaliks in the Northern part of India (expected age from 0.5-2.5 Ma, (Kumar et al., 1999; Kumaravel et al., 2005; Mandal et al., 2019)) and the Charavathur formation from the Southern part of India (expected age > 2.5 Ma, Poulose, 1965, Nair and Chauhan, 1984, King, W. 1882, Rajendran, C.P., & Dr.Soman, K. 1987). This chapter compares the results of the multiple aliquot BSL measurements with single aliquot BSL measurements and tried to understand the discrepancy in context of the expected ages of these sites.

6.2. Sample Details

6.2.1. Upper Shivaliks

Geological description: The Shivalik mountain range is the outermost mountain range of the Himalayan orogenic belt formed by the collision of Indian and Eurasian plate that

began during the Cenozoic- Paleocene time. The Himalayas span a significant region of Pakistan, India, Bhutan, Myanmar and Nepal. It is the land of the highest peak (Mount Everest) ~ 8.8 km high from sea level and hosts a number of rivers and hot springs. The collision resulted in the disappearance of Tethys sea between the plates; eventually, many animal fossils are found in the Himalayas (Nanda et al., 2018). The region is continuously uplifting because of the subduction of Indian plate beneath the Eurasian plate at a rate of 10-50mm/year (Bilham et al., 1998; DeMets et al., 1994; Wesnousky et al., 1999). Folding of the plates leads to formation of various thrusts and faults. Based on the major fault line such as Main Boundary Thrust (MBT), Main Frontal Thrust (MFT) and Main Central Thrust (MCT), the division of the Himalayas from South to North is into the Outer Himalayas, or the sub Himalayas, followed by Lesser Himalayas and higher Himalayas. The MCT divides the higher and lesser Himalaya, MBT divides the lesser and sub Himalaya and MFT separates the sub Himalayas from Indo- Gangetic alluvial plain. The Shivaliks are formed by the fluvial deposition of sediments from the erosion of higher Himalayas. An upward coarsening is observed in the Shivaliks. It is further subcategorized into three formations the lower Shivaliks, middle Shivaliks and the upper Shivaliks.

The lower Shivaliks formed ~18-11 Ma ago, consists of Kamlial and Chinji formation. The middle Shivaliks formed ~11-5.26 Ma ago, consists of Nagri and Dhok-pathan formation and the upper Shivaliks ~ 5.26 -0.2 Ma ago, consists of Tatrot (5.26-2.5 Ma), Pinjour (2.5-1.7 Ma) and Boulder Conglomerate Formation (1.7-0.2Ma). The age constraints provided till date are majorly derived on the basis of paleomagnetic dating of the sediments in the region (Kumar et al., 1999; Kumaravel et al., 2005, 2005; Mandal et al., 2019).

The lithology of the Upper Shivaliks primarily consist of:

- **Conglomerates** (large boulders embedded in sandy or clayey matrices)
- **Sandstone** (coarse-grained, often cross-bedded)
- **Siltstone and claystone** (fine-grained deposits from ancient floodplains)

Sandstone–Mudstone alterations are seen in the Shivaliks with occasional boulders in between the layers. The Upper Shivaliks have been tilted, folded, and faulted due to ongoing Himalayan tectonics (Bouscary, 2022). The presence of anticlines and synclines indicates compressional forces acting on these young sediments. These are known for their

vertebrate fossils, including remains of prehistoric mammals such as **elephants, rhinos, and hipparions** (extinct three-toed horses) (Deng and Ding, 2015).

Samples

Sediments from the boulder conglomerate formation were sampled (Table 6-1). The sample MS-BCFA is taken from a road cut section, while MS-BCFB is from a river cut section. The samples MS-BCFC, MS-BCFD, MS-BCFE are taken from the upper part of the Haripur Khol section also described in Sangode et al., (1996). The expected age of MS-BCFA and MS-BCFB is 0.2-1.7 Ma (Kumar et al., 1999; Kumaravel et al., 2005, 2005; Mandal et al., 2019).

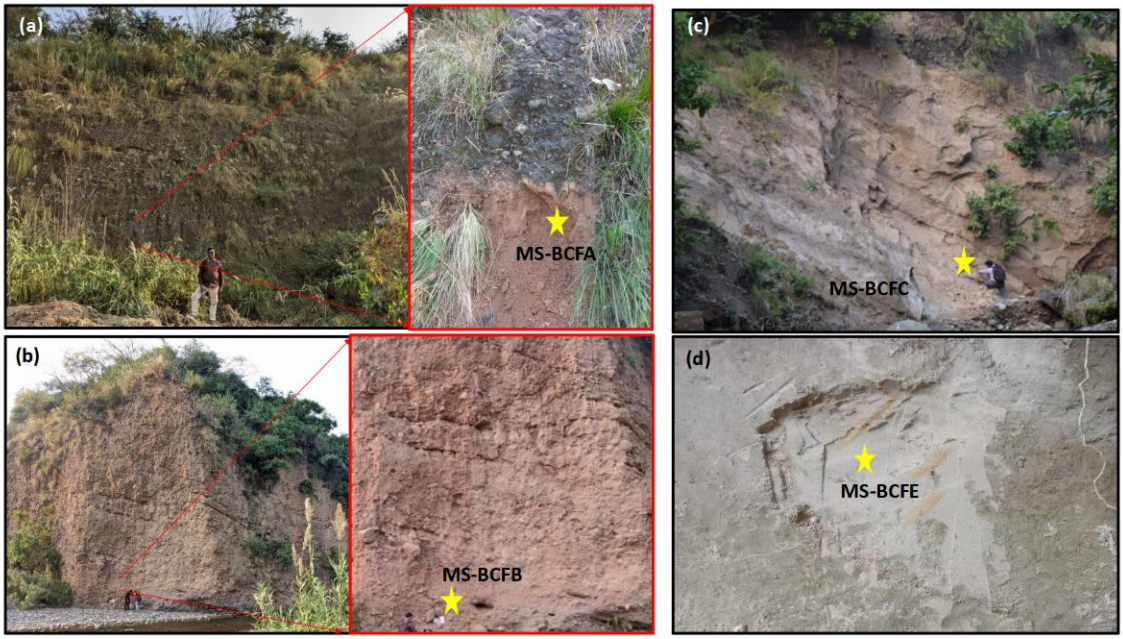

Figure 6-1: Field photos of the Upper Shivalik samples.

6.2.2. Cheravathur formation

Geological description: The geology of the Cheruvathur area in northern Kerala is characterized by a stratigraphic sequence that includes Precambrian basement rocks, Tertiary sediments, and Quaternary deposits, reflecting a complex geological history.

The basement rocks in the area consists of Archaean or Proterozoic Charnockitc gneisses and granites, high-grade metasedimentary and schistose gneissic rocks, acid intrusives (possibly Sargurs), dolerites and basalt dykes, pegmatites and granophyres. These form the crystalline basement over which younger formations rest unconformably.

This is followed by the Tertiary formations of Miocene age, correlated with the Warkalli Beds of southern Kerala, lie unconformably over the Precambrian basement and are marked by a kaolinized contact zone. They are primarily composed of lignite-bearing clay, sandstone, ferruginous grits, and shale beds. The sedimentary sequence consists of intercalations of sand and clay units with discrete lignite seams bounded by sandstone or shale (Poulose, 1965, Nair and Chauhan, 1984).

Key features of the Tertiary sediments include:

- **Sandstone:** Immature, loose, and friable with subangular to subrounded quartz grains and kaolin pebbles. Bedding and crossbedding are prominent.
- **Clays:** Alternating layers of greyish-white, fine, semi-plastic clays interbedded with sandstones. Brownish hues on the clays indicate iron infiltration during lateritization.
- **Lignite and Carbonaceous Material:** Lignite seams and carbonaceous sandy clays with remnants of semi-carbonized wood and resin.
- **Marcasite:** Impersistent seams and sticks of marcasite indicating reducing depositional environments.

The Tertiary sediments act as aquifers, with sandstone layers providing significant groundwater storage. The lateritic weathering of these sediments has also resulted in the development of thick caps of laterite. Laterites developed over both the crystalline basement and Tertiary sediments, formed under tropical weathering conditions (Poulose, 1965, Nair and Chauhan, 1984). The Tertiary formations in Cheruvathur, similar to the Varkalli-Quilon beds, are nearly horizontal and consist of unconsolidated sands and clays. The presence of carbonaceous material, marcasite sticks, and lignite seams indicates deposition under reducing conditions in a tropical to subtropical environment.

The lowlands are represented by sandy and alluvial flats, sandbars, and river terraces. The mudlands predominantly consist of laterite derived from the underlying crystalline rocks and sediments. The Quaternary deposits comprise sand and alluvium, occupying low-lying plains near the sea, backwaters, and paddy fields. The Tertiary sediments in Cheruvathur are comparable to the Warkalli Formation (Mio-Pliocene age) of southern Kerala, as identified by W. King in 1882. These formations are considered equivalent to the Cuddalore Sandstone of Tamil Nadu and provide vital insights into the depositional history of the region. The Varkala Cliff, part of the Kerala Khondalite Belt (KKB) in the Southern Granulite Terrain, serves as the type area for the Mio-Pliocene Warkalli Formation, which unconformably overlies the Precambrian basement and comprises

ferruginous and non-ferruginous sandstones, variegated clays, and carbonaceous clays with lignite seams. The Tertiary formations in the Varkala-Quilon area are classified into the calcareous Quilon Beds and the unconsolidated Warkalli Beds, with similarities to the Tertiaries of the Cannanore area, characterized by nearly horizontal strata and reducing environments (Sajinkumar et al., 2022).

Samples:

The studied section at Cheruvathur area, with a total thickness of 33 meters, represents a variety of lithologies. The stratigraphy of the Cheruvathur Formation reveals several meters of carbonaceous clay interbedded with lenticular layers of shale and lignite. The lignite units are notable for their abundance of plant fossils, including leaves, stems, twigs, and leaf impressions. Additionally, tubular stick-like and planar structures of marcasite, as well as traces of amber, are observed, followed by variegated clays and sandstone in the stratigraphic sequence.

The variegated lithological units, displaying evidence of chemical leaching, impart distinct coloration to the sand and clay layers. The clay units exhibit various shades of gray, red, and purple, while the sandstone units are predominantly ferruginous. Notably, layers of ferricrete deposits are observed at the base of the clay units at distinct intervals. Total 9 samples from the cliff section (shown in Figure 6.2 and Table 6-1) and one sample from the beach sand is collected for the study. CHR-OSL 3 is the topmost sample and is taken from red sandstone sandwiched between laterite, rich in ferrite. Followed by CHR-OSL1 and 2 are taken below the ferruginous layer and CHR-OSL 4, from a distant from CHR-OSL 1 and 2 but below the ferruginous layer. CHR-OSL-5 is taken from sand lenses, below the ferrite layer and CHR-OSL 6,7,8 and 9 from sandstone layers. In addition to these samples, CHR-OSL-0 is taken from 10 cm below the surface near the seashore.

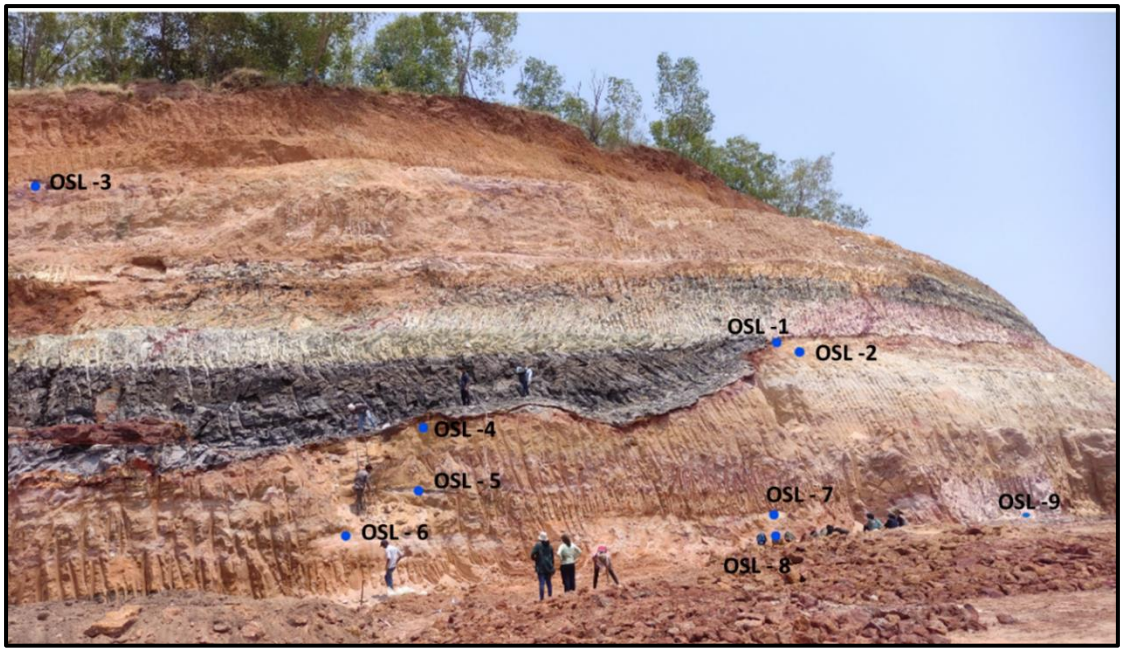

Figure 6-2:Field photo of the Charavathur cliff from which the samples are taken..

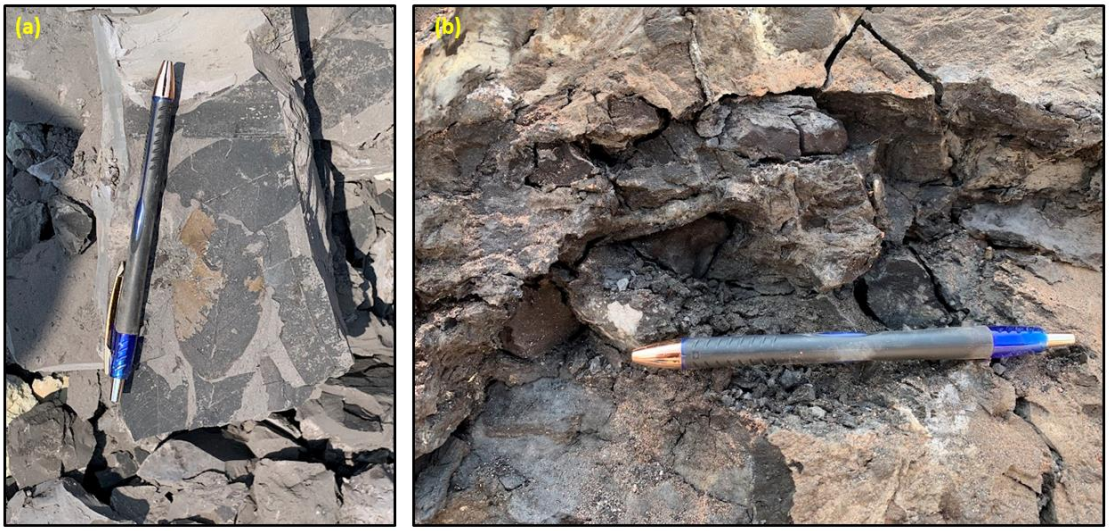

Figure 6-3: (a) A leaf fossil, (b) a tree stem fossil found in the cliff.

6.3. **Dose rate estimation**

To estimate the dose rate, the concentration of U and Th is estimated by thick source alpha counting. The K concentration is estimated by NaI scintillation counting. Cosmic ray dose rate is calculated from Prescott and Hutton, (1994) using the latitude, longitude, altitude and depth. The water content is calculated by estimating the weight of sample as it is, after drying it and after saturating it with water. The results are shown in Table 6-1. The dose rate of the Shivalik samples varied from 1.5- 2.2. Gy/ka and the dose rate of the

Charavathur samples varied from 0.16-0.36 Gy/ka. Although the Southern part of India is found to be rich in placer deposits and hence mostly have higher dose rate, these samples from the Charavathur cliff had a very low dose rate. The dose rate does not increase with depth. Additionally, a surface sample is also measured for the dose rate, which has a U, Th, and K content similar to the cliff samples. Hence, the possibility of leaching of radionuclide is discarded.

6.4. Equivalent dose estimation

Equivalent dose estimates are made on coarse grain quartz fraction (90-150 μm). Fast component of the BSL curve is used for analyses (0.2 s to 1 s is used as signal and 2.88 s to 4 s as background). The equivalent doses are estimated by both single aliquot and multiple aliquot methodology as discussed below.

6.4.1. Single aliquot regeneration protocol:

IR test is carried out following (Duller, 2003) to check the presence of feldspar in the extracted quartz samples. Based on which, either of BSL-SAR (Murray and Wintle, 2000a) or BSL-DSAR (Banerjee et al., 2001) is applied as given in the Table 6-2. The aliquots for which recuperation and recycling ratio are within 10% were accepted. Further based on the distribution of data and the values of kurtosis and skewness suitable age model (Bailey and Arnold, 2006; Galbraith et al., 1999) is chosen to estimate the equivalent dose. The shine down curve and the dose response curves for the samples are shown in Figure 6.4. The luminescence sensitivity of the Charavathur samples is relatively low as compared to the Shivalik samples; hence, these yielded higher errors in the DRC. The results of equivalent doses are given in Table 6-4.

The samples MS-BCFA and MS-BCFB are found to be in saturation. A decreasing equivalent dose is observed from the samples MS-BCFC, MS-BCFD and MS-BCFE samples and these samples are not in saturation as expected. The Charavathur samples are also not in saturation in SAR, as expected, given their reported tertiary formation age (>2.5 Ma; (Poulose, 1965, Nair and Chauhan, 1984)). Nor does the samples equivalent dose show a correlation with the depth. Instead, a mean equivalent dose of ~70 Gy is obtained for the complete cliff samples.

Table 6-1 Dose rate estimation of the samples.

SR. No.	Sample Name	Depth (m)	Latitude/ Longitude	Water content (%)	U(ppm)	Th (ppm)	K(%)	Cosmic ray dose rate (Gy/ka)	Dose Rate (Gy/ka)
Upper Shivaliks									
1	MS-BCFA	2.5	30°48.200 N, 77°55.707E	10	2.31±0.9	14±3	0.76±0.07	0.12±0.008	2.17 ±0.18
2	MS-BCFB	15	30°48.290 N, 77°56.126E	12	3.6±0.57	8 ±2	0.7±0.01	0.02±0.001	1.9± .17
3	MS-BCFC	10	30°28.778 N, 77°25.548E	23	2.48±0.41	6.71±1.42	0.75±0.04	0.03± 0.002	1.46±0.09
4	MS-BCFD	3	30°28.758 N, 77°25.528E	17	1.83±0.41	8.17±1.45	1.17±0.04	0.1±0.005	1.9±0.12
5	MS-BCFE	2.5	30°28.697 N, 77°25.425E	20	2.03±0.63	11.95±2.16	0.69±0.05	0.1±0.005	1.74±0.15
Charavathur Formation									
7	CHR-OSL-0	0.1	12°12.99 N, 77°9.756 E	-	0.83±0.16	2.62±0.50	0.003±0.055	0.22±0.01	0.525±0.073
8	CHR-OSL-3	10		18	0.42±0.12	2.77±0.43	0.10±0.04	0.04±0.005	0.36±0.04
9	CHR-OSL-1	26		27	0.66±0.12	2.33±0.46	-0.07±0.04	0.01±0.001	0.25±0.03
10	CHR-OSL-2	26		28	0.39±0.11	1.49±0.41	0.01±0.04	0.01±0.001	0.16±0.03
11	CHR-OSL-4	26		30	0.45±0.12	1.53±0.42	-0.09±0.07	0.01±0.001	0.16±0.02
12	CHR-OSL-5	26		17	0.18 ±0.1	1.12±0.3	0.1±0.05	0.01±0.001	0.20±0.04
13	CHR-OSL-6	26.1		20	0.37±0.12	2.07±0.45	0.01±0.03	0.01±0.001	0.2±0.03
14	CHR-OSL-7	31		24	0.46±0.09	0.86±0.31	0.0580.052	0.01±0.001	0.20± 0.04
15	CHR-OSL-8	31		18	0.33±0.13	1.48±0.49	-0.15±0.04	0.01±0.001	0.16±0.03
16	CHR-OSL-9	31		29	0.15±0.12	1.36±0.37	0.086±0.053	0.01±0.001	0.19±0.04

Table 6-2 Single aliquot regeneration protocols to estimate the equivalent dose.

Step no:	SAR(Murray and Wintle, 2000a)	DSAR(Banerjee et al., 2001)	Remarks
1	Preheat of 220-240 ℃ @2℃/s, 10 s	Preheat of 220-240 ℃ @2℃ /s, 60 s	Remove shallow traps
2		IRSL for 100s, @50℃	Remove signal from feldspar inclusion
3	BSL for 40 s, @125℃	BSL for 40 s, @125℃	**Lx**
4	Test Dose (25% of De)	Test Dose (25% of De)	Test dose to track sensitivity
5	Preheat of 220-240 ℃ @2℃/s, 10 s	Preheat of 220-240 ℃ @2℃ /s, 60 s	Remove shallow traps
6		IRSL for 100s, @50℃	Remove signal from feldspar inclusion
7	BSL for 40 s, @125℃	BSL for 40 s, @125℃	**Tx**
8	BSL for 100 s@200℃	BSL for 100 s@200℃	Hot Bleach
9	Regenerative dose	Regenerative dose	

Table 6-3 Multiple aliquot protocol to estimate the equivalent dose.

Step No	MAAD BSL Protocol	Measurement
1	Natural sample/ Natural + Additive dose	
2	Preheat (220-260 °C), 10 sec	
3	IRSL at 50 ºC for 100 s	
4	BSL at 125 ºC for 40 s	BSL signal
5	Test dose (Dt)	
6	Preheat (220-260 °C), 10 sec	
7	IRSL at 50 ºC for 100 s	
8	BSL at 125 ºC for 40 s	BSL (test dose signal)
9	Heat till 450 °C	
10	Test dose (Dt)	
11	TL Blue (220-260°C)	TL after annealing, blue emission (test dose signal)
12	IRSL at 50 ºC for 100 s	
13	BSL at 125 ºC for 40 s	BSL after annealing (test dose signal)

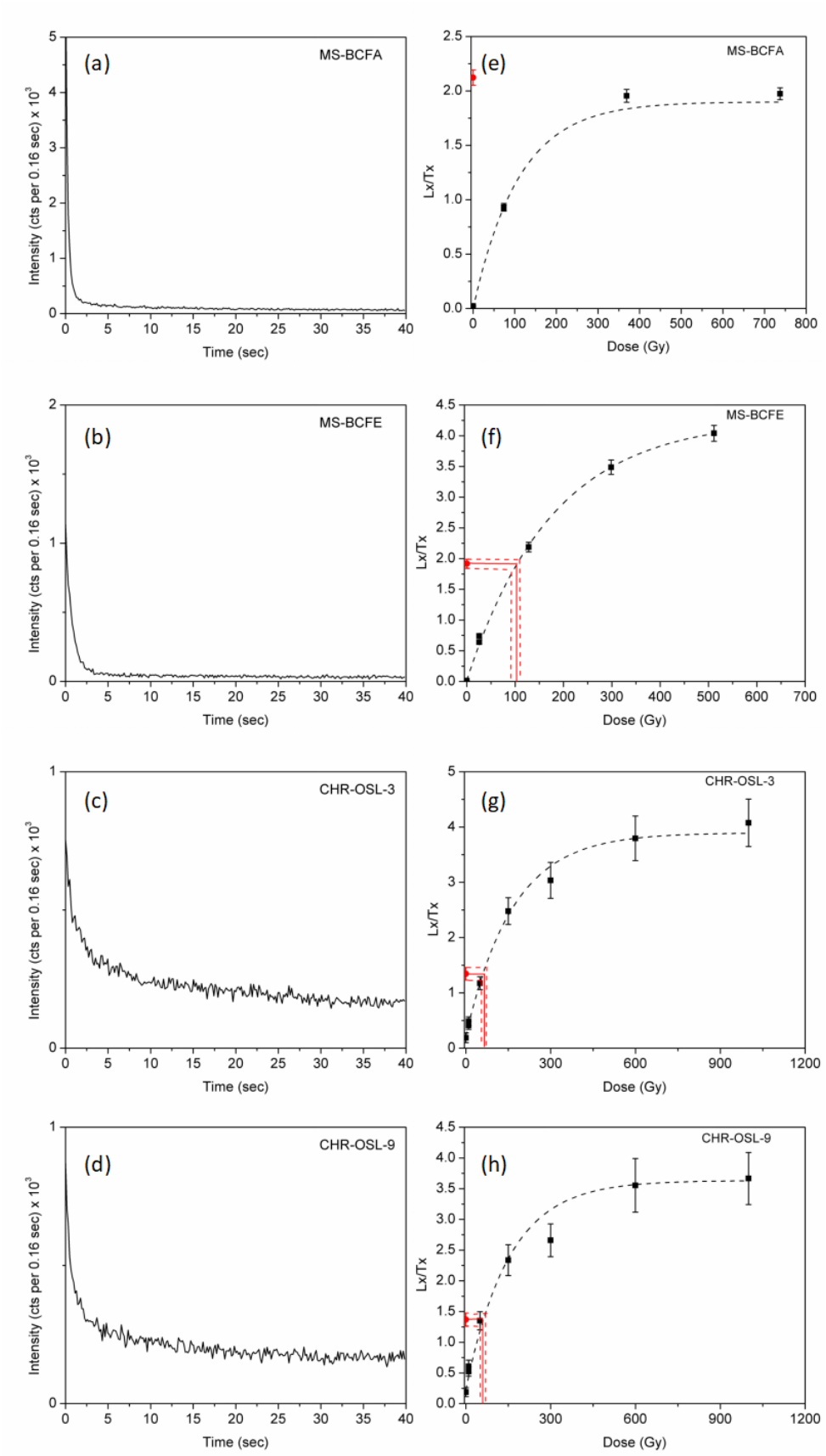

Figure 6-4 (a)-(d) shows the BSL shine down curves and (e)-(h) the SAR/DSAR dose response curves of Shivalik and Charavathur samples.

Table 6-4 Summary of Equivalent dose obtained from SAR and related parameters.

SR. No.	Sample Name	Expected age	Number of disc	Grain Size (um)	Protocol used	OD (%)	Recuperation	Model	Equivalent dose (Gy)	Age (ka)
Upper Shivaliks										
1	MS-BCFA	<1.7 Ma	0/5	90-150	SAR	-	5%	CAM	>218 ± 4	>100
2	MS-BCFB	<1.7 Ma	0/5	90-150	SAR	-	5%	CAM	>220 ± 4	>111
3	MS-BCFC	<0.7Ma	15/20	90-150	SAR	21	5%	CAM	176 ± 11	120± 11
4	MS-BCFD	<0.7Ma	17/20	90-150	SAR	18.5	5%	CAM	121 ±6	63±5
5	MS-BCFE	0.7 Ma	15/20	90-150	SAR	36	5%	MAM3	90 ±19	51±11
Charavathur formation										
7	CHR-OSL-0	0 Ma		90-150	DSAR	-	-	-	-	-
8	CHR-OSL-3		20/24	90-150	DSAR	16	5%	CAM	69±3	191±23
9	CHR-OSL-1		21/24	90-210	DSAR	52	10%	MAM3	71±15	287±68
10	CHR-OSL-2		19/22	90-210	DSAR	26	10%	CAM	66±4	408±84
11	CHR-OSL-4		15/24	90-210	DSAR	46	5%	MAM3	64±17	390±18
12	CHR-OSL-5		21/24	90-150	DSAR	24	10%	CAM	70±4	362±77
13	CHR-OSL-6		21/24	90-150	DSAR	27	10%	CAM	73±5	370±57
14	CHR-OSL-7		20/24	90-210	DSAR	29	10%	CAM	71±5	363±76
15	CHR-OSL-8		20/24	90-150	DSAR	30	10%	CAM	57±4	364±74
16	CHR-OSL-9	>2.5 Ma	17/24	90-150	DSAR	51	10%	MAM3	60±13	381±92

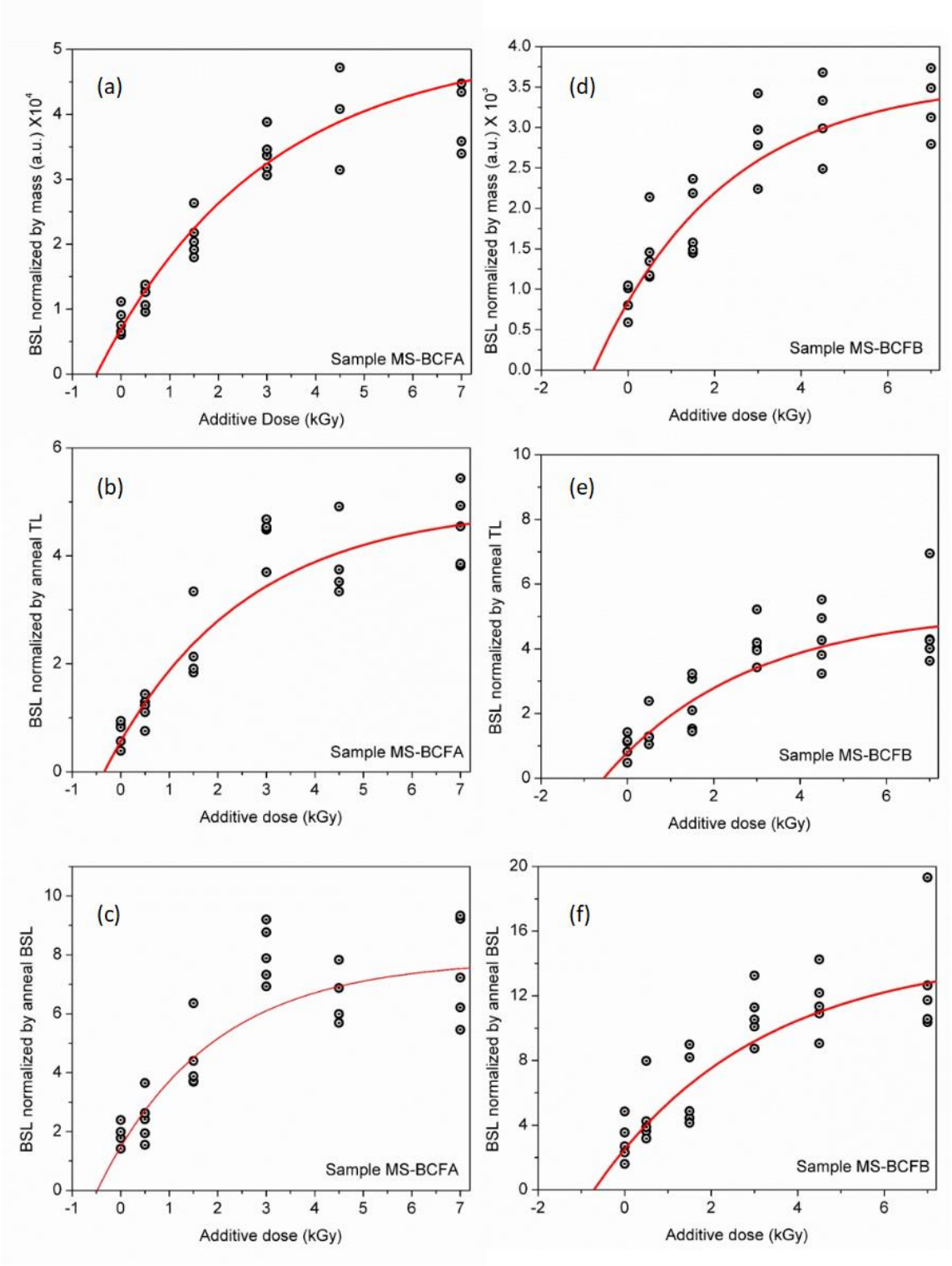

Figure 6-5 MAAD dose response curve of (a-c) MS-BCFA and (d-f) MS-BCFB, normalized by various normalization.

6.4.2. **Multiple aliquot additive protocol**

The multiple aliquot additive protocol as described in Table 6-3 is also applied to estimate the equivalent doses. For the samples that had feldspar inclusion (CHR-OSL series) an infrared stimulation for 100 s at 50℃ is given prior to BSL, otherwise it is skipped. As suggested in previous chapter, mass of the sample on the aliquot, BSL after annealing and TL after annealing (blue emission) are used as normalization for inter-aliquot comparison. The results are shown in Figure 6.5 for MS-BCF samples and Figure 6.6 for CHR-OSL samples. The saturation of BSL signals in general is found to be higher than SAR. An equivalent dose greater than SAR is obtained for all analysed samples and is summarised in Table 6-5. In sample CHR-OSL-3, an initial decrease in the BSL intensity is observed for the "additive + natural" dose, followed by increase with further additive doses and saturation. Additionally, the BSL after annealing and TL after annealing (blue emission) signals are found to carry negligible dependence on the additive dose, expect for few cases as shown in Figure 6.8, where BSL after annealing in CHR-OSL-8 had an initial dependence on the additive dose and hence is not used to construct the DRC. The mass normalized MAAD DRC for the infrared signal is also analysed for the CHR-OSL samples. Figure 6.7 shows the results, which indicate that the IRSL signals from feldspar contamination do not show an increase in intensity as shown by the BSL signal from quartz.

The equivalent dose obtained from the MAAD-BSL DRC does not increase with the depth. Hence, to understand the reason, the kinetics of the charge trapping and detrapping is investigated.

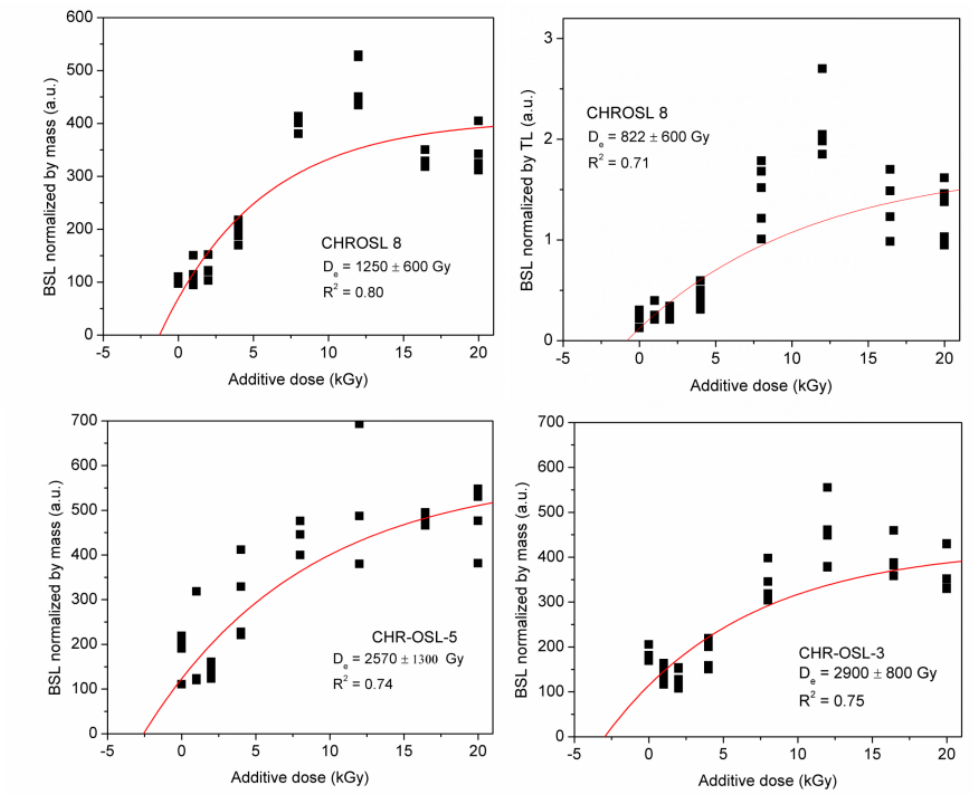

Figure 6-6 BSL MAAD dose response curve of CHR-OSL series sample normalized by various normalization.

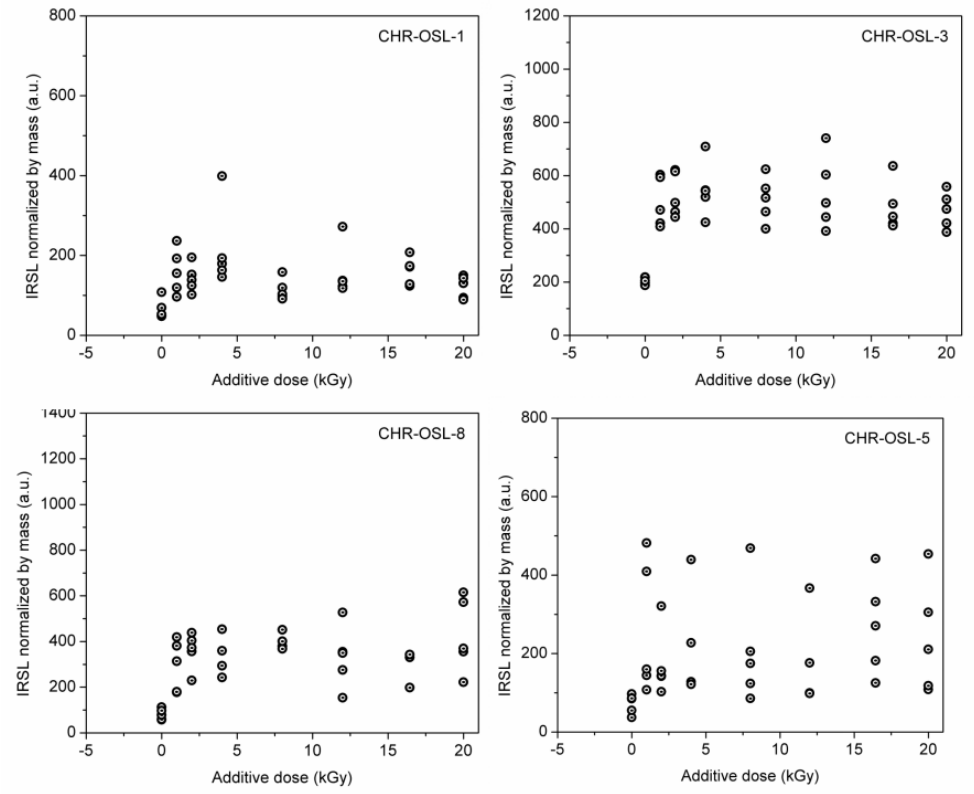

Figure 6-7 IRSL MAAD dose response curve of CHR-OSL series sample normalized by mass.

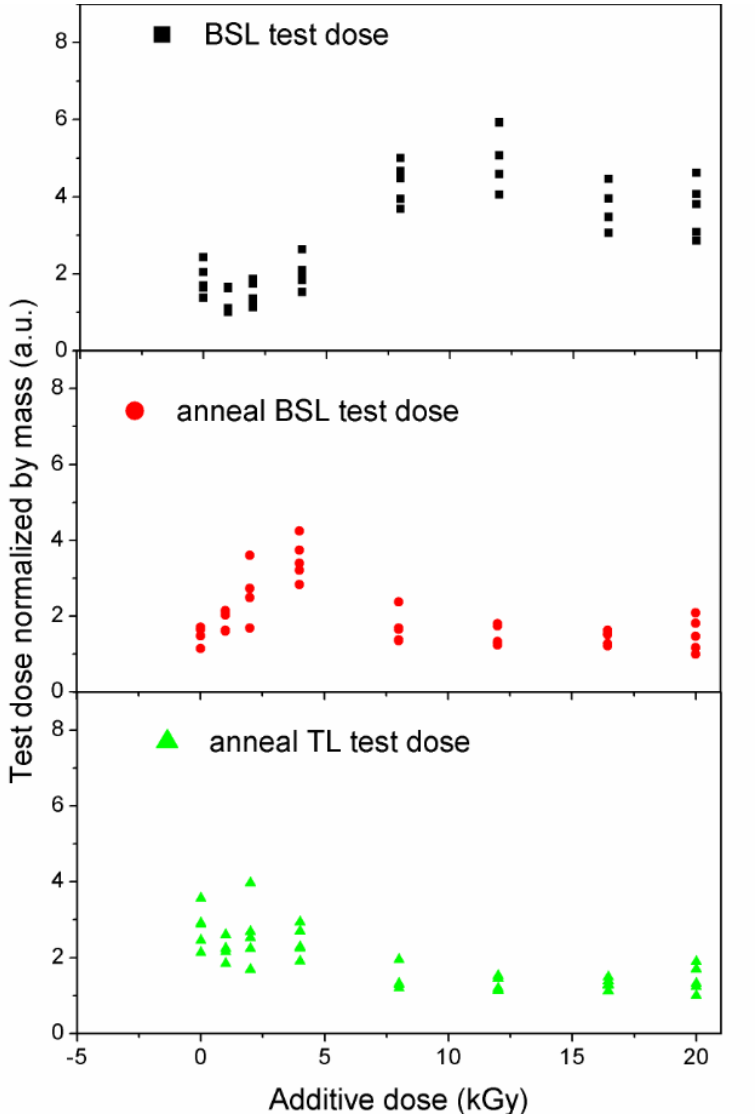

Figure 6-8 Test dose signal of sample CHR-OSL-8 normalized by mass.

Table 6-5 Summary of equivalent dose obtained from the MAAD protocol.

Sr. No.	**Sample Name**	**Expected Age (Ma)***	**Dose Rate (Gy/ka)**	**Expected Dose (Gy)**	Estimated Equivalent dose (Gy)		
					MAAD (mass normalized)	**MAAD (TL (after annealing, blue emission) normalization)**	**MAAD (BSL after annealing normalized)**
Shivalik samples							
1	MS-BCFA	0.5-1.7	2.17±0.18	1085-3700	503 ± 153	338 ± 127	483 ± 213
2	MS-BCFB	0.5-1.7	1.9± .17	955-3248	794 ± 261	547 ± 228	709 ± 286
Charavathur samples							
3	CHR-OSL-3	>2.5	0.36±0.04	>900	2900 ± 800	1835± 1843	2900± 2185
4	CHR-OSL-5	>2.5	0.20±0.04	>500	2570 ± 1300	2000 ± 1200	1840 ±1200
5	CHR-OSL-8	>2.5	0.16±0.03	>400	1250 ±600	822 ± 600	-

6.5. Kinetic Modelling

In order to understand the relatively low dose and age of Charavathur samples obtained in the SAR analysis and the inconsistent ages in stratigraphy obtained from the MAAD analysis, the kinetics equations governing the charge trapping and detrapping dynamics of luminescence mechanism are investigated.

6.5.1. Theory

For the single trap state in the crystal, which does not show any anomalous fading as in the case of quartz, the rate of change in number of charges (electrons/holes) in the trap due to build up by the ambient radioactivity and reduction due to thermal detrapping is given by (Li and Li, 2012; Randall and Wilkins, 1945)

$$\frac{dn}{dt} = \frac{\dot{D}}{D_0}(N - n) - nse^{\frac{-E}{kT}} \tag{6.1}$$

Where n is the number of charges in the traps, N is the total number of traps, t is the time, $\dot{D}$ (Gy/ka) is the ambient dose rate of the crystal, D_0(Gy) is the characteristics dose of saturation, s (s^{-1}) is the frequency factor, which is the frequency with which the electron oscillate in the potential of the trap, attempting to escape from there, E is the activation energy (trap depth) (eV), T is the ambient temperature (K) and k is the Boltzmann constant. The first part of the equation, defines the filling rate, which for a constant dose rate is high in the beginning of irradiation as more number of traps are available and the second term defines the emptying rate, which is proportional to number of charged traps and hence is significant when "n" increases. When the filling and emptying rate becomes equal, there is no further change in the number of charges in the trap, hence $\frac{dn}{dt}$ = 0 and an equilibrium is reached. At equilibrium, equation 6.1 can be written as,

$$\frac{\dot{D}}{D_0}(N - n) = nse^{\frac{-E}{kT}} \tag{6.2}$$

Dividing the equation by N and substituting $\frac{N}{N} = \varphi_s$, the saturation value and $\frac{n}{N} = \varphi_{eq}$, the equilibrium value, equation 6.2 can be re-written as

$$\frac{\varphi_{eq}}{\varphi_s} = \frac{\dot{D}}{(\dot{D}+sD_0\, e^{\frac{-E}{kT}})} \tag{6.3}$$

This equation gives the ratio of equilibrium to saturation intensity of the luminescence. The equation shows that the equilibrium value will depend on the natural dose rate, the kinetics of the trap and the ambient temperature and their role are discussed below.

6.5.2. Effect of Dose rate

The dose rate for the laboratory measurements (~0.04Gy/s) is very large as compared to the natural dose rates (1 Gy/ka = 3.17 x 10^{-11} Gy/s). The effect of this rate is investigated using equation 6.3. Two values of D_0 are chosen as shown in the previous sections for the BSL signals, 150 Gy (from the SAR) and 5500 Gy (form the MAAD). The activation energy and frequency factor are selected based on the literature. For the activation energy, large variation is seen in the estimated values in the literature. From 1.41±0.13 eV (Durcan, 2018) and 1.56 eV (Wang et al., 2024), 1.65 ± 0.04 eV (Spooner and Questiaux, 2000) 1.66 ± 0.02 eV (Biernacka et al., 2022a), 1.74 eV (Singarayer and Bailey, 2003), 1.70 ± 0.01 eV (Mineli et al., 2021) for quartz stimulated by blue light 470 ±20 nm and observed in UV (340±40 nm) via Hoya filter. Hence an average value of 1.65 ±0.04 eV is used in this work. The results (Figure 6.9) show that at lab dose rates; the thermal fading effects are negligible and the lab saturation can be considered as the true saturation of the charges in the traps. However, for natural dose rates, which are 4 Gy/ka or less, there is difference between the true saturation and the maximum value that will be attained in the nature. Suggesting that in nature, the traps will never be saturated (Figure 6.9).

Table 6-6 Summary of previously reported activation energy and frequency factor for the BSL signal of quartz.

Sr. No	**Activation energy (eV)**	**Frequency factor (s^{-1})**	**Reference**
1	1.41±0.13	4.25×10^{11}	Durcan, (2018)
2	1.56		Wang et al., (2024)
3	1.65 ± 0.04	1.30×10^{13}	Spooner and Questiaux, (2000)
4	1.66 ± 0.02	1.00×10^{13}	Biernacka et al., (2022a)
5	1.70 ± 0.01	7.76×10^{13}	Mineli et al., (2021)
6	1.74	8.90×10^{13}	Singarayer and Bailey, (2003)
Value taken	1.65 ± 0.04 eV	1.30×10^{13}	

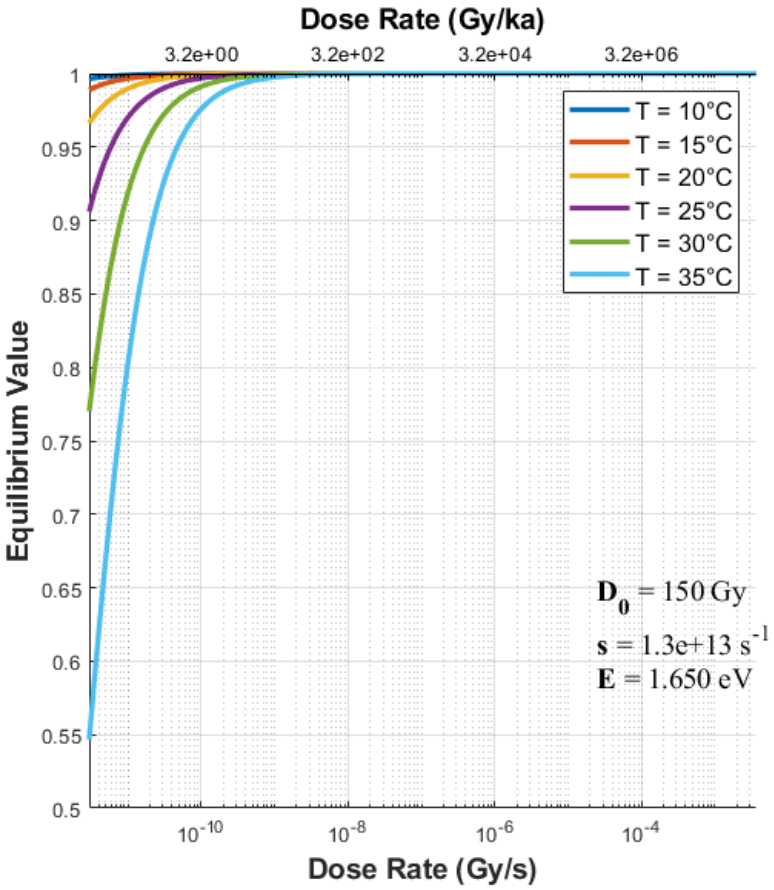
Dose Rate (Gy/ka)
3.2e+00
3.2e+02
3.2e+04
3.2e+06
Equilibrium Value
Dose Rate (Gy/s)
T = 10°C
T = 15°C
T = 20°C
T = 25°C
T = 30°C
T = 35°C
D0 = 150 Gy
s = 1.3e+13 s-1
E = 1.650 eV

(a)

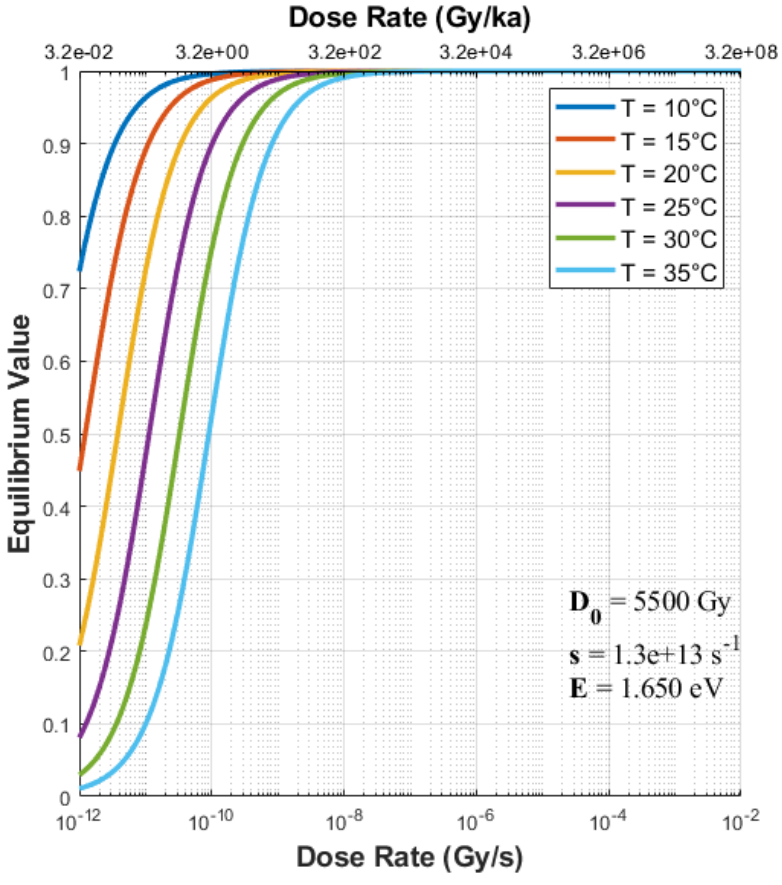
Dose Rate (Gy/ka)
3.2e-02
3.2e+00
3.2e+02
3.2e+04
3.2e+06
3.2e+08
Equilibrium Value
Dose Rate (Gy/s)
T = 10°C
T = 15°C
T = 20°C
T = 25°C
T = 30°C
T = 35°C
D0 = 5500 Gy
s = 1.3e+13 s-1
E = 1.650 eV

(b)

Figure 6-9 The variation of equilibrium value for the dose rate. (a) For D_0= 150 Gy and (b) for D_0=5500 Gy.

6.5.3. Effect of activation energy

Activation energy is an indicator of the stability of the trap. Higher the activation energy more is its thermal stability. Large variations are observed in the activation energy estimated for the BSL signals of the quartz as observed in Table 6-6, not only in different quartz samples of varying provenance, but also within multiple measurements in the same sample (Biernacka et al., 2022b). The equilibrium value variation is studied with the activation energy and the results are shown in Figure 6.10. Results indicate that the equilibrium value sharply decreases with the decrease in activation energy. For a trap having a characteristics dose (D_0) of 150 Gy, the activation energy ~1.65 eV corresponds to equilibrium level close to 1, except at very low dose rate (< 1Gy/ka), where the equilibrium level is around 0.9. However, for a trap with a characteristics dose (D_0) of 5500 Gy for the same activation energy, the equilibrium levels are less.

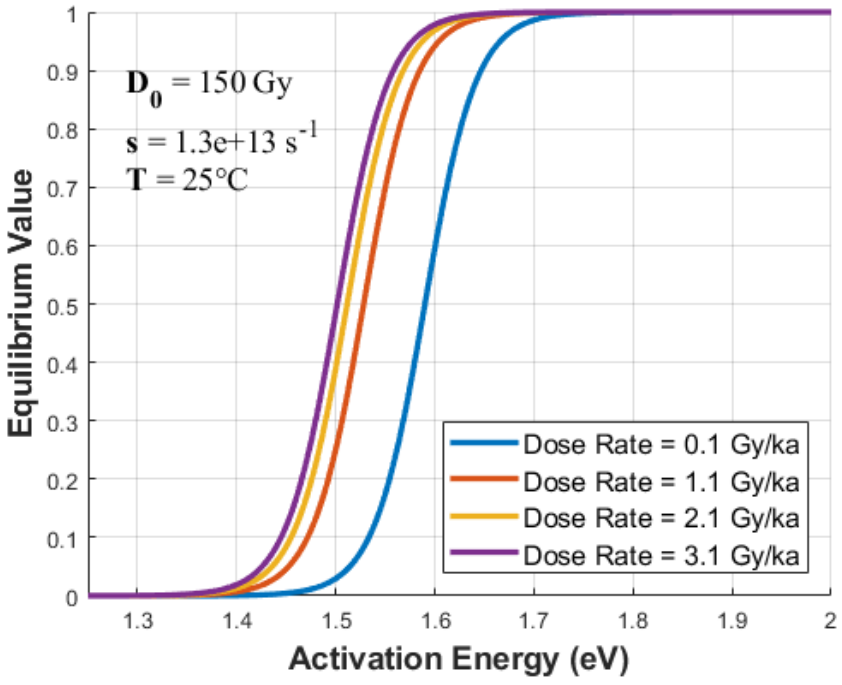

(a)

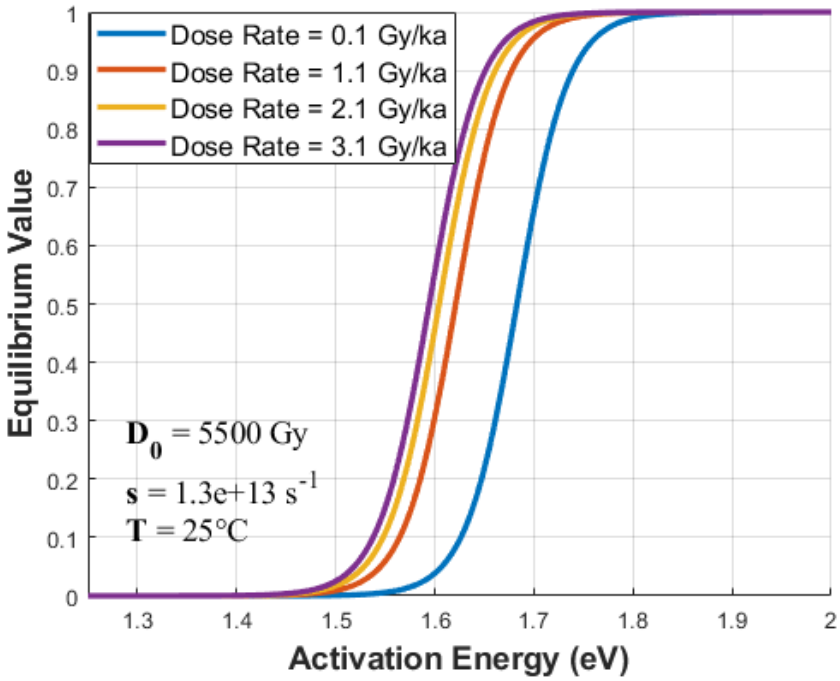

(b)

Figure 6-10 The variation of equilibrium value for the dose rate. (a) For D_0= 150 Gy and (b) for D_0=5500 Gy.

6.5.4. Effect of ambient temperature

Ambient temperature is another factor, which plays a major role and Figure 6.11 shows the effect of ambient temperature on the equilibrium value. As the temperature increases, the equilibrium value decreases. For a characteristics dose (D_0) of 150 Gy and dose rate >1 Gy/ka and temperatures ~ 35°C results in an equilibrium value close to 1, but for low dose rate ~ 0.1 Gy/ka equilibrium value is around 0.8, indicating that a maximum of 80% of the traps will be filled. For a characteristics dose (D_0) of 5500 Gy, ambient temperatures result in drastically lesser equilibrium value.

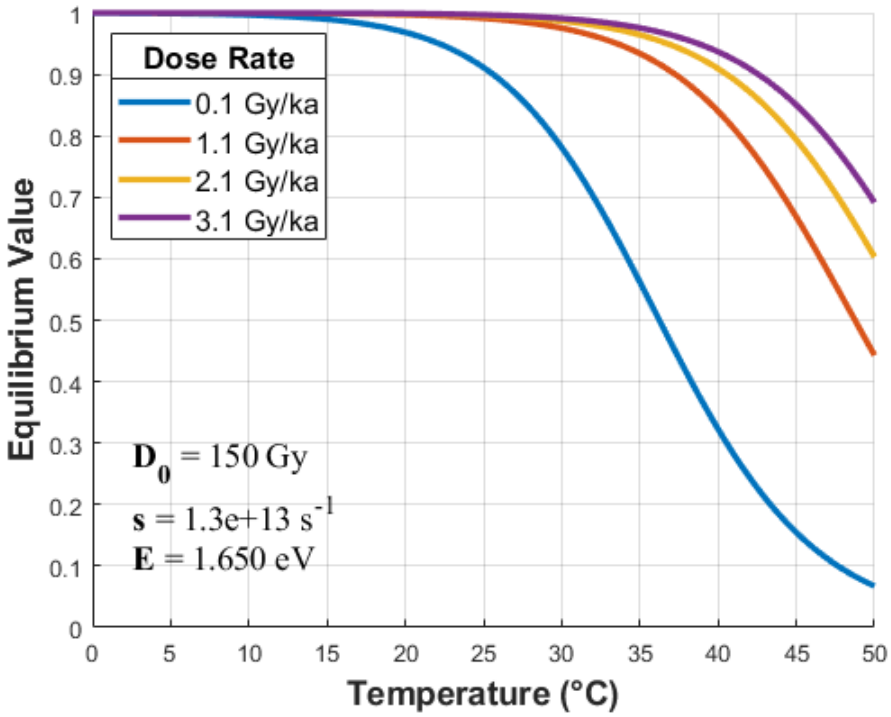

(a)

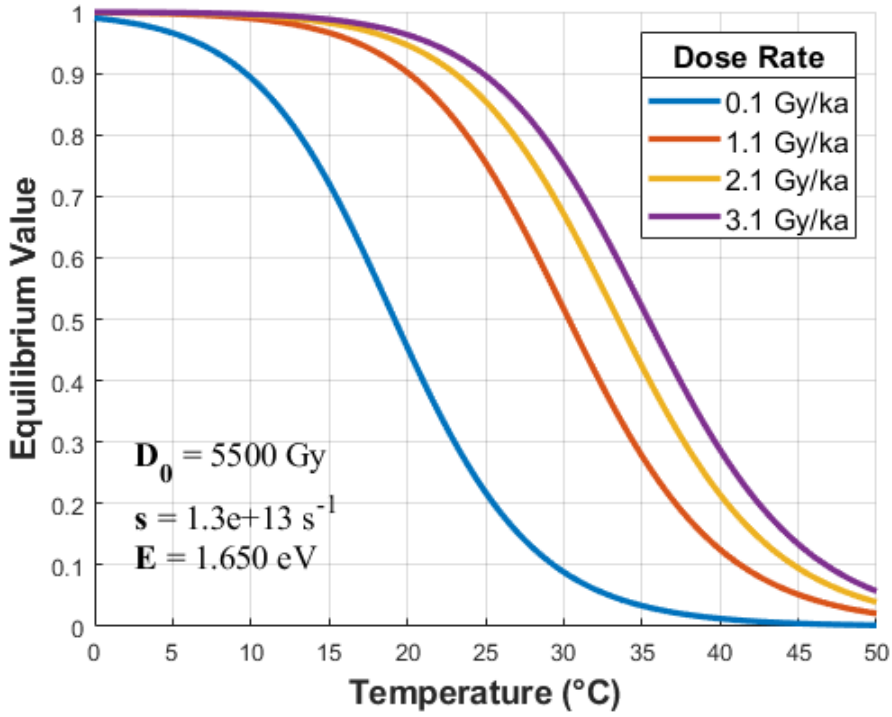

(b)

Figure 6-11 The variation of equilibrium value with ambient Temperature. (a) For D0= 150 Gy and (b) for D0=5500 Gy.

6.5.5. Laboratory and natural dose response curve

The discussion in previous sections show that due to the difference in the dose rate, the saturation obtained in the lab is different from the saturation obtained in the natural environment (in nature the saturation is not obtained instead it is the equilibrium value). Solving equation 6.1 to get the dose response curve by assuming that at time t=0, the number of trapped charges were also zero.

We get,

$$I = \frac{a}{b} I_0 \, (1 - e^{-bt}) \tag{6.4}$$

where $a = \frac{\dot{D}}{D_0}$ and $b = \frac{\dot{D}}{D_0} + se^{-\frac{E}{kT}}$

Equation 6.4 shows that the dose response curve is dependent on the dose rate and is lower for the natural dose rate as compared to laboratory dose rate. Figure 6.12 and 6.13 shows the simulated laboratory and natural dose response curve for varying kinetic parameters. The natural dose response curve is very sensitive to the activation energy. For a typical error of ± 0.04eV in kinetic energy (obtained in the experimental data), the natural dose response curve for the same temperature varies. Hence, signifies the need to precisely estimate the kinetic parameters viz. activation energy, ambient temperature and dose rate of the sample. Previously, many studies have reported that there are differences in the luminescence levels obtained in the laboratory and the natural measurements (Chapot et al., 2016, 2012; Rahimzadeh et al., 2023b; Tsukamoto et al., 2008), however, the reason was not explained satisfactorily. It is observed that in nature, field saturation is obtained the level of which is less than laboratory level. This is also validated by Figure 6.12 and 6.13. Further Li and Li, (2012) has also reported that because of inclusion of thermal effects, reliable doses can be estimated only till 100 ka, however, in these studies the natural signals are interpolated (as in SAR) or extrapolated (as in MAAD) on the laboratory dose response curve, but these should be inter/extrapolated on the natural dose response curve.

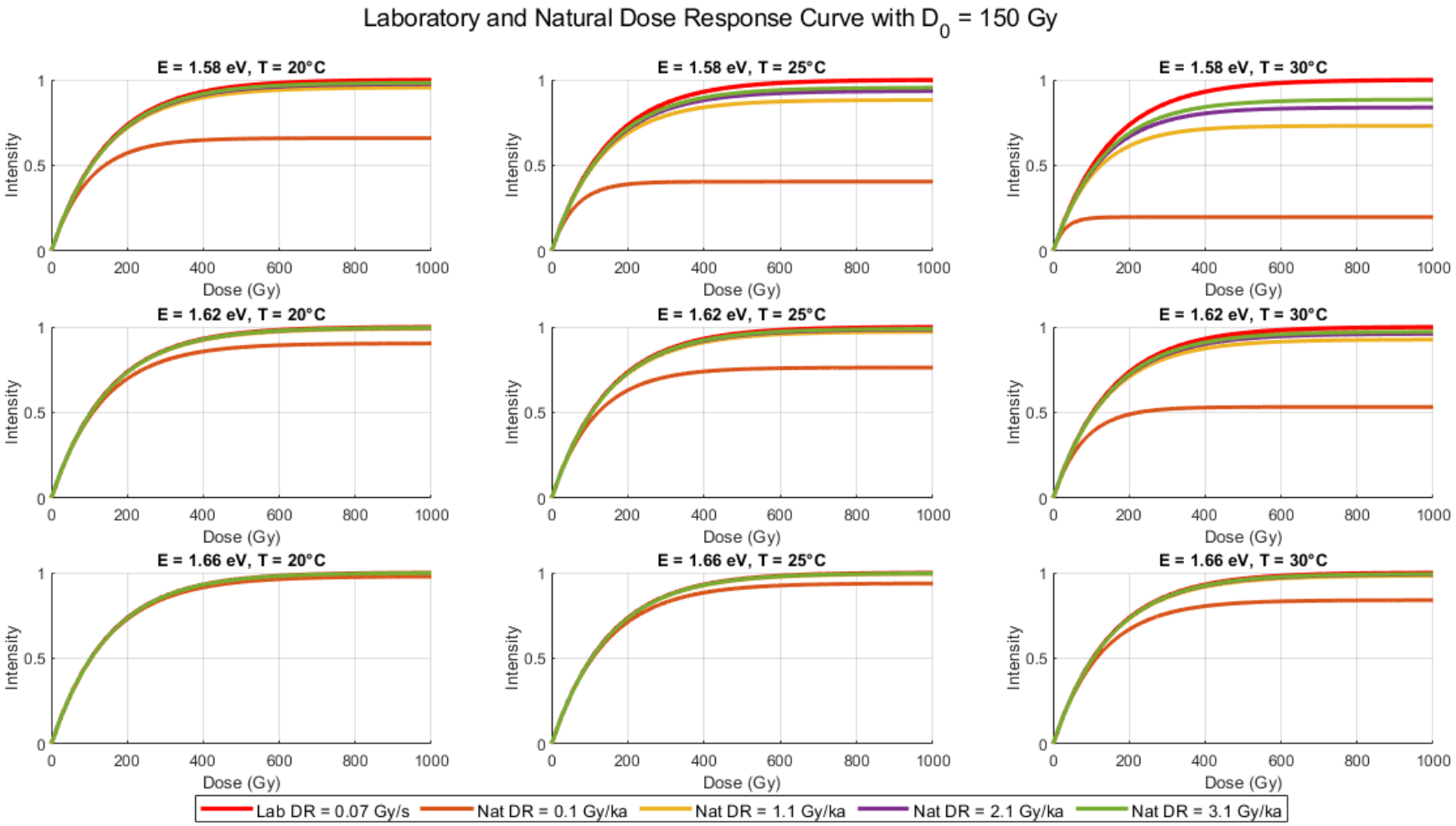

Figure 6-12 Laboratory and Natural dose response curve at various activation energy, temperature and dose rate for a characteristics dose of 150 Gy.

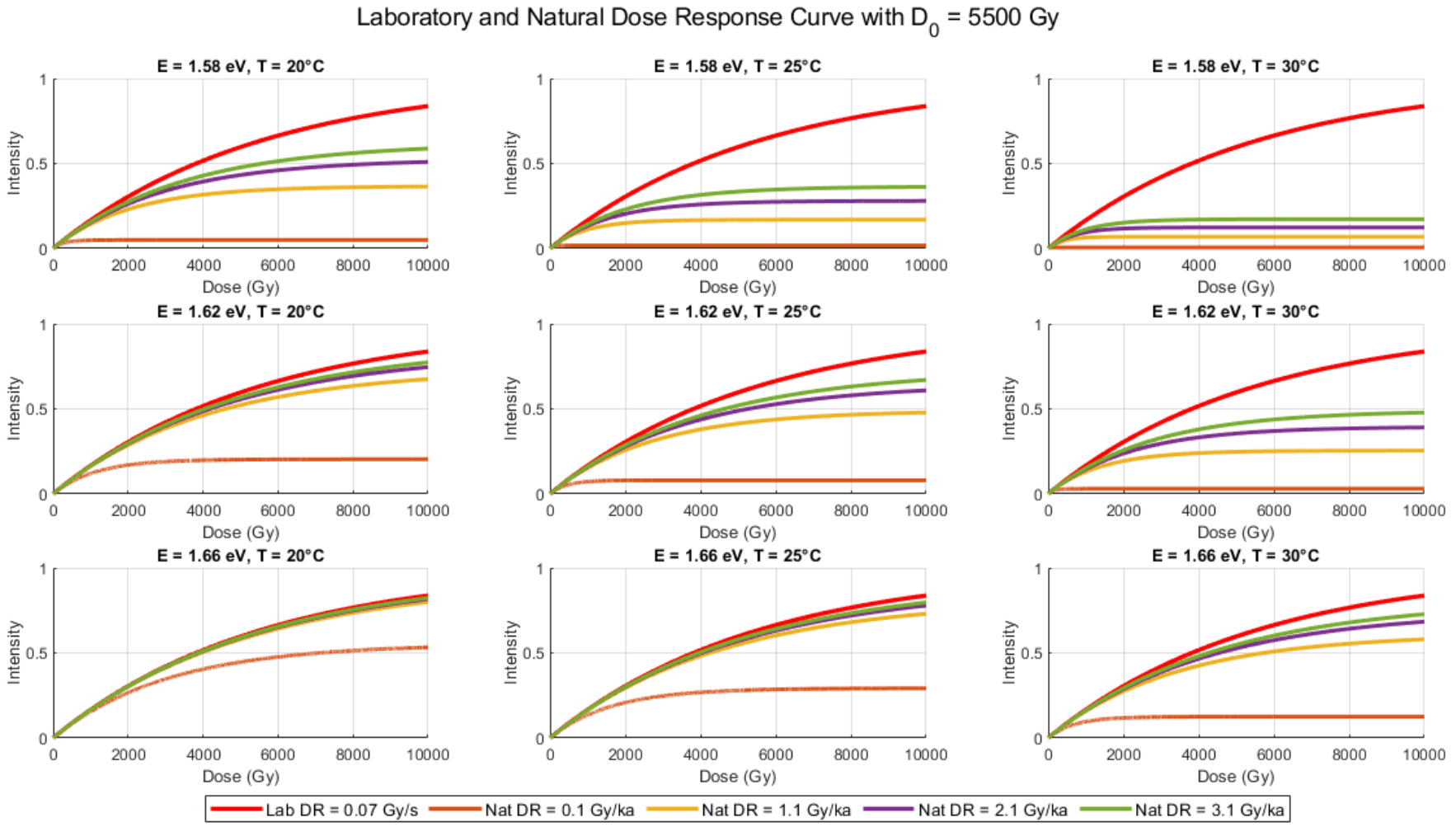

Figure 6-13 Laboratory and Natural dose response curve at various activation energy, temperature and dose rate for a characteristics dose of 5500 Gy.

6.6. Equilibrium value and Interpretation for natural samples

In this section, the maximum saturation level obtained in nature (equilibrium level) is calculated from equation 6.3 using the characteristics dose obtained from the laboratory dose response curve in SAR and MAAD analysis, dose rate estimated in lab and activation energy, frequency factor and ambient temperature are taken based on literature (Ajithkumar and Riya, 2022; Biernacka et al., 2022a). If the samples are in equilibrium, then the experimental equilibrium level can be calculated from ratio of measured equivalent dose and characteristics dose. The error of 0.04 eV for activation energy, $D_0/10$ for characteristics dose, 2 K in temperature is taken for theoretical calculation. The resultant error is calculated by error propagation. Results are summarized in Table 6-7 and are discussed below.

The Charavathur samples: From the SAR analysis the equilibrium value obtained from theoretical estimates is ~0.9, while the experimental ratio of equivalent dose to characteristics dose is around ~0.5. The experimental and theoretical values do not match within the errors. Hence, according to SAR these samples are not in equilibrium. In the MAAD methodology, the experimental equilibrium (D_e/D_0) and the theoretical equilibrium are near and within error, but the errors are very large. The experimental errors are high because we could estimate the equivalent dose with an error of 50%. However, the large theoretical errors are because of the characteristics of curves, wherein, a small error in the input parameter propagates to large error in the equilibrium value, except when we are near the edges of the S-shape theoretical curve (Figure 6.9-11). From both SAR and MAAD analysis, MAAD could explain the equilibrium level of the Charavathur samples, while SAR couldn't suggest conclusive explanation.

The Shivalik samples: In the SAR analysis, an equilibrium value near 1 is obtained and the natural signals are near to 1, suggesting that the traps are in saturation. However, in the MAAD analysis, the equilibrium value is very high, in comparison to the obtained equivalent dose, suggesting that the Shivalik samples are not in equilibrium. Since, MAAD could explain the equilibrium level in the Charavathur samples, here also the

Table 6-7 Equilibrium value estimates for the samples.

Sample name	Method	Calculated De (Gy)	Saturation value (Gy)	Activation energy (eV)	Frequency factor (s^{-1})	Dose rate (Gy/ka)	Ambient Temperature (K)	D_e/D_0	Theoretical equilibrium value
Upper Shivalik									
MS-BCFA	SAR	In saturation	218 ± 4	1.65±0.04	1.30E+13	2.17 ±0.18	298±2	-	0.99±0.01
MS-BCFA	MAAD	503±153	5800±800	1.65±0.04	1.30E+13	2.17 ±0.18	298±2	0.09±0.03	0.88±0.17
MS-BCFB	SAR	In saturation	220 ± 4	1.65±0.04	1.30E+13	1.9± .17	303±2	-	0.99±0.01
MS-BCFB	MAAD	794±261	5800±800	1.65±0.04	1.30E+13	1.9± .17	303±2	0.14±0.05	0.87±0.19
Charavathur Formation									
CHR-OSL-3	SAR	69±3	170±13	1.65±0.04	1.30E+13	0.36±0.04	303±2	0.41±0.04	0.94±0.1
CHR-OSL-3	MAAD	2900±800	9433±1495	1.65±0.04	1.30E+13	0.36±0.04	303±2	0.31±0.1	0.21±0.26
CHR-OSL-5	SAR	70±4	133±14	1.65±0.04	1.30E+13	0.20±0.04	303±2	0.53±0.06	0.91±0.13
CHR-OSL-5	MAAD	2570±1300	10847±6059	1.65±0.04	1.30E+13	0.20±0.04	303±2	0.24±0.18	0.11±0.16
CHR-OSL-8	SAR	57±4	157±15	1.65±0.04	1.30E+13	0.16±0.03	303±2	0.36±0.04	0.87±0.17
CHR-OSL-8	MAAD	1250±600	6756±2200	1.65±0.04	1.30E+13	0.16±0.03	303±2	0.19±0.11	0.14±0.19

MAAD deduced results seems more believable. However, still the estimated doses are lower than the expected doses (1000-3500 Gy) based on paleomagnetic dating defined chronology of the samples (Table 6-2) and suggests an underestimation of ages. There can be several reasons for this underestimation. Recent results of the ESR dating of fossils (dental enamel) from the Pinjor formation of the upper Shivaliks, which is lower in stratigraphy (hence older) compared to BCF, suggest a relatively younger age of 465 ka (Kaur et al., 2025) than that predicted by paleomagnetic dating (>1.7 Ma) (Kumar et al., 1999; Mandal et al., 2019; Rao et al., 1995). If these ESR ages are true compared to the paleomagnetic ages, then OSL age obtained from MAAD could be explained. Other possibility is that these estimated ages depict the exhumation age of BCF samples not the depositional age (Bouscary et al., 2024). In the present study, for the samples MS-BCFC, MS-BCFD, MS-BCFE shows an inversion of the OSL ages compared to the predicted paleomagnetic ages. This depicts that older samples are younger and it seems possible that OSL here depicts the age since when the samples have crossed their closure temperature, rather than the depositional ages.

6.7. **Conclusions**

In this chapter, two geological sections were studied which are previous predicted to have formed ~million year ago. The doses of both the samples are estimated by SAR and MAAD methodology. Following conclusion can be drawn.

1. For the Shivalik samples, the ages depict the exhumation age, rather than the depositional age.
2. For the Shivalik samples that were in saturation in SAR, MAAD could estimate the dose.
3. For the Charavathur samples, quartz BSL increases at least till 6000 Gy additive dose, while IRSL signal from the feldspar inclusion saturates after ~2000 Gy additive dose.
4. The Charavathur samples were in equilibrium, and this equilibrium level could be explained based on MAAD analysis, including the thermal effects rather than the SAR methodology.

Chapter 7: Summary and Future Outlook

7.1. Present Study

The objective of the present thesis is to develop a methodology for estimation of high radiation doses (HRDs) acquired by natural minerals. This research is driven by the need to extend the applicability and dating range of luminescence dating beyond its existing limits (~0.5 Ma). Hence, the thesis aimed to build an understanding of the luminescence mechanism of conventional minerals (quartz and feldspar) at high radiation doses and effect of HRDs on the natural crystals and their luminescence properties. Further, the thesis also explores new natural mineral for its use as potential natural dosimeters suitable for extending dating limits.

To achieve these objectives, the thesis investigates three natural minerals viz., quartz, feldspar and jarosite. Quartz and feldspar are well-established dosimeters used extensively in terrestrial geochronology but mismatch in ages is observed above 100 ka for quartz and 300 ka for feldspar (Buchanan et al., 2022; Chapot et al., 2016, 2012; Li et al., 2018; Murari et al., 2021; Rahimzadeh et al., 2023a, 2023b, 2021). Jarosite is explored considering its importance as a paleoclimate indicator, as it is formed in arid environment and is direct indicator of paleoaridity. Additionally, jarosite is also detected in Martian sediments by rovers as iron sulfate mineral. This provides possibility to study Martian surface processes, however, it is yet untested for its luminescence potential (Morris et al., 2000). Therefore, this study examines TL and BSL signals, dose–response curves, kinetics and normalization methods, focusing on saturation behavior, spectral characteristics, and the effects of high doses.

The major findings for jarosite are as follows:

1. *Luminescence response:* Jarosite demonstrates considerable luminescence potential for estimation of radiation doses and can be stimulated by both heat and light. The mineral responds to both blue and infrared stimulation, and emissions are visible in UV (280–

380 nm) and blue (400–480 nm) detection windows. HCl treatment enhances luminescence yield, likely due to the removal of surface gleying. TL glow peaks are recorded at approximately 100°C, 150°C, 300°C, and 350°C, with emissions detected across a broad spectral range (325–700 nm). The luminescence signals from jarosite are stable and reproducible, with TL showing <6% variability and BSL/IRSL <14% across repeated measurement cycles. Luminescence sensitivity varies between samples. Heating to 450°C alters signal intensity but not the shape of glow curves, a result supported by FTIR and CL-EDXS analyses.

2. *Kinetic analysis:* Fractional glow curve analysis suggests consistent kinetic characteristics for peaks below 300°C between annealed and unannealed samples. Deviations are observed at higher temperatures. Notably, the 300°C TL peak has an estimated lifetime of ~0.3 Ma at an ambient temperature of 30°C, whereas its lifetime is ~3 Ma at an ambient temperature of 10°C, making it suitable for dating older events in colder areas.
3. *Saturation and athermal fading:* Jarosite's BSL and IRSL signals each comprise three components. Saturation doses ranging from 590 Gy to 1600 Gy are obtained for different signals. While significant fading is observed in BSL (~6.6%/decade), IRSL (~7.4%/decade), and the 210°C TL peak (~4.3%/decade), the pIRIR225 signal (in both UV and blue detection windows) and the 350°C TL peak show no fading.
4. *Datable range:* Given a dose rate of ~2 mGy/year on Earth and ~65 mGy/year on Mars, jarosite can potentially date events up to ~800 ka and ~25 ka, respectively limited by the thermal stability of the traps.

The major findings for quartz are as follows:

1. *High-dose luminescence response and saturation behavior:* Quartz exhibits a significant TL signal increase in the 340–380°C range at doses up to ~18 kGy (rock) and ~10 kGy (sedimentary), particularly across the 325–700 nm spectral range. Saturation characteristics are primarily governed by trapping centres rather than recombination centres, and saturation doses are consistent across UV to red emissions.
2. *Bleachability and normalization challenges:* Luminescence bleachability is wavelength-dependent, with longer wavelengths showing lower bleachability. Standard normalization methods (e.g., zero/second glow) fail at high doses, and mass/weight-based normalization is more reliable beyond ~1 kGy.

3. *Sensitivity changes and pre-dose effects:* Pre-irradiation history significantly affects luminescence sensitivity. Emissions in the 340–380°C range and green/red 110°C signals increase after a high-dose pre-treatment, while UV 110°C emissions are quenched and blue emissions remain unaffected.
4. *Limitations of SAR-BSL protocol at high doses:* Although, the single aliquot regeneration (SAR) protocol works well for low-dose measurements, yet at higher regeneration doses, charge carry-over to the test dose measurements causes increase in the test signals, leading to early saturation of DRCs. Conventional SAR normalization methods are only reliable for doses below the saturation dose, and are not suitable for paleodoses near or beyond saturation.
5. *Preferred protocols and normalizations for high doses*: High-dose estimations are better handled using MAAD protocols combined with appropriate normalization methods. Techniques such as zero-glow, post-annealed BSL, and anneal TL (blue emission) show minimal regeneration dose dependence for test dose signal and offer more appropriate normalization for constructing DRCs in high-dose regime.
6. *Dose response behaviour and dose recovery:* BSL-Dose response curves built using suggested reliable normalization reflects a saturation around ~5800 Gy. Using this approach, a laboratory dose of 1000 Gy was accurately recovered, with a dose recovery ratio between 0.9 and 1.2.
7. *Methodology for old natural settings:* For samples where SAR shows saturation (e.g., in Shivaliks), the MAAD method successfully provides dose estimates, highlighting its suitability for high-dose scenarios. For Charavathur samples, dose equilibrium is better explained by MAAD, which accounts for thermal effects—demonstrating the limitations of SAR in complex geological contexts.

The major findings for feldspar are as follows:

1. TL measured in spectral emission 325-700 nm saturated around 1.5 kGy in rock sample and 6 kGy in sedimentary sample (chapter 3).
2. Further mass normalised IRSL from feldspar (chapter 6) saturates way early than quartz.

Previously, it is known that quartz saturates earlier than feldspar, but the work conducted in this thesis suggests that feldspar saturates earlier than quartz. This work also suggests that consideration of thermal effects in the dose response curve and appropriate normalizations are important to get reliable dose estimations. Considering these effects during natural antiquity,

this thesis shows that with the even BSL signal (BSL) having the best bleachability but considered low saturation dose can help date events that are million years old using suggested methods.

7.2. Future outlook

The quest to increase the luminescence dating limit had been long. Many new signals probing new traps are investigated in this regard. This thesis provides a different perspective then the conventional approach and aimed to understand luminescence properties at high radiation doses. The work suggests changes are required in the current methodology to date older samples and opens up new possibilities for study and establish the chronology of various earth surface and other planetary surface processes. These are summarized below:

1. *Dating of old samples:* The current work shows that the saturation dose of quartz BSL should be around 5 kGy, thus age estimates ~Ma should be possible limited by the thermal fading. Hence, this method can be applied to date older samples. Many studies have reported that the doses are underestimated in SAR (Dreimanis et al., 1978; Lowick et al., 2010b; Lowick and Preusser, 2011; Lu et al., 2007; Murray et al., 2007; Prescott and Robertson, 1997; Qin and Zhou, 2009; Timar-Gabor and Wintle, 2013; Wang et al., 2021). The current proposed normalizations including the thermal effects can be applied to these samples to test if dose underestimation is reduced or not.

2. *Re-investigation of other quartz protocols:* Most of the current protocols like Voilet Stimulated Luminescence (VSL), Thermally Transferred OSL (TT-OSL), Isothermal luminescence (ITL) are based on the SAR methodology wherein test dose is used for normalization. It is important to check if the test dose has a contribution from regenerative dose there also, which can be expected.

3. *Application to Martian studies*: As jarosite is reported at various locations on Mars, the high temperature (>300°C) traps in jarosite can be used for understanding the time scales (< 25 ka) of aeolian processes, reported by the Perseverance rover on Mars. It can also be used to map the cosmic ray flux on the surface of Mars and its variation with depth. For this the lower temperature trap 210°C peak bleaches in 20 min, with a saturation dose of 2600 Gy value and the higher temperature peak at 350°C bleaches in 105 minutes with a saturation dose of 1600 Gy, can be used to estimate the current

cosmic ray flux and the fluxes during the past Samples at depth can give estimates of the cosmic ray flux gradient. Thus, luminescence can provide very accurate spatial and temporal mapping of the flux, throughout the surface of Mars.

4. *Reducing errors in the MAAD estimates:* Currently, around 50% errors are observed in the equivalent dose or characteristics dose obtained from the MAAD analysis. The scatter in the data is also observed to be higher at radiation doses > 1kGy than at low doses. Further studies are needed to understand the reason for this scatter and to formulate method to reduce it.

5. *Understanding the role of recombination centers:* Chapter 4 investigated various properties of quartz at high doses in several spectral emissions. It was observed that properties like saturation does not depend on the emission spectrum but properties like bleachability, sensitivity after high previous dose is found to depend on the emitted spectrum. Since the emission properties depend on the recombination or hole centers, some insights obtained so far, highlight their importance and point towards the need to study them in detail.

6. *Inclusion of the methodology in OSL thermochronology and ESR dating:* Currently OSL thermochronology is limited to fast exhuming terrains due to the upper limit of dose estimation (King et al., 2016). The current methods can also be applied to increase the applicability of OSL thermochronology and to study the thermal history of different terrains. Similarly, ESR dating is based on the trapping of charges in the metastable states, and underestimation is obtained for ages obtained in ESR ages (Kabacińska et al., 2022), the similar methodology can be applied to estimate higher equivalent doses.

References

Adamiec, G., 2005. Properties of the 360 and 550nm TL emissions of the '110° C peak'in fired quartz. Radiat. Meas. 39, 105–110.

Adamiec, G., Aitken, M., 1998. Dose rate conversion factors. Health Phys.

Aitken, 1983. Thermoluminescence dating, Gff. https://doi.org/10.1080/11035898309455275

Aitken, M.J., 1998. Introduction to optical dating: the dating of Quaternary sediments by the use of photon-stimulated luminescence. Clarendon Press.

Aitken, M.J., 1985. Thermoluminescence Dating, Handbooks for archaeologists : a publication of the sub-committee for archaeology of the standing committee for the humanities. Academic Press.

Aitken, M.J., Bussell, G.D., Driver, H.S.T., 1979. Zero-glow monitoring (ZGM). Anc. TL 6, 13–15.

Aitken, M.J., Smith, B.W., 1988. Optical dating: recuperation after bleaching. Quat. Sci. Rev. 7, 387–393.

Ajithkumar, B., Riya, K.R., 2022. Temperature Variation in Kerala: Present and Future. Int. J. Environ. Clim. Chang. 12, 1185–1195.

Anil, D., Chauhan, N., Ajithprasad, P., Devi, M., Mahesh, V., 2022. Journal of Archaeological Science : Reports An Early Presence of Modern Human or Convergent Evolution ? A 247 ka Middle Palaeolithic Assemblage from Andhra Pradesh , India. J. Archaeol. Sci. Reports 45, 103565. https://doi.org/10.1016/j.jasrep.2022.103565

Ankjærgaard, C., 2019. Exploring multiple-aliquot methods for quartz violet stimulated luminescence dating. Quat. Geochronol. 51, 99–109. https://doi.org/https://doi.org/10.1016/j.quageo.2019.02.001

Ankjærgaard, C., Guralnik, B., Buylaert, J.P., Reimann, T., Yi, S.W., Wallinga, J., 2016. Violet stimulated luminescence dating of quartz from Luochuan (Chinese loess plateau): Agreement with independent chronology up to ~600 ka. Quat. Geochronol. 34, 33–46. https://doi.org/10.1016/j.quageo.2016.03.001

Ankjærgaard, C., Murray, A.S., Denby, P.M., Z, L.B., 2006. Measurement of optically and thermally stimulated electron emission from natural minerals 41, 780–786. https://doi.org/10.1016/j.radmeas.2006.05.012

Bailey, R.M., 1999. The form of the optically stimulated luminescence signal of quartz: implications for dating.

Bailey, R.M., Arnold, L.J., 2006. Statistical modelling of single grain quartz De distributions and an assessment of procedures for estimating burial dose. Quat. Sci. Rev. 25, 2475–2502. https://doi.org/10.1016/j.quascirev.2005.09.012

Bailiff, I.K., 1994. The pre-dose technique. Radiat. Meas. 23, 471–479.

Banerjee, D., Murray, A.S., Bøtter-Jensen, L., Lang, A., 2001. Equivalent dose estimation using a single aliquot of polymineral fine grains. Radiat. Meas. 33, 73–94.

Bateman, M.D., Frederick, C.D., Jaiswal, M.K., Singhvi, A.K., 2003. Investigations into the potential effects of pedoturbation on luminescence dating. Quat. Sci. Rev. 22, 1169–1176. https://doi.org/https://doi.org/10.1016/S0277-3791(03)00019-2

Bhattacharya, S., Mitra, S., Gupta, S., Jain, N., Chauhan, P., Parthasarathy, G., 2016a. Jarosite occurrence in the Deccan Volcanic Province of Kachchh, western India: Spectroscopic studies on a Martian analog locality. https://doi.org/10.1002/2015JE004949

Bhattacharya, S., Mitra, S., Gupta, S., Jain, N., Chauhan, P., Parthasarathy, G., 2016b.

Journal of Geophysical Research : Planets 402–431. https://doi.org/10.1002/2015JE004949.Received
Bhattacharya, S., Mitra, S., Gupta, S., Jain, N., Chauhan, P., Parthasarathy, G., 1955. Journal of geophysical research. Nature 175, 238. https://doi.org/10.1038/175238c0
Bhattacharya, S., Mitra, S., Gupta, S., Jain, N., Chauhan, P., Parthasarathy, G., Ajai, 2016c. Jarosite occurrence in the Deccan Volcanic Province of Kachchh, western India: Spectroscopic studies on a Martian analog locality. J. Geophys. Res. Planets 121, 402–431. https://doi.org/10.1002/2015JE004949
Biernacka, M., Chruścińska, A., Palczewski, P., Derkowski, P., 2022a. Determining the kinetic parameters of traps in quartz using the thermally modulated OSL method. J. Lumin. 252, 119289.
Biernacka, M., Chruścińska, A., Palczewski, P., Derkowski, P., 2022b. Determining the kinetic parameters of traps in quartz using the thermally modulated OSL method. J. Lumin. 252. https://doi.org/10.1016/j.jlumin.2022.119289
Bilham, R., Blume, F., Bendick, R., Gaur, V.K., 1998. Geodetic constraints on the translation and deformation of India: Implications for future great Himalayan earthquakes. Curr. Sci. 213–229.
Bishop, J.L., Murad, E., 2005. The visible and infrared spectral properties of jarosite and alunite. Am. Mineral. 90, 1100–1107.
Biswas, R.H., 2014. Development and application of luminescence to earth and planetary sciences: Some landmarks. Defect Diffus. Forum 357, 217–243. https://doi.org/10.4028/www.scientific.net/DDF.357.217
Biswas, R.H., Herman, F., King, G.E., Lehmann, B., Singhvi, A.K., 2020. Surface paleothermometry using low-Temperature thermoluminescence of feldspar. Clim. Past 16, 2075–2093. https://doi.org/10.5194/cp-16-2075-2020
Biswas, R.H., Morthekai, P., Gartia, R.K., Chawla, S., Singhvi, A.K., 2011. Thermoluminescence of the meteorite interior: A possible tool for the estimation of cosmic ray exposure ages. Earth Planet. Sci. Lett. 304, 36–44. https://doi.org/10.1016/j.epsl.2011.01.012
Biswas, S.K., 1992. Tertiary stratigraphy of Kutch. Jour. Pal. Soc. India 37, 1–29.
Bohun, A., Öas, Ö.S., 1954. Fys. 3, 394 (1953). Czech. J. Phys 4, 91.
Bonde, A., Murray, A., Friedrich, W.L., 2001. Santorini: Luminescence dating of a volcanic province using quartz? Quat. Sci. Rev. 20, 789–793.
Bouscary, C., 2022. Sub-quaternary Himalayan Tectonics Inferred from Luminescence Thermochronometry.
Bouscary, C., King, G.E., Grujic, D., Lavé, J., Almeida, R., Hetényi, G., Herman, F., 2024. Sustained deformation across the Sub-Himalayas since 200 ka. Geology 52, 72–76.
Brown, N.D., Rhodes, E.J., Harrison, T.M., 2017. Using thermoluminescence signals from feldspars for low-temperature thermochronology. Quat. Geochronol. 42, 31–41. https://doi.org/https://doi.org/10.1016/j.quageo.2017.07.006
Buchanan, G.R., Tsukamoto, S., Zhang, J., Long, H., 2022. Testing the natural limits of infrared radiofluorescence dating of the Luochuan loess-palaeosol sequence, Chinese Loess Plateau. Radiat. Meas. 155, 106797. https://doi.org/10.1016/j.radmeas.2022.106797
Buylaert, J.-P., Murray, A.S., Thomsen, K.J., Jain, M., 2009. Testing the potential of an elevated temperature IRSL signal from K-feldspar. Radiat. Meas. 44, 560–565.
Buylaert, J., Jain, M., Murray, A.S., Thomsen, K.J., Thiel, C., Sohbati, R., 2012. A robust feldspar luminescence dating method for Middle and Late P leistocene sediments. Boreas 41, 435–451.
Buylaert, J.P., Murray, A.S., Huot, S., Vriend, M.G.A., Vandenberghe, D., De Corte, F., Van

Den Haute, P., 2006. A comparison of quartz OSL and isothermal TL measurements on Chinese loess. Radiat. Prot. Dosimetry 119, 474–478.
Caicedo, F.D., Asfora, V.K., Guzzo, P.L., Barros, V.S.M., 2021. Nuclear Inst . and Methods in Physics Research , B Investigation of the spectrally resolved TL signals of natural quartz single crystals sensitized by high-dose of gamma-radiation and moderate. Nucl. Inst. Methods Phys. Res. B 486, 37–47. https://doi.org/10.1016/j.nimb.2020.11.001
Chandel, H.N., Patel, A.D., Vaghela, H.R., Ubale, G.P., 2006. An effective and reusable sampling pipe for luminescence dating. Anc. Tl 24, 21–22.
Chapot, M.S., Roberts, H.M., Duller, G.A.T., Lai, Z.P., 2016. Natural and laboratory TT-OSL dose response curves: testing the lifetime of the TT-OSL signal in nature. Radiat. Meas. 85, 41–50.
Chapot, M.S., Roberts, H.M., Duller, G.A.T., Lai, Z.P., 2012. A comparison of natural- and laboratory-generated dose response curves for quartz optically stimulated luminescence signals from Chinese Loess. Radiat. Meas. 47, 1045–1052. https://doi.org/https://doi.org/10.1016/j.radmeas.2012.09.001
Chauhan, N., Anand, S., Palani Selvam, T., Mayya, Y.S., Singhvi, A.K., 2009. Extending the maximum age achievable in the luminescence dating of sediments using large quartz grains: A feasibility study. Radiat. Meas. 44, 629–633. https://doi.org/10.1016/j.radmeas.2009.06.009
Chauhan, N, Anand, S., Selvam, T.P., Mayya, Y.S., Singhvi, A.K., 2009. Extending the maximum age achievable in the luminescence dating of sediments using large quartz grains: A feasibility study. Radiat. Meas. 44, 629–633.
Chauhan, N., Singhvi, A.K., 2019. Changes in the optically stimulated luminescence (OSL) sensitivity of single grains of quartz during the measurement of natural OSL: Implications for the reliability of optical ages. Quat. Geochronol. 53, 101004. https://doi.org/https://doi.org/10.1016/j.quageo.2019.101004
Chauhan, N., Singhvi, A.K., 2011. Distribution in sar palaeodoses due to spatial heterogeniety of natural beta dose. Geochronometria 38, 190–198. https://doi.org/10.2478/s13386-011-0024-7
Chawla, S., Gundu Rao, T.K., Singhvi, A.K., 1998. Quartz thermoluminescence: Dose and dose-rate effects and their implications. Radiat. Meas. 29, 53–63. https://doi.org/10.1016/S1350-4487(97)00200-X
Chen, R., Lawless, J.L., Pagonis, V., 2022. On the various-heating-rates method for evaluating the activation energies of thermoluminescence peaks. Radiat. Meas. 150, 106692. https://doi.org/10.1016/j.radmeas.2021.106692
Chruścińska, A., Palczewski, P., Rerek, T., Biernacka, M., Lefrais, Y., 2021. Measurement of the paleodose in luminescence dating using the TM-OSL of quartz. Meas. J. Int. Meas. Confed. 167. https://doi.org/10.1016/j.measurement.2020.108448
Cloutis, E.A., Hawthorne, F.C., Mertzman, S.A., Krenn, K., Craig, M.A., Marcino, D., Methot, M., Strong, J., Mustard, J.F., Blaney, D.L., 2006. Detection and discrimination of sulfate minerals using reflectance spectroscopy. Icarus 184, 121–157.
Colarossi, D., Duller, G.A.T., Roberts, H.M., 2018. Exploring the behaviour of luminescence signals from feldspars: Implications for the single aliquot regenerative dose protocol. Radiat. Meas. 109, 35–44. https://doi.org/10.1016/j.radmeas.2017.07.005
Colarossi, D., Duller, G.A.T., Roberts, H.M., Tooth, S., Lyons, R., 2015. Comparison of paired quartz OSL and feldspar post-IR IRSL dose distributions in poorly bleached fluvial sediments from South Africa. Quat. Geochronol. 30, 233–238. https://doi.org/https://doi.org/10.1016/j.quageo.2015.02.015
Corpusculatre, L.D.P., 1991. Properties of the red tl peak of quartz relevant to thermoluminescence dating 18, 89–94.

Cruells, M., Roca, A., 2022. Jarosites: formation, structure, reactivity and environmental. Metals (Basel). 12, 802.
Curie, D., Garlick, G.F.J., 1963. Luminescence in crystals. (No Title).
Debenham, N.C., 1985. Use of U.V. emissions in TL dating of sediments. Nucl. Tracks Radiat. Meas. 10, 717–724. https://doi.org/10.1016/0735-245X(85)90080-8
Degda, N., Patel, N., Singhal, M., Murthy, K.V.R., Chauhan, N., Srinivas, M., 2024a. Thermally stable luminescence and dosimetric features of Ho (III) activated tungstate double perovskite. J. Lumin. 275, 120775.
Degda, N., Patel, N., Singhal, M., Murthy, K.V.R., Chauhan, N., Verma, V., Srinivas, M., 2024b. Luminescence and dosimetry investigations of Eu (III) doped Ca2CeVO6 novel double perovskite. Opt. Mater. (Amst). 155, 115861.
Degda, N., Patel, N., Verma, V., Murthy, K.V.R., Chauhan, N., Singhal, M., Srinivas, M., 2023. Photoluminescence and thermoluminescence kinetic features of Eu3+ doped Sr2YVO6 double perovskite phosphor. Opt. Mater. (Amst). 142, 114019.
DeMets, C., Gordon, R.G., Argus, D.F., Stein, S., 1994. Effect of recent revisions to the geomagnetic reversal time scale on estimates of current plate motions. Geophys. Res. Lett. 21, 2191–2194.
Deng, T., Ding, L., 2015. Paleoaltimetry reconstructions of the Tibetan Plateau: progress and contradictions. Natl. Sci. Rev. 2, 417–437.
Desai, B.G., Saklani, R.D., 2012. Significance of the trace fossil Balanoglossites Mägdefrau, 1932 from the Lower Cretaceous Guneri member (Bhuj formation) of the Guneri dome, Kachchh, India. Swiss J. Palaeontol. 131, 255–263.
Devi, M., Chauhan, N., Singhvi, A.K., 2024. Post-violet infrared stimulated luminescence (pVIRSL) dating protocol for potassium feldspar. Quat. Geochronol. 79, 101487.
Doran, P.T., Clifford, S.M., Forman, S.L., Nyquist, L., Papanastassiou, D.A., Stewart, B.W., Sturchio, N.C., Swindle, T.D., Cerling, T., Kargel, J., McDonald, G., Nishiizumi, K., Poreda, R., Rice, J.W., Tanaka, K., 2004. Mars chronology: assessing techniques for quantifying surficial processes. Earth-Science Rev. 67, 313–337. https://doi.org/https://doi.org/10.1016/j.earscirev.2004.04.001
Dosimetry, R.P., 1996. 96/01061 Computerised glow curve deconvolution: Application to thermoluminescence dosimetry. Fuel Energy Abstr. 37, 64. https://doi.org/10.1016/0140-6701(96)87174-8
Dreimanis, A., Hutt, G., Raukas, A., Whippey, P.W., 1978. Dating methods of Pleistocene deposits and their problems: I. Thermoluminescence dating. Geosci. Canada.
Duller, G.A.T., 2008. Luminescence Dating: guidelines on using luminescence dating in archaeology.
Duller, G.A.T., 2003. Distinguishing quartz and feldspar in single grain luminescence measurements. Radiat. Meas. 37, 161–165.
Duller, G.A.T., 1994. Luminescence dating of sediments using single aliquots: new procedures. Quat. Sci. Rev. 13, 149–156.
Duller, G.A.T., 1991. Equivalent dose determination using single aliquots. Int. J. Radiat. Appl. Instrumentation. Part D. Nucl. Tracks Radiat. Meas. 18, 371–378.
Duller, G.A.T., Wintle, A.G., 2012. A review of the thermally transferred optically stimulated luminescence signal from quartz for dating sediments. Quat. Geochronol. 7, 6–20. https://doi.org/10.1016/j.quageo.2011.09.003
Durcan, J.A., 2018. Assessing the reproducibility of quartz OSL lifetime determinations derived using isothermal decay 120, 234–240.
Durrani, S.A., Khazal, K.A.R., McKeever, S.W.S., Riley, R.J., 1977. Studies of changes in the thermoluminescence sensitivity in quartz induced by proton and gamma irradiations. Radiat. Eff. 33, 237–244. https://doi.org/10.1080/00337577708233112

Dutkiewicz, A., Prescott, J.R., 1997. Thermoluminescence Ages and Palaeoclimate From the. Quat. Sci. Rev. 16, 367–385.
Dutrizac, J.E., Jambor, J.L., 2000. Jarosites and Their Application in Hydrometallurgy. Rev. Mineral. Geochemistry 40, 405–452. https://doi.org/10.2138/rmg.2000.40.8
Dutrizac, J.E., Kaiman, S., 1976. Synthesis and properties of jarosite-type compounds. Can. Mineral. 14, 151–158.
Duval, M., 2022. Electron Spin Resonance dating of Quaternary materials. Cuaternario y Geomorfol. 36, 237–254. https://doi.org/10.17735/cyg.v36i3-4.95281
Fairchild, J.G., 1933. Artificial jarosites—the separation of potassium from cesium. Am. Mineral. J. Earth Planet. Mater. 18, 543–547.
Farmer, V.C., 1974. The infrared spectra of minerals. Mineral. Soc. Monogr. 4, 331–363.
Fattahi, M., Stokes, S., 2003. Dating volcanic and related sediments by luminescence methods: A review. Earth-Science Rev. 62, 229–264. https://doi.org/10.1016/S0012-8252(02)00159-9
Fattahi, M., Stokes, S., 2000. Extending the time range of luminescence dating using red TL (RTL) from volcanic quartz. Radiat. Meas. 32, 479–485. https://doi.org/10.1016/S1350-4487(00)00105-0
Fattahi, M, Stokes, S., 2000. Extending the time range of luminescence dating using red TL (RTL) from volcanic quartz. Radiat. Meas. 32, 479–485.
Fattahi, M., Stokes, S.C., Lamothe, M., 2004. Red luminescence emission from potassium feldspars stimulated by infrared. Anc. TL 22, 35–44.
Fleming, S., 1969. The acquisition of radiothermoluminescence by ancient ceramics.
Fleming, S.J., 1979. Thermoluminescence techniques in archaeology. Clarendon Press.
Franklin, A.D., Prescott, J.R., Scholefield, R.B., 1995. The mechanism of thermoluminescence in an Australian sedimentary quartz. J. Lumin. 63, 317–326.
Frechen, M., Schweitzer, U., Zander, A., 1996. Improvements in sample preparation for the fine grain technique. Anc. TL 14, 15–17.
Frost, R.L., Weier, M.L., Martens, W., 2005. Thermal decomposition of jarosites of potassium, sodium and lead. J. Therm. Anal. Calorim. 82, 115–118.
Galbraith, R.F., 1990. The radial plot: Graphical assessment of spread in ages. Int. J. Radiat. Appl. Instrumentation. Part 17, 207–214. https://doi.org/10.1016/1359-0189(90)90036-W
Galbraith, R.F., Roberts, R.G., Laslett, G.M., Yoshida, H., Olley, J.M., 1999. Optical dating of single and multiple grains of quartz from Jinmium rock shelter, northern Australia: Part I, experimental design and statistical models. Archaeometry 41, 339–364. https://doi.org/10.1111/j.1475-4754.1999.tb00987.x
Garlick, G.F.J., Gibson, A.F., 1948. The electron trap mechanism of luminescence in sulphide and silicate phosphors. Proc. Phys. Soc. 60, 574.
Garvie, L.A.J., Rez, P., Alvarez, J.R., Buseck, P.R., 1998. Interband transitions of crystalline and amorphous SiO2: An electron energy-loss spectroscopy (EELS) study of the low-loss region. Solid State Commun. 106, 303–307. https://doi.org/10.1016/S0038-1098(98)00021-0
Gliganic, L.A., Roberts, R.G., Jacobs, Z., 2012. Natural variations in the properties of TL and IRSL emissions from metamorphic and volcanic K-feldspars from East Africa: Assessing their reliability for dating. Radiat. Meas. 47, 659–664. https://doi.org/https://doi.org/10.1016/j.radmeas.2012.03.001
Gobrecht, H., Hofmann, D., 1966. Spectroscopy of traps by fractional glow technique. J. Phys. Chem. Solids 27, 509–522. https://doi.org/10.1016/0022-3697(66)90194-6
Guérin, G., Mercier, N., Adamiec, G., 2011. Dose-rate conversion factors: update. Anc. Tl 29, 5–8.

Hashimoto, T., Yokosaka, K., Habuki, H., 1987. Emission properties of thermoluminescence from natural quartz-blue and red TL response to absorbed dose. Int. J. Radiat. Appl. Instrumentation. Part 13, 57–66. https://doi.org/10.1016/1359-0189(87)90008-2
Herman, F., Rhodes, E.J., Braun, J., Heiniger, L., 2010. Uniform erosion rates and relief amplitude during glacial cycles in the Southern Alps of New Zealand, as revealed from OSL-thermochronology. Earth Planet. Sci. Lett. 297, 183–189. https://doi.org/10.1016/j.epsl.2010.06.019
Howari, F.M., Sharma, M., Xavier, C.M., Nazzal, Y., AlAydaroos, F., 2021. Chronological Analysis and Remote Sensing of Craters on the Surface of Mars . Front. Environ. Sci. .
Hunter, P.G., Spooner, N.A., Smith, B.W., 2018. Thermoluminescence emission from quartz at 480 nm as a high-dose radiation marker. Radiat. Meas. 120, 143–147. https://doi.org/10.1016/j.radmeas.2018.04.001
Huntley, D.J., 2006. An explanation of the power-law decay of luminescence. J. Phys. Condens. Matter 18, 1359–1365. https://doi.org/10.1088/0953-8984/18/4/020
Huntley, D.J., 1994. Further Thermoluminescence Dates From the Dune. Quat. Sci. Rev. 13, 201–207.
Huntley, D.J., Godfrey-Smith, D.I., Thewalt, M.L.W., 1985. Optical dating of sediments. Nature 313, 105–107. https://doi.org/10.1038/313105a0
Huntley, D.J., Hutton, J.T., Prescott, J.R., 1993. The stranded beach-dune sequence of south-east South Australia: A test of thermoluminescence dating, 0-800 ka. Quat. Sci. Rev. 12, 1–20. https://doi.org/10.1016/0277-3791(93)90045-N
Huntley, D.J., Lamothe, M., 2001. Ubiquity of anomalous fading in K-feldspars and the measurement and correction for it in optical dating. Can. J. Earth Sci. 38, 1093–1106. https://doi.org/10.1139/cjes-38-7-1093
Huntley, D.J., Prescott, J.R., 2001. Improved methodology and new thermoluminescence ages for the dune sequence in south-east South Australia. Quat. Sci. Rev. 20, 687–699. https://doi.org/10.1016/S0277-3791(00)00022-6
Huntley, D.J., Short, M.A., Dunphy, K., 1996. Deep traps in quartz and their use for optical dating. Can. J. Phys. 74, 81–91.
Hütt, G., Jaek, I., Tchonka, J., 1988. Optical dating: K-feldspars optical response stimulation spectra. Quat. Sci. Rev. 7, 381–385.
Inami, T., Nishiyama, M., Maegawa, S., Oka, Y., 2000. Magnetic structure of the kagomé lattice antiferromagnet potassium jarosite KFe 3 (OH) 6 (S O 4) 2. Phys. Rev. B 61, 12181.
Jain, M., 2009. Extending the dose range: Probing deep traps in quartz with 3.06 eV photons. Radiat. Meas. 44, 445–452. https://doi.org/10.1016/j.radmeas.2009.03.011
Jain, M., Andersen, C.E., Bøtter-Jensen, L., Murray, A.S., Haack, H., Bridges, J.C., 2006. Luminescence dating on Mars: OSL characteristics of Martian analogue materials and GCR dosimetry. Radiat. Meas. 41, 755–761. https://doi.org/10.1016/j.radmeas.2006.05.018
Jain, M., Andersen, C.E., Hajdas, W., Edmund, J.M., Bøtter-Jensen, L., 2007a. OSL response to proton irradiation in some natural dosemeters: Implications for martian sediment dating. Nucl. Instruments Methods Phys. Res. Sect. A Accel. Spectrometers, Detect. Assoc. Equip. 580, 652–655. https://doi.org/10.1016/j.nima.2007.05.112
Jain, M., Bøtter-Jensen, L., Murray, A.S., Denby, P.M., Tsukamoto, S., Gibling, M.R., 2005. Revisiting TL: dose measurement beyond the OSL range using SAR. Anc. TL 23, 9–24.
Jain, M, Bøtter-Jensen, L., Singhvi, A.K., 2003. Dose evaluation using multiple-aliquot quartz OSL: test of methods and a new protocol for improved accuracy and precision. Radiat. Meas. 37, 67–80.
Jain, M., Duller, G.A.T., Wintle, A.G., 2007b. Dose response, thermal stability and optical

bleaching of the 310 °C isothermal TL signal in quartz. Radiat. Meas. 42, 1285–1293. https://doi.org/10.1016/j.radmeas.2007.08.008
Jain, M., Murray, A.S., Bøtter-Jensen, L., 2003. Characterisation of blue-light stimulated luminescence components in different quartz samples: Implications for dose measurement. Radiat. Meas. 37, 441–449. https://doi.org/10.1016/S1350-4487(03)00052-0
Kabacińska, Z., Buylaert, J.P., Yi, S., Timar-Gabor, A., 2022. Revisiting natural and laboratory electron spin resonance (ESR) dose response curves of quartz from Chinese loess. Quat. Geochronol. 70. https://doi.org/10.1016/j.quageo.2022.101306
Kalita, J.M., Chithambo, M.L., 2022. Thermally-assisted optically stimulated luminescence from deep electron traps in microcline. Radiat. Meas. 154, 106786. https://doi.org/10.1016/j.radmeas.2022.106786
Kars, R.H., Wallinga, J., Cohen, K.M., 2008. A new approach towards anomalous fading correction for feldspar IRSL dating - tests on samples in field saturation. Radiat. Meas. 43, 786–790. https://doi.org/10.1016/j.radmeas.2008.01.021
Kaur, A.P., Skinner, A., Patnaik, R., 2025. Electron Spin Resonance (ESR) dating of fossil mammals from the Pinjor Formation, Upper Siwaliks, India. Quat. Int. 744, 109920.
Kelly, A., Knowles, K.M., 2020. Crystallography and crystal defects. John Wiley & Sons.
Khoury, H.J., Guzzo, P.L., Souza, L.B.F., Farias, T.M.B., Watanabe, S., 2008. TL dosimetry of natural quartz sensitized by heat-treatment and high dose irradiation 43, 487–491. https://doi.org/10.1016/j.radmeas.2008.01.028
King, W. (1882). The Warkalli beds and associated deposits at Quilon in Travancore. *Records of the Geological Survey of India, Vol. XV, Part 2.*

King, G.E., Guralnik, B., Valla, P.G., Herman, F., 2016. Trapped-charge thermochronometry and thermometry: A status review. Chem. Geol. 446, 3–17.
Kitis, G., Kiyak, N.G., Polymeris, G.S., Pagonis, V., 2010. Investigation of OSL signals from very deep traps in unfired and fired quartz samples. Nucl. Instruments Methods Phys. Res. Sect. B Beam Interact. with Mater. Atoms 268, 592–598.
Klingelhöfer, G., Morris, R. V, Bernhardt, B., Schröder, C., Rodionov, D.S., de Souza, P.A.J., Yen, A., Gellert, R., Evlanov, E.N., Zubkov, B., Foh, J., Bonnes, U., Kankeleit, E., Gütlich, P., Ming, D.W., Renz, F., Wdowiak, T., Squyres, S.W., Arvidson, R.E., 2004. Jarosite and hematite at Meridiani Planum from Opportunity's Mossbauer Spectrometer. Science 306, 1740–1745. https://doi.org/10.1126/science.1104653
Knoll, F.G., 2000. Radiation Detection and Measurement, 3rd ed - Glenn F.pdf.
Kolb, T., Tudyka, K., Kadereit, A., Lomax, J., Poręba, G., Zander, A., Zipf, L., Fuchs, M., 2022. The µ Dose system: determination of environmental dose rates by combined alpha and beta counting–performance tests and practical experiences. Geochronology 4, 1–31.
Kotler, J.M., Hinman, N.W., Yan, B., Stoner, D.L., Scott, J.R., 2008. Glycine identification in natural jarosites using laser desorption Fourier transform mass spectrometry: implications for the search for life on Mars. Astrobiology 8, 253–266.
Krbetschek, M.R., Götze, J., Dietrich, A., Trautmann, T., 1997. Spectral information from minerals relevant for luminescence dating. Radiat. Meas. 27, 695–748. https://doi.org/10.1016/S1350-4487(97)00223-0
Kreutzer, S., Burow, C., Dietze, M., Fuchs, M.C., Schmidt, C., Fischer, M., Friedrich, J., Mercier, N., Smedley, R.K., Christophe, C., 2024. Package 'Luminescence.'
Kuhn, R., Trautmann, T., Singhvi, A.K., Krbetschek, M.R., Wagner, G.A., Stolz, W., 2000. Study of thermoluminescence emission spectra and optical stimulation spectra of quartz from different provenances. Radiat. Meas. 32, 653–657. https://doi.org/10.1016/S1350-4487(00)00090-1

Kumar, R., Ghosh, S.K., Sangode, S.J., 1999. Evolution of a Neogene fluvial system in a Himalayan foreland basin, India. Spec. Pap. Geol. Soc. Am. 328, 239–256. https://doi.org/10.1130/0-8137-2328-0.239
Kumaravel, V., Sangode, S.J., Kumar, R., Siva Siddaiah, N., 2005. Magnetic polarity stratigraphy of Plio-Pleistocene Pinjor Formation (type locality), Siwalik Group, NW Himalaya, India. Curr. Sci. 88, 1453–1561.
Lai, Z., Murray, A., 2006. Red TL of quartz extracted from Chinese loess : Bleachability and saturation dose 41, 836–840. https://doi.org/10.1016/j.radmeas.2006.04.017
Lancaster, N., Greeley, R., 1990. Sediment volume in the north polar sand seas of Mars. J. Geophys. Res. Solid Earth 95, 10921–10927.
Lepper, K., McKeever, S.W.S., 2000. Characterization of fundamental luminescence properties of the mars soil simulant JSC Mars-1 and their relevance to absolute dating of martian eolian sediments. Icarus 144, 295–301. https://doi.org/10.1006/icar.1999.6295
Lepper, K., WS McKeever, S., 2002. An objective methodology for dose distribution analysis. Radiat. Prot. Dosimetry 101, 349–352.
Li, B., Jacobs, Z., Roberts, R.G., 2022. Bayesian analysis of De distributions in optical dating: Towards a robust method for dealing with outliers. Quat. Geochronol. 67, 101230. https://doi.org/https://doi.org/10.1016/j.quageo.2021.101230
Li, B., Li, S.-H., 2006. Comparison of De estimates using the fast component and the medium component of quartz OSL. Radiat. Meas. 41, 125–136.
Li, B., Li, S.H., 2012. Determining the cooling age using luminescence-thermochronology. Tectonophysics 580, 242–248. https://doi.org/10.1016/j.tecto.2012.09.023
Li, B., Roberts, R.G., Jacobs, Z., Li, S.-H., 2014. A single-aliquot luminescence dating procedure for K-feldspar based on the dose-dependent MET-pIRIR signal sensitivity. Quat. Geochronol. 20, 51–64.
Li, Y., Tsukamoto, S., Long, H., Zhang, J., Yang, L., He, Z., Frechen, M., 2018. Testing the reliability of fading correction methods for feldspar IRSL dating: A comparison between natural and simulated-natural dose response curves. Radiat. Meas. 120, 228–233. https://doi.org/10.1016/j.radmeas.2018.06.025
Liu, L., Yang, S., Liu, X., Cheng, T., Li, P., Zhou, J., Chen, Z., Luo, Y., 2022. Effects of the size of the test dose on the SAR protocol for quartz optically stimulated luminescence dating of loess in the eastern Tibetan Plateau. Quat. Geochronol. 72, 101365. https://doi.org/10.1016/j.quageo.2022.101365
Lowick, S.E., Preusser, F., 2011. Investigating age underestimation in the high dose region of optically stimulated luminescence using fine grain quartz. Quat. Geochronol. 6, 33–41. https://doi.org/10.1016/j.quageo.2010.08.001
Lowick, Sally E., Preusser, F., Pini, R., Ravazzi, C., 2010a. Underestimation of fine grain quartz OSL dating towards the Eemian: Comparison with palynostratigraphy from Azzano Decimo, northeastern Italy. Quat. Geochronol. 5, 583–590. https://doi.org/10.1016/j.quageo.2009.12.003
Lowick, Sally E., Preusser, F., Wintle, A.G., 2010b. Investigating quartz optically stimulated luminescence dose-response curves at high doses. Radiat. Meas. 45, 975–984. https://doi.org/10.1016/j.radmeas.2010.07.010
Lowick, Sally E, Preusser, F., Wintle, A.G., 2010. Investigating quartz optically stimulated luminescence dose–response curves at high doses. Radiat. Meas. 45, 975–984.
Lu, Y. C., Wang, X.L., Wintle, A.G., 2007. A new OSL chronology for dust accumulation in the last 130,000 yr for the Chinese Loess Plateau. Quat. Res. 67, 152–160. https://doi.org/10.1016/j.yqres.2006.08.003
Lu, Y C㲋, Wang, X.L., Wintle, A.G., 2007. A new OSL chronology for dust accumulation in the last 130,000 yr for the Chinese Loess Plateau. Quat. Res. 67, 152–160.

Mahaney, W.C., 1984. Quaternary dating methods., Quaternary dating methods. https://doi.org/10.1016/0168-9622(86)90024-2
Mandal, S.K., Scherler, D., Romer, R.L., Burg, J.P., Guillong, M., Schleicher, A.M., 2019. Multiproxy Isotopic and Geochemical Analysis of the Siwalik Sediments in NW India: Implication for the Late Cenozoic Tectonic Evolution of the Himalaya. Tectonics 38, 120–143. https://doi.org/10.1029/2018TC005200
Marescotti, P., Carbone, C., Comodi, P., Frondini, F., Lucchetti, G., 2010. Mineralogical and chemical evolution of ochreous precipitates from the Libiola Fe-Cu-sulphides mine eastern Liguria, Italy. Acta Mineral. Abstr. Ser. 6, 346.
May, C.E., Partridge, J.A., 1964. Thermoluminescent kinetics of alpha-irradiated alkali halides. J. Chem. Phys. 40, 1401–1409.
Mayya, Y.S., Morthekai, P., Murari, M.K., Singhvi, A.K., 2006. Towards quantifying beta microdosimetric effects in single-grain quartz dose distribution. Radiat. Meas. 41, 1032–1039.
McKeever, S.W.S., 1985. Thermoluminescence of solids. Cambridge University Press.
McKeever, S.W.S., 1984. Thermoluminescence in quartz and silica. Radiat. Prot. Dosimetry 8, 81–98.
McKeever, S.W.S., Banerjee, D., Blair, M., Clifford, S.M., Clowdsley, M.S., Kim, S.S., Lamothe, M., Lepper, K., Leuschen, M., McKeever, K.J., Prather, M., Rowland, A., Reust, D., Sears, D.W.G., Wilson, J.W., 2003. Concepts and approaches to in situ luminescence dating of martian sediments. Radiat. Meas. 37, 527–534. https://doi.org/https://doi.org/10.1016/S1350-4487(03)00025-8
Medlin, W.L., 1963. Thermoluminescence in quartz. J. Chem. Phys. 38, 1132–1143.
Mejdahl, V., Bøtter-Jensen, L., 1997. Experience with the SARA OSL method. Radiat. Meas. 27, 291–294.
Mejdahl, V., Wintle, A.G., 2020. Thermoluminescence applied to age determination in archaeology and geology, in: Thermoluminescence and Thermoluminescent Dosimetry. CRC Press, pp. 133–190.
Miallier, D., Fain, J., Montret, M., Pilleyre, T., Sanzelle, S., Soumana, S., 1994. Sun bleaching of the red TL of quartz: preliminary observations. Anc. TL 12, 1–4.
Miallier, D., Fain, J., Montret, M., Pilleyre, T., Sanzelle, S., Soumana, S., 1991. Properties of the red TL peak of quartz relevant to thermoluminescence dating. Int. J. Radiat. Appl. Instrumentation. Part D. Nucl. Tracks Radiat. Meas. 18, 89–94.
Mineli, T.D., Sawakuchi, A.O., Guralnik, B., Lambert, R., Jain, M., Pupim, F.N., Rio, I. de., Guedes, C.C.F., Nogueira, L., 2021. Variation of luminescence sensitivity, characteristic dose and trap parameters of quartz from rocks and sediments. Radiat. Meas. 144, 106583. https://doi.org/https://doi.org/10.1016/j.radmeas.2021.106583
Monti, A.M., Fasoli, M., Panzeri, L., Martini, M., 2019. Investigation of the spectrally resolved TL peaks of quartz in the 70°C–220°C temperature region. Radiat. Meas. 127, 106141. https://doi.org/10.1016/j.radmeas.2019.106141
Morris, R. V, Golden, D.C., Bell III, J.F., Shelfer, T.D., Scheinost, A.C., Hinman, N.W., Furniss, G., Mertzman, S.A., Bishop, J.L., Ming, D.W., Allen, C.C., Britt, D.T., 2000. Mineralogy, composition, and alteration of Mars Pathfinder rocks and soils: Evidence from multispectral, elemental, and magnetic data on terrestrial analogue, SNC meteorite, and Pathfinder samples. J. Geophys. Res. Planets 105, 1757–1817. https://doi.org/https://doi.org/10.1029/1999JE001059
Morthekai, P., Jain, M., Dartnell, L., Murray, A.S., Bøtter-Jensen, L., Desorgher, L., 2007. Modelling of the dose-rate variations with depth in the Martian regolith using GEANT4. Nucl. Instruments Methods Phys. Res. Sect. A Accel. Spectrometers, Detect. Assoc. Equip. 580, 667–670. https://doi.org/10.1016/j.nima.2007.05.118

Morthekai, P., Jain, M., Murray, A.S., Thomsen, K.J., Bøtter-Jensen, L., 2008. Fading characteristics of martian analogue materials and the applicability of a correction procedure. Radiat. Meas. 43, 672–678. https://doi.org/10.1016/j.radmeas.2008.02.019
Morthekai, P., Singhal, M., Sharma, S.K., Sivasubramaniam, S., Kamarasu, M., Singh, P., Chauhan, N., Kumar, K., Nawaz, S.A., Khonde, N., 2025. Investigating historical attribution: luminescence dating of bricks from a submerged structure in southeastern India. Front. Environ. Archaeol. 4. https://doi.org/10.3389/fearc.2025.1464315
Murari, M.K., Kreutzer, S., Frouin, M., Friedrich, J., Lauer, T., Klasen, N., Schmidt, C., Tsukamoto, S., Richter, D., Mercier, N., Fuchs, M., 2021. Infrared Radiofluorescence (IR-RF) of K-Feldspar: An Interlaboratory Comparison. Geochronometria 48, 95–110. https://doi.org/10.2478/geochr-2021-0007
Murray, A., Arnold, L.J., Buylaert, J.-P., Guérin, G., Qin, J., Singhvi, A.K., Smedley, R., Thomsen, K.J., 2021. Optically stimulated luminescence dating using quartz, Nature Reviews Methods Primers. https://doi.org/10.1038/s43586-021-00068-5
Murray, A., Olley, J., 2002. … and Accuracy in the Optically Stimulated Luminescence Dating of Sedimentary …. Geochronometria 21, 1–16.
Murray, A.S., Mejdahl, V., 1999. Comparison of regenerative-dose single-aliquot and multiple-aliquot (SARA) protocols using heated quartz from archaeological sites. Quat. Sci. Rev. 18, 223–229. https://doi.org/10.1016/S0277-3791(98)00055-9
Murray, A.S., Roberts, R.G., 1998. Measurement of the equivalent dose in quartz using a regenerative-dose single-aliquot protocol. Radiat. Meas. 29, 503–515. https://doi.org/10.1016/S1350-4487(98)00044-4
Murray, A.S., Svendsen, J.I., Mangerud, J., Astakhov, V.I., 2007. Testing the accuracy of quartz OSL dating using a known-age Eemian site on the river Sula, northern Russia. Quat. Geochronol. 2, 102–109.
Murray, A.S., Wintle, A.G., 2000a. Luminescence dating of quartz using an improved single-aliquot regenerative-dose protocol. Radiat. Meas. 32, 57–73. https://doi.org/10.1016/S1350-4487(99)00253-X
Murray, A.S., Wintle, A.G., 2000b. Application of the single-aliquot regenerative-dose protocol to the 375 °C quartz TL signal. Radiat. Meas. 32, 579–583. https://doi.org/10.1016/S1350-4487(00)00089-5
Nagar, Y.C., 2007. Methodological aspects of radiation dosimetry of natural radiation environment using luminescence techniques: New minerals and application.
Nambi, K.S. V, 1977. Thermoluminescence : Its Understanding and Applications 94.
Nanda, A.C., Sehgal, R.K., Chauhan, P.R., 2018. Siwalik-age faunas from the Himalayan foreland Basin of South Asia. J. Asian Earth Sci. 162, 54–68.
Nair, S. and Chauhan, A. L., 1984. *Stratigraphy and Sedimentary Clays of Tertiary Formations in Parts of Cannanore District, Kerala State. Progress Report for the Field Season 1974-75.* Geological Survey of India.

Niyonzima, P., Oehler, S., King, G.E., Schmidt, C., 2024. Investigating thermoluminescence signal saturation in quartz and feldspar using emission spectrometry. Radiat. Meas. 177, 107262.
Ogundare, F.O., Chithambo, M.L., Oniya, E.O., 2006. Anomalous behaviour of thermoluminescence from quartz: A case of glow peaks from a Nigerian quartz. Radiat. Meas. 41, 549–553. https://doi.org/10.1016/j.radmeas.2006.03.001
Oniya, E.O., 2014. Luminescence Sensitisation of Natural Quartz Using Pre-Exposure Dose and Thermal Activation Techniques.
Pagonis, V., Kitis, G., Furetta, C., 2006. Numerical and practical exercises in thermoluminescence, Numerical and Practical Exercises in Thermoluminescence.

https://doi.org/10.1007/0-387-30090-2
Palczewski, P., Biernacka, M., Chruścińska, A., 2025. Testing TM-OSL on different quartz samples to illustrate the advantages of the technique. Geochronometria 52, 1–17. https://doi.org/10.20858/geochr/200792
Palczewski, P., Biernacka, M., Chruścińska, A., 2022. Dose-response of the fast OSL component in quartz at the range of high doses. https://doi.org/10.13140/RG.2.2.34379.05924
Peng, J., Dong, Z.B., Han, F.Q., 2015. tgcd: An R package for analyzing thermoluminescence glow curves. SoftwareX 5, 112–120. https://doi.org/10.1016/j.softx.2016.06.001
Polymeris, G.S., 2016. Thermally assisted OSL (TA-OSL) from various luminescence phosphors; an overview. Radiat. Meas. 90, 145–152. https://doi.org/10.1016/j.radmeas.2016.01.035
Polymeris, G.S., Şahiner, E., Kadioğlu, Y.K., Meriç, N., 2018. Properties of quartz TA–OSL signal with a peculiar decay shape for SAR TA–OSL applications. Radiat. Meas. 120, 176–180.
Polymeris, G.S., Şahiner, E., Meriç, N., Kitis, G., 2015. Experimental features of natural thermally assisted OSL (NTA-OSL) signal in various quartz samples; Preliminary results. Nucl. Instruments Methods Phys. Res. Sect. B Beam Interact. with Mater. Atoms 349, 24–30. https://doi.org/10.1016/j.nimb.2015.01.079
Porat, N., 2006. Use of magnetic separation for purifying quartz for luminescence dating. Anc. TL 24, 33–36.
Poulose, K. V. (1965). Report on reconnaissance geological mapping of the coastal Tertiaries in parts of Ernakulam, Trichur, Palghat, Calicut, and Cannanore districts, Kerala State. Field Season 1964-1965. *(Unpublished GSI Progress Report).*

Prasad, A.K., Poolton, N.R.J., Kook, M., Jain, M., 2017. Optical dating in a new light: A direct, non-destructive probe of trapped electrons. Sci. Rep. 7, 1–15. https://doi.org/10.1038/s41598-017-10174-8
Prescott, J.R., Huntley, D.J., Hutton, J.T., 1993. Estimation of equivalent dose in thermoluminescence dating—the Australian slide method. Anc. TL 11, 1–5.
Prescott, J.R., Hutton, J.T., 1994. Cosmic ray contributions to dose rates for luminescence and ESR dating: Large depths and long-term time variations. Radiat. Meas. 23, 497–500. https://doi.org/10.1016/1350-4487(94)90086-8
Prescott, J.R., Robertson, G.B., 1997. Sediment dating by luminescence: A review. Radiat. Meas. 27, 893–922. https://doi.org/10.1016/S1350-4487(97)00204-7
Preusser, F., Chithambo, M.L., Götte, T., Martini, M., Ramseyer, K., Sendezera, E.J., Susino, G.J., Wintle, A.G., 2009. Quartz as a natural luminescence dosimeter. Earth-Science Rev. 97, 184–214. https://doi.org/10.1016/j.earscirev.2009.09.006
Qin, J.T., Zhou, L.P., 2009. Stepped-irradiation SAR: A viable approach to circumvent OSL equivalent dose underestimation in last glacial loess of northwestern China. Radiat. Meas. 44, 417–422. https://doi.org/10.1016/j.radmeas.2009.06.008
Rahimzadeh, N., Tsukamoto, S., Thiel, C., Frechen, M., 2023a. Progress and pitfalls of the SAR protocol for the quartz violet stimulated luminescence (VSL) signal: A case study from Sardinia. Quat. Geochronol. 75, 101433. https://doi.org/https://doi.org/10.1016/j.quageo.2023.101433
Rahimzadeh, N., Tsukamoto, S., Zhang, J., Long, H., 2021. Natural and laboratory dose response curves of quartz violet stimulated luminescence (VSL): Exploring the multiple aliquot regenerative dose (MAR) protocol. Quat. Geochronol. 65. https://doi.org/10.1016/j.quageo.2021.101194
Rahimzadeh, N., Zhang, J., Tsukamoto, S., Long, H., 2023b. Characteristics of the quartz

isothermal thermoluminescence (ITL) signal from the 375° C peak and its potential for extending the age limit of quartz dating. Radiat. Meas. 161, 106899.
Rajapara, H.M., 2014. Some Unresolved Problems of Mineral Luminescence Relevant to Radiation Dosimetry.
Randall, J.T., Wilkins, M.H.F., 1945. Phosphorescence and electron traps-I. The study of trap distributions. Proc. R. Soc. London. Ser. A. Math. Phys. Sci. 184, 365–389.
Rangarajan, V.G., Bharti, R., Mondal, S.K., Pradhan, C., Dutta, S., 2018. Remote Sensing for Martian Studies: Inferences from Syrtis Major. J. Indian Soc. Remote Sens. 46, 1537–1551. https://doi.org/10.1007/s12524-018-0826-7
Rajendran, C.P., & Dr.Soman, K. (1987). Systematic stratigraphic studies of cenozoic sediment of Kerala with special reference to Warkalli and Quilon formations. Ph.D. thesis. Cochin University of Science and Technology.

Rao, A.R., Nanda, A.C., Sharma, U.N., Bhalla, M.S., 1995. Magnetic polarity stratigraphy of the Pinjor Formation (Upper Siwalik) near Pinjore, Haryana. Source Curr. Sci. 68, 1231–1236.
Reynolds, G.A., 2007. the Jarosite Group of Compounds – Stability , Decomposition and Conversion.
Rhodes, E.J., 1992. Optical dating of quartz from sediments.
Rink, W.J., Rendell, H., Marseglia, E.A., Luff, B.J., Townsend, P.D., 1993. Thermoluminescence spectra of igneous quartz and hydrothermal vein quartz. Phys. Chem. Miner. 20, 353–361. https://doi.org/10.1007/BF00215106
Roberts, R.G., Galbraith, R.F., Olley, J.M., Yoshida, H., Laslett, G.M., 1999. Optical dating of single and multiple grains of quartz from Jinmium rock shelter, northern Australia: Part II, results and implications. Archaeometry 41, 365–395. https://doi.org/10.1111/j.1475-4754.1999.tb00988.x
Roberts, R.G., Spooner, N.A., Questiaux, D.G., 1994. Palaeodose underestimates caused by extended-duration preheats in the optical dating of quartz. Radiat. Meas. 23, 647–653.
Roca, A., 2022. Jarosites: Formation, Structure, Reactivity and Environmental.
Rodrigues, K., Huot, S., Keen-Zebert, A., 2022. Exploring the application of blue and red thermoluminescence for dating volcanic glasses. Radiat. Meas. 153, 106731. https://doi.org/10.1016/j.radmeas.2022.106731
Şahiner, E., Meriç, N., Polymeris, G.S., 2017. Thermally assisted OSL application for equivalent dose estimation; comparison of multiple equivalent dose values as well as saturation levels determined by luminescence and ESR techniques for a sedimentary sample collected from a fault gouge. Nucl. Instruments Methods Phys. Res. Sect. B Beam Interact. with Mater. Atoms 392, 21–30. https://doi.org/10.1016/j.nimb.2016.12.001
Sajinkumar, K.S., Santosh, M., Rani, V.R., Anand, S., Pradeepkumar, A.P., Chavan, A., Thrivikramji, K.P., Ramachandran, P. V., 2022. The Tertiary sequence of Varkala coastal cliffs, southwestern India: An ideal site for Global Geopark. Int. J. Geoheritage Park. 10, 308–321. https://doi.org/10.1016/j.ijgeop.2022.05.003
Sangode , S . J ., Kumar , R . & Ghosh, S.. K.., 1996. Sangode , S . J ., Kumar , R . & Ghosh , S . K . 1996 . Magnetic polarity stratigraphy 683–704.
Sarkar, S., Moitra, H., Bhattacharya, S., Dagar, A., Ray, D., Gupta, S., Chavan, A., Shukla, A.D., Bhandari, S., 2022. Spectroscopic studies on the Puga Hot Spring Deposits, Ladakh, an astrobiological Martian analog site in India. J. Geophys. Res. Planets 127, e2022JE007299.
Sawakuchi, G.O., Okuno, E., 2004. Effects of high gamma ray doses in quartz. Nucl. Instruments Methods Phys. Res. Sect. B Beam Interact. with Mater. Atoms 218, 217–

221. https://doi.org/10.1016/j.nimb.2003.12.021
Schmidt, C., Halter, T., Hanson, P.R., Ulianov, A., Putlitz, B., King, G.E., Kreutzer, S., 2024. Zircon luminescence dating revisited. Geochronology 2024, 1–32.
Schmidt, C., Woda, C., 2019. Quartz thermoluminescence spectra in the high-dose range. Phys. Chem. Miner. 46, 861–875. https://doi.org/10.1007/s00269-019-01046-w
Singarayer, J.S., Bailey, R.M., 2003. Further investigations of the quartz optically stimulated luminescence components using linear modulation. Radiat. Meas. 37, 451–458. https://doi.org/https://doi.org/10.1016/S1350-4487(03)00062-3
Singarayer, J.S., Bailey, R.M., Rhodes, E.J., 2000. Potential of the slow component of quartz OSL for age determination of sedimentary samples. Radiat. Meas. 32, 873–880.
Singhal, M., Moitra, H., Mitra, S., Panda, A., Yadav, J.K., Sarma, D.S., Kumar, D., Chauhan, N., Gupta, S., Singhvi, A.K., 2025a. Luminescence characteristics of terrestrial Jarosite from Kachchh, India: A Martian analogue. Meteorit. Planet. Sci.
Singhal, M., Panda, M., Annalakshmi, O., Chauhan, N., 2025b. On the sensitivity normalization for blue stimulated luminescence of quartz. Radiat. Phys. Chem. 234, 112764.
Singhal, M., Panda, M., Shinde, S.H., Mondal, S., Annalakshmi, O., Chauhan, N., 2024. Study of thermoluminescence characteristics of quartz for high radiation doses (> 1kgy): implications for extending the luminescence dating range.
Singhvi, A., Kaushal, R., Parida, S., 2022. Luminescence dating and Quaternary Geology: The Indian Narrative. J. Palaeontol. Soc. India 67(1), 183–210.
Singhvi, A.K., 1985. Thermoluminescence d a t i n g of sediments 10, 137–161.
Singhvi, A.K., 1981. A possible correlation between the alpha efficiency and the anomalous fading characteristics. Anc. TL 14, 10.
Singhvi, A.K., Aitken, M.J., 1978. Americium-241 for alpha-irradiations. Anc. TL 2, 2–9.
Singhvi, A.K., Chauhan, N., Biswas, R.H., 2010. A survey of some new approaches in maximum age limit and accuracy of luminescence application to archaeological chronometry. Mediterr. Archaeol. Archaeom. 10, 9–15.
Singhvi, A.K., Mejdahl, V., 1985. Thermoluminescence dating of sediments. Nucl. Tracks Radiat. Meas. 10, 137–161.
Singhvi, A.K., Sharma, Y.P., Agrawal, D.P., 1982. Thermoluminescence dating of sand dunes in Rajasthan, IND. Nature 295, 313–315. https://doi.org/10.1038/295313a0
Singhvi, Ashok K, Stokes, S.C., Chauhan, N., Nagar, Y.C., Jaiswal, M.K., 2011. Changes in natural OSL sensitivity during single aliquot regeneration procedure and their implications for equivalent dose determination. Geochronometria 38, 231–241.
Singhvi, Ashok K., Stokes, S.C., Chauhan, N., Nagar, Y.C., Jaiswal, M.K., 2011. Changes in natural osl sensitivity during single aliquot regeneration procedure and their implications for equivalent dose determination. Geochronometria 38, 231–241. https://doi.org/10.2478/s13386-011-0028-3
Smith, B.W., 1988. Zircon from sediments: A combined OSL and TL auto-regenerative dating technique. Quat. Sci. Rev. 7, 401–406. https://doi.org/10.1016/0277-3791(88)90036-4
Smith, B.W., Rhodes, E.J., Stokes, S., Spooner, N.A., Aitken, M.J., 1990. Optical dating of sediments: initial quartz results from Oxford. Archaeometry 32, 19–31.
Smith, M.R., Bandfield, J.L., 2012. Geology of quartz and hydrated silica-bearing deposits near Antoniadi Crater, Mars. J. Geophys. Res. Planets 117.
Spooner, N. A., Questiaux, D.G., 2000. Kinetics of red, blue and UV thermoluminescence and optically-stimulated luminescence from quartz. Radiat. Meas. 32, 659–666. https://doi.org/10.1016/S1350-4487(00)00067-6
Spooner, N A, Questiaux, D.G., 2000. Kinetics of red , blue and UV thermoluminescence and

optically-stimulated luminescence from quartz 32, 659–666.
Stamoulis, K., Liritzis, I., Papachristodoulou, C., Ioannides, K.G., 2012. A re-evaluation of radiation dose-rate conversion factors. Mediterr. Archaeol. Archaeom. 12, 1–15.
Stevens, T., Buylaert, J.P., Murray, A.S., 2009. Towards development of a broadly-applicable SAR TT-OSL dating protocol for quartz. Radiat. Meas. 44, 639–645. https://doi.org/10.1016/j.radmeas.2009.02.015
Stokes, S., 1994. The timing of OSL sensitivity changes in a natural quartz. Radiat. Meas. 23, 601–605. https://doi.org/10.1016/1350-4487(94)90106-6
Thiel, C., Buylaert, J.P., Murray, A., Terhorst, B., Hofer, I., Tsukamoto, S., Frechen, M., 2011. Luminescence dating of the Stratzing loess profile (Austria) - Testing the potential of an elevated temperature post-IR IRSL protocol. Quat. Int. 234, 23–31. https://doi.org/10.1016/j.quaint.2010.05.018
Timar-Gabor, A., Constantin, D., Buylaert, J.P., Jain, M., Murray, A.S., Wintle, A.G., 2015. Fundamental investigations of natural and laboratory generated SAR dose response curves for quartz OSL in the high dose range. Radiat. Meas. 81, 150–156. https://doi.org/10.1016/j.radmeas.2015.01.013
Timar-Gabor, A., Vasiliniuc, Ş., Vandenberghe, D.A.G., Cosma, C., Wintle, A.G., 2012. Investigations into the reliability of SAR-OSL equivalent doses obtained for quartz samples displaying dose response curves with more than one component. Radiat. Meas. 47, 740–745. https://doi.org/https://doi.org/10.1016/j.radmeas.2011.12.001
Timar-Gabor, A., Wintle, A.G., 2013. On natural and laboratory generated dose response curves for quartz of different grain sizes from Romanian loess. Quat. Geochronol. 18, 34–40. https://doi.org/10.1016/j.quageo.2013.08.001
Tsukamoto, S., Duller, G.A.T., Wintle, A.G., 2008. Characteristics of thermally transferred optically stimulated luminescence (TT-OSL) in quartz and its potential for dating sediments. Radiat. Meas. 43, 1204–1218. https://doi.org/10.1016/j.radmeas.2008.02.018
Tsukamoto, S., Duller, G.A.T., Wintle, A.G., Muhs, D., 2011. Assessing the potential for luminescence dating of basalts. Quat. Geochronol. 6, 61–70. https://doi.org/10.1016/j.quageo.2010.04.002
Tsukamoto, S., Murray, A.S., Huot, S., Watanuki, T., Denby, P.M., Bøtter-Jensen, L., 2007. Luminescence property of volcanic quartz and the use of red isothermal TL for dating tephras. Radiat. Meas. 42, 190–197.
Tudyka, K., Miłosz, S., Adamiec, G., Bluszcz, A., Poręba, G., Paszkowski, Ł., Kolarczyk, A., 2018. μDose: A compact system for environmental radioactivity and dose rate measurement. Radiat. Meas. 118, 8–13.
Vandenberghe, D., Kasse, C., Hossain, S.M., De Corte, F., Van den Haute, P., Fuchs, M., Murray, A.S., 2004. Exploring the method of optical dating and comparison of optical and 14C ages of Late Weichselian coversands in the southern Netherlands. J. Quat. Sci. Publ. Quat. Res. Assoc. 19, 73–86.
Velasco, F., Herrero, J.M., Suárez, S., Yusta, I., Alvaro, A., Tornos, F., 2013. Supergene features and evolution of gossans capping massive sulphide deposits in the Iberian Pyrite Belt. Ore Geol. Rev. 53, 181–203. https://doi.org/https://doi.org/10.1016/j.oregeorev.2013.01.008
Viñals, J., Roca, A., Arranz, M., 2003. Autoclave Alkaline Decomposition and Cyanidation of Jarosite-Beudantite Phases from Rio Tinto Gossan Ores. Can. Metall. Q. 42, 29–40. https://doi.org/10.1179/cmq.2003.42.1.29
Viñals, J., Roca, A., Cruells, M., Núñez, C., 1995. Characterization and cyanidation of Rio Tinto gossan ores. Can. Metall. Q. 34, 115–122. https://doi.org/https://doi.org/10.1016/0008-4433(94)00022-C
Visocekas, R., Spooner, N.A., Zink, A., Blanc, P., 1994. Tunnel afterglow, fading and

infrared emission in thermoluminescence of feldspars. Radiat. Meas. 23, 377–385.
Wallinga, J., Murray, A., Wintle, A., 2000. The single-aliquot regenerative-dose (SAR) protocol applied to coarse-grain feldspar. Radiat. Meas. 32, 529–533.
Wang, C., Huang, C., Fan, A., Li, S., 2024. Quaternary Geochronology The D e underestimation caused by the unstable medium component in the initial OSL signal from lava-baked quartz and correction strategies. Quat. Geochronol. 82, 101532. https://doi.org/10.1016/j.quageo.2024.101532
Wang, L., Zhang, Yuhang, Gao, D., Sha, X., Chen, X., Zhang, Yanqiu, Zhang, J., Zhang, X., Cao, Y., Wang, Y., Li, X., Xu, S., Yu, H., Chen, B., 2024. Concentration- and temperature- dependent luminescence quenching and optical transition of Sr2GdTaO6: Eu3+ phosphor for potential applications in white LEDs. Results Phys. 56, 107238. https://doi.org/https://doi.org/10.1016/j.rinp.2023.107238
Wang, X., Peng, J., Adamiec, G., 2021. Extending the age limit of quartz OSL dating of Chinese loess using a new multiple-aliquot regenerative-dose (MAR) protocol with carefully selected preheat conditions. Quat. Geochronol. 62. https://doi.org/10.1016/j.quageo.2020.101144
Wang, X.L., Lu, Y.C., Wintle, A.G., 2006. Recuperated OSL dating of fine-grained quartz in Chinese loess. Quat. Geochronol. 1, 89–100. https://doi.org/10.1016/j.quageo.2006.05.020
Watanuki, T., Murray, A.S., Tsukamoto, S., 2005. Quartz and polymineral luminescence dating of Japanese loess over the last 0.6 Ma: Comparison with an independent chronology. Earth Planet. Sci. Lett. 240, 774–789. https://doi.org/https://doi.org/10.1016/j.epsl.2005.09.027
Wesnousky, S.G., Kumar, S., Mohindra, R., Thakur, V.C., 1999. Uplift and convergence along the Himalayan Frontal Thrust of India. Tectonics 18, 967–976.
Westaway, K.E., Roberts, R.G., 2006. A dual-aliquot regenerative-dose protocol (DAP) for thermoluminescence (TL) dating of quartz sediments using the light-sensitive and isothermally stimulated red emissions. Quat. Sci. Rev. 25, 2513–2528. https://doi.org/10.1016/j.quascirev.2005.06.010
Wills, A.S., Harrison, A., Ritter, C., Smith, R.I., 2000. Magnetic properties of pure and diamagnetically doped jarosites: model kagomé antiferromagnets with variable coverage of the magnetic lattice. Phys. Rev. B 61, 6156.
Wintle, A.G., 2008. Luminescence dating: Where it has been and where it is going. Boreas 37, 471–482. https://doi.org/10.1111/j.1502-3885.2008.00059.x
Wintle, A.G., 1997. Luminescence dating: Laboratory procedures and protocols. Radiat. Meas. 27, 769–817. https://doi.org/10.1016/S1350-4487(97)00220-5
Wintle, Ann G, 1973. Anomalous fading of thermo-luminescence in mineral samples. Nature 245, 143–144.
Wintle, Ann G., 1973. © 1973 Nature Publishing Group. Nat. Phys. Sci. 241, 20.
Wintle, A.G., Huntley, D.J., 1979. Thermoluminescence dating of a deep-sea sediment core [7]. Nature 279, 710–712. https://doi.org/10.1038/279710a0
Wintle, A.G., Murray, A.S., 2006. A review of quartz optically stimulated luminescence characteristics and their relevance in single-aliquot regeneration dating protocols. Radiat. Meas. 41, 369–391. https://doi.org/10.1016/j.radmeas.2005.11.001
Woda, C., Schilles, T., Rieser, U., Mangini, A., Wagner, G.A., 2002. POINT DEFECTS AND THE BLUE EMISSION IN FIRED QUARTZ AT HIGH DOSES : A COMPARATIVE LUMINESCENCE AND EPR STUDY 100, 261–264.
Xu, H., Zhao, Æ.Y., Vogel, Æ.S.C., Hickmott, D.D., Daemen, Æ.L.L., Hartl, M.A., 2010. Thermal expansion and decomposition of jarosite : a high-temperature neutron diffraction study 73–82. https://doi.org/10.1007/s00269-009-0311-5

Yoshida, H., Roberts, R.G., Olley, J.M., Laslett, G.M., Galbraith, R.F., 2000. Extending the age range of optical dating using single ‘supergrains’ of quartz. Radiat. Meas. 32, 439–446.
Yukihara, E.G., McKeever, S.W.S., 2011. Optically stimulated luminescence: fundamentals and applications. John Wiley & Sons.
Yukihara, E.G., McKeever, S.W.S., Andersen, C.E., Bos, A.J.J., Bailiff, I.K., Yoshimura, E.M., Sawakuchi, G.O., Bossin, L., Christensen, J.B., 2022. Luminescence dosimetry. Nat. Rev. Methods Prim. 2. https://doi.org/10.1038/s43586-022-00102-0
Zhang, J., Tsukamoto, S., 2022. A simplified multiple aliquot regenerative dose protocol to extend the dating limit of K-feldspar pIRIR signal. Radiat. Meas. 157, 106827. https://doi.org/10.1016/j.radmeas.2022.106827
ZIMMERMAN, D.W., 1971. Thermoluminescent dating using fine grains from pottery. Archaeometry 13, 29–52.
Zimmerman, J., 1971. The radiation-induced increase of the 100 C thermoluminescence sensitivity of fired quartz. J. Phys. C Solid State Phys. 4, 3265–3276. https://doi.org/10.1088/0022-3719/4/18/032
Zimmermans, D.W., 1972. Relative thermoluminescence effects of alpha- and beta- radiation. Radiat. Eff. 14, 81–92. https://doi.org/10.1080/00337577208230476

List of Publication

1. **Singhal, Malika**, Madhusmita Panda, S. H. Shinde, Sandip Mondal, O. Annalakshmi, and Naveen Chauhan. "Study of thermoluminescence characteristics of quartz for high radiation doses (> 1kGy): Implications for extending the luminescence dating range." *Radiation Measurements* 178 (2024): 107300. https://doi.org/10.1016/j.radmeas.2024.107300

2. **Singhal, Malika,** Madhusmita Panda, O. Annalakshmi, and Naveen Chauhan. "On the sensitivity normalization for blue stimulated luminescence of quartz." *Radiation Physics and Chemistry* 234 (2025): 112764. https://doi.org/10.1016/j.radphyschem.2025.112764

3. **Singhal, Malika,** Himela Moitra, Souvik Mitra, Aurovinda Panda, Jayant Kumar Yadav, D. Srinivasa Sarma, Devender Kumar, Naveen Chauhan, Saibal Gupta, and Ashok Kumar Singhvi. "Luminescence characteristics of terrestrial Jarosite from Kachchh, India: A Martian analogue." *Meteoritics & Planetary Science* (2025). https://doi.org/10.1111/maps.70021

4. Degda, Naresh, Nimesh Patel, Vishwnath Verma, K. V. R. Murthy, Naveen Chauhan, **Malika Singhal**, and M. Srinivas. "Photoluminescence and thermoluminescence kinetic features of Eu3+ doped Sr2YVO6 double perovskite phosphor." *Optical Materials* 142 (2023): 114019. https://doi.org/10.1016/j.optmat.2023.114019

5. Sajwan, Shruti, Manisha Sharma, Santosh Kachhap, **Malika Singhal**, Akhilesh Kumar Singh, Mohit Tyagi, Partha Sarathi Sarkar, Naveen Chauhan, and Sunil Kumar Singh. "Structural and Optical Properties of Zn2. 95Ga2-xSnO8: xCr3+: An excellent X-ray Charging-Based Persistent Phosphor." *Journal of Alloys and Compounds* (2024): 173405. https://doi.org/10.1016/j.jallcom.2023.173405

6. Degda, Naresh, Nimesh Patel, **Malika Singhal**, K. V. R. Murthy, Naveen Chauhan, and M. Srinivas. "Thermally Stable Luminescence and Dosimetric Features of Ho (III) Activated Tungstate Double Perovskite." *Journal of Luminescence* (2024): 120775. https://doi.org/10.1016/j.jlumin.2024.120775

7. Degda, Naresh, Nimesh Patel, **Malika Singhal**, K. V. R. Murthy, Naveen Chauhan, Vishwnath Verma, and M. Srinivas. "Luminescence and Dosimetry Investigations of Eu (III) Doped Ca2CeVO6 Novel Double Perovskite." Optical Materials (2024): 115861. https://doi.org/10.1016/j.optmat.2024.115861

8. Morthekai, Paulramasamy, **Malika Singhal**, Suchinder K. Sharma, Sudhakar Sivasubramaniam, Muthalankurichi Kamarasu, Priyanka Singh, Naveen Chauhan, Kamlesh Kumar, Sheikh Ali Nawaz, and Nitesh Khonde. "Investigating historical attribution: luminescence dating of bricks from a submerged structure in southeastern India." *Frontiers in Environmental Archaeology* 4 (2025): 1464315. https://doi.org/10.3389/fearc.2025.1464315

9. Sajwan, Shruti, **Malika Singhal,** Pradeep Kumar Vishwakarma, Naveen Chauhan, and Sunil Kumar Singh. "Advanced luminescent material for multikey static and dynamic

anticounterfeiting and information encryption." *ACS Applied Optical Materials* 3, no. 7 (2025): 1535-1546. https://doi.org/10.1021/acsaom.5c00138

10. Sharma, Ankit, **Malika Singhal**, Naveen Chauhan, and Suchinder K. Sharma. "Structure–defect–luminescence correlation in Cr3+-doped Zn2TiO4." *Materials Science and Engineering: B* 323 (2026): 118661. https://doi.org/10.1016/j.mseb.2025.118661

Under review:

1. Monika Devi, **Malika Singhal,** Parth Khaduri, Naveen Chauhan, Ashok Kumar Singhvi. Applicability of Post Violet-Infrared Single Aliquot Regenerative (pVIR-SAR) Dose Protocol for Different Types of Samples using Potassium Feldspars.

2. Pandya, Jalaja, **Malika Singhal**, Navinder Singh, and Naveen Chauhan DFT Investigations of Major Defects in Quartz Crystal: Implications for Luminescence and ESR Dosimetry and Dating

Under preparation:

1**. Malika Singhal,** Linto Alappat, Madhusmita Panda, O. Annalakshmi, Naveen Chauhan. Insights into the luminescence mechanism over Ma timescale from the Charavathur Tertiary Formation (Southern India)

Workshop/Conference/Symposium

International

1. **Malika Singhal**, Madhusmita Panda, S. H. Shinde, Sandip Mondal, O. Annalakshmi, and Naveen Chauhan. “Thermoluminescence characteristics of quartz at high radiation doses (>1kGy)”, 2024 UK Luminescence and ESR meeting (UKLUM2024), Oxford, UK (11-13th September 2024).

2. **Malika Singhal**, Souvik Mitra, Himela Moitra, Saibal, Naveen Chauhan, and Ashok Kumar Singhvi. “Dosimetric Investigation of Jarosite: A Martian Analogue”, Meteoroids, Meteors and Meteorites: Messengers from Space” (MetMeSS-2024), Ahmedabad, India (20-22 November 2024).

3. **Malika Singhal,** Madhusmita Panda, Ozhimuthu Annalakshmi, Parth Chauhan, and Naveen Chauhan. "Do Sensitivity Normalization Methods Limit the Upper Range of Luminescence Dating Using BSL Quartz?." AGU24 (2024).

4. **Malika Singhal,** Madhusmita Panda, Sachin Mahatre, Santosh Shinde, Sandip Mondal, O. Annalakshmi, Naveen Chauhan. “Investigating high-dose thermoluminescence characteristics of quartz” 7th International Conference on Luminescence & its Applications-2023 (ICLA - 2023), Hyderabad, India, (3rd-6th July 2023).

National

1. **Malika Singhal,** Souvik Mitra, Saibal, Naveen Chauhan, and Ashok Kumar Singhvi. "Luminescence Characteristics of terrestrial Jarosite from Kachchh, India: A Martian Analogue" 3rd Symposium on "Meteoroids, Meteors and Meteorites: Messengers from Space" (MetMeSS-2023), Ahmedabad, India (1-3 November 2023).

2. **Malika Singhal,** Naveen Chauhan. "Exploring the Influence of Regenerative Dose on Test Dose Signal in SAR BSL: Implications for Dating Beyond Saturation Limits". 5th Workshop on Luminescence Dating and its Application. Ahmedabad, India (21-23 February 2024).

3. **Malika Singhal**, Naveen Chauhan. "Exploring the potential of olivine as a natural dosimeter for luminescence dating". 4th Workshop on Luminescence Dating and its Application. IISER Kolkata, India (1-3 February 2023).

4. **Malika Singhal**, Kuljeet Kaur Marhas, Naveen Chauhan, Manish N. Sanghani. "Luminescence Characterization of Minerals from Murchison and Murray". Meteoroids, Meteors and Meteorites: Messengers from Space" (MetMeSS), Ahmedabad, India (November 29-30, 2021)

Grants and Awards

1. 2024-DST-SERB travel grant for attending UKLum2024; Sanction Order: ITS/2024/003684.

2. 2024- Award for best oral presentation in UKLUM2024 held at Oxford University, UK; Prize money: 200 GBP.

Radiation Measurements 178 (2024) 107300

Contents lists available at ScienceDirect

Radiation Measurements

journal homepage: www.elsevier.com/locate/radmeas

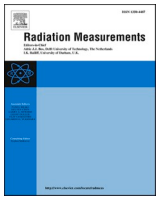

Study of thermoluminescence characteristics of quartz for high radiation doses (>1kGy): Implications for extending the luminescence dating range

Malika Singhal [a,b], Madhusmita Panda [c], S.H. Shinde [d], Sandip Mondal [d], O. Annalakshmi [c,e], Naveen Chauhan [a,*]

[a] AMOPH division, Physical Research Laboratory, Navrangpura, Ahmedabad, 380009, India
[b] Indian Institute of Technology, Gandhinagar, 382355, India
[c] Indira Gandhi Centre of Atomic Research, Kalpakkam, Tamil Nadu, 603102, India
[d] Bhabha Atomic Research Centre, Trombay, Mumbai, 400085, India
[e] Homi Bhabha National Institute, IGCAR, Kalpakkam, Tamil Nadu, 603102, India

ARTICLE INFO

Keywords:
Quartz
High dose response
Thermoluminescence
Multispectral
Normalization
Bleachability
Previous dose effects

ABSTRACT

Quartz is an omnipresent abundant natural mineral, used for luminescence dating. Lately, quartz optically stimulated luminescence (OSL) technique is widely used to estimate the equivalent doses (D_e) for dating geological events (up to 250 Gy, limited by saturation). Some works report thermoluminescence (TL) saturation around ~ (10–40) kGy. Still dose estimates for such high radiation dose (HRD) range are not achieved. Significant research exists about luminescence response for low dose ranges (<250 Gy) but limited studies are done for HRDs (>1 kGy). This work characterizes the luminescence response of quartz for HRDs (1–21 kGy) to improve existing understanding of luminescence mechanism. Results show that the characteristics of the trap (<200 °C) differ significantly at HRDs than low doses. TL in multi-spectral detection (UV–Visible) band suggest an increase in 340–380 °C peak intensity up to 11 kGy dose. The measurements of saturation dose suggest that it depends on the trapping centres but is independent of recombination centres for the samples used for study. The traps are found bleachable by sunlight, reducing TL signal to residual levels in 1 h. Further, the bleachability is found to be anti-correlated with luminescence emission wavelength. At HRDs luminescence sensitivity is influenced by dose given in previous cycle which is difficult to correct by routine normalization procedures. The work also explores the various normalization methods to find appropriate method for HRD estimation and recommends the use of mass normalization as other normalization methods do not correct the sensitivity changes at HRDs adequately.

1. Introduction

Luminescence dating has contributed considerably towards the understanding of the earth surface processes in the late quaternary period (Murray et al., 2021). Quartz and feldspar are two major minerals primarily used in luminescence dating. Feldspar offers to date older sediments but it is prone to anomalous fading, has slow signal bleachability (Buylaert et al., 2011; Kars et al., 2008) and weathers faster than quartz. In contrast, quartz has excellent bleachability (Murray and Wintle, 2000) and has no fading (except for volcanic quartz (Fattahi and Stokes, 2003)).

Dosimetric thermoluminescence (TL) peaks of quartz are present at temperatures higher than 300 °C and have a lifetime greater than 10^8 years at ambient temperature of 15 °C (Aitken, 1985). Spooner and Questiaux (2000) obtained a lifetime of 1.7×10^7 years for 325 °C trap at ambient temperature 20 °C and at heating rate of 5 °C/s, while a lifetime of 10^7 and 10^9 years for 325 °C and 375 °C peak respectively at heating rate of 5 °C/s at 25 °C was obtained by Ngoc et al. (2024, 2021). Some other works (Han et al., 2000) have reported greater lifetime such as 1.07×10^{12}, 1.92×10^{12} and 4.06×10^{12} years for 320 °C, 370 °C and 420 °C traps respectively, at ambient temperature of 20 °C and heating rate of 10 °C/s. Sufficiently larger lifetime of quartz makes it suitable for dating Ma events The signal in quartz is known to saturate generally around ~250 Gy (Chawla et al., 1998; Huntley et al., 1996; Murray and Wintle, 2000; Wintle and Murray, 2006) compared to feldspar (~2000Gy) (Thiel et al., 2011). Considering stable and fast to bleach signal, quartz is always a preferred mineral and rigorously explored for signals suitable for dating older sediments. Protocols such as thermally

* Corresponding author.
E-mail address: chauhan@prl.res.in (N. Chauhan).

https://doi.org/10.1016/j.radmeas.2024.107300
Received 31 May 2024; Received in revised form 29 August 2024; Accepted 17 September 2024
Available online 18 September 2024

transferred-optically stimulated luminescence (TT-OSL), violet stimulated luminescence (VSL) (Jain, 2009; Wang et al., 2006) are developed suggesting dose saturation in excess to 1 kGy but with limited success (Ankjærgaard et al., 2016; Duller and Wintle, 2012). Some studies report saturation of TL signals for dosimetric peaks around 10–40 kGy, but age estimations have not become a reality in this dose range (Durrani et al., 1977; Sawakuchi and Okuno, 2004; Schmidt and Woda, 2019; Woda et al., 2002). The possibility to increase the dosimetry and dating range till 10 kGy is of great importance as there are several interesting natural processes which date beyond the current dating limits. Besides this, radiation dosimetry in high dose range can be useful for radiation dose assessment, and space related applications. This suggests that attempts to comprehend basic physics and luminescence mechanisms at high radiation doses (HRDs) should be stepped up.

Quartz is known to emit luminescence in several emission bands that are majorly classified as UV, blue, green and red emissions (Götze et al., 2021; Krbetschek et al., 1997; Preusser et al., 2009; Rink et al., 1993). UV emission reaches early saturation around 250 Gy (Adamiec, 2005; Chawla et al., 1998; Wintle, 1997) and shows a supralinear increase thereafter (Chawla et al., 1998). Therefore, it is used for dose estimation below 250 Gy. In blue, many studies report very high saturation ~40 kGy, but no dose estimates at these HRDs are made (Hashimoto et al., 1987; Schmidt and Woda, 2019). Further sensitivity changes are reported in blue TL at HRDs (Hashimoto et al., 1987). Studies using red TL emission from volcanic quartz have obtained saturation dose ~6 kGy and are fairly studied for dose estimation (Fattahi and Stokes, 2000; Hashimoto et al., 1987; Miallier et al., 1991). The saturation characteristics for quartz in different emissions, the role of electron traps and recombination centres in saturation is still not understood (Ankjærgaard et al., 2006; Lowick et al., 2010). Therefore, there is a need to develop more understanding about the luminescence response of quartz at HRDs, which requires systematic study of luminescence characteristics of different emissions with variable doses. This study attempts a detailed simultaneous analysis of dose saturation across the entire spectral region from UV to red for various HRDs. This will further help in developing an understanding about the associated issues such as defect creations, sensitivity changes, TL peak shifts, emission spectrum changes and possibly help in deconvoluting complex convolution of glow peaks linked with different dose ranges. The study also addresses the effect of normalization, predose (previous measurement cycle dose), bleachability on the TL characteristics at HRDs.

2. Methodology

2.1. Samples

This study utilizes four quartz samples from varying provenances and deposition history in order to capture variability in the luminescence characteristics from different types of samples in high dose regime. Thus, samples are chosen from Northern India (Himalayan river sediment sample YS-5), Western India (Deccan traps sediment sample, KG-1), Northwestern India (Aravalli's range quartzite rock (RQ-1) and sediment (SR-23) samples). The samples from rock and sediment from same provenance are generally known to have varied characteristics (Sawakuchi et al., 2011). The mineralogy of quartzite rock sample RQ-1 was confirmed using XRD. The sample KG-1 is naturally high dosed and is in field saturation. It was used to study the bleaching effect and natural luminescence in different spectral windows. Details of these samples are given in Table 1. Of the four samples used in this study, detailed investigations are carried out on the sample YS-5, because of the less inter-aliquot scatter and clear observability of signal saturation.

2.2. Sample preparation

All the samples were processed under subdued red light by first treating them with 1 N HCl to remove carbonates, followed by 30% H_2O_2 to remove organic impurities. The samples were dried at a temperature of 45 °C. A grain size fraction of 90–150 μm was sieved and magnetically separated using Frantz® magnetic separator (Model LB-1) to separate heavy minerals at 0.5 A and further quartz and feldspar at 1.5 A current (Porat, 2006). Cleaned quartz was treated with 40% HF for 60 min to remove alpha skin (~20 μm) and then with 37% HCl for 30 min to remove any fluorides. IR test was done to check feldspar contamination and negligible IR signal was observed (Smith et al., 1990). The rock quartz (RQ-1) sample was obtained by crushing the rock and separating a grain size of 90–150 μm through sieving. This fraction is treated with 10% HF for 5 min to remove surface defects formed, if any, due to crushing and then with 37% HCl for 30 min to remove any fluoride contamination (Toyoda et al., 2000). Monolayer of the sample was mounted on stainless steel disc using Silkospray™ and used for all TL measurements. A sample size of 5 mm was used on the disc for measurement, thus enabling an average measurement of approximately 1000 grains at a time.

Table 1
Sample details.

Sl. No.	Sample Name	Provenance	Latitude and Longitude	Remarks
1	YS-5	Yamuna Basin	29°45′47.80″N 77° 8′ 29.20″E	Himalayan river sediment, Northern India
2	SR-23	Sabarmati Basin	24°29′12.00″N 73°13′ 18.00″E	Sediment sample from Aravalli range, Northwestern India
3	KG-1	Khari Gorge, Bhuj	23° 15′ 3.24″ N 69° 37′ 48.72″ E	Deccan trap sediment, Western India, natural luminescence in saturation in SAR- BSL[a]
4	RQ-1	Sabarmati Basin	24°29′12.00″N 73°13′18.00″E	Quartzite rock sample from Aravalli range, Northwestern India

[a] SAR-BSL: Single Aliquot Regenerative- Blue Stimulated Luminescence.

2.3. Instrumentation

Measurements were done in Risø TL/OSL DA-15 automated reader equipped with EMI 9635 QA Photomultiplier tube, Sr^{90}/Y^{90} beta source (dose rate 0.044 Gy/s), and optical head containing Blue and IR LEDs for stimulation (Bøtter-Jensen et al., 2010; Thomsen et al., 2006). A linear heating rate of 2 °C/s was employed to heat the samples. A Co-60 gamma source having a dose rate of 0.183 Gy/s in a GC1200 assembly, manufactured indigenously by BRIT (Board of Radiation & Isotope Technology) in India was used for irradiating samples with HRDs >1 kGy having a 2 sigma uncertainty of 3.5%. All quartz samples were positioned at the center of the gamma chamber to ensure uniform exposure during irradiation. For multi-spectral TL studies, an EMCCD based high sensitivity spectrometer is often required. However, due to the high cost and unavailability of the required instrument, measurements were done using several interference filters as done in many previous studies (Caicedo et al., 2021; Monti et al., 2019; Spooner and Questiaux, 2000). Optical filters used for present study are listed in Table 2 and their spectral transmissions are shown in Fig. 1.

These filters were used in combination with BG39 filter (output from 325 to 700 nm) to reduce IR blackbody background. In addition, suitable

Table 2
Specification of different optical filters used in the study.

Filter Name	Central wavelength (nm)	Bandwidth (nm)
UV_{340}	340	80
$Blue_{447}$	447	60
$Blue_{475}$	475	50
$Green_{520}$	520	70
$Yellow_{550}$	550	100
Red_{620}	620	60

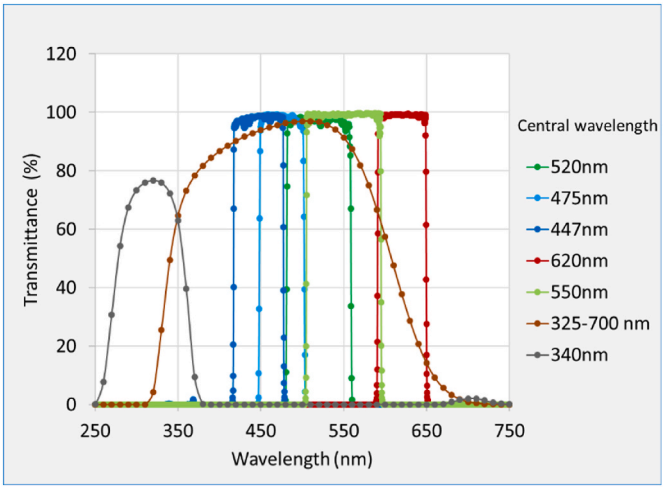

Fig. 1. The intensity transmittance of various optical band pass filters used in the study and mentioned in Table 2. (Data obtained from official website of the filter supplying companies, i.e., www.schott.com, https://hoyafilter.com/, www.edmundoptics.in).

neutral density (ND) filters were also used wherever the counts were significantly high and can lead PMT to non-linear region. Osram ultra-vitalux 300 W solar simulator lamp was used to bleach the samples of previous luminescence signals in addition to natural sunlight whenever needed.

2.4. Measurements

To study the luminescence characteristics for known dose, the signal due to prior dose was removed by bleaching the sediment samples YS-5 and SR-23 in solar lamp for 24 h. This reduced the previous TL signals in the samples. As the sensitivity of rock sample (RQ-1) was low and it didn't yield a measurable S/N ratio, it was sensitized by annealing at 450 °C for 30 min. This removed the previous TL signal and enhanced the dose sensitivity as well as stabilizing it. The residuals are shown in Fig. S9. Following this, the samples were irradiated with known doses. Apart from KG-1, all samples were irradiated with gamma radiation from 1 to 21 kGy. The following experiments were conducted.

2.4.1. Trap characterization

It has been reported that quartz has several traps (Aitken, 1985; Khoury et al., 2008). Hence a T_{max}-T_{stop} analysis was carried out (Garlick and Gibson, 1948; McKeever, 1985; Pagonis et al., 2006). The sample was irradiated with a dose of 50 Gy, and preheated till T_{stop} (from 30 to 450 °C, in steps of 10 °C) followed by a measurement of TL 450 °C. To avoid irradiation of samples multiple times (as is done in T_{max}-T_{stop}), the activation energy (E_a) was estimated using the repeated initial rise method (fractional glow technique) (Gobrecht and Hofmann, 1966), thus enabling the study of trap characteristics at HRDs. This method enables the determination of E_a of trap of any order. The initial part which is known to follow first-order kinetics of the glow curve was analysed. The method here was applied on 50 Gy, 3000 Gy and 18000 Gy dosed samples. The irradiated samples were heated till T_{stop} (from 30 to 450 °C, in steps of 5 °C), cooled and heated again. The blackbody subtracted intensity was used to compute the activation energy using Arrhenius relation between intensity and temperature (Pagonis et al., 2006). Additionally, to observe the effect of HRD on trap characteristics after annealing, a dose of 50 Gy was administered and activation energy was re-estimated.

2.4.2. Thermoluminescence glow curves and dose response

The TL glow curves of all the samples were measured for variable doses in the range 1–21 kGy in spectrum range (325–700 nm) using a BG39 filter. A preheat of 260 °C for 10 s was used to remove the contribution from shallow traps, which generally overpowers the signal from higher temperature peaks (>300 °C) (Spooner and Questiaux, 2000). Multiple aliquot additive dose (MAAD) response curves were obtained using mass normalized integrated TL intensity in 340–380 °C temperature range. The MAAD protocol ensures the measurement of samples at similar sensitivity. The measurement protocol is provided in Table 3. Three aliquots were measured for each dose point. For samples SR-23 and YS-5, a test dose of 21 Gy was added to measure low-temperature peak 80–100 °C TL peak for using it to monitor zero glow sensitivity. The saturation dose was found by fitting a single saturating exponential equation, $I = I_0\left(1 - e^{-D/D_0}\right)$, where I_0 is the saturation intensity and D_0 is the characteristics dose (Murray and Wintle, 2000). The maximum dose (saturation dose) ($2D_0$), which corresponds to 86% of the maximum intensity was calculated (Wintle and Murray, 2006). Additionally, a preheat of 350 °C was used based on T_{max}-T_{stop} analysis to remove shallower traps in the region 300–400 °C and $2D_0$ was calculated.

2.4.3. Multi-spectral studies

Multi-spectral studies were carried out using various bandpass filters (details in Table 2). The variation of TL response in different transmission bands was studied for the sample YS-5 for an irradiation dose of 1 kGy and a test dose of 21 Gy (zero glow) by heating linearly up to 450 °C at a rate of 2 °C/s. Following this, the dose response curve (DRC) is obtained for HRD as per section 2.4.2. in various spectral regions and $2D_0$ was estimated.

2.4.4. Signal resetting by sunlight

For dating applications, an important requirement for any signal is its resetting before burial by sunlight or heat or the reduction of signal to residual level before burial. The TL dating method can be applied to sunlight resettable events by subtracting the residual dose found by laboratory experiments (Singhvi and Mejdahl, 1985). Thus, bleachability of different TL spectral bands by sunlight and the magnitude of the residuals was investigated. The aliquots of naturally irradiated quartz sample KG-1 were exposed to sunlight for time periods of 30 s, 1 min, 10 min, 30 min, 1 h, 2 h and 3 h. Their respective TL responses were measured following sunlight exposure.

2.4.5. Sensitivity normalization

For inter-aliquot comparisons proper normalization of signal corresponding to a given dose is required. It may include normalization by mass, which assumes homogeneity in luminescence sensitivity of the grains throughout the sample; or by luminescence response of same or another peak, which assumes the signal to be proportional to mass or dosimetric signal being used and takes care of sensitivity fluctuations during measurements. These methods are well tested and characterized for low doses, but are yet not investigated for HRDs and needs to be verified for HRDs. Hence, the zero glow and second glow normalized signal corresponding to a test dose of 21Gy were compared with mass normalized signal as per protocol given in Table 4. The zero glow normalization was obtained by dividing the integrated TL1 signal intensity in the range 340–380 °C with the integrated TL1 intensity in the range of 80–100 °C. Similarly, in the second glow normalization, the

Table 3
Protocol to measure the dose response curve (DRC).

Sl. No.	Operation	Remarks
1.	Dose (1–21 kGy)	Laboratory doses for DRC
2.	Preheat 260 °C for 10 s	Removal of shallow traps
3.	Test Dose (21 Gy)	Dose for zero glow normalization
4.	TL 450 °C (@ 2 °C/s)	Luminescence intensity
5.	Mass normalization	

Table 4
Protocol to study various normalization method.

Step no.	Operation	Remarks
1	Fresh sample	
2	Irradiation with variable high radiation doses to different batches in range 1–21 kGy	
3	Preheat 260 °C (10s)	
4	Test dose (TD1) 21 Gy	
5	TL 450 °C (@ 2 °C/s)	TL1 (recording the zero glow 110 °C and first glow 340–380 °C peak signal)
6	Test dose (TD2) 21 Gy	
7	TL 450 °C (@2 °C/s)	TL2 (recording the second glow 110 °C peak signal)

integrated TL1 intensity in range 340–380 °C is normalized with the integrated TL2 intensity in range 80–100 °C, obtained after test dose TD2.

2.4.6. High radiation predose (HRpD) effect

Here high radiation predose (HRpD) effect implies the effect of dose given in previous measurement cycle that is propagated to its next measurements. Effect of HRpDs on the TL signals of the samples was studied by examining the TL intensity of various trapping and recombination centres. Fresh samples were divided into 8 batches and each batch was given a different dose in range 1–21 kGy followed by TL wash up to 450 °C to remove signal stored due to this dose. Then an identical dose was given to all batches followed by TL measurement (Table 5). The measurements were made in various wavelength bands to see the characteristics of various recombination centres.

3. Results

3.1. Trap characteristics

The TL glow curves of sample YS-5 measured following varying preheat temperatures are shown in Fig. 2. Several traps are observed and are marked with black arrows. Results shows that at least three traps are present beyond 300 °C. Further, Fig. 3 shows the T_{max}- T_{stop} graph for the sample YS-5. Multiple traps are visible for temperatures <200 °C and a continuum in T_{stop} is observed for temperatures >200 °C and T_{max} is found to increase towards end. The activation energy estimated at various doses is shown in Fig. 4(a), the curve for 50 Gy shows multiple plateaus, in agreement with the multiple traps observed in TL glow curve (Fig. 2). Towards the end the errors increase, because of poor signal to noise (S/N) ratio. However, at 3 kGy and 18 kGy significant differences in the activation energy of the quartz system are observed at low (<200 °C) temperatures and small variations at high (>350 °C) temperatures. The 110 °C peak has a low lifetime (~8 h) (Aitken, 1985). The time of gamma irradiation of samples with 3 and 18 kGy and time of transportation of samples is significantly higher than lifetime of

Table 5
Protocol to measure the HRpDs response of various peaks of quartz in different wavelength range.

Step no.	Operation	Remarks
1	Fresh sample (8 Batches)	
2	Irradiation with variable high radiation doses to different batches in range 1–21 kGy	X-axis
3	TL 450 °C (@ 2 °C/s)	
4	Same test dose 34 Gy to all aliquot	
5	TL 450 °C (@ 2 °C/s)	Y-axis (Observations using different detection filters)

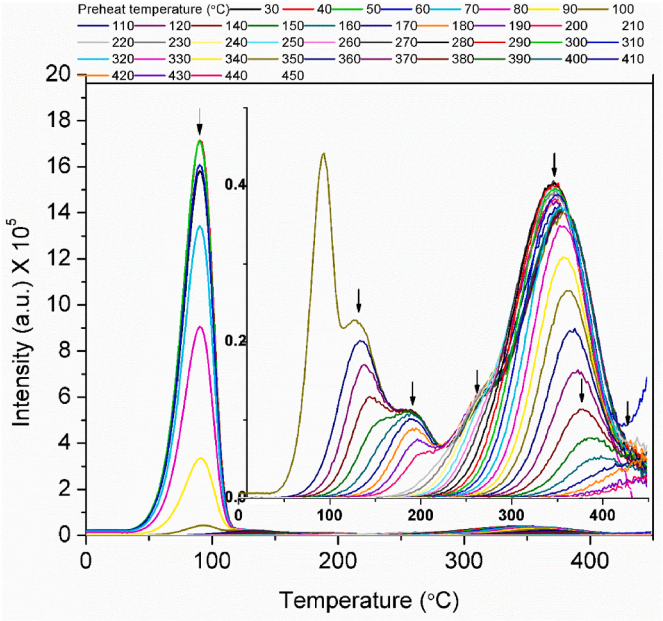

Fig. 2. TL glow curves of sample YS-5 recorded after various preheat temperatures. A dose of 50 Gy is given in each cycle. The visibly distinct peaks are marked by black arrow, measured in visible using BG39 Filter (325–700 nm).

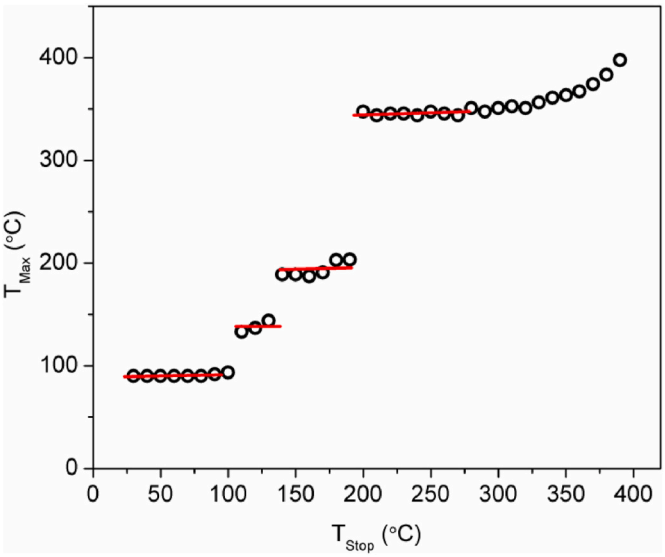

Fig. 3. T_{max}-T_{stop} graph for sample YS-5, dose 50 Gy, measured in visible using BG39 Filter (325–700 nm).

low-temperature peak leading to thermal fading, hence activation energy for this peak for HRDs could not be calculated. Further, for HRDs, the activation energy distribution for higher temperatures becomes like a continuum, rather than plateaus that are observed at 50 Gy. Further Fig. 4(b) shows the comparison of activation energies for 50 Gy doses before and after different HRD treatment of samples. Results shows that the crystal tries to restore E_a once the high doses are removed.

3.2. Dose response characteristics

Fig. 5(a), S2(a) and S3(a) represent the TL glow curves of the quartz samples (YS-5, RQ-1 and SR-23) for increasing HRDs. The TL peak intensity increases with HRD maintaining the glow curve shapes throughout the temperature range. Insets of Fig. 5(a) and S3(a) show the

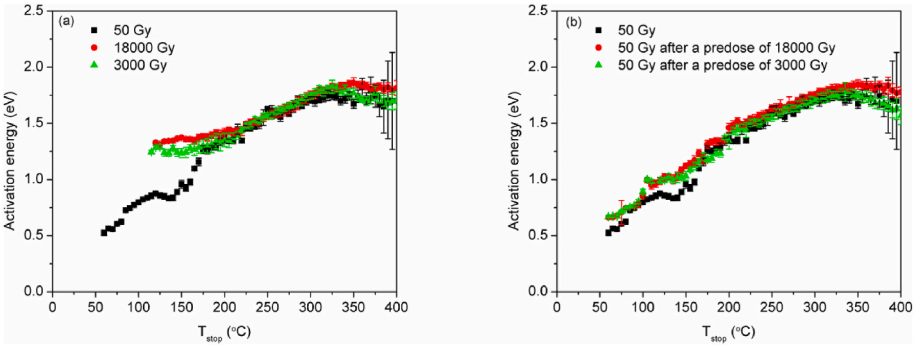

Fig. 4. Activation energy of sample YS-5 (a) at different doses, (b) at 50 Gy dose but after different HRpD removed by heating up to 450 °C, measured in visible using BG39 Filter (325–700 nm).

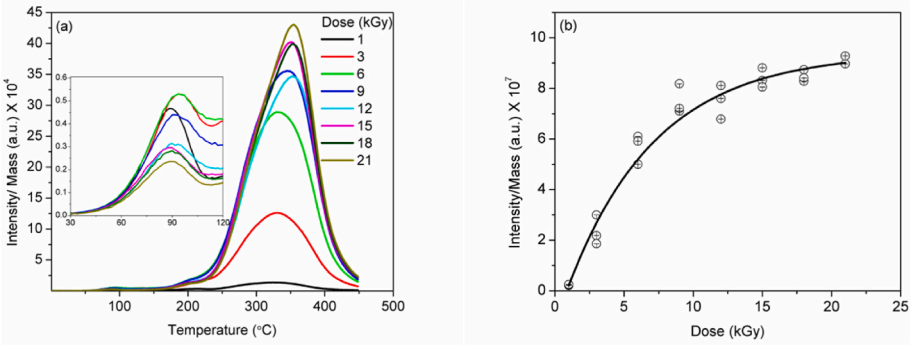

Fig. 5. a) Thermoluminescence glow curves of sample YS-5 (sedimentary quartz sample) at various high doses measured in visible using BG39 Filter (325–700 nm). b) Dose response curve of peak from temperature 340–380 °C, normalized by the mass. The $2D_0$ value is 11 ± 1 kGy. Each TL glow curve for a given dose is obtained by point wise averaging of three aliquots.

110 °C zero glow peak response to a dose of 21 Gy, appearing around 90 °C in these experiments. Such a shift in the peak has previously been reported (theoretically and experimentally) and is due to changes in heating rate (Pagonis et al., 2006). At a heating rate of 2 °C/s it appears at 90 °C, but at 5 °C/s, it is at 110 °C (see Supplementary Fig. S1). For the sample YS-5, dose quenching (Bailiff, 1994; Oniya, 2014) in the low-temperature (80–100 °C) peak is observed with the increase in the HRD Fig. 5(a), inset. However, no quenching is observed for the sample SR-23, Fig. S3(a) inset. Fig. 5(b)–S2(b), and S3(b) show the DRC for 340–380 °C peak. The estimated saturation dose ($2D_0$) is ~18 kGy in the annealed rock quartz sample (RQ-1), and 8.12 ± 1.8 kGy and 11 ± 1 kGy for the sedimentary samples, SR-23 and YS-5 respectively. In the initial part of the DRC of sample RQ-1, supralinearity is observed with an increase in dose. This changed to linear characteristics after 6 kGy, and to sublinearity after 15 kGy. Fig. 6 shows the DRC comparison for a preheat temperature of 260 °C and 350 °C and the $2D_0$ is 9.2 ± 1.3 and 13.3 ± 1 kGy respectively. The saturation dose is found to increase by 40% in the case when higher preheat is used.

A slight shift in peak maxima is observed in all the glow curves towards higher temperatures with increase in dose. The extent of peak shift is measured from the TL glow curves by noting the temperature corresponding to maximum intensity in the >300 °C temperature region. With increase in dose, the peak maximum shifts towards higher temperature by 35 °C from 1 to 15 kGy for sample RQ-1, 25 °C from 1 to 12 kGy dose for the sample YS-5, after which signal saturates and no further shift in peak maximum is observed. However, for the sample SR-23, peak temperature first decreases by 10 °C from 1 to 3 kGy, then it increases by 15 °C till 12 kGy.

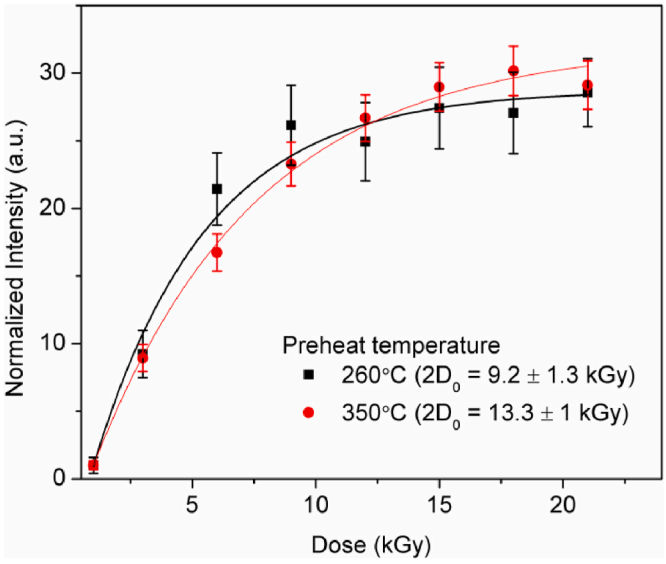

Fig. 6. DRC of sample YS-5 for different preheat. Intensity is integrated from 250°C to 450 °C and is normalized by mass and counts corresponding to 1 kGy dose in both case. Each point in graph is an average of measurement on 3 aliquots. Measurements made in visible spectral range 325–700 nm.

3.3. Multi-spectral emission studies

Fig. 7 and S10 shows the glow curves for the samples irradiated with 1 kGy dose in different transmission bands (Table 2). The low-temperature peak is most prominent in UV emission for 21 Gy test

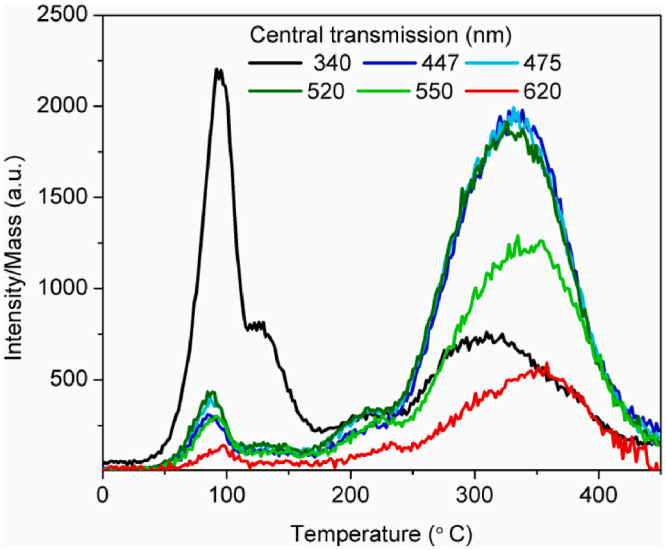

Fig. 7. TL glow curves of sample YS-5 in different transmission bands. An irradiation of 1000 Gy is given and on measurement after a preheat of 260 °C, 10 s, a small dose of 21 Gy is given for zero glow normalization. The intensity of the curves is not to be compared, because of differences in transmitivity, PMT efficiency and diameter of the filters.

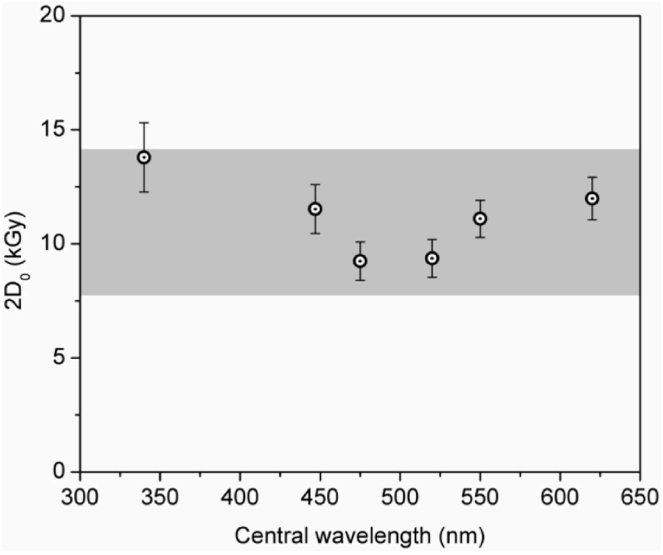

Fig. 9. Plot of TL saturation dose ($2D_0$ (kGy)) for different emission wavelengths for the sample YS-5.

dose after a TL 450 °C wash (supplementary, Fig. S4). It is observed that the high-temperature peak (>300 °C) has emissions in all selected spectral bands. However, the relative intensity of low-temperature peak w.r.t. high-temperature peak varies. The ratio is lower for higher wavelengths and maximum for the UV emission (340 ± 40 nm). The DRC in red and UV are shown in Fig. 8 (rest in Supplementary Fig. S5). All the DRCs have $2D_0$ within 2σ (Grey Band) of the mean 11 kGy as shown in Fig. 9. DRC for all emissions for annealed RQ-1 are shown in supplementary, Fig. S6. It shows a similar linear increase with dose in all emissions and no saturation is observed.

3.4. Signal resetting by sunlight

Fig. 10 shows the effect of sunlight exposure on TL intensity of the sample KG-1 in various spectral regions. The mass normalized TL signal of bleached aliquot is further normalized by the mass normalized counts of non-exposed aliquot. The counts in red emission in the present setup are an order less than other emissions, thus has larger error. The high-temperature region is further divided into two regions of 320–330 °C and 370–380 °C, integrated mass normalized counts in these regions are plotted in supplementary, Fig. S7. The bleachability of the region 370–380 °C is less than that of 320–330 °C. Further, it is found to

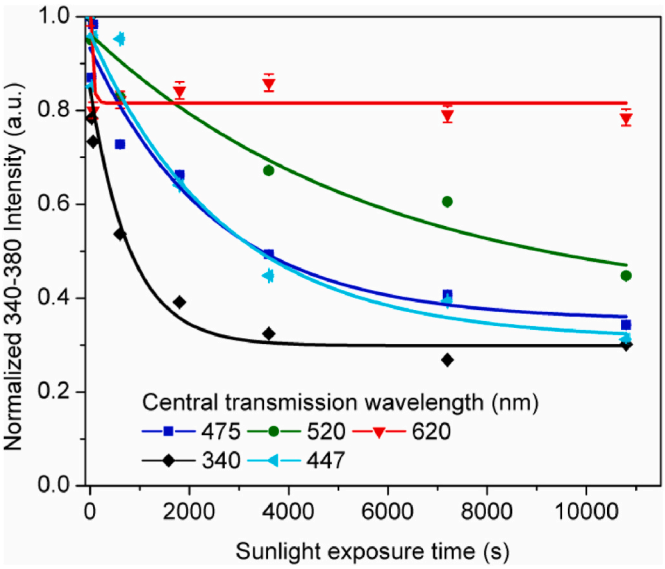

Fig. 10. Signal bleachability of 340–380 °C region, of sample KG-1 exposed to sunlight for different time period for different transmission wavelengths.

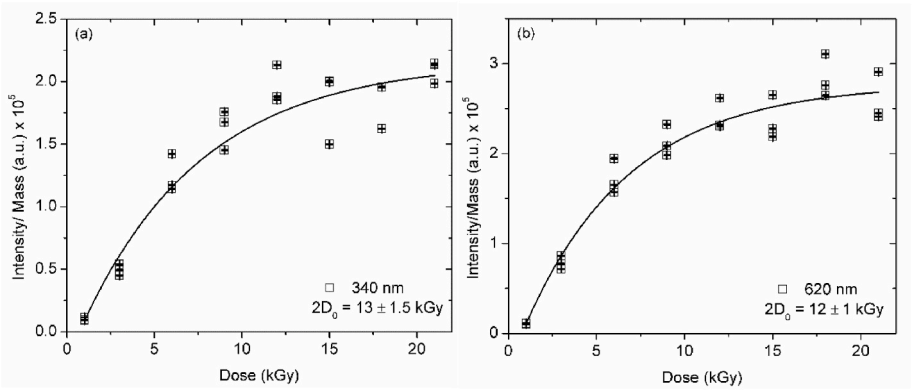

Fig. 8. The dose response curves of sample YS-5 in UV and red spectral windows of 340–380 °C peak, normalized by mass.

decrease with increasing emission wavelength. The red signal is found to be the least bleachable for both regions.

3.5. Sensitivity normalization

Fig. 11 shows the comparison of DRC for signal normalized by mass, zero glow and second glow TL signals for the sample YS-5 in visible emission (325–700 nm). Normalization results for specific emission bands are shown in Fig. S8. The $2D_0$ of 11 ± 1 kGy, 143 ± 55 kGy, 19.6 ± 2.6 kGy for mass normalization, zero glow normalization and second glow normalization are obtained respectively. Zero glow normalization shows linear increase with dose and no saturation is observed. Such huge differences implicate caution during normalization.

3.6. High radiation predose (HRpD)

The results for HRpD experiment (Table 5) on sample RQ-1 are shown in Fig. 12(a) and (b). The 340–380 °C peak intensity for a 34 Gy test dose is dependent on the HRpD. This dependence is observed in all emission bands. For low doses, intensity first increases with previous dose and then saturates after 10 kGy dose. Similarly, for the low-temperature peak, the intensity for the same 34 Gy test dose is dependent on the previous dose except for the blue emission. The low-temperature UV emission, sensitivity decreases with increase in HRpD and becomes constant around 10 kGy. For low-temperature 447 and 475 nm emission bands, sensitivity has negligible dependence on HRpD. However, for 520, 550 and 620 nm emission, low-temperature peak intensity increases with HRpD.

4. Discussion

Till date, the use of quartz for dosimetry and dating is limited to a dose of ~250 Gy (Chawla et al., 1998; Fleming, 1969; Huntley et al., 1996) using conventional UV (340 nm) emission. The lack of understanding of quartz luminescence characteristics at HRD limits the application for HRD estimation. The results obtained provide new insights about the luminescence phenomenon at HRD as discussed below.

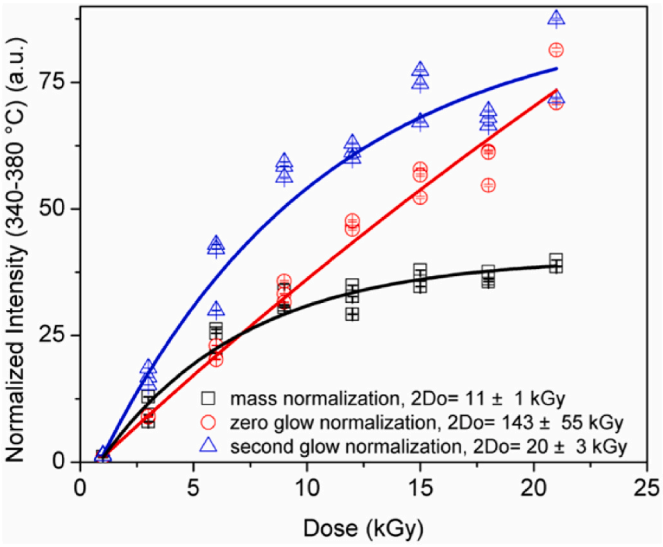

Fig. 11. Dose response curve of sample YS-5 with different normalization technique. The counts are integrated from 340 to 380 °C temperature range. The graph has been normalized by the counts of 1 kGy dose. Measurements made in visible spectral range 325–700 nm.

4.1. Dose response and trap characteristics

The DRCs measured in visible region using BG39 bandpass filter for HRDs indicate that saturation dose is about 50–100 times higher (~10−18 kGy) (Fig. 5, S2 and S3) than conventional methods, which implicates a potential to increase the dating limit by two order of magnitude. This result is in agreement with previous studies (Durrani et al., 1977; Kuhn et al., 2000; Ogundare et al., 2006; Sawakuchi and Okuno, 2004; Schmidt and Woda, 2019; Woda et al., 2002). Additionally, the DRCs show saturation (Figs. S3 and 5) of signal which is unexpected if new defects centres are created during HRD. In such cases, defect creation should be a continuous process and saturation should not be observed. The damage to crystal structure can be associated with unpredictable luminescence behaviour instead of monotonous increase towards saturation with increasing dose (Hegde et al., 2019).

Trap kinetic parameters such as τ, E_a and s, also give insights into the trap structure with the changing HRDs. Fig. 4 shows the activation energy (E_a) estimated for different radiation doses. Results show that low-temperature traps (<200 °C) are majorly affected during HRDs as their activation energy increases. This signifies that the potential energy at the site of these electronic states is modified due to accumulation of large trapped charges. Higher activation energy indicates towards lesser probability of eviction at room temperature and strongly bound charges, which are difficult to evict. However, the deeper traps at temperatures >200 °C are much more stable in terms of changes in activation energy, with HRD. This is in agreement with study by Hunter et al. (2018) on the blue emission for 210 °C and 350 °C peaks, which show that the kinetic parameters remain unaltered at HRDs. Annealing samples by heating to 450 °C reduces the activation energy of the low-temperature traps (Fig. 4(b)). This again indicates that permanent defect creation does not occur due to HRD and after removal of charges from trapping centre, crystal tries to restore the original configuration of traps in crystal.

4.2. Peak shift with dose

Fig. 5(a), S2(a) and S3(a) shows a shift in the TL peak maximum temperature towards higher temperature with increase in dose. McKeever (1985) suggested that for non-first order kinetics TL glow peak temperature shifts to lower temperatures with increase in dose as observed for high-temperature (250–450 °C) TL peak at 3 kGy for the sample SR-23 (Fig. S3(a)). However, for doses >3 kGy, the peak maximum for high-temperature (250–450 °C) TL peak shifts to higher temperatures with dose. Similarly, a shift in peak maximum to higher temperature is observed for the samples RQ-1 and YS-5 (Figs. S2(a) and 5(a)) for the high-temperature (250–450 °C) TL peak. Such a shift can be explained based on the variable electron capture cross-sections of different traps, resulting in different saturation (suggested by Ogundare et al. (2006)). Fig. 2 suggests that there are multiple traps contributing to TL signal in quartz above 300 °C. Traps beyond 200 °C could not be distinguished in Fig. 3 because of the overpowering intensity from 350 °C peak. For deep traps having peak temperature >350 °C the saturation dose is significantly higher (Fig. 6). Presence of multiple traps with different saturation characteristics, results in continuous increase in intensity of deeper traps even after comparatively shallow traps are saturated resulting in shift of peak maxima towards higher temperature. Durrani et al. (1977) have reported that the saturation dose of all traps at HRDs in quartz is similar ~ 10^4 Gy. However, due to the low dose resolution in their study, it was difficult to observe changes in saturation of different traps. Schmidt and Woda (2019) have also reported on the shifting of blue TL peak maximum to higher temperature with increase in doses, which is consistent with the results of present study.

4.3. Multi-spectral studies

Quartz TL is complex in nature, consisting of several traps and recombination centres or emissions. The luminescence spectral

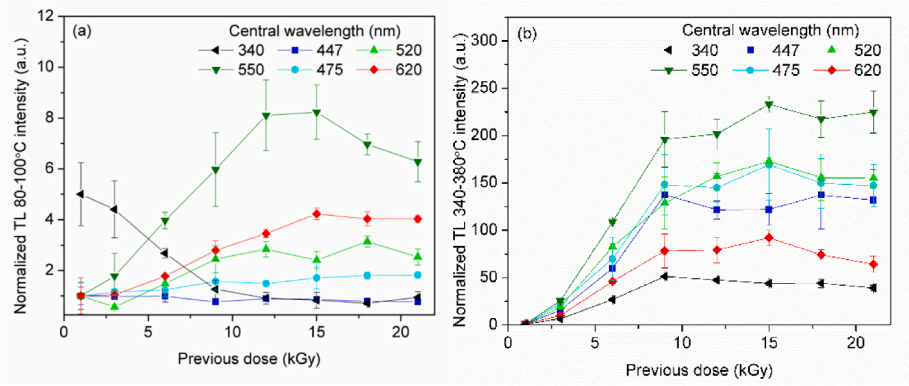

Fig. 12. The response of sample RQ-1 (a) 80–100 °C peak counts (b) 340–380 °C peak counts, to a test dose of 34 Gy after the previous high dose was followed by heating to 450 °C as per Table 5. The legends give the transmission in different filters which are given in Table 2.

characteristics measured using different filter combinations spanning the full transmission range from UV to red (300–660 nm) are shown in Figs. 7–10 and Fig. 12.

Fig. 7 shows TL glow curves of quartz in various transmission bands ranging from UV to red for sample YS-5. Similarly, TL glow curves were also measured for all samples in the mentioned bands and are shown in Fig. S10. Same number of peaks are observed in all bands, however the relative intensity of different peak changes, in accordance with previous studies (Adamiec, 2005; Hashimoto et al., 1987). With the increase in HRD from 1 to 21 kGy, increase in the signal intensity in all emissions is observed (Fig. 8, S5, S6). This is different from the observation mentioned by Schmidt and Woda (2019) that with increase in dose to kGy level some emissions in quartz become diminished while blue emissions dominate.

Figs. 8 and 9 shows that the saturation dose ($2D_0$) is similar for all emissions within 2 sigma of the mean. This possibly suggests that for measured samples, the recombination centres may not have any role in dose saturation and it is mainly controlled by the charge population of the trapping centre. Possibly, there is an excess of recombination centres, thus sufficient numbers are available for all the emission bands. Similar estimates are made by other researchers like, the saturation dose for red TL agrees with our results (Miallier et al., 1991; Roberts and Westaway, 2006). Some works also report an increase in TL intensity in blue up to ~10 kGy (Hashimoto et al., 1987; Hunter et al., 2018; Schmidt and Woda, 2019). Study by Lowick et al. (2010) on TL also shows an increasing luminescence emission in both blue and UV until 1.2 kGy, although they didn't record for higher doses. Besides this, study using the optically and thermally stimulated electrons (OSE and TSE), Ankjærgaard et al. (2006) have shown that trapping centres in quartz do not saturate till 10 kGy and may even go beyond that. Collectively, the results of present study agree with these previous results.

4.4. Signal resetting

It is observed that bleachability of 320–330 °C TL peak region is better than 370–380 °C region (Fig. S7) for all emissions and accords with earlier observations (Wintle, 1997). It is seen that for higher emission wavelengths, the bleachability is low (Fig. 10, S7). The UV emissions has the least residuals (most bleachable) and red has the maximum residual (least bleachable). Although it appears to be linked to recombination centre, the exact mechanism is not yet clear and need more investigation. One of the possibilities could be that the charges in the recombination centres associated with higher wavelength emission (i.e., red emission) are tightly bound and are thus slow to bleach, however more detailed investigations are needed. The results are consistent with the previous findings on blue, UV TL (Singhvi et al., 1982) and red TL (Lai and Murray, 2006; Miallier et al., 1994). This indicates that the role of recombination centres is overlooked and needs more attention.

4.5. Normalization, dose quenching

Ideally for adequate normalization, the observed dose signal and corresponding test dose signal should have identical sensitivity changes with the measurement cycle and dose. It is expected that the saturation dose should be independent of normalization method and various normalization methods should give identical saturation dose. Fig. 11, shows that saturation characteristics of different normalization methods does not match. Here, the mass normalization is taken as standard normalization for reference, as it is not influenced by any other signal characteristics. The deviations of zero glow and second glow normalization suggest that low-temperature peak and 340–380 °C peak does not respond to dose in similar way. The increase in the zero glow normalized signal intensity beyond mass normalized intensity in Fig. 11 is due to decrease in the low-temperature peak intensity with dose as shown in Fig. 5(b) resulting from quenching of signal during high dose irradiation (Bailiff, 1994; Oniya, 2014). The trap competition can significantly influence the normalization process. During zero glow normalization irradiation fills charges in traps 80–100 °C peak when high-temperature peaks (340–380 °C) are already filled, whereas for second glow normalization, irradiation fills 80–100 °C traps while high-temperature traps (340–380 °C) are empty. However, as evident from Fig. 4(b), the low-temperature trap system (<200 °C) tries to restore after HRD but does not exactly match the original trap system; differences in the saturation of mass and second glow normalized DRC are observed. Thus, the choice of normalization technique at HRDs is crucial. In the present case mass normalization is found to provide better results as shown in Fig. 11 as it is unaffected by the intrinsic characteristics traps and more suitable to normalize inter-aliquot variations.

4.6. High radiation predose (HRpD) effects

Fig. 12 (a) shows that 110 °C TL sensitivity in different emissions is drastically affected by the HRpD. Different emission centres are affected differently. The UV emissions are quenched by HRpD, while blue is unaffected (in comparison to other) and green and red are enhanced. For the 340–380 °C TL, all centres signal is enhanced, but to different extents. The enhancement is greatest in yellow-green (550 nm), followed by green (520 nm) and blue (447 and 475 nm). HRpD effects have been observed in several studies (Oniya, 2014; Stoneham and Stokes, 1991; Zimmerman, 1971). However, the majority of these studies are done in the ultraviolet or blue luminescence emissions. The decreased response of low-temperature TL peak emission in the ultraviolet region (290–390 nm) is in agreement with observation of Jain et al. (2003). Further, the study by (Hunter et al., 2018) shows sensitization of high-temperature peak (350 °C) by HRpD similar to current observations. Woda et al.

(2002) have shown that different EPR centres in quartz respond differently to HRpD e.g. the Ge-Li and Ge-Na centre first increases with dose than decreases, whereas, the Al centre continuously increases. However, there have always been ambiguity on the matter of which centre corresponds to which emission. The results further signify the importance of recombination centres in the luminescence response. The enhancement in the sensitivity of 340–380 °C TL intensity and the lack of correlated enhanced signal for test dose, restricts us to use single aliquot regenerative type protocols to estimate doses for HRD. However, since the DRC shows dose response till ~10 kGy and ~18 kGy (annealed rock quartz), dose estimation for HRD should be advanced with additive approach.

5. Conclusions

Present work investigated quartz samples from different provenance at high radiation doses (1–21 kGy), for several properties like dose-response, trap characteristics, bleachability, normalization and pre-dose effects. Quartz has the potential to estimate doses 50–100 times the present limit. The work enhances the role of recombination centres in the luminescence mechanism.

This study leads to the following major conclusions;

1. Activation energy for the traps present at temperature <200 °C, increases at HRDs. Further, after removal of high dose the activation energy decreases and approaches the low dose values.
2. TL signal in 340–380 °C temperature range of quartz increase with doses up to 18 kGy for annealed rock quartz and around 11 kGy for sedimentary quartz in the spectral range of 325–700 nm.
3. The spectral analysis of the luminescence emission signifies that the trapping centres are majorly responsible for saturation in the samples and the saturation dose is similar within error for all emissions wavelengths from UV to red.
4. The TL signal (340–380 °C) is bleachable by sunlight. The bleachability is found to be anticorrelated with emission wavelength and the mechanism needs further investigation.
5. Zero glow and second glow normalization are not appropriate for sensitivity correction at HRDs and mass normalization should be used.
6. HRpD enhances the signal intensity of all emissions in the 340–380 °C temperature range and green and red 80–100 °C emissions, while there is a quenching of the UV 80–100 °C and blue 80–100 °C is independent in comparison to others.

CRediT authorship contribution statement

Malika Singhal: Writing – original draft, Methodology, Investigation, Formal analysis, Data curation, Conceptualization. **Madhusmita Panda:** Writing – review & editing, Methodology, Data curation. **S.H. Shinde:** Writing – review & editing, Methodology. **Sandip Mondal:** Writing – review & editing, Methodology. **O. Annalakshmi:** Writing – review & editing, Methodology, Data curation. **Naveen Chauhan:** Writing – review & editing, Supervision, Resources, Methodology, Investigation, Formal analysis, Conceptualization.

Declaration of competing interest

The authors declare that they have no known competing financial interests or personal relationships that could have appeared to influence the work reported in this paper.

Data availability

Data will be made available on request.

Acknowledgement

The authors would like to thank Dr. Munish Kumar, BARC for help with gamma irradiation of samples and discussion on the manuscript, Dr. V. Sathian, Head, RSS, RSSD, BARC, Smt. M. Menaka, Head, RAMS, IGCAR and Dr. Balasubramanian Venkatraman, director IGCAR for providing high-dose irradiation facility. The work carried out at PRL is supported by the Department of Space, Government of India.

Appendix A. Supplementary data

Supplementary data to this article can be found online at https://doi.org/10.1016/j.radmeas.2024.107300.

References

Adamiec, G., 2005. Properties of the 360 and 550nm TL emissions of the '110° C peak'in fired quartz. Radiat. Meas. 39, 105–110.
Aitken, M.J., 1985. Thermoluminescence Dating, Handbooks for Archaeologists : a Publication of the Sub-committee for Archaeology of the Standing Committee for the Humanities. Academic Press.
Ankjærgaard, C., Guralnik, B., Buylaert, J.P., Reimann, T., Yi, S.W., Wallinga, J., 2016. Violet stimulated luminescence dating of quartz from Luochuan (Chinese loess plateau): agreement with independent chronology up to ~600 ka. Quat. Geochronol. 34, 33–46. https://doi.org/10.1016/j.quageo.2016.03.001.
Ankjærgaard, C., Murray, A.S., Denby, P.M., Z, L.B., 2006. Measurement of Optically and Thermally Stimulated Electron Emission from Natural Minerals, 41, pp. 780–786. https://doi.org/10.1016/j.radmeas.2006.05.012.
Bailiff, I.K., 1994. The pre-dose technique. Radiat. Meas. 23, 471–479.
Bøtter-Jensen, L., Thomsen, K.J., Jain, M., 2010. Review of optically stimulated luminescence (OSL) instrumental developments for retrospective dosimetry. Radiat. Meas. 45, 253–257. https://doi.org/10.1016/j.radmeas.2009.11.030.
Buylaert, J.P., Thiel, C., Murray, A.S., Vandenberghe, D.A.G., Yi, S., Lu, H., 2011. Irsl and post-ir irsl residual doses recorded in modern dust samples from the Chinese loess plateau. Geochronometria 38, 432–440. https://doi.org/10.2478/s13386-011-0047-0.
Caicedo, F.D., Asfora, V.K., Guzzo, P.L., Barros, V.S.M., 2021. Nuclear Inst . and Methods in Physics Research , B Investigation of the spectrally resolved TL signals of natural quartz single crystals sensitized by high-dose of gamma-radiation and moderate. Nucl. Instrum. Methods Phys. Res. B 486, 37–47. https://doi.org/10.1016/j.nimb.2020.11.001.
Chawla, S., Gundu Rao, T.K., Singhvi, A.K., 1998. Quartz thermoluminescence: dose and dose-rate effects and their implications. Radiat. Meas. 29, 53–63. https://doi.org/10.1016/S1350-4487(97)00200-X.
Duller, G.A.T., Wintle, A.G., 2012. A review of the thermally transferred optically stimulated luminescence signal from quartz for dating sediments. Quat. Geochronol. 7, 6–20. https://doi.org/10.1016/j.quageo.2011.09.003.
Durrani, S.A., Khazal, K.A.R., McKeever, S.W.S., Riley, R.J., 1977. Studies of changes in the thermoluminescence sensitivity in quartz induced by proton and gamma irradiations. Radiat. Eff. 33, 237–244. https://doi.org/10.1080/00337577708233112.
Fattahi, M., Stokes, S., 2003. Dating volcanic and related sediments by luminescence methods: a review. Earth Sci. Rev. 62, 229–264. https://doi.org/10.1016/S0012-8252(02)00159-9.
Fattahi, M., Stokes, S., 2000. Extending the time range of luminescence dating using red TL (RTL) from volcanic quartz. Radiat. Meas. 32, 479–485. https://doi.org/10.1016/S1350-4487(00)00105-0.
Fleming, S., 1969. The Acquisition of Radiothermoluminescence by Ancient Ceramics.
Garlick, G.F.J., Gibson, A.F., 1948. The electron trap mechanism of luminescence in sulphide and silicate phosphors. Proc. Phys. Soc. 60, 574.
Gobrecht, H., Hofmann, D., 1966. Spectroscopy of traps by fractional glow technique. J. Phys. Chem. Solid. 27, 509–522. https://doi.org/10.1016/0022-3697(66)90194-6.
Götze, J., Pan, Y., Müller, A., 2021. Mineralogy and mineral chemistry of quartz: a review. Mineral. Mag. 85, 639–664. https://doi.org/10.1180/mgm.2021.72.
Han, Z.-Y., Li, S.-H., Tso, M.-Y.W., 2000. Lifetime estimation of thermoluminescence traps in granitic quartz. Radiat. Eff. Defect Solid 152, 307–314.
Hashimoto, T., Yokosaka, K., Habuki, H., 1987. Emission properties of thermoluminescence from natural quartz-blue and red TL response to absorbed dose. Int. J. Radiat. Appl. Instrumentation. Part 13, 57–66. https://doi.org/10.1016/1359-0189(87)90008-2.
Hegde, V., Chauhan, N., Kumar, V., Viswanath, C.S.D., Mahato, K.K., Kamath, S.D., 2019. Effects of high dose gamma irradiation on the optical properties of Eu3+ doped zinc sodium bismuth borate glasses for red LEDs. J. Lumin. 207, 288–300. https://doi.org/10.1016/j.jlumin.2018.11.023.
Hunter, P.G., Spooner, N.A., Smith, B.W., 2018. Thermoluminescence emission from quartz at 480 nm as a high-dose radiation marker. Radiat. Meas. 120, 143–147. https://doi.org/10.1016/j.radmeas.2018.04.001.
Huntley, D.J., Short, M.A., Dunphy, K., 1996. Deep traps in quartz and their use for optical dating. Can. J. Phys. 74, 81–91.

Jain, M., 2009. Extending the dose range: probing deep traps in quartz with 3.06 eV photons. Radiat. Meas. 44, 445–452. https://doi.org/10.1016/j.radmeas.2009.03.011.
Jain, M., Bøtter-Jensen, L., Singhvi, A.K., 2003. Dose evaluation using multiple-aliquot quartz OSL: test of methods and a new protocol for improved accuracy and precision. Radiat. Meas. 37, 67–80.
Kars, R.H., Wallinga, J., Cohen, K.M., 2008. A new approach towards anomalous fading correction for feldspar IRSL dating - tests on samples in field saturation. Radiat. Meas. 43, 786–790. https://doi.org/10.1016/j.radmeas.2008.01.021.
Khoury, H.J., Guzzo, P.L., Souza, L.B.F., Farias, T.M.B., Watanabe, S., 2008. TL Dosimetry of Natural Quartz Sensitized by Heat-Treatment and High Dose Irradiation, 43, pp. 487–491. https://doi.org/10.1016/j.radmeas.2008.01.028.
Krbetschek, M.R., Götze, J., Dietrich, A., Trautmann, T., 1997. Spectral information from minerals relevant for luminescence dating. Radiat. Meas. 27, 695–748. https://doi.org/10.1016/S1350-4487(97)00223-0.
Kuhn, R., Trautmann, T., Singhvi, A.K., Krbetschek, M.R., Wagner, G.A., Stolz, W., 2000. Study of thermoluminescence emission spectra and optical stimulation spectra of quartz from different provenances. Radiat. Meas. 32, 653–657. https://doi.org/10.1016/S1350-4487(00)00090-1.
Lai, Z., Murray, A., 2006. Red TL of Quartz Extracted from Chinese Loess : Bleachability and Saturation Dose, 41, pp. 836–840. https://doi.org/10.1016/j.radmeas.2006.04.017.
Lowick, S.E., Preusser, F., Wintle, A.G., 2010. Investigating quartz optically stimulated luminescence dose-response curves at high doses. Radiat. Meas. 45, 975–984. https://doi.org/10.1016/j.radmeas.2010.07.010.
McKeever, S.W.S., 1985. Thermoluminescence of Solids. Cambridge University Press.
Miallier, D., Fain, J., Montret, M., Pilleyre, T., Sanzelle, S., Soumana, S., 1994. Sun bleaching of the red TL of quartz: preliminary observations. Anc. TL 12, 1–4.
Miallier, D., Fain, J., Montret, M., Pilleyre, T., Sanzelle, S., Soumana, S., 1991. Properties of the red TL peak of quartz relevant to thermoluminescence dating. Int. J. Radiat. Appl. Instrumentation. Part D. Nucl. Tracks Radiat. Meas. 18, 89–94.
Monti, A.M., Fasoli, M., Panzeri, L., Martini, M., 2019. Investigation of the spectrally resolved TL peaks of quartz in the 70°C–220°C temperature region. Radiat. Meas. 127, 106141. https://doi.org/10.1016/j.radmeas.2019.106141.
Murray, A., Arnold, L.J., Buylaert, J.-P., Guérin, G., Qin, J., Singhvi, A.K., Smedley, R., Thomsen, K.J., 2021. Optically stimulated luminescence dating using quartz. Nature Rev. Methods. Prim. https://doi.org/10.1038/s43586-021-00068-5.
Murray, A.S., Wintle, A.G., 2000. Luminescence dating of quartz using an improved single-aliquot regenerative-dose protocol. Radiat. Meas. 32, 57–73. https://doi.org/10.1016/S1350-4487(99)00253-X.
Ngoc, T., Ca, N.X., Thanh, N.T., Hung, N.M., Du, P.T., Thuy, T.T.C., Huong, N.T., Van Do, P., 2024. Thermoluminescence properties and new insights on the UV-vis absorption features of colorless quartz after γ-ray irradiation. RSC Adv. 14, 19154–19166.
Ngoc, T., Van Tuyen, H., Thi, L.A., Hung, L.X., Ca, N.X., Thanh, L.D., Van Do, P., Son, N. M., Thanh, N.T., Quang, V.X., 2021. The role of sodium ions in the thermoluminescence peaks of laboratory-irradiated natural quartz. Radiat. Meas. 141, 106539. https://doi.org/10.1016/j.radmeas.2021.106539.
Ogundare, F.O., Chithambo, M.L., Oniya, E.O., 2006. Anomalous behaviour of thermoluminescence from quartz: a case of glow peaks from a Nigerian quartz. Radiat. Meas. 41, 549–553. https://doi.org/10.1016/j.radmeas.2006.03.001.
Oniya, E.O., 2014. Luminescence Sensitisation of Natural Quartz Using Pre-exposure Dose and Thermal Activation Techniques.
Pagonis, V., Kitis, G., Furetta, C., 2006. Numerical and practical exercises in thermoluminescence, numerical and practical exercises in thermoluminescence. https://doi.org/10.1007/0-387-30090-2.
Porat, N., 2006. Use of magnetic separation for purifying quartz for luminescence dating. Anc. TL 24, 33–36.
Preusser, F., Chithambo, M.L., Götte, T., Martini, M., Ramseyer, K., Sendezera, E.J., Susino, G.J., Wintle, A.G., 2009. Quartz as a natural luminescence dosimeter. Earth Sci. Rev. 97, 184–214. https://doi.org/10.1016/j.earscirev.2009.09.006.
Rink, W.J., Rendell, H., Marseglia, E.A., Luff, B.J., Townsend, P.D., 1993. Thermoluminescence spectra of igneous quartz and hydrothermal vein quartz. Phys. Chem. Miner. 20, 353–361. https://doi.org/10.1007/BF00215106.
Roberts, R.G., Westaway, K.E., 2006. A Dual-Aliquot Regenerative-Dose Protocol (DAP) for Thermoluminescence (TL) Dating of Quartz Sediments Using the Light-Sensitive and Isothermally Stimulated Red Emissions.
Sawakuchi, A.O., Blair, M.W., DeWitt, R., Faleiros, F.M., Hyppolito, T., Guedes, C.C.F., 2011. Thermal history versus sedimentary history: OSL sensitivity of quartz grains extracted from rocks and sediments. Quat. Geochronol. 6, 261–272. https://doi.org/10.1016/j.quageo.2010.11.002.
Sawakuchi, G.O., Okuno, E., 2004. Effects of high gamma ray doses in quartz. Nucl. Instrum. Methods Phys. Res. Sect. B Beam Interact. Mater. Atoms 218, 217–221. https://doi.org/10.1016/j.nimb.2003.12.021.
Schmidt, C., Woda, C., 2019. Quartz thermoluminescence spectra in the high-dose range. Phys. Chem. Miner. 46, 861–875. https://doi.org/10.1007/s00269-019-01046-w.
Singhvi, A.K., Mejdahl, V., 1985. Thermoluminescence dating of sediments. Nucl. Tracks Radiat. Meas. 10, 137–161.
Singhvi, A.K., Sharma, Y.P., Agrawal, D.P., 1982. Thermoluminescence dating of sand dunes in Rajasthan. IND. Nature 295, 313–315. https://doi.org/10.1038/295313a0.
Smith, B.W., Rhodes, E.J., Stokes, S., Spooner, N.A., Aitken, M.J., 1990. Optical dating of sediments: initial quartz results from Oxford. Archaeometry 32, 19–31.
Spooner, N.A., Questiaux, D.G., 2000. Kinetics of red, blue and UV thermoluminescence and optically-stimulated luminescence from quartz. Radiat. Meas. 32, 659–666. https://doi.org/10.1016/S1350-4487(00)00067-6.
Stoneham, D., Stokes, S., 1991. An investigation of the relationship between the 110° C TL peak and optically stimulated luminescence in sedimentary quartz. Int. J. Radiat. Appl. Instrum. Nucl. Tracks Radiat. Meas. 18, 119–123.
Thiel, C., Buylaert, J.P., Murray, A., Terhorst, B., Hofer, I., Tsukamoto, S., Frechen, M., 2011. Luminescence dating of the Stratzing loess profile (Austria) - testing the potential of an elevated temperature post-IR IRSL protocol. Quat. Int. 234, 23–31. https://doi.org/10.1016/j.quaint.2010.05.018.
Thomsen, K.J., Bøtter-Jensen, L., Denby, P.M., Moska, P., Murray, A.S., 2006. Developments in luminescence measurement techniques. Radiat. Meas. 41, 768–773. https://doi.org/10.1016/j.radmeas.2006.06.010.
Toyoda, S., Rink, W.J., Schwarcz, H.P., Rees-Jones, J., 2000. Crushing effects on TL and OSL on quartz: relevance to fault dating. Radiat. Meas. 32, 667–672.
Wang, X.L., Lu, Y.C., Wintle, A.G., 2006. Recuperated OSL dating of fine-grained quartz in Chinese loess. Quat. Geochronol. 1, 89–100. https://doi.org/10.1016/j.quageo.2006.05.020.
Wintle, A.G., 1997. Luminescence dating: laboratory procedures and protocols. Radiat. Meas. 27, 769–817. https://doi.org/10.1016/S1350-4487(97)00220-5.
Wintle, A.G., Murray, A.S., 2006. A review of quartz optically stimulated luminescence characteristics and their relevance in single-aliquot regeneration dating protocols. Radiat. Meas. 41, 369–391. https://doi.org/10.1016/j.radmeas.2005.11.001.
Woda, C., Schilles, T., Rieser, U., Mangini, A., Wagner, G.A., 2002. POINT DEFECTS AND THE BLUE EMISSION IN FIRED QUARTZ AT HIGH DOSES : A COMPARATIVE LUMINESCENCE AND EPR STUDY, 100, pp. 261–264.
Zimmerman, J., 1971. The radiation-induced increase of the 100 C thermoluminescence sensitivity of fired quartz. J. Phys. C Solid State Phys. 4, 3265–3276. https://doi.org/10.1088/0022-3719/4/18/032.

Radiation Physics and Chemistry 234 (2025) 112764

Contents lists available at ScienceDirect

Radiation Physics and Chemistry

journal homepage: www.elsevier.com/locate/radphyschem

On the sensitivity normalization for blue stimulated luminescence of quartz

Malika Singhal [a,b,*], Madhusmita Panda [c], O. Annalakshmi [c,d], Naveen Chauhan [a]

[a] Atomic Molecular and Optical Physics Division, Physical Research Laboratory, Ahmedabad, Gujarat, 380009, India
[b] Indian Institute of Technology, Palaj, Gandhinagar, Gujarat, 382355, India
[c] Indira Gandhi Centre of Atomic Research, Kalpakkam, Tamil Nadu, 603102, India
[d] Homi Bhabha National Institute, IGCAR, Kalpakkam, Tamil Nadu, 603102, India

ARTICLE INFO

Handling Editor: Dr. Chris Chantler

Keywords:
Quartz
Blue stimulated luminescence (BSL)
Single aliquot regeneration (SAR)
Multiple aliquot additive dose (MAAD)
Multiple aliquot regenerative (MAR)
Normalizations

ABSTRACT

In the single aliquot regeneration (SAR) dating method for quartz, the maximum dating limit depends on the saturation dose of sensitivity-corrected luminescence signal (L/T) and is generally found to be around ~250 Gy. Since saturation is the restraining aspect in luminescence dating, it is important to understand the factors that influence it. This paper, investigates the blue stimulated luminescence (BSL) signals of quartz of different provenance using the multiple aliquot additive dose (MAAD) methodology. Results show that the BSL signal increases beyond the saturation limits of SAR. The early saturation in the SAR is observed primarily due to a disproportional increase in the test dose signal (T) at higher doses resulting from its dependence on the prior regeneration dose. The work further searches for normalization methods, which are independent of regeneration doses at high doses. Results show that zero glow thermo-luminescence (TL), BSL (after annealing, UV emission) and TL (after annealing, blue emission) normalization carry negligible previous dose information. These normalization signals are tested for constructing dose-response curve (DRC) using MAAD and multiple aliquot regeneration (MAR) methods. Laboratory generated DRCs are found to be best fitted with double saturating exponential with a second exponential saturation dose of 5800 ± 800 Gy. However, the scatter in the BSL, multiple aliquot data at higher doses (~kGy) is significant and needs future investigation. The proposed methodology yields higher equivalent doses for the natural samples than SAR but still found to be lower than expected doses.

1. Introduction

Optically stimulated luminescence (OSL) dating is extensively used as a chronological tool to understand earth surface processes and human evolution. Huntley et al. (1985) is the first one to show that quartz luminescence can be stimulated by optical light. This discovery made possible the direct dating of sediment transport events, wherein the luminescence clock is reset by sunlight. Thereafter, over the years, OSL has been observed for other minerals like feldspar, zircon, calcite, gypsum etc. (Godfrey-Smith et al., 1988; Guilheiro et al., 2021; Nagar, 2007; Smith, 1988). Among these, quartz and feldspar are the mineral of choice for OSL dating as these two are ubiquitous minerals and can be used for dating in a variety of settings. The natural dose (paleodose; estimated as equivalent dose; D_e) accumulated in these minerals is divided by the dose rate to estimate burial age of sediments (Aitken, 1985). Quartz provides the advantage over feldspar as its luminescence signal resets faster (Murray and Wintle, 2000), is stable unlike feldspar (Wintle, 1973) and is more resistant to weathering. However, quartz luminescence signal saturates around 250 Gy (Chawla et al., 1998), which is lower than feldspar (~2000 Gy (Thiel et al., 2011)). The early saturation of the signal limits the use of quartz to date comparatively younger (<100 ka) events compared to feldspar.

In quartz, several signals are probed over the years some of which include slow component (S_3) OSL dating (Singarayer et al., 2000), thermally transferred optically stimulated luminescence (TT-OSL; Duller and Wintle, 2012; Wang et al., 2006; Wang et al., 2007), red thermo-luminescence (TL), dual-aliquot protocol (DAP; Roberts and Westaway, 2006), isothermal TL (ITL; Jain et al., 2005) and violet stimulated luminescence (VSL; Ankjærgaard et al., 2016; Jain, 2009). These signals are proposed to extend the dating limits of quartz with limited success (Colarossi et al., 2015; Rahimzadeh et al., 2023a, 2023b and ref within). Still, the blue stimulated luminescence (BSL) of quartz is the most widely used signal for dating in which trapped electrons are stimulated by 470 ± 30 nm wavelength and luminescence is detected in 340 ± 40 nm (UV)

* Corresponding author. Atomic Molecular and Optical Physics Division, Physical Research Laboratory, Ahmedabad, Gujarat, 380009, India
E-mail address: malikasinghal97@gmail.com (M. Singhal).

https://doi.org/10.1016/j.radphyschem.2025.112764
Received 12 December 2024; Received in revised form 22 March 2025; Accepted 26 March 2025
Available online 26 March 2025

wavelength range. The measured BSL signal is related to 325 °C TL trap (Murray and Wintle, 2000) and have a thermal stability of 10^7–10^8 years suggesting its suitability for dating up to million years (Aitken, 1985; Biernacka et al., 2022; Durcan, 2018; Spooner and Questiaux, 2000 and ref therein).

The luminescence sensitivity $\left(\frac{counts\ /time}{dose \times weight}\right)$ of quartz of different origins is drastically different, mainly due to variation in intrinsic/substitutional defects and crystallinity (Topaksu et al., 2012). However, a similar methodology to estimate equivalent dose can be used for the quartz of different origins due to the associated broad emissions with the defects (Topaksu et al., 2012). The main complexity of dose estimations is due to significant variations in the luminescence sensitivity during measurements (Aitken, 1985), which is primarily associated with changes in the intrinsic defects. In the early days of the development of luminescence dating, additive measurement procedures such as multiple aliquot additive dose (MAAD) protocols, R-Γ method (Wintle and Huntley, 1979), total bleach method (Singhvi et al., 1982), Australian slide method (Prescott et al., 1993) were formulated to estimate the equivalent dose (D_e). In majority of these procedures, each aliquot was used only once for measurement, so the effect of sensitivity changes, which occur during repetitive measurements was avoided. These procedures however involved extrapolation of fitted curves to estimate the dose, requires longer measurement time, involved more manual work and a larger quantity of sample (Aitken, 1985; Fleming, 1979; Mejdahl and Wintle, 2020). Hence, attempts were made to identify appropriate signals that can track the sensitivity changes and can be used for normalization after establishing a correlation with measured signals (Stokes, 1994). This resulted in the development of well-known and mostly used single aliquot regeneration (SAR) protocol (Murray and Mejdahl, 1999; Murray and Roberts, 1998; Murray and Wintle, 2000). SAR provided a scope to study the distribution in doses and, associated causes of scatter in doses in the depositional environment such as sediment mixing, bleaching and dose heterogeneity.

The SAR procedure provides reliable dose estimates for doses up to ~250–300 Gy for quartz, after which the signal saturates and does not increase further with increase in dose. However, several researchers suggested that the signal of quartz increases beyond ~250 Gy and the DRC (Dose Response curve) is better fitted with "single plus saturating exponential" (Chapot et al., 2012; Timar-Gabor et al., 2012). Further, recent investigations from the authors (Singhal et al., 2024) suggested that the normalization methods that work at low radiation doses, do not work for high radiations (>1 kGy) due to disproportionate variation of normalizing signals. Several other researchers (Dreimanis et al., 1978; Lowick et al., 2010a; Lowick and Preusser, 2011; Y. C. Lu et al., 2007; Murray et al., 2007; Prescott and Robertson, 1997; Qin and Zhou, 2009; Timar-Gabor and Wintle, 2013; Wang et al., 2021) also reported that at high radiation doses (~> 250Gy), paleodoses are underestimated by SAR. Thus, it is important to investigate the validity of SAR protocol and adopted normalization procedures for higher doses (~>300 Gy).

To understand the cause of underestimation, experiments were done to measure anomalous fading, thermal instability, saturation of natural signal, stepped irradiation (Bonde et al., 2001; Li and Li, 2006; Qin and Zhou, 2009; Singhvi et al., 2011; Yoshida et al., 2000) and other parameter and their correlation with underestimation was studied. Most of these factors are associated with the processes that occur in nature. However, some studies show the role of laboratory procedures could also result in paleodose underestimation. Previously, Wang et al. (2021) have shown that multiple aliquot regeneration (MAR) protocol can be used to extend the dating limits for quartz. Similarly, Zhang and Tsukamoto (2022) have shown for feldspar that protocol used for estimation of D_e affects the upper range to which the date can be estimated. Since, different signals (VSL, TT-OSL, etc.) originate from different traps inside the crystal, the consequently, the maximum dose that can be estimated with them can vary. However, for the same signal, the saturation dose should not depend on the laboratory protocol.

Hence, the present work investigates the dependence of saturation dose of quartz on various experimental parameters and procedures to answer some of these questions. BSL characteristics at doses greater than SAR saturation (~250 Gy) are studied, and for clarity doses greater than 250 Gy are defined as D_{GSS} (doses greater than SAR saturation) throughout the manuscript.

2. Methodology

2.1. Sample and sample preparation

Five quartz samples were used in the study from different parts of India to capture variability in luminescence characteristics as given in Table 1. RQ-1 is a rock sample from Sabarmati basin, Western India (24°29′12″N, 73°13′18″E). PRL-1 is a flood deposited sedimentary sample of high sensitivity from Bharathpuzha basin, Southern India (10° 46′ 44.0292″ N, 76° 34′ 30.36″ E). MS-BCFA (30° 48.200′N, 76° 55.707′E) and MS-BCFB (30° 48.290′N 76° 56.126′E), are sedimentary deposit in the boulder conglomerate formation of upper Shivaliks, in Northern India. YS11 (28° 53′ 52.90″ N, 77° 13′ 59.90″ E) is a surface sedimentary samples of the Yamuna river basin, India.

The samples were processed in subdued red light. A standard chemical treatment is followed to extract quartz (Aitken, 1985). All sedimentary samples were treated with 1 N hydrochloric acid for atleast 1 h or until the reaction stops indicating elimination of carbonates. Next, samples were treated with 30 % hydrogen peroxide to eliminate organic contaminants for at least 24 h or until the reaction stops and dried at 45 °C. A grain size fraction of 90–150 μm was separated by dry sieving. To separate heavy minerals, quartz and feldspar, magnetic separator was used (Frantz magnetic separator (Model LB-1)) at ~0.5 and 1.5 A (Porat, 2006). After cleaning, quartz was subjected to 60 min of 40 % hydrofluoric acid treatment to eliminate the alpha affected outer 20-μm skin and 30 min of 37 % hydrochloric acid treatment to eliminate fluorides. The quartz sample (RQ-1), quartzite rock (pure quartz), was crushed and the 90–150 μm grain size was separated by sieving. As it was mainly quartz, evident from XRD (Singhal et al., 2024), free from carbonates and organic matter, it was treated with 10 % hydrofluoric acid for 5 min to remove surface defects, and 37 % hydrochloric acid for 30 min to remove fluorides (Aitken, 1985, pg. 182; Singhal et al., 2024; Toyoda et al., 2000).

2.2. Instrumentation

The measurements are done in Risø TL/OSL reader DA-20 DASH

Table 1
Sample details.

Sr. No.	Sample name	Latitude, Longitude	Provenance	Remarks
1.	RQ-1	24°29′12″N, 73°13′18″E	Sabarmati basin, Western India	Rock sample
2.	PRL-1	10° 46′ 44.0292″ N, 76° 34′ 30.36″ E	Bharathpuzha basin, Southern India	Bright sedimentary sample; flood deposit; natural dose 21.5 Gy
3.	MS-BCFA	30° 48.200′N, 76° 55.707′E	Boulder Conglomerate Formation, Shivaliks, Northern India	Natural signal in saturation in SAR, independent age from paleomagnetic study
4.	MS-BCFB	30° 48.290′N, 76° 56.126′E	Boulder Conglomerate Formation, Shivaliks, Northern India	Natural signal in saturation in SAR, independent age from paleomagnetic study
5.	YS11	28° 53′ 52.90″ N, 77° 13′ 59.90″ E	Yamuna Basin, Indo-gangetic plain, India	Dull sedimentary sample

head equipped in Luminescence Physics and Application Laboratory at Physical Research Laboratory, Ahmedabad, India. For the stimulation of the samples, 470 ± 30 nm wavelength blue LED is used, and detection is done in UV (340 ± 40 nm) using a U340 Hoya optical band-pass filter and blue: 440 ± 40 nm using Scott (BG39 and BG3) filters. Bialkali photomultiplier tube (ET9107B) is used which is most sensitive in the blue-ultraviolet region (Bøtter-Jensen et al., 2003). A heating of 2 °C/s was used for preheat/TL (used for normalization) during measurements. A monolayer of the samples is mounted on stainless steel disc using Silkospray™. IR depletion ratio (Duller, 2003) was estimated for the samples to check for the feldspar contamination at various doses and was found to be negligible. Luminescence measurements are done in ultrapure nitrogen environment. For irradiation of the samples, a beta source (Sr-90) delivering dose at a rate of 4.92 Gy/min at sample position is used. Additionally, a gamma (Co-60) radiation facility, having a dose rate of 10.98 Gy/min, at Indira Gandhi Centre of Atomic Research, Kalpakkam, India is used for bulk irradiation of the samples.

2.3. Measurements

Throughout the experiments, the fast component of the BSL signal is investigated using early background subtraction method. In this, 0.2 s–1 s is used as signal and 2.88 s–4 s is taken as background. Further, the dose response curve (DRC) is fitted with single saturating exponential equation i.e., $I = I_0\left(1 - e^{-\left(\frac{D}{D_0}\right)}\right)$, until mentioned otherwise with I_0 as the saturation intensity and D_0 as the characteristics dose and $2D_0$ is the saturation dose.

2.3.1. Multiple aliquot additive dose (MAAD) measurements

For the MAAD measurements, a set of 5 aliquots (3, if inter-aliquot scatter is less) are taken for each dose points. The mass of sample on each is carefully measured to a precision of 0.01 mg. Each set is given a known dose. BSL measurements are done at 125 °C for 40 s after preheating to 220–260 °C for 10 s (decided on the basis of SAR preheat plateau (Murray and Wintle, 2000)). The luminescence emission measurements were done in ultraviolet (340 ± 40 nm) using Hoya U-340 filter. The measurement protocol steps are tabulated in Table 2. The saturation dose is estimated by fitting the saturating exponential to the measured dose response curve.

2.3.2. Single aliquot regeneration (SAR) measurements

The SAR (Murray and Wintle, 2000) measurements are done on single aliquots using test dose sensitivity normalization as per protocol given in Table 2. BSL signal at 125 °C for 40 s is measured after preheating samples aliquots to 220–260 °C for 10 s. A test dose signal for a dose of 40 Gy (<30 % of saturation dose) is used to monitor and correct luminescence signal for the sensitivity changes during measurements. A hot bleach of BSL at 200 °C for 100 s is used to remove any signal in between the SAR cycles. A 0 Gy dose is used to measure the recuperation and a repetitive dose is used to measure the recycling. Any aliquot having recuperation >5 % or recycling ratio deviating more than 10 % of unity is discarded. Saturation dose is obtained after fitting the DRC with single saturating exponential. Following experiments were conducted to investigate the effect of test dose on saturation dose.

Effect of regeneration dose on test dose signal: In this, experiments were carried out to investigate the effect of regeneration dose on test dose signals. The details of experiments are given below.

1. The variation of test dose signal (T_X/T_N) for 2 constant alternately repetitive high and low regeneration doses during SAR cycle is investigated. The protocol used is as per Table 3. All measurements are normalized w.r.t first test dose signal (T_X/T_N).
2. The effect of variation in test dose on saturation dose is investigated. For this, the increasing test doses viz. 7, 70, 280 and 860 Gy were used in SAR protocol provided in Table 2 and respective DRC is constructed.
3. SAR procedures strongly relies on correlation of regeneration and test dose signal. A constant L_X/T_X ratio with SAR cycle for a fixed regeneration and test dose is one of the prerequisites for the use of any test dose correction. The L_X/T_X variation with SAR cycle is studied for high and low regeneration doses. Three sets of regeneration dose (R) and test dose (T) are chosen with R, T as (28, 7), (280, 7) and (860,70) Gy and repetitively measured using SAR procedures.
4. Murray and Roberts (1998) suggested that 110 °C TL peak counts could also be used to correct for the sensitivity changes as it is correlated with OSL signal. Hence, the use of 110 °C TL peak for normalization within the SAR methodology is tested, and its effect on saturation is investigated. The DRC is obtained by normalizing the BSL signal (Step 3, Table 2) by 110 °C peak intensity counts (Step 5, Table 2) (emission 340 ± 40 nm). The results of the saturation obtained by this normalization are compared with the standard SAR protocol (Table 2).
5. Additionally, experiments were conducted to investigate TL and BSL signals, with and without annealing of samples for identifying their potential for normalization of BSL signals at high radiation doses. It was suggested by Singhal et al. (2024), that after annealing to 450 °C, blue emission 110 °C TL peak is independent of the predose effect. Hence, BSL, TL in blue emission (400–480 nm), zero glow normalization, are investigated for their dependence on regeneration dose as per protocol given in Table 4.

2.3.3. Comparison of protocols

Three protocols (SAR, MAAD and MAR) are used to estimate the equivalent dose of samples MS-BCFA and MS-BCFB. For MAAD and MAR, mass normalizations and the normalizations which passed the criteria of being independent of regeneration doses (in the previous experiments) are used to construct dose response curve. In MAAD, doses

Table 2
Protocol used for DRC of BSL signals.

Step No.	MAAD BSL	SAR BSL (Murray and Wintle, 2000)
1	Natural sample + (additive doses)	Natural sample
2	Preheat (220–260 °C), 10 s	Preheat(220–260 °C), 10 s
3	OSL at 125 °C($\mathbf{L_x}$)	OSL at 125 °C($\mathbf{L_x}$)
4	Mass normalized	Test dose
5		Preheat (220–260 °C), 10 s
6		OSL at 125 °C($\mathbf{T_x}$ = 40 Gy)
7		Blue bleach 200 °C for 100 s
8		Regenerative dose(Ri)
9		Go to step 2

Table 3
Protocol used for T_x/T_N ratio variation.

Step No	Measurement
1	Regenerative dose 426 Gy
2	Preheat (220–260 °C), 10 s
3	OSL at 125 °C($\mathbf{L_x}$)
4	Test dose (8.5 Gy)
5	Preheat (220–260 °C), 10 s
6	OSL at 125 °C($\mathbf{T_x}$)
7	Blue bleach 200 °C for 100 s
8	Regenerative dose (8.5 Gy)
9	Preheat (220–260 °C), 10 s
10	OSL at 125 °C($\mathbf{L_x}$)
11	Test dose (8.5 Gy)
12	Preheat (220–260 °C), 10 s
13	OSL at 125 °C ($\mathbf{T_x}$)
14	Blue bleach 200 °C for 100 s
15	Go to step no. 1

Table 4
Protocol to study various signals for suitability as normalizations.

Step No	SAR BSL	Measurement
1	Natural sample	
2	Test dose	
3	TL (220–260 °C)	Zero glow (TL, UV emission)
4	Additive dose	
5	Preheat(220–260 °C), 10 s	
6	OSL at 125 °C	L
7	Test dose	
8	TL blue (220–260 °C)	TL blue emission
9	OSL at 125 °C	BSL
10	Heat till 450 °C	
10	Test dose (Dt)	
11	TL Blue (220–260 °C)	TL after annealing, blue emission
12	OSL at 125 °C	BSL after annealing

in addition to natural dose are given to the sample and the natural dose is extrapolated. For the MAR, DRC from zero is constructed and the normalized natural dose is interpolated. To construct the DRC from zero, the natural sample is bleached in solar lamp for 24 h to remove previous signal followed by gamma irradiation.

3. Results

3.1. Comparison of dose response curves

Fig. 1 shows the mass normalized MAAD BSL shine down curves. A natural dose of 21.5 Gy was present in PRL-1. MS-BCFA and MS-BCFB were found to be in dose saturation in SAR BSL. Hence in Fig. 1 the shine down curves are shown for doses given in addition to natural dose. Whereas, in RQ-1 and YS-11, no initial dose was present. It is observed that the intensity of BSL increases beyond D_{GSS}. An increase in the medium and slow component is also observed with dose. Fig. 2 shows the comparison of SAR and mass normalized MAAD DRC for RQ-1 and PRL-1. The errors in the DRC of PRL-1 becomes significant towards high doses. Previously, it is observed by several researchers that the mass normalizations may result in large scatter (Jain et al., 2003), which is a sample dependent observation. Results show that the mass normalized MAAD DRC has higher saturation than the SAR DRC. For the sample RQ-1, the $2D_0$ for MAAD is 1080 ± 90 Gy and SAR is 260 ± 20 Gy, similarly for the sample PRL-1, MAAD $2D_0$ is 2181 ± 1158 Gy while SAR $2D_0$ is 259 ± 27 Gy.

3.2. Effect of test dose

Fig. 3 and S1 show the variation of T_X/T_N for the sample RQ-1 and PRL-1 respectively. In both the graphs, two trends are clearly visible. 1) An overall linear increase in the sensitivity with the SAR cycle and 2) a systematic change in the T_X/T_N ratio in accordance with the regeneration dose alteration. For all high dose regeneration points, the T_X/T_N ratio is higher than the T_X/T_N corresponding to the previous lower dose regeneration points. Similarly, Fig. 4 and S2 show the variation of $2D_0$ with test doses. The graphs are normalized by the luminescence intensity corresponding to the maximum dose. For the sample RQ-1, saturation dose increases from 120 ± 40 Gy to 408 ± 20 Gy with increasing test dose. Similarly, for the sample PRL-1, the saturation dose increases from 201 ± 8 Gy to 545 ± 27 Gy. Fig. 5 and S3 show the variation of L_X/T_X for same regeneration and test dose (R,T), with SAR cycle. The luminescence signals are normalized by the first L_X/T_X signal. It is observed that when dose for R and T signals is less than D_{GSS}, the L_X/T_X remains constant with constant regeneration dose in SAR cycle. However, for constant regeneration dose > D_{GSS} given in SAR sequence (Table 2), L_X/T_X is not constant but decreases with the SAR cycle (Fig. 5 and S3). The decrease is more for higher regeneration doses Fig. S3.

3.3. Normalization methods

Fig. 6 and S4 show the comparison of SAR DRCs using BSL and TL (UV emission) test dose normalization. The saturation dose ($2D_0$) is higher for the TL (UV emission) normalization for both the samples RQ-1 and PRL-1. However, the recycling ratio is 80 % or less. Fig. 7 shows the dependence of different normalization methods (BSL, BSL after annealing, TL (UV emission), TL (blue emission) and TL after annealing (blue emission)) on regeneration dose and their effect on the DRCs for the sample RQ-1 using multiple aliquot measurements. It is observed that BSL test dose has a carry-over of charge from the prior regeneration dose, as test dose signal increase is proportional to the regeneration dose (Fig. 7a). However, after annealing the sample to 450 °C, the carry-over signal is significantly reduced in BSL signal (Fig. 7b). Corresponding DRCs for BSL and BSL (after annealing) normalizations are shown in Fig. 7f and g. For BSL normalized by "BSL test dose", the signal saturates around ~250 Gy, whereas BSL normalized by "BSL after annealing" signal increases up to 1100 Gy, which is the maximum dose given in the experiment. For TL zero glow normalization (Fig. 7c) the test dose signal is unaffected by the prior regeneration dose. Fig. 7h shows the DRC constructed, using TL zero glow normalization. Additionally, Fig. 7d, e shows the results for TL (blue emission) and TL after annealing (blue emission) used as normalization. TL after annealing (blue emission) is also independent of regeneration dose given. The corresponding DRCs are shown in Fig. 7i and j. The errors plotted are the standard deviation of the mean (Taylor, 1997) estimated for each point considering the scatter in the data. A relatively higher error is observed at 1100 Gy for the BSL test dose, however, for the same aliquots in the TL and annealed BSL normalization data, the errors are not so significant. This suggests that there is further uncertainty associated with the method of de-trapping of charges (BSL/anneal BSL/TL/anneal TL). Fig. S5 shows the results for the sample PRL-1.

3.4. Protocol comparison

Fig. 8, shows the mass normalized MAAD DRC for the sample MS-BCFA. The equivalent dose is obtained by extrapolating the DRC curves on the negative dose axis. Fig. 9 shows the mass normalized MAR DRC for the sample MS-BCFA. In the initial part of the MAR DRC, a change in the slope is observed, indicating presence of two traps as also pointed by some earlier studies (Chapot et al., 2016; Lowick et al., 2010b; Singhal et al., 2024; Timar-Gabor et al., 2012). Hence, the DRC is fitted with double saturating exponential as shown in Fig. 9, with equation $I = I_{01}\left(1-\exp\left(-\frac{D}{D_{01}}\right)\right) + I_{02}\left(1-\exp\left(-\frac{D}{D_{02}}\right)\right)$ where, $2D_{01}$ and $2D_{02}$ are the characteristics dose indicating two trap system. The fitted value of $2D_{01}$ is between 120 ± 30 Gy and $2D_{02}$ is between 5800 ± 800 Gy. The equivalent dose is obtained by interpolating the natural point on the graph. Table 5, summarizes equivalent doses estimated using SAR, MAR and MAAD methodologies using various normalizations. The equivalent doses obtained by MAAD are the highest. Dose response curves of TL after annealing (blue emission) and BSL (after annealing) of sample MS-BCFA and of sample MS-BCFB are shown in Supplementary Figs. S6–S15. It is observed that the errors in the data becomes significant at radiation doses >1 kGy.

4. Discussion

As of now, quartz is known to saturate ~250 (±100) Gy as suggested by several earlier research (Chawla et al., 1998; Duller, 2008; Wintle, 2008; Wintle and Murray, 2006). However, it is also suggested that the saturation dose is protocol dependent (Murray et al., 2021; Wang et al., 2021; Zhang and Tsukamoto, 2022). Thus, it is crucial to identify the measurement variables that affect the luminescence saturation dose, as it influences the luminescence-dating limit. This study investigated

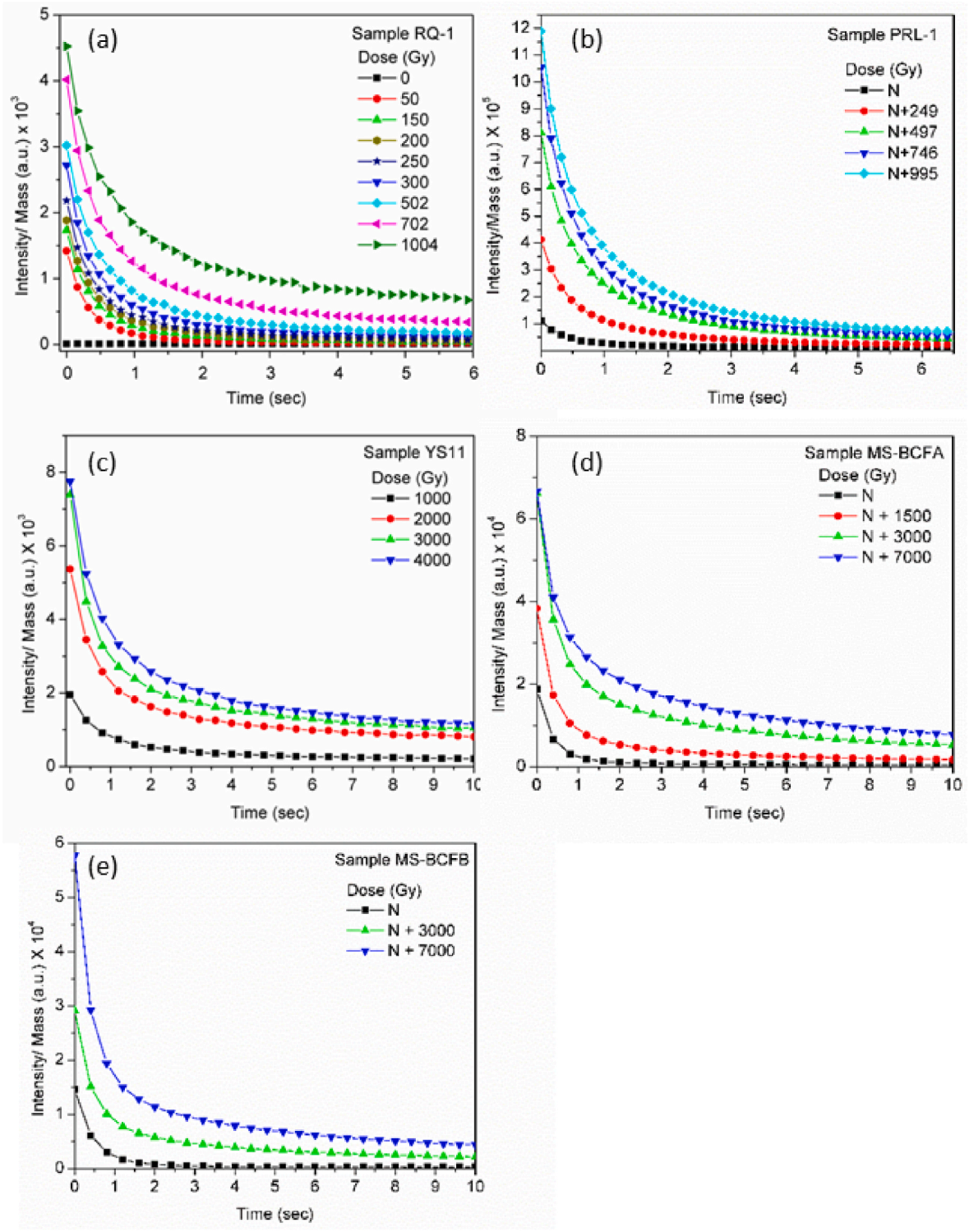

Fig. 1. Shine down curve of sample (a) RQ-1 and (b) PRL-1 (c) YS11, (d) MS-BCFA, (e) MS-BCFB, normalized by mass and average of 5 aliquot data respectively. RQ-1 is average of 3 aliquots, as the scatter was less. 'N' stands for natural dose.

procedures, which can be used for estimating higher radiation doses for extending the dating limit by comparing DRCs for BSL measured at 125 °C. The results suggest that BSL signals in general do not saturate as early as observed during SAR procedure (Fig. 2), suggesting the need for improvement in laboratory measurement protocols. The protocols such as MAAD and MAR provide much higher saturation doses (Figs. 2, 7 and 8, S5-14) compared to SAR and also supported by previous research works (Y C Lu et al., 2007; Murray et al., 2021; Wang et al., 2021). This indicates that the saturation in SAR is somewhat protocol induced and the cause needs to be probed. The SAR protocol is known to produce very reliable results for low doses (<D_0~250Gy), which is verified against other standard techniques and methodologies (Murray and Olley, 2002; Vandenberghe et al., 2004; Watanuki et al., 2005). However, SAR's early saturation compared to other luminescence protocols warrants careful investigation of its applicability for doses near and beyond saturation limit.

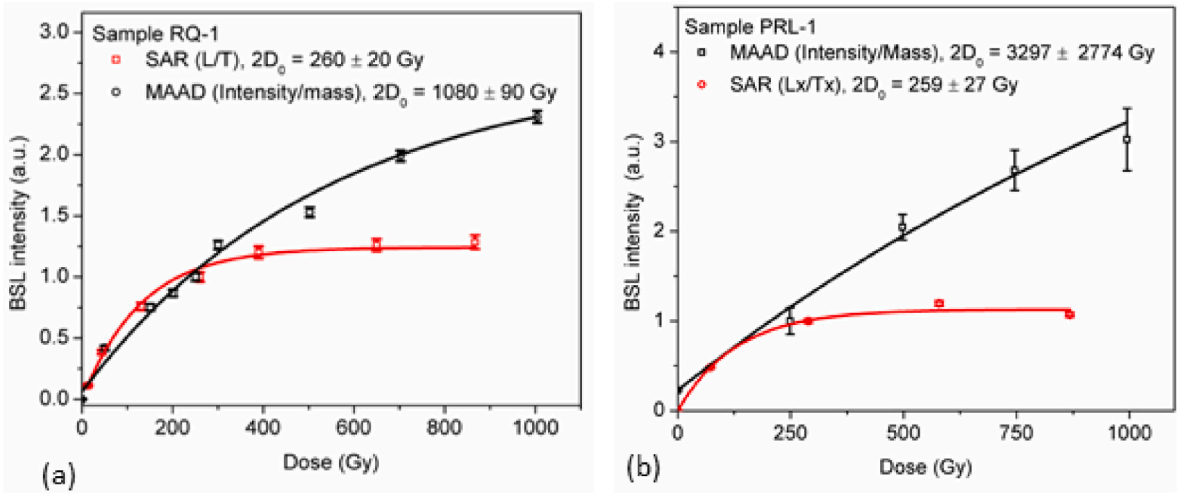

Fig. 2. *Comparison between MAAD and SAR BSL dose response of sample (a) RQ-1, (b) PRL-1. The saturation dose is obtained by fitting the single saturating exponential equation* $I = I_0\backslash(1 - exp\ ((x - x_c)/D_0))$.

Table 5
Equivalent dose measurement using various normalization methods.

Sr. No.	Sample Name	Expected Age (Ma)*	Dose Rate (Gy/ka)	Expected Dose (Gy)	Estimated Equivalent dose (Gy)						
					SAR	**MAAD (mass normalized)**	**MAAD (TL (after annealing, blue emission) normalization)**	**MAAD (BSL after annealing normalized)**	**MAR (mass normalized)**	**MAR (TL (after annealing, blue emission) normalization)**	**MAR (BSL after annealing normalized)**
1	MS-BCFA	0.5-1.7	2.17 ± 0.18	1085–3700	>218 ± 4	503 ± 153	338 ± 127	483 ± 213	310 ± 80	380 ± 100	325 ± 125
2	MS-BCFB	0.5-1.7	1.91 ± 0.17	955–3248	>220 ± 4	794 ± 261	547 ± 228	709 ± 286	280 ± 80	120 ± 20	100 ± 60

* the expected age is based on the paleo-magnetic studies by (Kumar et al., 1999; Mandal et al., 2019; Rao et al., 1995).

One of the important differences in the measurement techniques is in normalization methods. Therefore, the effect of normalization is investigated in SAR and other protocols. In SAR protocol, the luminescence signal is normalized by signal corresponding to an immediate test dose, expecting it to correlate with the luminescence signal (Murray and Wintle, 2000). This is in fact the case for doses less than saturation doses; however, more investigation for doses near and higher than saturation is required. For this, the variation in T_x/T_N for a fixed test dose is studied for multiple cycles of constant alternate low (~8 Gy) and high (~426 Gy) regeneration doses (Table 3). The periodic variation of T_X/T_N ratio correlates with alternating regeneration doses (Fig. 3 and S1) suggests a regeneration dose dependence of test dose signal for doses near or higher than saturation. This can significantly influence the saturation limit. During L/T measurement, as the regeneration dose increases, the dividing factor, i.e., test dose signal (T) also increases. This increase in the denominator of L/T will reduce the proportional increase in L/T with dose resulting in early saturation of SAR DRC. On comparison of SAR-BSL protocol (Table 2) with TT-OSL protocol (Chapot et al., 2016; Duller and Wintle, 2012), it is evident that the test dose signal in SAR-BSL is the main signal (L_x) in TT-OSL, difference lies in the fact that in TT-OSL a dose between two OSL measurements is not given. Hence the test dose will show significant dependence on the regeneration dose. This contribution becomes even more pronounced at higher doses. Some previous studies have also reported dependency of BSL test dose signal on regeneration dose (Jain et al., 2003; Rhodes, 1992).

The regeneration dose dependency in the test dose can be minimized either by increasing the size of test dose such that the percentage contribution from the regeneration dose to the test dose is suppressed or by adopting another normalization procedure. Results (Fig. 4 and S2) show that the growth curve modifies with increasing test dose and saturation doses are high for high-test doses. Similar observations are made by Colarossi et al. (2018) for feldspars, Palczewski et al. (2022) for

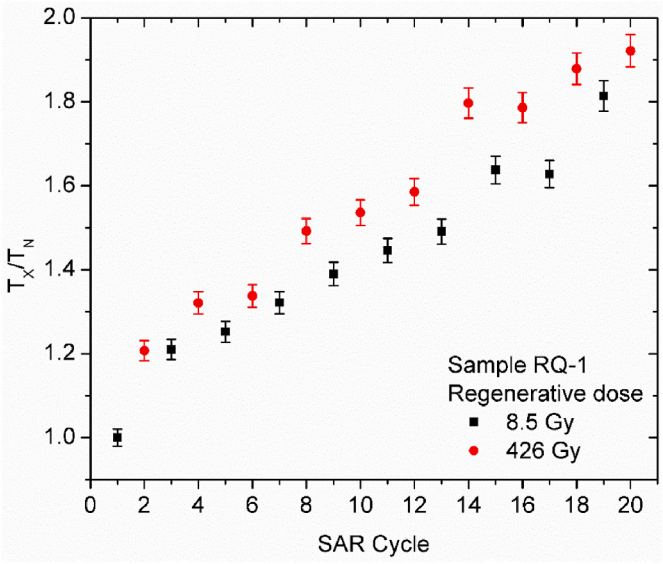

Fig. 3. T_X/T_N ratio of sample RQ-1 for alternative high and low regenerative doses and fixed test dose of 8.5 Gy.

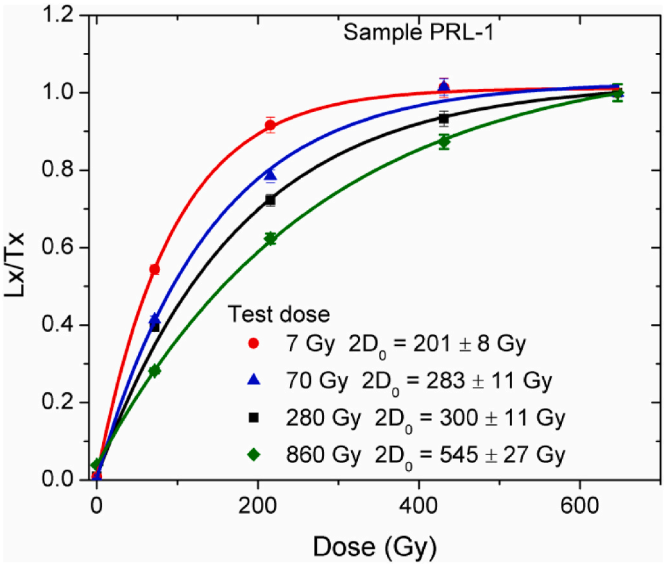

Fig. 4. The DRC of sample PRL-1, for 4 different test doses. The curves are fitted with single saturating exponential.

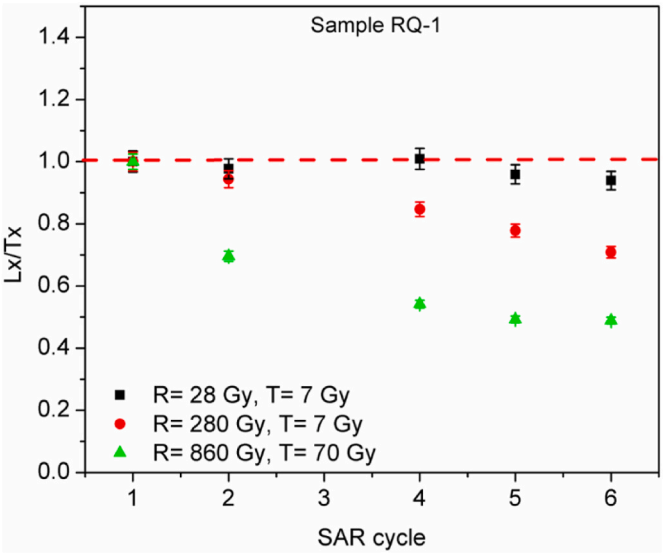

Fig. 5. Lx/Tx variation with SAR cycle, for fixed regenerative and test dose.

TM-OSL for quartz, however, a decrease in saturation is observed by Liu et al. (2022). Several authors (Chauhan and Singhvi, 2019; Murray and Mejdahl, 1999; Murray and Roberts, 1998; Singhvi et al., 2011) suggested that 110 °C peak is correlated with BSL signal, so it can also be used to track sensitivity changes similar to test dose BSL signal. The feasibility of using the 110 °C (UV emission) peak as a normalization signal was investigated. The integrated counts within the maximum peak temperature ±5 °C are used for normalization of BSL signal, and a DRC with a higher saturation dose was observed (Fig. 6 and S4). However, in this, the estimated recycling ratio is below suggested limit of 10 % of unity. The differences can again be attributed to the fact that 110 °C TL peak and BSL sensitivity are not correlated at higher doses (Singhal et al., 2024). The experiment to monitor L/T above D_{GSS} for a constant regeneration dose in SAR cycle suggested that the L/T is not constant but decreases with number of cycles (Fig. 4). This implies that at higher doses (>~D_{GSS}), SAR test dose signal (TL or OSL) is inappropriate for correcting luminescence signal for the sensitivity changes occurring during measurement procedures and require a revisit of normalization

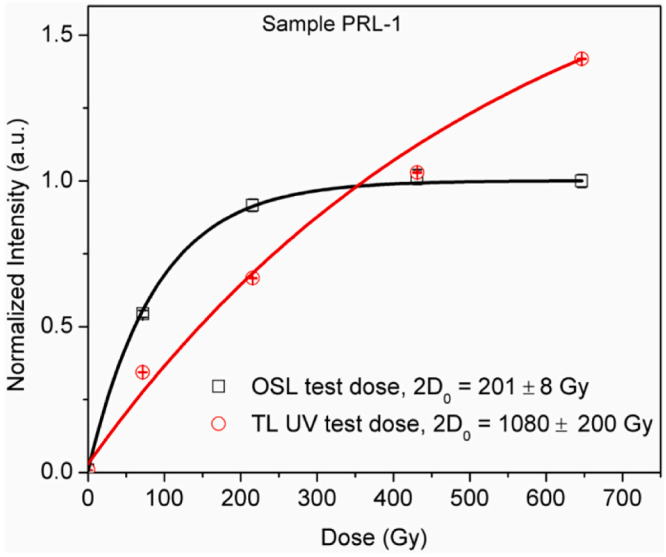

Fig. 6. DRC of sample PRL-1. The black curve is BSL-SAR normalized by SAR test dose as per given in Table 2. The red curve is OSL dose normalized by 110 °C counts obtained from step 5 in the SAR protocol given in Table 2. (For interpretation of the references to colour in this figure legend, the reader is referred to the Web version of this article.)

methods. Further, as the regeneration dose signal is propagated to next OSL measurements, it is not possible to correct for this propagation of charge within SAR methodology.

It is important to identify alternative methods that can be used for estimating D_{GSS}. Other methodologies such as MAAD and MAR are useful, since in these methods, aliquots are measured only once and sensitivity correction is not required. However, in these methods as well, normalization is required for removing inter-aliquot variability due to inhomogeneity in masses and sediment grains. Experiments done to identify the suitable normalization procedure (Table 4) suggest that zero dose normalization is the best method (Fig. 7 and S5). However, in cases, when the samples subsets are irradiated with different high radiation doses (>1 kGy) then zero glow normalization is also not possible due to radiation quenching of 110 °C peak (Schmidt and Woda, 2019; Singhal et al., 2024) which again depends on dose in dosimetric traps (>300°C; Singhal et al., 2024). In such cases, test dose BSL or TL (blue; Singhal et al. (2024)) signals after annealing can be used for normalizations, as they are found to be independent of the regeneration dose (Fig. 7 and S5). Previous studies by Timar-Gabor et al. (2015) have also reported that the use of zero glow TL 110 °C normalized MAAD DRCs has higher saturation doses than 2000 Gy and supports the argument.

Normally, BSL signal is considered to be arising from a single trap corresponding to 325 °C peak (Aitken, 1998; Wintle and Murray, 2006), so a single saturating exponential is considered to explain the nature of fitting. Some of the works also use linear fitting for very low doses (~10 Gy) as at low doses single saturating exponential approaches linear approximation. However, interestingly for doses near saturation of SAR signal, different types of fitting procedures are reported as single saturating exponential is unable to explain the dose response. Some of the works use a combination of linear and saturating exponential curves (Lowick et al., 2010a; Rodrigues et al., 2022) while some others used double saturating exponentials as they are found to fit well (Ankjærgaard, 2019; Chapot et al., 2012; Timar-Gabor et al., 2012). However, the physical reason for such fittings is not explained. The results obtained in the present study (Table 4 and Fig. 7, S11-15) indicate towards the existence of two trap systems because a difference in slope for doses in range 0–300 Gy and 300–1000 Gy is observed (Fig. 7). A similar change in slope is observed in many previous studies (Chawla et al., 1998; Rodrigues et al., 2022; Singhal et al., 2024) however, these

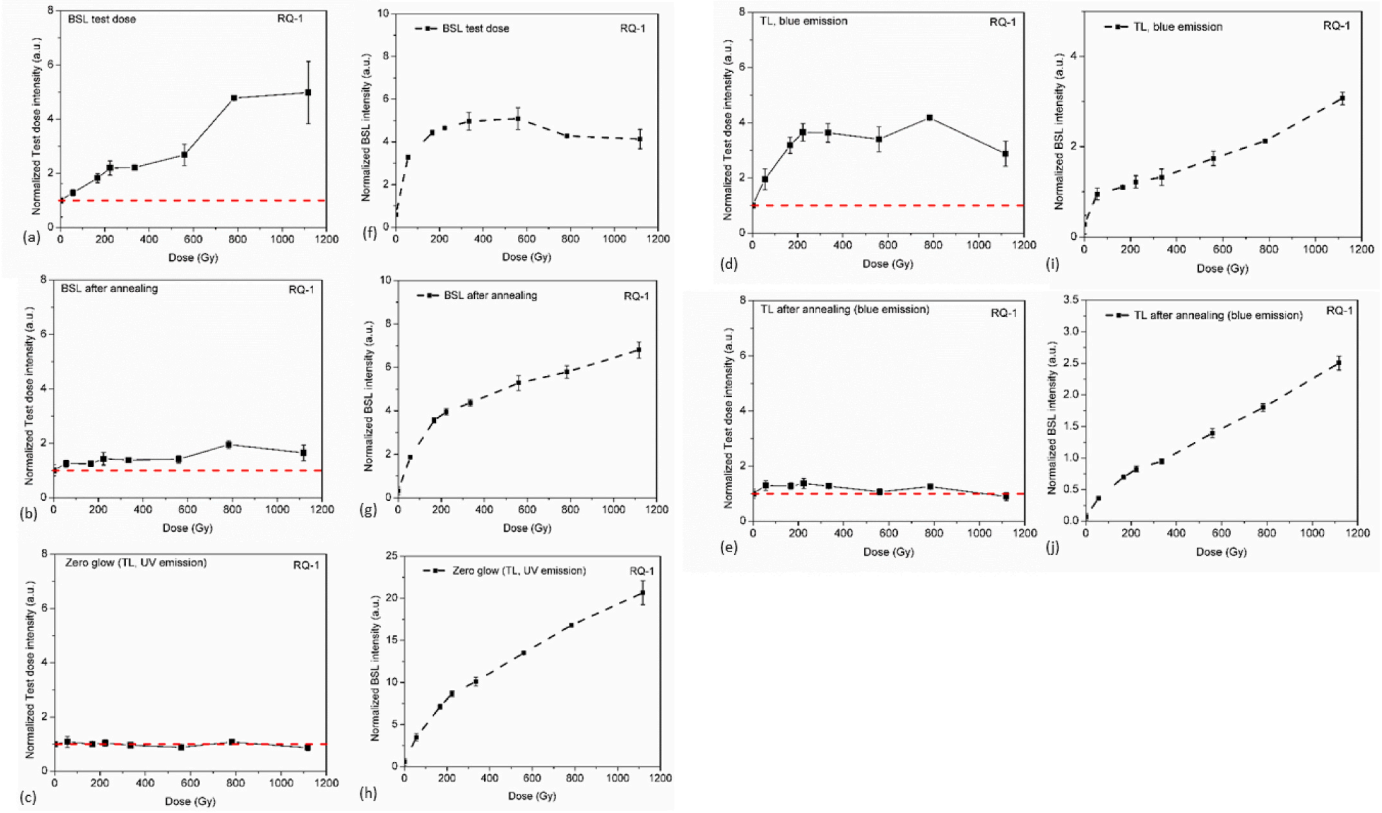

Fig. 7. RQ-1 data, with different normalization. (a–e) shows the variation of fixed test dose signal with regeneration doses, (f–j) shows the dose response curve obtained by using the mentioned normalization in the graph.

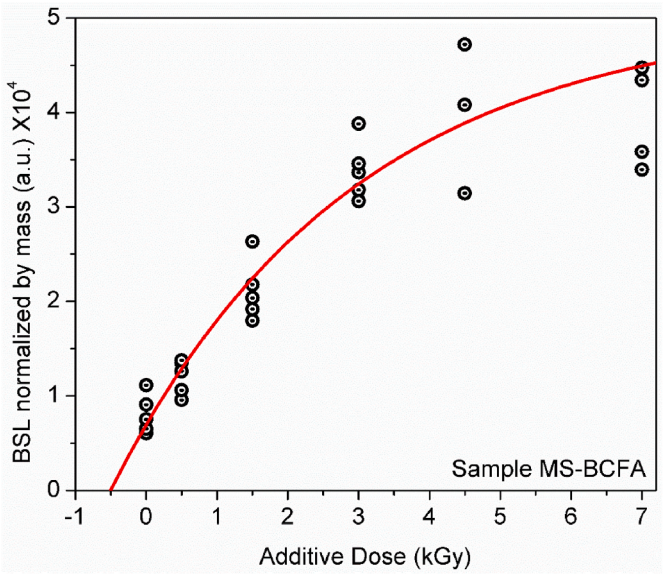

Fig. 8. MAAD dose response curve of MS-BCFA, normalized by mass.

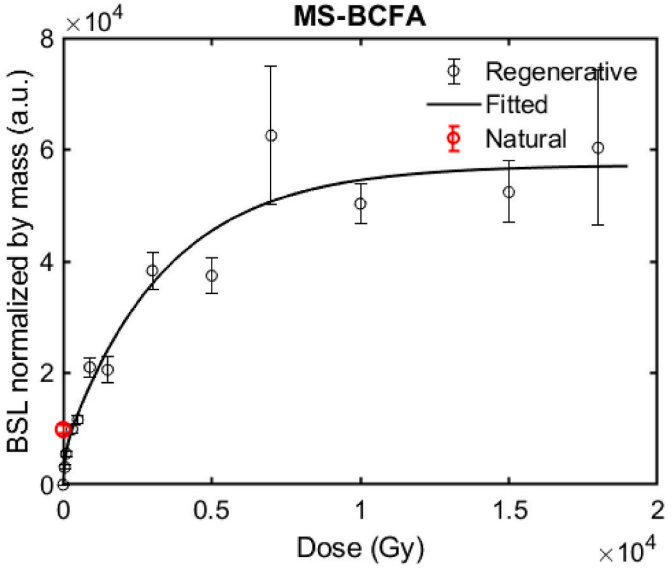

Fig. 9. MAR dose response curve of MS-BCFA normalized by mass.

studies either focus on the low dose range (from 0 to ~ 1000 Gy) or high dose range (>1000 Gy) and provide a limited picture of dose response curve. In the present study, dose response is constructed from 0 Gy till the second saturating exponential also results in saturation (Fig. 9 and S11-S15). Thus for the present work, double saturating exponential is used for fitting. The MAR saturation dose for natural samples MS-BCFA and MS-BCFB is found to be significantly higher (~5800 Gy) than the SAR saturation ($2D_0$~ 220 Gy). The estimated doses for MS-BCFA is higher than SAR saturation but lower than MAAD. For MS-BCFB, there exists inconsistency within the MAR D_e estimated from different normalizations and the values are lower than D_e estimated using SAR. In MAAD DRC, onset of saturation can be seen after N+3000 Gy for both the samples MS-BCFA and MS-BCFB and further data points are needed to observe the saturation dose. The D_e estimated by extrapolating fitted curve to negative dose axis yielded higher D_e values (500 and 700 Gy respectively) than the SAR saturation ($2D_0$~ 220 Gy). Based on the better consistency within different normalization obtained in the study

and higher D_e values, it can be concluded that MAAD can be used for estimating doses greater then SAR saturation. However, still the estimated doses are lower than the doses expected (1000–3500 Gy) based on paleomagnetic dating based chronology of the samples (Table 5) suggesting an underestimation of ages. There can be several reason for this underestimation. Recent results of the ESR dating of fossils (dental enamel) from the Pinjor formation of the upper Shivaliks, which is lower in stratigraphy compared to BCF, suggest a relatively younger age of 465 ka (A. P. Kaur, 2024) than that predicted by paleomagnetic dating (>1.7 Ma) (Kumar et al., 1999; Mandal et al., 2019; Rao et al., 1995). Other possibility is that these estimated ages depict the exhumation age of BCF samples not the depositional age (Bouscary et al., 2024). It may also be possible that the samples are in field saturation that differs from laboratory saturation (Chapot et al., 2016; Y C Lu et al., 2007; Rahimzadeh et al., 2021) and laboratory measurements estimated field saturation dose, not the dose corresponding to depositional age. In order to find out the exact reason for such underestimation a more detailed study with multiple controlled age samples is required. More samples, having signals in SAR saturation or those that demonstrate underestimation near saturation, should be measured by recommended normalization utilizing MAAD methods to identify the best method for D_e estimation (Dreimanis et al., 1978; Lowick et al., 2010a; Lowick and Preusser, 2011; Y. C. Lu et al., 2007; Murray et al., 2007; Prescott and Robertson, 1997; Qin and Zhou, 2009; Timar-Gabor and Wintle, 2013; Wang et al., 2021). Although MAAD and MAR protocols look promising for higher doses, but these protocols also have identified limitations like extrapolation in MAAD and inherent signal scatter due to variability in sensitivity of grains of the sample. Experiments using MAAD and MAR protocol (Table 4) yielded large scatter in the data at a higher doses (~kGy) (Figs. 8, 9, S6-14). Generally, this trend is also observed in literature (Chawla et al., 1992; Huntley et al., 1993; Timar-Gabor et al., 2015) although, these studies uses lesser doses (<kGy). At kGy doses, the errors can further increase due to statistical nature of dose absorption, which needs more investigation in future. For MAAD measurements larger amount of sample is required to minimise heterogeneity due to statistics. For lesser number of aliquots errors are often higher as observed in Fig. 9. In this study, measurements were made on 5 aliquots for each dose point with a sample size covering 8 mm on the stainless steel disc. However, still the scatter is prominent and could not be reduced further due to limited sample and irradiation time constraints.

This discussion indicates, that there is need to understand the physics of luminescence for high radiation dosimetry and investigate the controlled age old samples for understanding the applicability of luminescence dating for old samples.

5. Conclusion

The study helps in understanding the quartz DRC characteristics of BSL signals near saturation of SAR and beyond. Following major conclusions can be drawn from this work.

1. Laboratory protocol influences the saturation dose that can be estimated using BSL signals. A significant variation is observed in the saturation obtained from SAR and MAAD methodology, with MAAD DRC saturating later.
2. SAR methods are widely used and work well at low radiation doses, however, as regeneration dose increases, the carry-over charge from regeneration dose cycle to the test dose cycle results in increased test dose signal (T). Thus, the increase in T, reduces proportional increase in L/T and results in early saturation of SAR DRCs. The normalization provides reliable results for doses less than D_{GSS} using SAR, however, for paleodoses estimation near saturation or beyond, these normalization procedures are inappropriate.
3. The dependency of regeneration dose is reduced only after annealing. Zero glow, BSL after annealing and TL after annealing (blue emission)) are observed to carry negligible regeneration dose dependence and can be used for normalization. Hence MAAD and MAR methods normalized by these normalizations are preferred for high dose estimations.
4. The DRCs constructed using these normalizations need to be fitted by double saturating exponential. Second saturation is observed ~5800 Gy in this study. Hence, BSL signals can be used to estimate doses way beyond the saturation of SAR.
5. Equivalent doses above the SAR saturation could be estimated with MAAD. Further tests on other samples with well constrained age is required to understand high dose response of luminescence better.

CRediT authorship contribution statement

Malika Singhal: Writing – original draft, Validation, Methodology, Investigation, Formal analysis, Data curation, Conceptualization. **Madhusmita Panda:** Writing – review & editing, Methodology, Data curation. **O. Annalakshmi:** Writing – review & editing, Supervision, Resources, Methodology. **Naveen Chauhan:** Writing – review & editing, Supervision, Resources, Methodology, Investigation, Formal analysis, Conceptualization.

Declaration of competing interest

The authors declare that they have no known competing financial interests or personal relationships that could have appeared to influence the work reported in this paper.

Acknowledgement

The authors would like to thank Prof. Parth Chauhan, IISER Mohali for help in collecting the boulder conglomerate samples, Smt. M. Menaka, Head, RAMS, IGCAR for providing high-dose irradiation facility. The authors thank 8 anonymous reviewers for their suggestions in improving the manuscript. The work carried out at PRL is supported by the Department of Space, Government of India.

Appendix A. Supplementary data

Supplementary data to this article can be found online at https://doi.org/10.1016/j.radphyschem.2025.112764.

Data availability

Data will be made available on request.

References

Aitken, M.J., 1985. Thermoluminescence Dating, Handbooks for Archaeologists : a Publication of the Sub-committee for Archaeology of the Standing Committee for the Humanities. Academic Press.
Aitken, M.J., 1998. Introduction to Optical Dating: the Dating of Quaternary Sediments by the Use of Photon-Stimulated Luminescence. Clarendon Press.
Ankjærgaard, C., 2019. Exploring multiple-aliquot methods for quartz violet stimulated luminescence dating. Quat. Geochronol. 51, 99–109. https://doi.org/10.1016/j.quageo.2019.02.001.
Ankjærgaard, C., Guralnik, B., Buylaert, J.P., Reimann, T., Yi, S.W., Wallinga, J., 2016. Violet stimulated luminescence dating of quartz from Luochuan (Chinese loess plateau): Agreement with independent chronology up to ~600 ka. Quat. Geochronol. 34, 33–46. https://doi.org/10.1016/j.quageo.2016.03.001.
Biernacka, M., Chruścińska, A., Palczewski, P., Derkowski, P., 2022. Determining the kinetic parameters of traps in quartz using the thermally modulated OSL method. J. Lumin. 252, 119289.
Bonde, A., Murray, A., Friedrich, W.L., 2001. Santorini: luminescence dating of a volcanic province using quartz? Quat. Sci. Rev. 20, 789–793.
Bøtter-Jensen, L., Andersen, C.E., Duller, G.A.T., Murray, A.S., 2003. Developments in radiation, stimulation and observation facilities in luminescence measurements. Radiat. Meas. 37, 535–541. https://doi.org/10.1016/S1350-4487(03)00020-9.
Bouscary, C., King, G.E., Grujic, D., Lavé, J., Almeida, R., Hetényi, G., Herman, F., 2024. Sustained deformation across the Sub-Himalayas since 200 ka. Geology 52, 72–76.
Chapot, M.S., Roberts, H.M., Duller, G.A.T., Lai, Z.P., 2012. A comparison of natural- and laboratory-generated dose response curves for quartz optically stimulated

luminescence signals from Chinese Loess. Radiat. Meas. 47, 1045–1052. https://doi.org/10.1016/j.radmeas.2012.09.001.
Chapot, M.S., Roberts, H.M., Duller, G.A.T., Lai, Z.P., 2016. Natural and laboratory TT-OSL dose response curves: testing the lifetime of the TT-OSL signal in nature. Radiat. Meas. 85, 41–50.
Chauhan, N., Singhvi, A.K., 2019. Changes in the optically stimulated luminescence (OSL) sensitivity of single grains of quartz during the measurement of natural OSL: implications for the reliability of optical ages. Quat. Geochronol. 53, 101004. https://doi.org/10.1016/j.quageo.2019.101004.
Chawla, S., Dhir, R.P., Singhvi, A.K., 1992. Thermoluminescence chronology of sand profiles in the Thar desert and their implications. Quat. Sci. Rev. 11, 25–32.
Chawla, S., Gundu Rao, T.K., Singhvi, A.K., 1998. Quartz thermoluminescence: dose and dose-rate effects and their implications. Radiat. Meas. 29, 53–63. https://doi.org/10.1016/S1350-4487(97)00200-X.
Colarossi, D., Duller, G.A.T., Roberts, H.M., Tooth, S., Lyons, R., 2015. Comparison of paired quartz OSL and feldspar post-IR IRSL dose distributions in poorly bleached fluvial sediments from South Africa. Quat. Geochronol. 30, 233–238. https://doi.org/10.1016/j.quageo.2015.02.015.
Colarossi, D., Duller, G.A.T., Roberts, H.M., 2018. Exploring the behaviour of luminescence signals from feldspars: implications for the single aliquot regenerative dose protocol. Radiat. Meas. 109, 35–44. https://doi.org/10.1016/j.radmeas.2017.07.005.
Dreimanis, A., Hutt, G., Raukas, A., Whippey, P.W., 1978. Dating methods of Pleistocene deposits and their problems: I. Thermoluminescence dating. Geosci. 5, 2.
Duller, G.A.T., 2003. Distinguishing quartz and feldspar in single grain luminescence measurements. Radiat. Meas. 37, 161–165.
Duller, G.A.T., 2008. Luminescence Dating: Guidelines on Using Luminescence Dating in Archaeology.
Duller, G.A.T., Wintle, A.G., 2012. A review of the thermally transferred optically stimulated luminescence signal from quartz for dating sediments. Quat. Geochronol. 7, 6–20. https://doi.org/10.1016/j.quageo.2011.09.003.
Durcan, J.A., 2018. Assessing the Reproducibility of Quartz OSL Lifetime Determinations Derived Using Isothermal Decay, vol. 120, pp. 234–240.
Fleming, S.J., 1979. Thermoluminescence Techniques in Archaeology. Clarendon Press.
Godfrey-Smith, D.I., Huntley, D.J., Chen, W.-H., 1988. Optical dating studies of quartz and feldspar sediment extracts. Quat. Sci. Rev. 7, 373–380. https://doi.org/10.1016/0277-3791(88)90032-7.
Guilheiro, J.M., Tatumi, S.H., Soares, A.d.F., Courrol, L.C., Barbosa, R.F., Rocca, R.R., 2021. Correlation study between OSL, TL and PL emissions of yellow calcite. J. Lumin. 233, 117881. https://doi.org/10.1016/j.jlumin.2020.117881.
Huntley, D.J., Godfrey-Smith, D.I., Thewalt, M.L.W., 1985. Optical dating of sediments. Nature 313, 105–107. https://doi.org/10.1038/313105a0.
Huntley, D.J., Hutton, J.T., Prescott, J.R., 1993. The stranded beach-dune sequence of south-east South Australia: a test of thermoluminescence dating, 0-800 ka. Quat. Sci. Rev. 12, 1–20. https://doi.org/10.1016/0277-3791(93)90045-N.
Jain, M., 2009. Extending the dose range: probing deep traps in quartz with 3.06 eV photons. Radiat. Meas. 44, 445–452. https://doi.org/10.1016/j.radmeas.2009.03.011.
Jain, M., Bøtter-Jensen, L., Singhvi, A.K., 2003. Dose evaluation using multiple-aliquot quartz OSL: test of methods and a new protocol for improved accuracy and precision. Radiat. Meas. 37, 67–80. https://doi.org/10.1016/S1350-4487(02)00165-8.
Jain, M., Bøtter-Jensen, L., Murray, A.S., Denby, P.M., Tsukamoto, S., Gibling, M.R., 2005. Revisiting TL: dose measurement beyond the OSL range using SAR. Anc. TL 23, 9–24.
Kaur, A.P., 2024. Multidisciplinary perspectives on early-to-middle pleistocene (2.58-0.63 Ma) contexts in the siwalik hills and implications for hominin adaptations in northern India. Unpublished PhD dissertation. IISER Mohali.
Kumar, R., Ghosh, S.K., Sangode, S.J., 1999. Evolution of a Neogene fluvial system in a Himalayan foreland basin, India. Spec. Pap. Geol. Soc. Am. 328, 239–256. https://doi.org/10.1130/0-8137-2328-0.239.
Li, B., Li, S.-H., 2006. Comparison of De estimates using the fast component and the medium component of quartz OSL. Radiat. Meas. 41, 125–136.
Liu, L., Yang, S., Liu, X., Cheng, T., Li, P., Zhou, J., Chen, Z., Luo, Y., 2022. Effects of the size of the test dose on the SAR protocol for quartz optically stimulated luminescence dating of loess in the eastern Tibetan Plateau. Quat. Geochronol. 72, 101365. https://doi.org/10.1016/j.quageo.2022.101365.
Lowick, S.E., Preusser, F., 2011. Investigating age underestimation in the high dose region of optically stimulated luminescence using fine grain quartz. Quat. Geochronol. 6, 33–41. https://doi.org/10.1016/j.quageo.2010.08.001.
Lowick, S.E., Preusser, F., Pini, R., Ravazzi, C., 2010a. Underestimation of fine grain quartz OSL dating towards the Eemian: comparison with palynostratigraphy from Azzano Decimo, northeastern Italy. Quat. Geochronol. 5, 583–590. https://doi.org/10.1016/j.quageo.2009.12.003.
Lowick, S.E., Preusser, F., Wintle, A.G., 2010b. Investigating quartz optically stimulated luminescence dose-response curves at high doses. Radiat. Meas. 45, 975–984. https://doi.org/10.1016/j.radmeas.2010.07.010.
Lu, Y.C., Wang, X.L., Wintle, A.G., 2007. A new OSL chronology for dust accumulation in the last 130,000 yr for the Chinese Loess Plateau. Quat. Res. 67, 152–160. https://doi.org/10.1016/j.yqres.2006.08.003.
Mandal, S.K., Scherler, D., Romer, R.L., Burg, J.P., Guillong, M., Schleicher, A.M., 2019. Multiproxy isotopic and geochemical analysis of the siwalik sediments in NW India: implication for the late cenozoic tectonic evolution of the himalaya. Tectonics 38, 120–143. https://doi.org/10.1029/2018TC005200.
Mejdahl, V., Wintle, A.G., 2020. Thermoluminescence applied to age determination in archaeology and geology. In: Thermoluminescence and Thermoluminescent Dosimetry. CRC Press, pp. 133–190.
Murray, A.S., Mejdahl, V., 1999. Comparison of regenerative-dose single-aliquot and multiple-aliquot (SARA) protocols using heated quartz from archaeological sites. Quat. Sci. Rev. 18, 223–229. https://doi.org/10.1016/S0277-3791(98)00055-9.
Murray, A., Olley, J., 2002. Precision and accuracy in the optically stimulated luminescence dating of sedimentary quartz. Geochronometria 21, 1–16.
Murray, A.S., Roberts, R.G., 1998. Measurement of the equivalent dose in quartz using a regenerative-dose single-aliquot protocol. Radiat. Meas. 29, 503–515. https://doi.org/10.1016/S1350-4487(98)00044-4.
Murray, A.S., Wintle, A.G., 2000. Luminescence dating of quartz using an improved single-aliquot regenerative-dose protocol. Radiat. Meas. 32, 57–73. https://doi.org/10.1016/S1350-4487(99)00253-X.
Murray, A.S., Svendsen, J.I., Mangerud, J., Astakhov, V.I., 2007. Testing the accuracy of quartz OSL dating using a known-age Eemian site on the river Sula, northern Russia. Quat. Geochronol. 2, 102–109. https://doi.org/10.1016/j.quageo.2006.04.004.
Murray, A., Arnold, L.J., Buylaert, J.-P., Guérin, G., Qin, J., Singhvi, A.K., Smedley, R., Thomsen, K.J., 2021. Optically stimulated luminescence dating using quartz. Nature Reviews Methods Primers. https://doi.org/10.1038/s43586-021-00068-5.
Nagar, Y.C., 2007. Methodological Aspects of Radiation Dosimetry of Natural Radiation Environment Using Luminescence Techniques: New Minerals and Application.
Palczewski, P., Biernacka, M., Chruścińska, A., 2022. Dose-response of the fast OSL component in quartz at the range of high doses. https://doi.org/10.13140/RG.2.2.34379.05924.
Porat, N., 2006. Use of magnetic separation for purifying quartz for luminescence dating. Anc. TL 24, 33–36.
Prescott, J.R., Robertson, G.B., 1997. Sediment dating by luminescence: a review. Radiat. Meas. 27, 893–922. https://doi.org/10.1016/S1350-4487(97)00204-7.
Prescott, J.R., Huntley, D.J., Hutton, J.T., 1993. Estimation of equivalent dose in thermoluminescence dating—the Australian slide method. Anc. TL 11, 1–5.
Qin, J.T., Zhou, L.P., 2009. Stepped-irradiation SAR: a viable approach to circumvent OSL equivalent dose underestimation in last glacial loess of northwestern China. Radiat. Meas. 44, 417–422. https://doi.org/10.1016/j.radmeas.2009.06.008.
Rahimzadeh, N., Tsukamoto, S., Zhang, J., Long, H., 2021. Natural and laboratory dose response curves of quartz violet stimulated luminescence (VSL): exploring the multiple aliquot regenerative dose (MAR) protocol. Quat. Geochronol. 65. https://doi.org/10.1016/j.quageo.2021.101194.
Rahimzadeh, N., Tsukamoto, S., Thiel, C., Frechen, M., 2023a. Progress and pitfalls of the SAR protocol for the quartz violet stimulated luminescence (VSL) signal: a case study from Sardinia. Quat. Geochronol. 75, 101433. https://doi.org/10.1016/j.quageo.2023.101433.
Rahimzadeh, N., Zhang, J., Tsukamoto, S., Long, H., 2023b. Characteristics of the quartz isothermal thermoluminescence (ITL) signal from the 375° C peak and its potential for extending the age limit of quartz dating. Radiat. Meas. 161, 106899.
Rao, A.R., Nanda, A.C., Sharma, U.N., Bhalla, M.S., 1995. Magnetic polarity stratigraphy of the Pinjor formation (upper siwalik) near pinjore, Haryana. Source Curr. Sci. 68, 1231–1236.
Rhodes, E.J., 1992. Optical Dating of Quartz from Sediments.
Roberts, R.G., Westaway, K.E., 2006. A Dual-Aliquot Regenerative-Dose Protocol (DAP) for Thermoluminescence (TL) Dating of Quartz Sediments Using the Light-Sensitive and Isothermally Stimulated Red Emissions.
Rodrigues, F.C.G., Porat, N., Mineli, T.D., Del Río, I., Niyonzima, P., Nogueira, L., Pupim, F. do N., Silva, C.G., Baker, P., Fritz, S., Wahnfried, I., Kiefer, G., Sawakuchi, A.O., 2022. Extended-range luminescence dating of central and eastern amazonia sandy terrains. Front. Earth Sci. 10, 1–11. https://doi.org/10.3389/feart.2022.888443.
Schmidt, C., Woda, C., 2019. Quartz thermoluminescence spectra in the high-dose range. Phys. Chem. Miner. 46, 861–875. https://doi.org/10.1007/s00269-019-01046-w.
Singarayer, J.S., Bailey, R.M., Rhodes, E.J., 2000. Potential of the slow component of quartz OSL for age determination of sedimentary samples. Radiat. Meas. 32, 873–880.
Singhal, M., Panda, M., Shinde, S.H., Mondal, S., Annalakshmi, O., Chauhan, N., 2024. Study of Thermoluminescence Characteristics of Quartz for High Radiation Doses (>1kgy): Implications for Extending the Luminescence Dating Range.
Singhvi, A.K., Sharma, Y.P., Agrawal, D.P., 1982. Thermoluminescence dating of sand dunes in Rajasthan. IND. Nature 295, 313–315. https://doi.org/10.1038/295313a0.
Singhvi, A.K., Stokes, S.C., Chauhan, N., Nagar, Y.C., Jaiswal, M.K., 2011. Changes in natural OSL sensitivity during single aliquot regeneration procedure and their implications for equivalent dose determination. Geochronometria 38, 231–241.
Smith, B.W., 1988. Zircon from sediments: a combined OSL and TL auto-regenerative dating technique. Quat. Sci. Rev. 7, 401–406. https://doi.org/10.1016/0277-3791(88)90036-4.
Spooner, N.A., Questiaux, D.G., 2000. Kinetics of red, blue and UV thermoluminescence and optically-stimulated luminescence from quartz. Radiat. Meas. 32, 659–666. https://doi.org/10.1016/S1350-4487(00)00067-6.
Stokes, S., 1994. The timing of OSL sensitivity changes in a natural quartz. Radiat. Meas. 23, 601–605. https://doi.org/10.1016/1350-4487(94)90106-6.
Taylor, J., 1997. Introduction to Error Analysis, the Study of Uncertainties in Physical Measurements.
Thiel, C., Buylaert, J.P., Murray, A., Terhorst, B., Hofer, I., Tsukamoto, S., Frechen, M., 2011. Luminescence dating of the Stratzing loess profile (Austria) - testing the potential of an elevated temperature post-IR IRSL protocol. Quat. Int. 234, 23–31. https://doi.org/10.1016/j.quaint.2010.05.018.
Timar-Gabor, A., Wintle, A.G., 2013. On natural and laboratory generated dose response curves for quartz of different grain sizes from Romanian loess. Quat. Geochronol. 18, 34–40. https://doi.org/10.1016/j.quageo.2013.08.001.
Timar-Gabor, A., Vasiliniuc, Ş., Vandenberghe, D.A.G., Cosma, C., Wintle, A.G., 2012. Investigations into the reliability of SAR-OSL equivalent doses obtained for quartz

samples displaying dose response curves with more than one component. Radiat. Meas. 47, 740–745. https://doi.org/10.1016/j.radmeas.2011.12.001.
Timar-Gabor, A., Constantin, D., Buylaert, J.P., Jain, M., Murray, A.S., Wintle, A.G., 2015. Fundamental investigations of natural and laboratory generated SAR dose response curves for quartz OSL in the high dose range. Radiat. Meas. 81, 150–156. https://doi.org/10.1016/j.radmeas.2015.01.013.
Topaksu, M., Correcher, V., Garcia-Guinea, J., Topak, Y., Göksu, H.Y., 2012. Comparison of thermoluminescence (TL) and cathodoluminescence (ESEM-CL) properties between hydrothermal and metamorphic quartzes. Appl. Radiat. Isot. 70, 946–951. https://doi.org/10.1016/j.apradiso.2012.03.017.
Toyoda, S., Rink, W.J., Schwarcz, H.P., Rees-Jones, J., 2000. Crushing effects on TL and OSL on quartz: relevance to fault dating. Radiat. Meas. 32, 667–672.
Vandenberghe, D., Kasse, C., Hossain, S.M., De Corte, F., Van den Haute, P., Fuchs, M., Murray, A.S., 2004. Exploring the method of optical dating and comparison of optical and 14C ages of Late Weichselian coversands in the southern Netherlands. J. Quat. Sci. Publ. Quat. Res. Assoc. 19, 73–86.
Wang, X.L., Lu, Y.C., Wintle, A.G., 2006. Recuperated OSL dating of fine-grained quartz in Chinese loess. Quat. Geochronol. 1, 89–100. https://doi.org/10.1016/j.quageo.2006.05.020.
Wang, X.L., Wintle, A.G., Lu, Y.C., 2007. Testing a single-aliquot protocol for recuperated OSL dating. Radiat. Meas. 42, 380–391. https://doi.org/10.1016/j.radmeas.2006.12.015.
Wang, X., Peng, J., Adamiec, G., 2021. Extending the age limit of quartz OSL dating of Chinese loess using a new multiple-aliquot regenerative-dose (MAR) protocol with carefully selected preheat conditions. Quat. Geochronol. 62. https://doi.org/10.1016/j.quageo.2020.101144.
Watanuki, T., Murray, A.S., Tsukamoto, S., 2005. Quartz and polymineral luminescence dating of Japanese loess over the last 0.6 Ma: comparison with an independent chronology. Earth Planet Sci. Lett. 240, 774–789. https://doi.org/10.1016/j.epsl.2005.09.027.
Wintle, A.G., 1973. Anomalous fading of thermo-luminescence in mineral samples. Nature 245, 143–144.
Wintle, A.G., 2008. Luminescence dating: where it has been and where it is going. Boreas 37, 471–482. https://doi.org/10.1111/j.1502-3885.2008.00059.x.
Wintle, A.G., Huntley, D.J., 1979. Thermoluminescence dating of a deep-sea sediment core [7]. Nature 279, 710–712. https://doi.org/10.1038/279710a0.
Wintle, A.G., Murray, A.S., 2006. A review of quartz optically stimulated luminescence characteristics and their relevance in single-aliquot regeneration dating protocols. Radiat. Meas. 41, 369–391. https://doi.org/10.1016/j.radmeas.2005.11.001.
Yoshida, H., Roberts, R.G., Olley, J.M., Laslett, G.M., Galbraith, R.F., 2000. Extending the age range of optical dating using single 'supergrains' of quartz. Radiat. Meas. 32, 439–446.
Zhang, J., Tsukamoto, S., 2022. A simplified multiple aliquot regenerative dose protocol to extend the dating limit of K-feldspar pIRIR signal. Radiat. Meas. 157, 106827. https://doi.org/10.1016/j.radmeas.2022.106827.

The Meteoritical Society

Meteoritics & Planetary Science 1–18 (2025)
doi: 10.1111/maps.70021

Luminescence characteristics of terrestrial Jarosite from Kachchh, India: A Martian analogue

Malika SINGHAL[1,2]*, Himela MOITRA[3], Souvik MITRA[4], Aurovinda PANDA[5], Jayant Kumar YADAV[5], D. Srinivasa SARMA[5], Devender KUMAR[5], Naveen CHAUHAN[1], Saibal GUPTA[3], and Ashok Kumar SINGHVI[1]

[1]Atomic and Molecular Physics Division, Physical Research Laboratory, Ahmedabad, India
[2]Indian Institute of Technology, Gandhinagar, Palaj, India
[3]Department of Geology and Geophysics, Indian Institute of Technology, Kharagpur, India
[4]Department of Geology, Presidency University, Kolkata, India
[5]CSIR-National Geophysical Research Institute, Hyderabad, India

***Correspondence**
Malika Singhal, Atomic and Molecular Physics Division, Physical Research Laboratory, Ahmedabad 380009, India.
Email: malikasinghal97@gmail.com

(Received 18 January 2025; revision accepted 09 July 2025)

Abstract–In this study, naturally occurring jarosite samples from Kachchh, India (considered to be Martian analogue) were characterized using Fourier Transform Infrared Spectroscopy (FTIR), Cathodoluminescence–Energy Dispersive X-ray Spectroscopy (CL-EDXS), and Luminescence (thermoluminescence [TL], blue and infrared stimulated luminescence [BSL and IRSL]) methods. FTIR and CL-EDXS studies suggested that jarosite preserves its luminescence characteristics even after annealing the samples to 450°C. This facilitated luminescence studies (TL/BSL/IRSL) to assess the potential use of luminescence-dating methods to establish the chronology of jarosite formation or its transport. Jarosite exhibited TL, BSL, and IRSL signals with varied sensitivities. The TL glow curve of jarosite comprised glow peaks at 100, 150, 300, and 350°C, reproducible over multiple readout cycles. The least bleachable TL glow peak at 350°C is reduced to $(1/e)^{th}$ of its glow peak intensity (i.e., 36%) with ~100 min of light exposure under a sunlamp. BSL and IRSL optical decay signals comprised three components. These signals exhibited athermal fading of g ~ 6%/decade, but pIRIR signal at 225°C showed a near zero fading. The saturation doses ($2D_0$) ranged from 700 Gy to 2600 Gy for different signals, which suggests a dating range of ~25 ka using a reported Martian total dose rate of 65 Gy/ka, primarily due to cosmic rays. Multiple TL glow peaks and their widely differing stability also offer promise to discern changes in cosmic ray fluxes over a century to millennia time scale through inverse modeling and laboratory experiments.

INTRODUCTION

Considerable efforts are being made to understand the surface processes on Mars, largely through remote sensing methods (Howari et al., 2021; Lancaster & Greeley, 1990; Rangarajan et al., 2018). To date, the chronological information on surface processes is established through crater counting, which is a relative dating method that has a poor resolution and needs calibration (Doran & Doran, 2004). With the anticipation of sample return and onsite measurements by space missions, instruments are being developed and modeling/measurements of the properties of rocks on the Martian surface are being carried out (Jain et al., 2006; Lepper & McKeever, 2000; Morthekai et al., 2007, 2008; Tsukamoto et al., 2011).

Luminescence techniques and, in particular, thermoluminescence (TL), have been used to understand the radiation, thermal history, and the metamorphic grades

of meteorites and lunar samples (Biswas et al., 2011; Geake & Walker, 1967; Sears et al., 2013). More recent efforts include the development of optically stimulated luminescence (OSL) readers for onsite dating using luminescence characteristics of minerals reportedly present in Martian sediments. Reports on rocks such as pyroxene, olivine, gypsum, obsidian, anhydrite, and various meteorites are now available (Jain et al., 2006; Lepper & McKeever, 2000; McKeever et al., 2003).

Luminescence dating is widely used for establishing chronologies of events associated with earth surface processes (Rhodes, 2011; Singhvi et al., 2022). It utilizes radiation-induced luminescence in natural minerals. A luminescence age is estimated by measuring the total luminescence and then scaling it with the annual rate of luminescence production in the mineral. Appropriate laboratory calibration enables conversion of luminescence intensity to radiation dose units (energy deposited per unit mass) and is termed paleodose. The annual rate of dose deposition (i.e., dose rate) responsible for luminescence production is estimated by measuring the concentration of natural radioactivite elements in ambient environment viz. U, Th, and K and the cosmic rays through the use of standard prescriptions. In the case of Mars, the radiation dose is predominantly from cosmic rays (Morthekai et al., 2007) with a small contribution from U, Th, and K present in the surrounding soil matrix.

The use of luminescence signal for chronology requires that it to be stable over geological times, which has to be ascertained for each sample/mineral phase/grain used for dating. Stability of a luminescence signal is determined by:

a. thermal kinetics, which depends on the ambient temperature, crystal properties, and trap depth of trapping centers. Trapping of charges in these centers is assumed to follow the Arrhenius equation and
b. temperature independent, athermal quantum mechanical tunneling effects, which result in a reduction in trapped charges at a time-dependent rate (Wintle, 1973). Laboratory measurements and modeling are used to correct for such a signal loss over time (Huntley, 2006; Kars et al., 2008).

Several minerals and materials are used as luminescence chronometers. These include quartz, feldspar, gypsum, calcite, olivine, zircon, pyroxene, basalts, and volcanic ashes (Aitken, 1985; Biswas et al., 2013; Clark-Balzan et al., 2021; Jain et al., 2006; Nagar, 2007; Zhang & Wang, 2020). The abundance of quartz on Mars is negligible (Smith & Bandfield, 2012). Most of the feldspar on the Martian surface is of basaltic origin and should therefore be prone to athermal fading (Wintle, 1973). Morthekai et al. (2008) reported that athermal fading for the basalts cannot be adequately corrected. Further, presently available models do not ensure proper corrections (Biswas et al., 2013; Gliganic et al., 2012; Rajapara, 2014), and to an extent, this limits the use of basaltic feldspars as a geochronometer on Mars.

Spectroscopic measurements from Mars missions viz., *Curiosity*, *Mars Pathfinder*, and others, suggested the presence of jarosite on the surface of Mars. Morris et al. (2000) used optical and Mössbauer spectroscopic data from the Pathfinder mission to confirm the presence of jarosite. Rovers, *Opportunity* (MER-B) and *Curiosity* (Klingelhöfer et al., 2004) reconfirmed the presence of jarosite on Mars using Mossbauer spectroscopy. The formation of jarosite requires a wet (but water-limited) acidic environment, and therefore, its very presence implies the existence of water. Additionally, jarosite has the ability to incorporate foreign molecules in its structure; for example, glycine has been detected in natural jarosite on Earth (Kotler et al., 2008). This adds value to the mineral in detecting biological activity on Mars.

Since jarosite is a widespread mineral on the Martian surface, it can be used to study surface processes on Mars and establish the associated timing of related processes. This work attempts to characterize the luminescence dosimetry and dating properties of jarosite in order to explore its feasibility for dating Martian surfaces.

FORMATION AND CHEMICAL PROPERTIES

Jarosite is an anhydrous sulphate of the "alunite super group" with a general composition $AFe_3(SO_4)_2(OH, H_2O)$, where A is a metal (such as Ag, 1/2Pb, Na, K Rb Tl, 1/2Hg, or hydronium). For jarosite, A is potassium. In nature, five kinds of metal substitutions can occur, forming hydronium (hydronium jarosite), sodium (natrojarosite), silver (argentojarosite), lead (plumbojarosite) and ammonium (ammoniojarosite) (Roca, 2022).

Jarosite forms through the weathering of sulphide ores in acidic sulphate soils or through the oxidation of iron by microorganisms under bioleach environments (Roca, 2022). Its occurrences are reported from USA, Brazil, Canada, Iran, Romania, Greece, and India (Bhattacharya et al., 2016; Klingelhöfer et al., 2004; Marescotti et al., 2010; Reynolds, 2007; Velasco et al., 2013; Viñals et al., 1995, 2003). Jarosite occurs in four distinctive settings, viz. (a) in sulphide ores due to oxidation or in arid areas with pyrite-bearing rocks; (b) as nodules in clays; (c) as segments of acid soils; and (d) as hypogene minerals (Dutrizac & Jambor, 2000). Synthetic jarosite can be prepared by heating the metal sulfate and sulfuric acid solution at ~100°C, leading to its precipitation (Dutrizac & Kaiman, 1976; Fairchild, 1933).

Jarosite structure comprises alternating tetrahedral and octahedral sheets. $Fe(O, OH)_6$ occupies octahedral

TABLE 1. Sample details.

Sr. No.	Samples	Formation	Latitude	Longitude	Main lithology
1	56B2	Guneri	23°47′07″ N	68°50′22″ E	Shale, Sandstone, Laterite
2	57D2	Guneri	23°47′01″ N	68°50′22″ E	Shale, Sandstone, Laterite
3	65B2	Naredi	23°34′47″ N	68°38′52″ E	Shale, Limestone
4	66B2	Naredi	23°34′43″ N	68°38′38″ E	Shale, Limestone
5	67F2	Naredi	23°34′31″ N	68°38′36″ E	Shale, Limestone
6	68B2	Harudi	23°31′28″ N	68°41′08″ E	Shale, Limestone

sites connected by four hydroxyl groups, with a neighboring octahedral sheet and with two oxygen atoms of [SO_4] at a tetrahedral site (Xu et al., 2010). Metals (Ag, Pb, Na, K Rb Tl, Hg, etc.) reside in a 12-fold coordinated site, linked to 6 atoms of O from neighboring [SO_4] and 6 atoms from OH in $Fe(O, OH)_6$.

Numerous studies on the thermal stability of jarosite exist. Neutron diffraction studies on deuterated jarosite show that jarosite is stable up to 277°C, beyond which it decomposes into yavapaiite, hematite, and D_2O vapor (Xu et al., 2010). At 302°C, diffraction peaks of yavapaiite and hematite appear, and jarosite gets decomposed at 327°C as follows,

$$KFe_3(SO_4)_2(OD)_6 \rightarrow KFe_3(SO_4)_2 + Fe_2O_3 + 3D_2O \quad (1)$$

Thermogravimetric and mass spectrometric analysis show successive mass loss from 130°C to 330°C in K jarosite, which has been attributed to the loss of water. The weight loss at 500°C has been attributed to the loss of sulfur (Frost et al., 2005). For Na-jarosite, mass loss occurs between 215°C and 230°C, followed by further mass losses at 352°C and 555°C. For Pb-jarosite, mass loss occurs at 390°C and 418°C. The presence of Fe^{3+} in jarosite is responsible for its magnetic properties (Inami et al., 2000; Wills et al., 2000). It may be noted that jarosite decomposes in both the alkaline and acidic media, but it does not dissolve in water (Cruells & Roca, 2022).

SAMPLES AND METHODS

Sample details

Table 1 provides the details of six natrojarosite samples collected from Kachchh, India, for this study. The samples were from different stratigraphic units in sediment successions at Kachchh. The relevant part of the Mesozoic succession is described by Desai and Saklani (2012), and the Tertiary stratigraphy is documented in Biswas (1992). Samples 57D2 and 56B2 are from the Guneri member of the Mesozoic Bhuj Formation. Samples 65B2, 66B2, and 67F2 are from the Upper Paleocene to Lower Eocene Naredi Formation, and sample 68B2 is from the Middle Eocene Harudi Formation. The host rocks are predominantly shales, with natrojarosite occurring in veins that cut across and are also parallel to the layering. Bhattacharya et al. (2016) established the presence of jarosite in the Matanumadh Formation of Kachchh using X-ray diffraction and FTIR methods, and the mode of occurrence was used by them to present the locality as a mineralogical Martian analogue. The present study includes jarosite samples from a location near the Matanumadh Formation given in Table 1 and shown in Figure 1.

Measurement techniques

FTIR spectra of the powder samples were measured using a NICOLET 6700 (Thermo Fisher Scientific Instruments, USA) at the Central Research Facility at the Indian Institute of Technology Kharagpur. CL imaging was performed using a Hitachi S-3400 N scanning electron microscope at the CSIR-National Geophysical Research Institute, Hyderabad, with a 15 kV electron beam. The EDXS spectra were measured with the electron beam focused on luminescing phases, using the Oxford Ultim max 40 system, and Aztec© software was used to obtain the EDXS spectra.

TL and OSL were measured on fine grain (4–11 μm) fractions of Jarosite samples using a commercial Risoe TL/OSL reader DA-15 (with facilities for linear heating, blue [450–490 nm] or infrared [817–883 nm] LEDs for optical stimulation) at the Physical Research Laboratory, Ahmedabad. The detection units comprised an EMI 9635 QA photomultiplier tube coupled to a Schott BG-39 filter (330–625 nm) for TL; U340 (300–380 nm) for BSL and pIRIR225; and Schott BG39 + BG3 transmitting in 400–480 nm for IRSL and pIRIR 225 (Bøtter-Jensen et al., 2003; Thomsen et al., 2006). A Sr^{90}/Y^{90} beta source, calibrated for fine grain quartz (4–11 μm grains), was used. The dose rate for quartz was 0.033 and 0.056 Gy/s. The corresponding absorbed dose for fine grain jarosite calculated using the stopping power was 0.038 and 0.066 Gy/s, respectively. A calibrated alpha source, Am^{241}

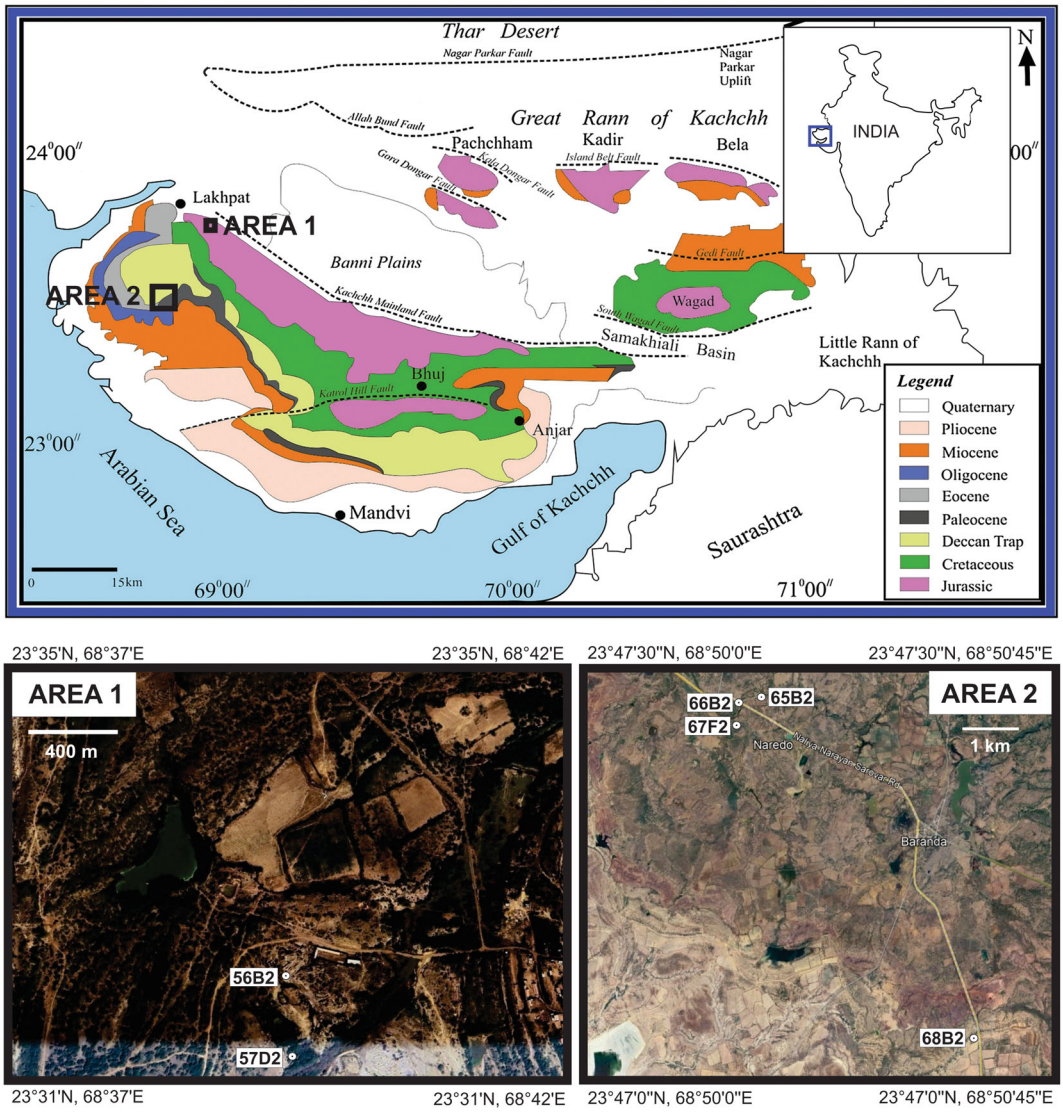

FIGURE 1. Map showing the location of samples used in this study. The blue inset on the map of India shows the geological map of the Kutch region, modified after Biswas (1992), Karanth and Gadhavi (2007) and Bhattacharya et al. (2016). Insets with open black boxes are for Area 1 showing the locations for samples 56B2 and 57D2, and Area 2 for samples 65B2, 66B2, 67F2 and 68B2 on satellite images from Google Earth Pro.

with a strength of 0.074 $\mu m^{-2} min^{-1}$ was used for alpha irradiations (Singhvi & Aitken, 1978). A linear heating rate of 2°C/s up to 450°C was used for TL measurements.

Thick source alpha counting and sodium thallium-activated (NaI(Tl)) scintillation counter were used to estimate the U, Th, and K concentration in the sample.

Measurements

Samples were characterized using Cathodo-luminescence–Energy Dispersive X-ray Spectroscopy (CL-EDXS) and Fourier Transform Infrared Spectroscopy (FTIR), and for their thermally and optically stimulated luminescence characteristics. Key issues examined were the effect of heating on luminescence and attendant properties to establish the use of jarosite for geochronometry.

Sample characterization

The studies were carried out to characterize jarosite before and after annealing to 450°C. For FTIR, finely powdered samples were pressed into pellets after mixing them with dehydrated KBr powder in a weight ratio of 1:300. FTIR spectra of the powder samples were collected in transmittance mode in the spectral range of 4000–400 cm^{-1} at a spectral resolution of 4 cm^{-1}, and both, the samples as received and their fractions annealed to 450°C were measured.

For CL-EDXS measurements, samples were placed on 15 × 4 mm stubs with a double-sided tape. The samples were carbon-coated using a Hitachi E-1010 Ion Sputter carbon coating unit operating under a vacuum of 1 Pascal with a current of ~14 amperes. The samples were examined in the CL mode, and the X-ray spectrum was taken by focusing the electron beam on the luminescent phases. EDXS on luminous portions was measured, and at least 10 brightest luminescent points for each sample (natural and annealed) were probed. EDXS spectra yielded elemental data in weight percentages corresponding to each spot. To make calculations and visualization easier, the average weight % of elements across all measured spots in a sample was calculated for both natural and annealed samples. Comparative analysis was then carried out by plotting the elements against their average weight percentages for each set of samples to understand the differences between the natural and annealed (to 450°C) conditions.

Luminescence measurements

The measurements were carried out in an oxygen free ultrapure nitrogen environment. Though the samples were collected as bulk rock in daylight, but once received, the entire laboratory processing and analysis was carried out under subdued red light (>630 nm). Pretreatment of the grains with 1 N HCl for 2 min increased the luminescence yield in comparison to the samples as received and therefore, all samples were treated with HCl, and then measurements were carried out on fine grains mounted on standard stainless steel discs. Sample 56B2, had the highest luminescence sensitivity (LS, luminescence per unit mass) and per unit radiation dose (counts/(mg/Gy)) and was therefore used for most of the analysis for TL/OSL properties. The following measurements were carried out.

a. *TL and OSL characteristics*: The TL glow curves were recorded from room temperature up to 450°C at a heating rate of 2°C/s. Measurements were done on natural samples (as received) and the same samples after an irradiation of 19 Gy to investigate the effect of heating above the decomposition temperature of jarosite on the glow curve. Blue stimulated luminescence (BSL) was recorded at 200°C for 100 s after a preheat of 250°C for 10 s, and infrared stimulated luminescence (IRSL) was measured at 50°C and 225°C for 100 s and after a preheat of 250°C for 60 s.
b. *TL Sensitivity*: LS of 80–100°C glow peak was measured for all the samples by heating to 250°C, irradiating with 19 Gy beta dose, and normalizing the photon counts (luminescence intensity) by the weight. The effect of heating on LS was compared by integrating the photon counts between 50°C and 200°C (by heating to 250°C and 450°C) and weight normalizing the integrated photon counts. The protocol is given in Figure S1a.
c. *Reproducibility*: The protocol in Figure S1b was used to measure the effect of repeated irradiation, heating, and measurement (TL/BSL/IRSL) cycles to check the reproducibility of the signals.
d. *Thermal stability*: Kinetic parameters such as activation energy [E(eV)], frequency factor [$s(s^{-1})$], and the lifetime of charges in their trap [$\tau(s)$] were estimated using the fractional glow method (Gobrecht & Hofmann, 1966; Pietkun et al., 1992; Shalgaonkar & Narlikar, 1972). Three aliquots of the sample 56B2 were irradiated with a 325 Gy beta dose, heated to 40°C (T_i), cooled to room temperature, and then heated again to $T_i + 10$°C. This was repeated till 450°C. The activation energy and lifetime for each cycle were estimated from the Arrhenius plot and by fitting the luminescence intensity with temperature using the equation.

$$I = -\frac{dn}{dt} = nse^{\frac{-E}{kT}} \quad (2)$$

e. *TL bleachability*: Bleachability of various TL glow peaks by light exposure under solar simulator lamp (Osram, Ultravitalux, 300 watts filtered through a window glass) was investigated. In this, aliquots of sample 56B2 were annealed to 450°C, irradiated (300 Gy) and bleached under a solar lamp for time periods varying from 0 to 1000 min. The integrated photon counts (±5°C of the peak counts) of glow peaks 150°C, 210°C, 300°C, and 350°C were weight normalized and plotted with bleach times.
f. *Dose–response curve*: The growth of luminescence signal (TL/BSL/IRSL) with radiation dose was studied. Single aliquot regenerative (SAR) type protocol was used to construct the dose–response curves (DRC) (Murray & Wintle, 2000). The DRC was fitted with the following single saturating exponential equation

$$I = I_0\left(1 - e^{-\frac{D}{D_0}}\right) \quad (3)$$

where, I is the intensity at dose (D), and D_0 is the saturation dose defined as the dose where the intensity is 66% of maximum intensity (I_0). The maximum dose that can be estimated is twice the characteristics dose (D_0), after which the error increases.

The recycling ratio (ratio of luminescence produced by the same dose but at different cycles of the protocol) and recuperation (ratio of luminescence due to zero dose to natural dose) were measured for a repeated and

TABLE 2. Various protocols used to estimate the dose.

Step. No.	TL450	$BLSL200_{UV}$ (modified after Wintle and Murray (2006))	$IR50_{blue}$ (Wallinga et al., 2000)	$pIRIR225_{blue}$ (Buylaert et al., 2009)	$pIRIR225_{UV}$ (Buylaert et al., 2009)
1	Natural dose/ Regenerative dose	Natural dose/Regenerative dose	Natural/ Regenerative dose	Natural/ Regenerative dose	Natural dose/ Regenerative dose
2	TL 250°C	Preheat 250°C for 10 s	Preheat 250°C for 60 s	Preheat 250°C, 60 s	Preheat 250°C, 60 s
3	TL 450°C	BSL at 200°C for 100 s	IRSL at 50°C for 100 s	IRSL at 50°C, 100 s	IRSL at 50°C, 100 s
4	Go to step 1	Test dose	Test dose	IRSL at 225°C, 200 s	IRSL at 225°C, 200 s
5		Preheat 250°C for 10 s	Preheat 250°C for 60 s	Test dose	Test dose
6		BSL at 200°C for 100 s	IRSL at 50°C for 100 s	Preheat 250°C, 60 s	Preheat 250°C, 60 s
7		Go to step 1	Go to step 1	IRSL at 50°C, 100 s	IRSL at 50°C, 100 s
8				IRSL at 225°C, 200 s	IRSL at 225°C, 200 s
9				Go to step 1	Go to step 1
Emission under investigation (nm)	330–625	280–380	400–480	400–480	280–380

zero doses, respectively. For TL, as the samples showed good reproducibility, a regenerative measurement protocol without any sensitivity correction was used. For BSL and IRSL, the sensitivity correction used test dose normalization. A modified version of protocols suggested by Wintle and Murray (2006) was used to construct the dose–response curve (DRC) for BSL 200_{UV}. Here, the measurement was carried out at 200°C to prevent recapture of charges in glow peaks <200°C.

For IRSL, measurements were made at 50°C in the blue detection window (Wallinga et al., 2000); IRSL at an elevated temperature of 225°C was also measured in UV and blue detection windows after the measurement of IR50 (named pIRIR225) (Buylaert et al., 2009). The measurement protocols are given in Table 2.

g. *Athermal fading*: Athermal fading rates were estimated by irradiating the sample to a fixed (100 Gy) beta dose, followed by measurement after variable time delays. The protocol is given in Figure S1c (Huntley, 2006; Huntley & Lamothe, 2001; Kars et al., 2008).

h. *Dose rate estimation*

1. *Alpha and charge particle luminescence induction efficiency*: The track length of charge particles in a crystal matrix depends on their charge, mass, and energy. Thus, dose deposition by alpha particles with higher charge and mass is confined to short track lengths (~μm) resulting in a very high ionization charge density implying loss of charges being trapped and a consequent reduction in luminescence production per unit dose of alpha as compared to weakly ionizing beta particles (Aitken, 1985; Zimmermans, 1972). For low energy alpha particles, as in the case of terrestrial sediments, a ratio of luminescence produced per unit dose of alpha to beta, called alpha efficiency (a-value), is measured and included in the computation of annual dose rate. The a-value is measured by bleaching the samples for 5 h and irradiating using ^{241}Am, in a vacuum alpha irradiator (Singhvi & Aitken, 1978) for 120 min. The protocols used to recover the dose, as per Table 2, were used to measure the "a-value." On the Martian surface, the major source of ionizing radiation is largely high energy protons, and limited studies so far (Jain et al., 2007) suggest that the luminescence production efficiency would be in the range 0.5 to 1. Pending these measurements for the case of Jarosite, we used a luminescence production efficiency of 1 for an integrated cosmic ray flux on Mars.

2. *Radioactivity measurements*: Thick source alpha counting was used to estimate radioactive element concentration. In this, a thick layer (~2 mm) of sample in direct contact with ZnS:Ag scintillator was kept in a perspex holder over a photomultiplier tube. Alpha-induced scintillations/unit area/unit time were measured to estimate U and Th concentration. NaI-scintillation counting was used to measure K

concentration through the 1.46 MeV gamma ray from ^{40}K. The sample was mounted in plastic vials and compared with the gamma ray counts provided by the standard (AR grade KCl), counted under identical geometry and after appropriate correction for instrument and Compton background. The concentration was estimated by the peak area comparison method.

RESULTS

FTIR and CL-EDX studies were carried out to ascertain possible structural changes in Jarosite due to heating.

FTIR

The mid-infrared spectra (Figure 2) of samples 57D2, 57D2A and 66B2A were typical of jarosite (Bhattacharya et al., 2016; Bishop & Murad, 2005; Cloutis et al., 2006; Farmer, 1974; Sarkar et al., 2022). Spectra of 57D2 and 66B2 were nearly identical. The difference between the spectra of the annealed and non-annealed samples suggests that the non-annealed sample has a higher overall absorbance, indicating a larger proportion of crystalline jarosite. The spectral absorptions attributed to jarosite used in this study are listed in Table 3.

CL-EDXS studies

The comparison of EDXS spectras for natural and annealed samples (Figure 3) indicated that in most samples, annealing leads to a relative decrease in oxygen and aluminum, and an increase in potassium and sulfur concentrations. The iron content for samples 66B2 and 57D2 remained unchanged after annealing and decreased for 65B2 and 68B2. The calcium concentration in 65B2 and 68B2 on annealing increased from 6.6% to 25.5% and 1.6% to 8.2%, respectively. These variations indicate that annealing alters elemental distribution to a limited extent, suggesting changes in crystal structure or elemental diffusion that are sample dependent.

Luminescence measurements

TL glow curves

Figure 4 shows the weight normalized TL glow curves of natural and irradiated jarosite. Natural jarosite comprises a broad glow peak from 200°C to 450°C, and the beta-irradiated samples had additional glow peaks at 100°C and 150°C. Figure 5 shows the TL glow curve of sample 56b2 at 260 Gy, where the 100°C and 150°C glow peaks cannot be distinguished. This suggests that jarosite has multiple convoluted glow peaks, possibly at 100°C, 150°C, 300°C, and 350°C.

Figure S2a shows the results for multiple cycles of irradiation and heating to 250°C, that is, below the temperature for loss of stoichiometric water. Figure S2b shows the luminescence intensity variation with cycles of repeated irradiation and readout. Figure S3a,b shows changes in glow curve shape and luminescence sensitivity after cut heating to 450°C. In both cases and for all the glow peaks in multiple cycles of heating to 250°C and 450°C, the reproducibility of luminescence intensity was within 1% and 6%, respectively. This

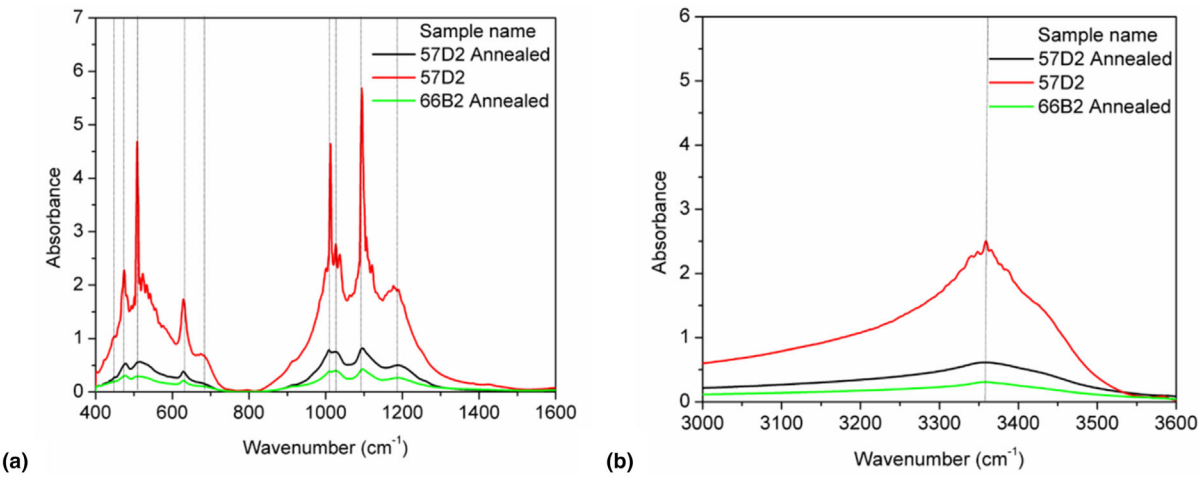

FIGURE 2. Mid-infrared spectra of samples 57D2, 57D2 Annealed, and 66B2 Annealed from (a) 400 to 1600 cm^{-1} to study the fundamental absorptions and (b) from 3000 to 3600 cm^{-1} to study the absorptions due to the hydroxyl ion. These show that jarosite signatures are preserved even after annealing to 450°C. The marked lines are discussed in Table 3.

TABLE 3. FTIR spectral absorption attributes of jarosite.

Wave number	Molecular transition	Attribute
449	$\nu 2$ (SO_4)-2	Fundamental bending vibrations in sulphate ion
474	M-O(M:Al/Fe)	Metal-oxygen vibrations
508	M-O(M:Al/Fe)	Metal-oxygen vibrations
629	$\nu 4$ (SO_4)-2	Fundamental stretching vibrations in sulphate ion
673	$\nu 4$ (SO_4)-2	Fundamental stretching vibrations in sulphate ion
1012	δ(OH)	In-plane bending vibrations of hydroxyl ion
1025	δ(OH)	In-plane bending vibrations of hydroxyl ion
1094	$\nu 3$ (SO_4)-2	Fundamental stretching vibrations in sulphate ion
1189	$\nu 3$ (SO_4)-2	Fundamental stretching vibrations in sulphate ion
3358	ν (OH)	Fundamental stretching vibrations in hydroxyl ion

suggests that despite heating, the luminescing phase remains unaltered, and these accord with FTIR and EDXS results.

Figure 6 shows that the LS of samples from different locations is variable. Guneri jarosite has the highest LS. After heating to 450°C, LS for samples 66B2, 57D2, and 56B2 decreased, while it increased for the samples 65B2, 67F2, and 68B2. Further, Figure 5 shows that heating to 450°C changes the LS of the sample; however, the glow curve shape does not change.

Stability: Kinetic Parameters

Figure 7 provides the plot of activation energies with a maximum temperature of heating for both unannealed and annealed samples. Regions of plateau are marked as a suggestion of a charge trap. The activation energy was the same for annealed and non-annealed samples till 300°C, after which deviation is observed. Table 4 provides the data. Assuming first-order kinetics, the lifetime for the glow peak centered at 350°C in the case of the unannealed sample is ~0.3 Ma. For the annealed sample, two plateaus above 300°C are observed, with the highest lifetime of ~31 Ma for the glow peak at 360°C. Further, there exist regions of continuous increase in the activation energy (from room temperature to 100°C, from 240 to 300°C), suggesting additional nearby lying traps.

TL DRC and fading

ince TL glow curves show reproducibility within a ~5%–6%, regeneration protocol (Table 2) based DRC was constructed, without the use of conventional test dose sensitivity correction. Figure 8a,c show the DRC of sample 56B2. The growth curve was fitted to a single saturating exponential, with equal weightage to all data points. Low temperature (210°C glow peak) and high temperature (350°C glow peak) DRC was constructed from step 2 and step 3 of Table 2, respectively. TL glow peaks at 210 and 350°C have saturation doses ~2600 and 1600 Gy, respectively. The recycling ratio and recuperation were within 10 and 5%, respectively, suggesting that the regeneration protocol was suitable for estimating the absorbed doses using TL. Athermal fading (Figure 8b,d) with a g-value of 4.27%/decade and near zero was observed for the 210 and 350°C glow peaks. "a"-value (Table 5) for alpha particles was 0.075 and 0.051 for the 210°C and 350°C glow peaks, respectively.

Bleaching of luminescence under a solar lamp

The bleachability of sample 56B2 is shown in Figure 9. In this, the intensities of glow peaks 150°C, 210°C, 300°C, and 350°C were weight normalized. TL reduce to 1/e (36%) of the maximum intensity after 16, 20, 70, and 105 min of solar lamp exposure for glow peaks at 150°C, 210°C, 300°C, and 350°C respectively. This rate would be expectedly faster on the Martian surface due to the higher intensity of solar UV penetrating to the surface (Haberle, 2015; Solomon et al., 2005).

Optically Stimulated Luminescence

Blue Stimulated Luminescence (BSL) characteristics

A typical blue stimulated luminescence decay curve (measured at 200°C, after a preheat of 250°C in the ultraviolet detection window; named $BSL200_{UV}$) is shown in Figure 10 for sample 56B2 irradiated to 350 Gy (natural signal bleached using blue LED for 100 s at 200°C). The decay comprises three components (Figure S6) and relevant parameters are summarized in Table S1.

Figure S7 shows the reproducibility of different components of the BSL optical decay curve on repeated irradiation (40 Gy) and blue light stimulation. Reproducibility of three components of $BSL200_{UV}$ was within 10%. The reproducibility experiments suggested a need for LS correction in constructing DRC (Figure 10).

The saturation dose for $BSL200_{UV}$ is 867 ± 85 Gy. This signal has athermal fading rate of 6.64 ± 0.82%/decade and, a-value of 0.093 ± 0.01.

Infrared Stimulated Luminescence (IRSL) characteristics

The jarosite samples also showed infrared stimulated luminescence in blue (400–480 nm). The optical decay curves of IRSL at 50°C (IRSL50) are shown in Figures 10 and S8. Figure S9 shows the reproducibility of the sample.

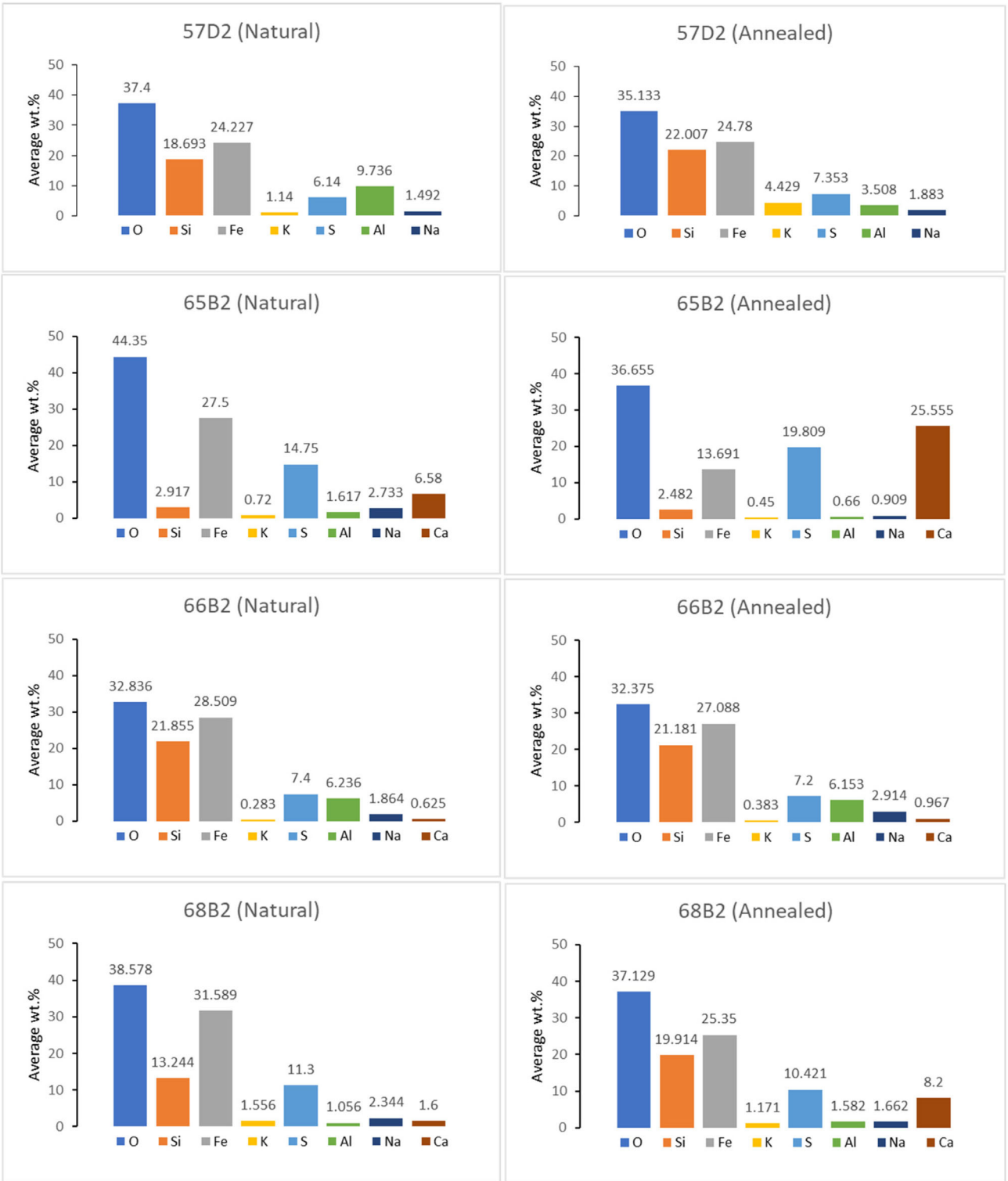

FIGURE 3. Elemental composition of phases luminescing under CL. Natural and annealed samples. Annealing was at 450°C.

For IRSL measurements, the average deviation between repeated signals was 3%, 3%, and 14% for the fast, medium, and slow components, respectively.

DRC and fading. The saturation dose for IRSL50 is 1180 ± 180 Gy, and the athermal fading g-value was $7.4 \pm 0.7\%$/decade. Recuperation and recycling were

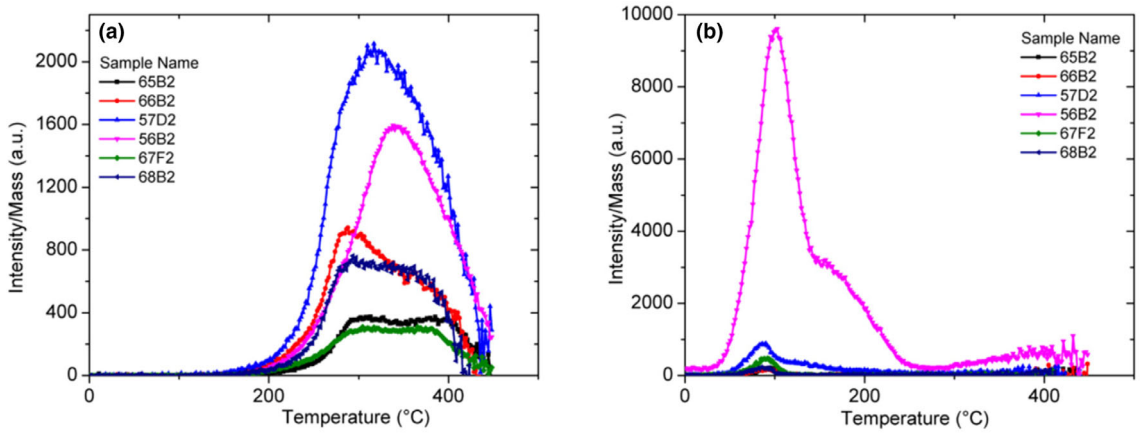

FIGURE 4. TL Glow Curves of samples in emission range 325–700 nm; (a) Natural grains with HCl wash. (b) Beta-irradiated (19 Gy) grain after a preheat of 450°C.

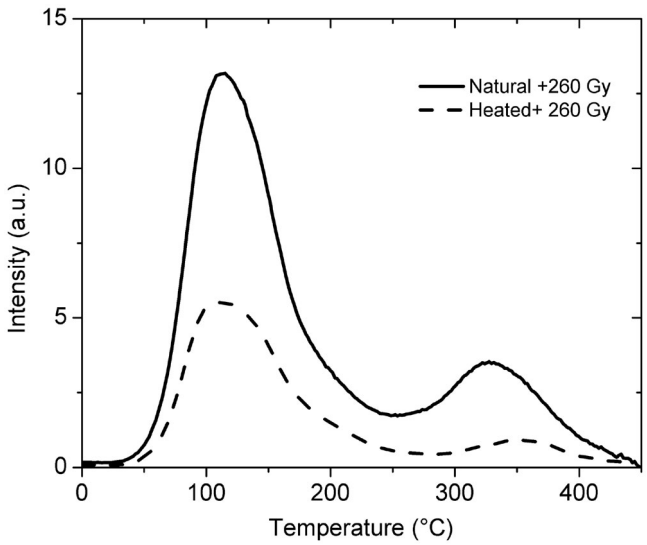

FIGURE 5. Sample 56B2. TL when the natural sample is given a dose of 260 Gy and when the same heated sample is given a dose of 260 Gy.

< 10%. Further, the saturation dose for pIRIR225 UV detection window is 817 ± 95 Gy and for pIRIR225 blue detection window is 685 ± 36 Gy. Near zero athermal fading is obtained for both the pIRIR225 signals. The "a-values" are of 0.058 ± 0.005, 0.041 ± 0.004, and 0.029 ± 0.002 for IR50 (blue), pIRIR225 (blue), and pIRIR225 (UV), respectively. The results are shown in Figure 10.

DOSE RATE

Table 6 provides the details of the measured radionuclide concentration. Radionuclide dose for the present samples based on the measured radioactivity for concentration is 1.62 ± 0.6 mGy/year. The thin atmosphere of Mars implies a higher cosmic ray dose contribution to the dose rate compared to the Earth. Calculation done using GEANT4 simulation (Morthekai et al., 2007) yields a cosmic dose rate estimation of 63 mGy/year for the solar minimum condition. Summing this with the measured internal dose rate approximates an average total dose rate of ~65 mGy/year for the Martian surface, assuming a luminescence induction efficiency of 1.

DISCUSSION

Jarosite is abundant on Mars and its use for dosimetry and dating can inform both on cosmic ray fluxes through time and on time scales of various surface processes on Mars. This study characterized six jarosite samples from an analog site in Kachchh, India. Jarosite exhibited TL/BSL/IRSL. TL glow peaks were observed at 100°C, 150°C, 300°C, and 350°C in the detection range of 330–625 nm (Figures 4 and 6). The similarity in glow curve shapes after heating and remeasurement of TL suggests that heating of jarosite at ~277°C and at ~352°C do not interfere with its luminescing phases (Figure 5). However, a change in the LS of the samples with heating did occur (Figure 6). Samples that show enhancement in the sensitivity were accompanied by a decrease in iron and an increase in calcium, but for the samples that exhibited a decrease in sensitivity, the iron content remains unchanged (Figures 3 and 5b). As iron is a well-established quencher of luminescence properties, the increase in luminescence sensitivity with a decrease in iron content appears plausible (Nambi, 1977). Further, as jarosite signatures are visible in the

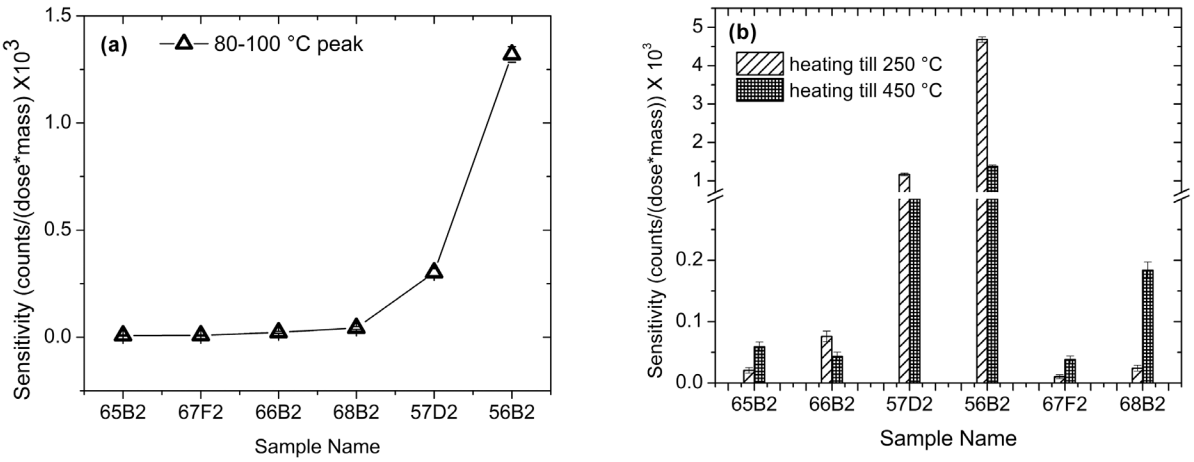

FIGURE 6. (a) Sensitivity of 80–100°C peak was measured for all samples by heating to 250°C, then giving a dose of 19 Gy. (b) Effect of heating to 250°C and 450°C on the sensitivity of 50–200°C peak.

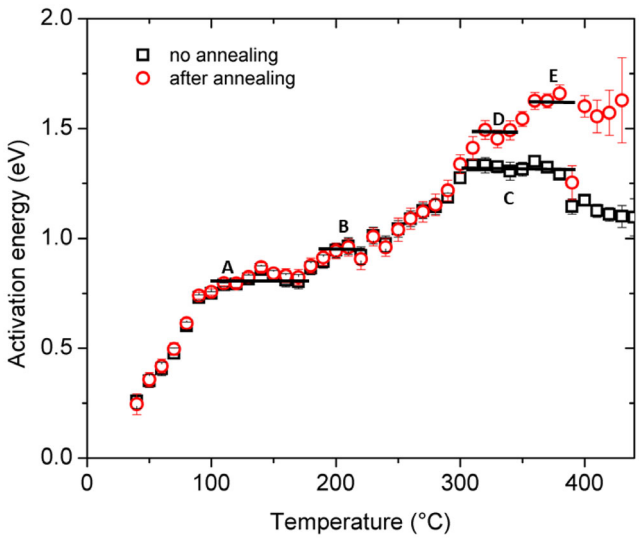

FIGURE 7. Activation energy versus maximum heating temperature graph for 56B2 obtained by Fractional glow curve method. Observation in emission range 330–625 nm.

annealed FTIR spectra, it is reasonable to infer that complete breakdown of jarosite does not occur on heating up to 450°C.

Luminescence dating depends on the basic premise that the initial luminescence signal was zero or near zero. This could occur in two contexts: First, the formation event, where the radiation-induced luminescence is ab initio zero. The second is bleaching due to daylight exposure and burial thereafter. Laboratory studies on bleaching show that the glow peaks could be bleached in 100 min (Figure 9) under a sunlamp. On Mars, higher UV flux due to a thin atmosphere (5–38 g/cm^2; Haberle, 2015; Solomon et al., 2005; Figures S4 and S5) would ensure an even more effective bleaching, given that UV has a higher cross-section for photo-bleaching (Spooner, 1987). The least bleachable glow peak (350°C) attains residual after 105 min of exposure to a solar lamp (Figure 9).

The upper limit of dating and dose estimates is constrained by the saturation of the luminescence intensity with radiation dose and the stability of the charges in the trap. Various signals of jarosite show variable saturation. The saturation doses were 800 Gy ($BSL200_{UV}$); 1180 Gy (IRSL50 blue detection), 1600 Gy TL450 (350 peak) (Figures 8 and 10). pIRIR225 UV detection window exhibited a saturation dose ~750 Gy, and for pIRIR225 blue detection window, the saturation dose was 590 Gy (Figure 10). All these signals can be used for dating and dosimetry.

From the thermal stability analysis, a similarity in annealed and non-annealed values suggests that the trap structure remains unaltered till 300°C, after which deviation occurs. However, a notional lifetime of 0.3 Ma for the non-annealed samples puts a constraint on dating only young events on the surface (Figure 7, Table 2).

Various other dating relevant parameters like athermal fading, alpha efficiency were measured. The athermal fading rate measurements for BSL200, IRSL50, and TL450 (210 peak) yielded g values of 7.6, 7.4, and 4.3%/decade respectively and these have to be corrected for dose estimates. Alternatively, pIRIR225 signals and TL450 (350 peak) signals with near zero athermal fading can be useful (Figures 8 and 10, Table 5).

A new possibility for future studies is provided by the present results, and these relate to ascertaining the validity of athermal fading rates as estimated in the laboratory. These arise from the fact that the saturation/equilibrium doses in different optical

TABLE 4. Kinetic parameters for 56B2.

Sample as received followed by 325 Gy beta dose					Samples after heating to 450°C for 10 s followed by 325 Gy beta dose				
Peak	Peak Temperature (°C)	Activation energy E (eV)	Frequency factor s (s^{-1})	Lifetime (s) at 27°C	Peak	Peak Temperature (°C)	Activation energy E (eV)	Frequency factor s (s^{-1})	Lifetime (s) at 27°C
A	150	0.82 ± 0.04	$(2 \pm 1) \times 10^{9}$	$(5.4 \pm 3.5) \times 10^{4}$	A	150	0.83 ± 0.04	$(2.15 \pm 0.3) \times 10^{9}$	$(125 \pm 24) \times 10^{4}$
B	210	0.94 ± 0.04	$(8.5 \pm 5.3) \times 10^{8}$	$(1.1 \pm 0.3) \times 10^{7}$	B	210	0.93 ± 0.04	$(1.1 \pm 0.1) \times 10^{9}$	$(3.5 \pm 3) \times 10^{7}$
C	300	1.32 ± 0.03	$(9.4 \pm 10) \times 10^{9}$	$(4.8 \pm 3.6) \times 10^{12}$	D	300	1.47 ± 0.04	$(2.75 \pm 2.25) \times 10^{11}$	$(13 \pm 13) \times 10^{12}$
					E	360	1.63 ± 0.04	$(7.2 \pm 1.3) \times 10^{11}$	$(5 \pm 7) \times 10^{15}$

windows are different for the same mineral type but with the same dose rate. This would imply that the equivalent doses in different optical windows should scale in proportion to their thermal and athermal fading. We envisage that a rigorous study of kinetic parameters and inverse modeling should enable arriving at a field data-based estimate of the athermal fading and will offer a comparison with the values measured in the laboratory. This will be instructive in elucidating the basic mechanism of athermal fading. The alpha efficiency of jarosite for a particular detection window (BG39, blue and UV) correlates with athermal fading g-value. Lower g-value corresponds to lower alpha efficiency, as suggested by Singhvi (1981) and, this needs to be explored further. Future studies on jarosite samples from other locations are now needed to establish working parameters a-value/charge particle induction efficiency for possible dating signals. These values can be assumed for estimating the dose and date without in situ measurement (e.g., Schmidt et al., 2018).

POTENTIALS FOR LUMINESCENCE STUDIES USING JAROSITE

1. *Mars surface processes*: The high temperature (>300°C) traps in jarosite can be used for dating, and the relevant age can be calculated by the following classic equation

$$\text{Age} = \frac{\text{Total dose accumulated}}{\text{Annual accumulation of dose}}. \quad (4)$$

Dividing the saturation dose by the annual dose rate gives a working dating range of ~25,000 years to understand time scales of eolian processes, reported by the *Perseverance* rover on Mars.

2. *Mapping of cosmic ray flux on the surface of Mars and its variation with depth*: The TL glow of lower temperature trap at 210°C, bleaches in 20 min and has a saturation dose of 2600 Gy value, and the higher temperature glow peak at 350°C bleaches in 105 min with a saturation dose of 1600 Gy. This can, with some ingenuity, be used to estimate the current cosmic ray flux and the fluxes during the past. A rover containing a TL readout instrument can be used to first bleach the latent signal at the surface of interest and remeasure it after a designated time to obtain an absolute measurement of the absorbed cosmic ray flux by the surface. Samples at depth can give insights into the cosmic ray flux gradient. The aspect of long-term changes in cosmic ray fluxes

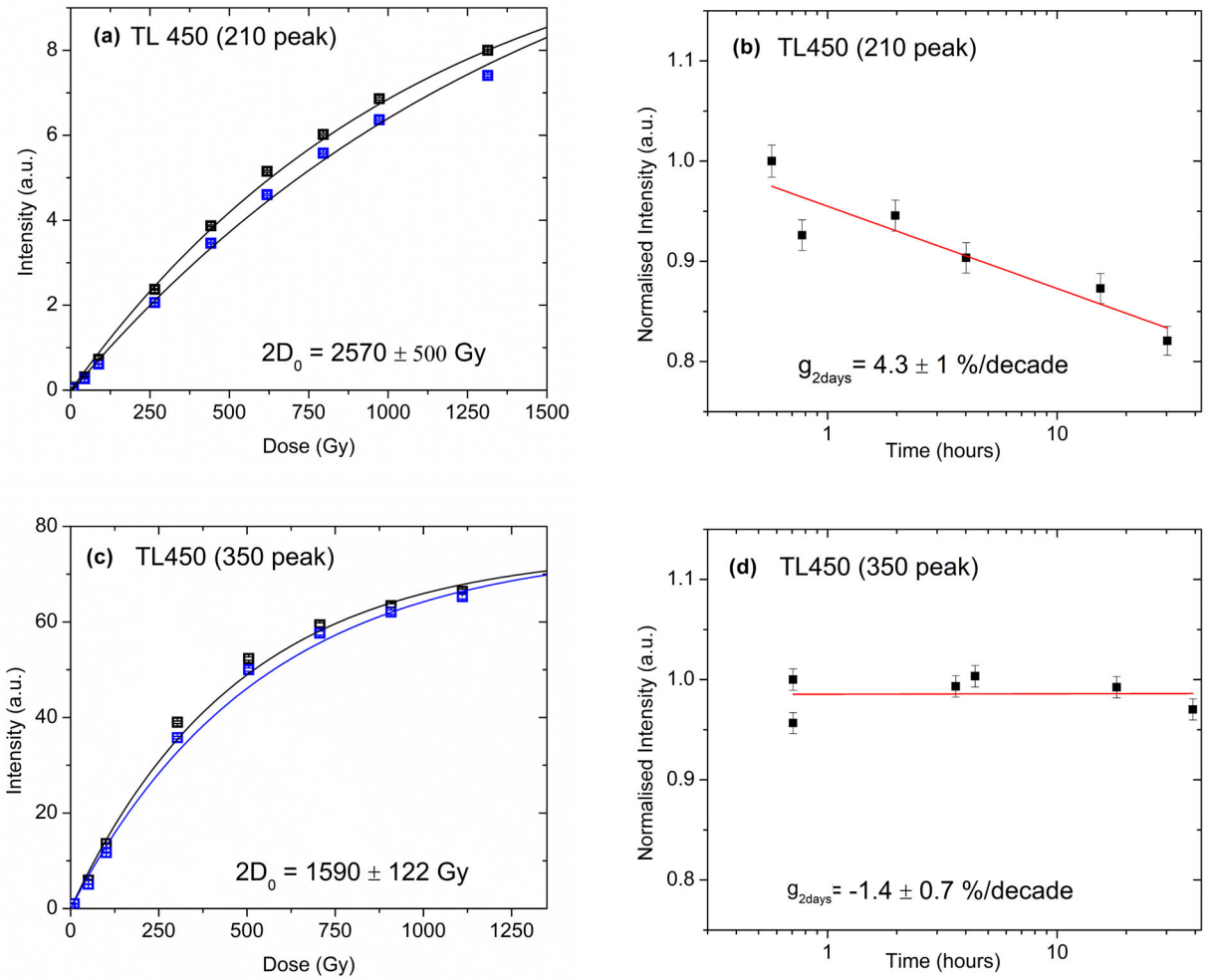

FIGURE 8. Sample 56B2 TL dose–response curve and fading. TL intensity comprises (a, b) Integrated photon count 220–220°C. (c, d) Integrated photon counts are from 340°C to 360°C. Individual lines show data from different aliquots.

TABLE 5. Dose–response parameters.

Sr. No.	Protocol name	No. of disc	Saturation dose ($2D_0$) (Gy)	g-value (%/decade) (average of 10 aliquots)	Alpha efficiency	Recycling ratio (%)	Recuperation (%)
1	TL450 (210 peak)	2	2570 ± 500	4.3 ± 1	0.075 ± 0.004	<10	<2
2	TL450 (350 peak)	2	1590 ± 122	-1 ± 0.7	0.051 ± 0.004	<10	<1
3	$BSL200_{UV}$	3	867 ± 85	7.6 ± 0.6	0.093 ± 0.01	<10	<2
4	$IR50_{Blue}$	3	1180 ± 181	7.4 ± 0.7	0.058 ± 0.005	<10	<2
5	$pIRIR225_{UV}$	3	817 ± 95	0.7 ± 0.2	0.029 ± 0.002	<10	<2
6	$pIRIR225_{blue}$	3	685 ± 36	-0.5 ± 0.4	0.041 ± 0.004	<10	<2

through inverse modeling will be developed elsewhere. Thus, luminescence can provide very accurate spatial and temporal mapping of the flux throughout the surface of Mars.

3. *Terrestrial studies for late quaternary climate change*: Jarosite formation is indicative of the start of aridity in the region, and thus a proxy for climate change. On Earth, various lakes have jarosite deposits (Long

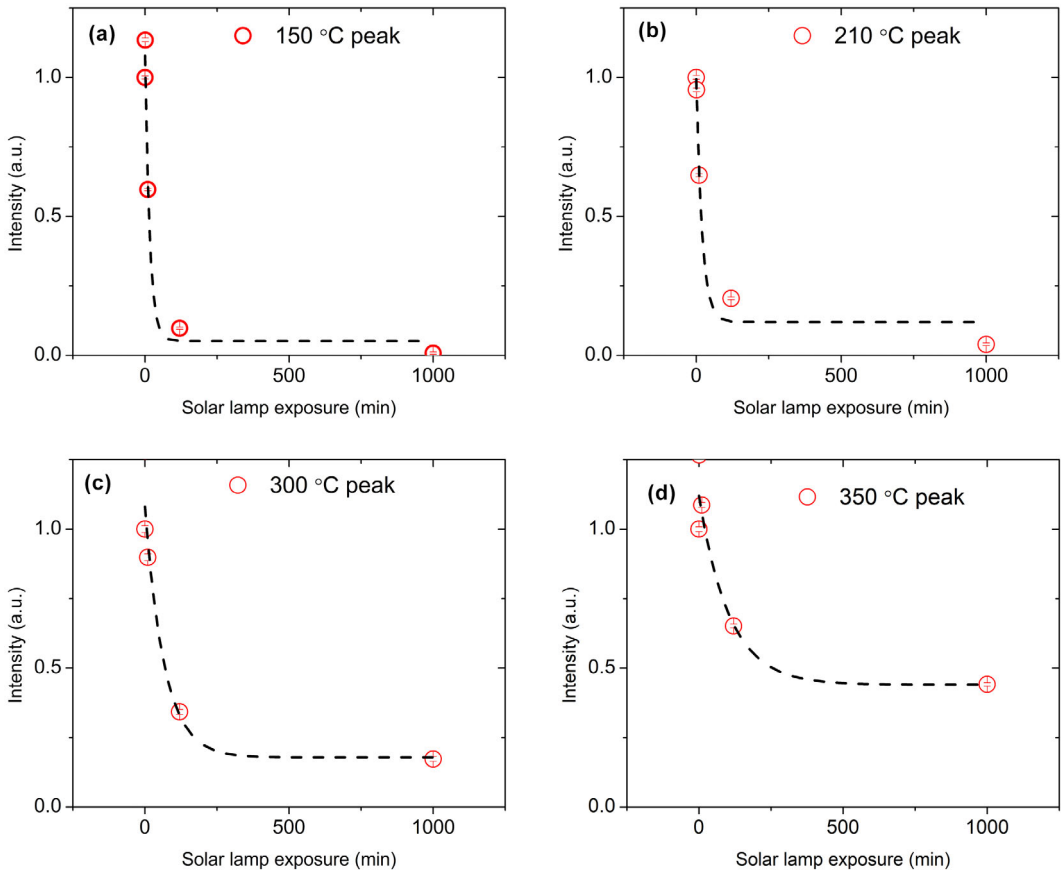

FIGURE 9. Solar lamp resetting of annealed sample 56B2 after a dose of 300 Gy for (a) 150°C peak, (b) 210°C peak, (c) 300°C peak and (d) 350°C TL peaks. Each red data point is an average of measurements on three aliquots. The dashed black curves were fitted with $y = a.e^{-b.t}$.

et al., 1992). Since this study shows the possibility of directly dating the jarosite formation and not the minerals and organics found nearby, it can give added understanding of contemporary climates.

SUMMARY AND CONCLUSION

The following are the major findings of this study:

1. HCl increases the luminescence yield, possibly due to the removal of gleying.
2. In the detection window of 330–625 nm, TL glow peaks of Jarosite are observed at 100°C, 150°C, 300°C, and 350°C.
3. Jarosite luminescence can be stimulated by both blue and infrared light, and detection in both blue (400–480 nm) and UV (280–380 nm) is seen.
4. The luminescence signals are reproducible under repeated cycles of irradiation and readout. The reproducibility of TL was <6% and that of BSL/IRSL (<14%).
5. Luminescence sensitivity (LS) of the samples was variable. Samples from the Guneri formation had the highest sensitivity. Heating up to 450°C changed the LS, but the glow curve shapes remained the same. This is also supported by FTIR and CL-EDXS.
6. Fractional glow curve analysis suggests that the kinetic parameters of glow peaks below 300°C are similar for both the annealed and non-annealed samples. For higher temperature glow peaks, deviation occurs. The glow peak at 300°C has an estimated lifetime of ~0.3 Ma, and this is suitable for dating.
7. Both BSL and IRSL comprise three components.
8. Saturation doses of various luminescence signals range from 590 Gy to 1600 Gy. Any or all of these could be used for dating.
9. Jarosite shows large fading of the BSL and IRSL, that is, around 6.64 and 7.4%/decade. However, no fading is observed for the pIRIR225 in the blue and UV detection window and for the TL glow peak at 350°C.

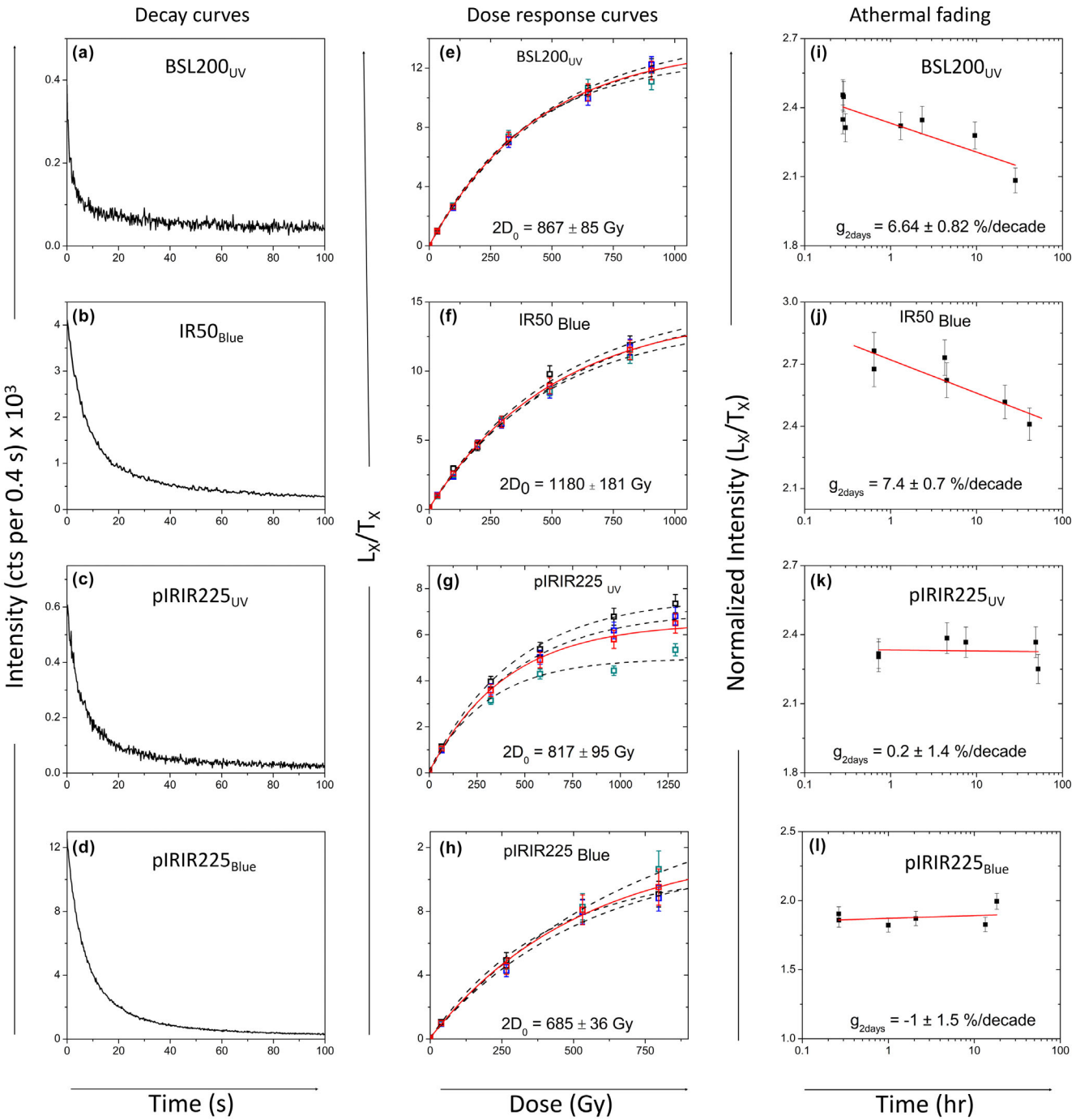

FIGURE 10. Optical decay curves (a–d); Dose–response curves (e–h), each dashed line is data on individual aliquot and solid line is average; Fading characteristics (i–l) of $BSL200_{Uv}$, $IR50_{Blue}$, $pIRIR225_{UV}$, and $pIRIR225_{Blue}$ respectively.

10. The average dose rate on the Martian surface is ~65 mGy/year, giving a dating range of ~25,000 years.

Thus, the study suggests that jarosite provides an array of luminescence signals that can be used for dating recent eolian activity, mapping cosmic ray flux accumulation on Mars, and terrestrial paleoclimatic studies. Further, since pIRIR225 does not show fading, jarosite can be used for in situ dosimetry on Mars.

TABLE 6. Summary of dose rate; Sample 67F2.

	Concentration of radionuclide		Dose rate estimation technique
Internal dose rate (mGy/year)	U238 (ppm)	1.87 ± 0.1	ZnS alpha counting
	Th232 (ppm)	1.06 ± 0.35	ZnS alpha counting
	K (%)	0.78 ± 0.07	NaI Scintillator, gamma counting
	Total internal dose rate	1.62 ± 0.6 (mGy/year)	
External dose rate (mGy/year)	Cosmic Ray	63	Simulation; (Morthekai et al., 2007)
Total dose rate (mGy/year)		65	

Acknowledgments—The work carried out at PRL is supported by the Department of Space, Government of India. AKS thanks DST-SERB for a Year of Science Chair Professorship that facilitated this work. MS thanks Mr. Ranjan Mohanty for his help with QGIS. We thank Dr. I. Sfampa for her careful review and Prof. T. Jull for his assistance with the review process.

Data Availability Statement—The data that support the findings of this study are available from the corresponding author upon reasonable request.

Editorial Handling—Dr. Edward Cloutis

REFERENCES

Aitken, M. J. 1985. *Thermoluminescence Dating*. London: Academic Press.

Bhattacharya, S., Mitra, S., Gupta, S., Jain, N., Chauhan, P., Parthasarathy, G., and Ajai. 2016. Jarosite Occurrence in the Deccan Volcanic Province of Kachchh, Western India: Spectroscopic Studies on a Martian Analog Locality. *Journal of Geophysical Research: Planets* 121: 402–431.

Bishop, J. L., and Murad, E. 2005. The Visible and Infrared Spectral Properties of Jarosite and Alunite. *American Mineralogist* 90: 1100–1107.

Biswas, R. H., Morthekai, P., Gartia, R. K., Chawla, S., and Singhvi, A. K. 2011. Thermoluminescence of the Meteorite Interior: A Possible Tool for the Estimation of Cosmic Ray Exposure Ages. *Earth and Planetary Science Letters* 304: 36–44. https://doi.org/10.1016/j.epsl.2011.01.012.

Biswas, R. H., Williams, M. A. J., Raj, R., Juyal, N., and Singhvi, A. K. 2013. Methodological Studies on Luminescence Dating of Volcanic Ashes. *Quaternary Geochronology* 17: 14–25. https://doi.org/10.1016/j.quageo.2013.03.004.

Biswas, S. K. 1992. Tertiary Stratigraphy of Kutch. *Journal of the Palaeontological Society of India* 37: 1–29.

Bøtter-Jensen, L., McKeever, S. W. S., and Wintle, A. G. 2003. *Optically Stimulated Luminescence Dosimetry*. The Netherlands: Elsevier.

Buylaert, J. P., Murray, A. S., Thomsen, K. J., and Jain, M. 2009. Testing the Potential of an Elevated Temperature IRSL Signal from K-Feldspar. *Radiation Measurements* 44: 560–65. https://doi.org/10.1016/j.radmeas.2009.02.007.

Clark-Balzan, L., May, V. R., and Preusser, F. 2021. Luminescence Characteristics of Intraplate-Derived Olivines. *Geochronometria* 48: 73–94.

Cloutis, E. A., Cloutis, E., Hawthorne, F., Mertzman, S., Krenn, K., Craig, M., Marcino, D., et al. 2006. Detection and Discrimination of Sulfate Minerals Using Reflectance Spectroscopy. *Icarus* 184: 121–157.

Cruells, M., and Roca, A. 2022. Jarosites: Formation, Structure, Reactivity and Environmental. *Metals* 12: 802.

Desai, B. G., and Saklani, R. D. 2012. Significance of the Trace Fossil Balanoglossites Mägdefrau, 1932 from the Lower Cretaceous Guneri Member (Bhuj Formation) of the Guneri Dome, Kachchh, India. *Swiss Journal of Palaeontology* 131: 255–263.

Doran, P. T., and Doran, P. 2004. Mars Chronology: Assessing Techniques for Quantifying Surficial Processes. *Earth-Science Reviews* 67: 313–337. https://www.sciencedirect.com/science/article/pii/S001282520400039X.

Dutrizac, J. E., and Jambor, J. L. 2000. Jarosites and their Application in Hydrometallurgy. *Reviews in Mineralogy and Geochemistry* 40: 405–452. https://doi.org/10.2138/rmg.2000.40.8.

Dutrizac, J. E., and Kaiman, S. 1976. Synthesis and Properties of Jarosite-Type Compounds. *The Canadian Mineralogist* 14: 151–58.

Fairchild, J. G. 1933. Artificial Jarosites—The Separation of Potassium from Cesium. *American Mineralogist: Journal of Earth and Planetary Materials* 18: 543–47.

Farmer, V. C. 1974. *The Infrared Spectra of Minerals*. London: Mineralogical Society Monograph.

Frost, R. L., Weier, M. L., and Martens, W. 2005. Thermal Decomposition of Jarosites of Potassium, Sodium and Lead. *Journal of Thermal Analysis and Calorimetry* 82: 115–18.

Geake, J. E., and Walker, G. 1967. Laboratory Investigations of Meteorite Luminescence. *Proceedings of the Royal Society of London. Series A: Mathematical and Physical Sciences* 296: 337–346.

Gliganic, L. A., Roberts, R. G., and Jacobs, Z. 2012. Natural Variations in the Properties of TL and IRSL Emissions from Metamorphic and Volcanic K-Feldspars from East Africa: Assessing their Reliability for Dating. *Radiation Measurements* 47: 659–664. https://www.sciencedirect.com/science/article/pii/S1350448712000649.

Gobrecht, H., and Hofmann, D. 1966. Spectroscopy of Traps by Fractional Glow Technique. *Journal of Physics and Chemistry of Solids* 27: 509–522.

Haberle, R. M. 2015. Solar System/Sun, Atmospheres, Evolution of Atmospheres | Planetary Atmospheres: Mars. In *Encyclopedia of Atmospheric Sciences*, edited by G. R. North, J. Pyle, and F. Zhang, 168–177. Oxford: Academic Press. https://www.sciencedirect.com/science/article/pii/B9780123822253003121.

Howari, F. M., Sharma, M., Xavier, C. M., Nazzal, Y., and AlAydaroos, F. 2021. Chronological Analysis and Remote Sensing of Craters on the Surface of Mars. *Frontiers in*

Environmental Science 9: 605893. https://doi.org/10.3389/fenvs.2021.605893.

Huntley, D. J. 2006. An Explanation of the Power-Law Decay of Luminescence. *Journal of Physics. Condensed Matter* 18: 1359–65.

Huntley, D. J., and Lamothe, M. 2001. Ubiquity of Anomalous Fading in K-Feldspars and the Measurement and Correction for it in Optical Dating. *Canadian Journal of Earth Sciences* 38: 1093–1106.

Inami, T., Nishiyama, M., Maegawa, S., and Oka, Y. 2000. Magnetic Structure of the kagomé Lattice Antiferromagnet Potassium Jarosite $KFe_3(OH)_6(SO_4)_2$. *Physical Review B: Condensed Matter* 61: 12181.

Jain, M., Andersen, C. E., Bøtter-Jensen, L., Murray, A. S., Haack, H., and Bridges, J. C. 2006. Luminescence Dating on Mars: OSL Characteristics of Martian Analogue Materials and GCR Dosimetry. *Radiation Measurements* 41: 755–761.

Jain, M., Andersen, C. E., Hajdas, W., Edmund, J. M., and Bøtter-Jensen, L. 2007. OSL Response to Proton Irradiation in some Natural Dosemeters: Implications for Martian Sediment Dating. *Nuclear Instruments and Methods in Physics Research, Section A: Accelerators, Spectrometers, Detectors and Associated Equipment* 580: 652–55.

Karanth, R. V., and Gadhavi, M. S. (2007). Structural intricacies: Emergent thrusts and blind thrusts of Central Kachchh, Western India. *Current Science* 93: 1271–80.

Kars, R. H., Wallinga, J., and Cohen, K. M. 2008. A New Approach towards Anomalous Fading Correction for Feldspar IRSL Dating – Tests on Samples in Field Saturation. *Radiation Measurements* 43: 786–790.

Klingelhöfer, G., Morris, R. V., Bernhardt, B., Schroder, C., Rodionov, D. S., de Souza, P. A., Yen, A., et al. 2004. Jarosite and Hematite at Meridiani Planum from Opportunity's Mossbauer Spectrometer. *Science (New York, N.Y.)* 306: 1740–45.

Kotler, J. M., Hinman, N. W., Yan, B., Stoner, D. L., and Scott, J. R. 2008. Glycine Identification in Natural Jarosites Using Laser Desorption Fourier Transform Mass Spectrometry: Implications for the Search for Life on Mars. *Astrobiology* 8: 253–266.

Lancaster, N., and Greeley, R. 1990. Sediment Volume in the North Polar Sand Seas of Mars. *Journal of Geophysical Research: Solid Earth* 95: 10921–27.

Lepper, K., and McKeever, S. W. S. 2000. Characterization of Fundamental Luminescence Properties of the Mars Soil Simulant JSC Mars-1 and their Relevance to Absolute Dating of Martian Eolian Sediments. *Icarus* 144: 295–301.

Long, D. T., Fegan, N. E., McKee, J. D., Lyons, W. B., Hines, M. E., and Macumber, P. G. 1992. Formation of Alunite, Jarosite and Hydrous Iron Oxides in a Hypersaline System: Lake Tyrrell, Victoria, Australia. *Chemical Geology* 96: 183–202.

Marescotti, P., Carbone, C., Comodi, P., Frondini, F., and Lucchetti, G. 2010. Mineralogical and Chemical Evolution of Ochreous Precipitates from the Libiola Fe-Cu-Sulphides Mine Eastern Liguria, Italy. *Acta Mineralogica-Petrographica. Abstract Series* 6: 346. https://eurekamag.com/research/037/105/037105004.php.

McKeever, S. W. S., Banerjee, D., Blair, M., Clifford, S. M., Clowdsley, M. S., Kim, S. S., Lamothe, M., et al. 2003. Concepts and Approaches to In Situ Luminescence Dating of Martian Sediments. *Radiation Measurements* 37: 527–534. https://www.sciencedirect.com/science/article/pii/S1350448703000258.

Morris, R. V., Golden, D. C., Bell, J. F., III, Shelfer, T. D., Scheinost, A. C., Hinman, N. W., Furniss, G., et al. 2000. Mineralogy, Composition, and Alteration of Mars Pathfinder Rocks and Soils: Evidence from Multispectral, Elemental, and Magnetic Data on Terrestrial Analogue, SNC Meteorite, and Pathfinder Samples. *Journal of Geophysical Research: Planets* 105: 1757–1817. https://doi.org/10.1029/1999JE001059.

Morthekai, P., Jain, M., Dartnell, L., Murray, A. S., Bøtter-Jensen, L., and Desorgher, L. 2007. Modelling of the Dose-Rate Variations with Depth in the Martian Regolith Using GEANT4. *Nuclear Instruments and Methods in Physics Research, Section A: Accelerators, Spectrometers, Detectors and Associated Equipment* 580: 667–670.

Morthekai, P., Jain, M., Murray, A. S., Thomsen, K. J., and Bøtter-Jensen, L. 2008. Fading Characteristics of Martian Analogue Materials and the Applicability of a Correction Procedure. *Radiation Measurements* 43: 672–78.

Murray, A. S., and Wintle, A. G. 2000. Application of the Single-Aliquot Regenerative-Dose Protocol to the 375°C Quartz TL Signal. *Radiation Measurements* 32: 579–583.

Nagar, Y. C. 2007. Methodological Aspects of Radiation Dosimetry of Natural Radiation Environment Using Luminescence Techniques: New Minerals and Application.

Nambi, K. S. V. 1977. *Thermoluminescence: Its Understanding and Applications*. Sao Paulo: Instituto de Energia Atomica.

Pietkun, A., Polakiewicz, L., and Oczkowski, H. L. 1992. Measurement System for Fractional Glow Technique. *Acta Physica Polonica A* 81: 687–691.

Rajapara, H. M. 2014. Some Unresolved Problems of Mineral Luminescence Relevant to Radiation Dosimetry.

Rangarajan, V. G., Bharti, R., Mondal, S. K., Pradhan, C., and Dutta, S. 2018. Remote Sensing for Martian Studies: Inferences from Syrtis Major. *Journal of the Indian Society of Remote Sensing* 46: 1537–51. https://doi.org/10.1007/s12524-018-0826-7.

Reynolds, G. A. 2007. *The Jarosite Group of Compounds – Stability, Decomposition and Conversion*. Newcastle, NSW: University of Newcastle.

Rhodes, E. J. 2011. Optically Stimulated Luminescence Dating of Sediments Over the Past 200,000 Years. *Annual Review of Earth and Planetary Sciences* 39: 461–488. https://api.semanticscholar.org/CorpusID:64684744.

Roca, A. 2022. Jarosites: Formation, Structure, Reactivity and Environmental. *Metals* 12: 802.

Sarkar, S., Moitra, H., Bhattacharya, S., Dagar, A., Ray, D., Gupta, S., Chavan, A., Shukla, A. D., and Bhandari, S. 2022. Spectroscopic Studies on the Puga Hot Spring Deposits, Ladakh, an Astrobiological Martian Analog Site in India. *Journal of Geophysical Research: Planets* 127: e2022JE007299.

Schmidt, C., Bösken, J., and Kolb, T. 2018. Is there a Common Alpha-Efficiency in Polymineral Samples Measured by Various Infrared Stimulated Luminescence Protocols? *Geochronometria* 45: 160–172.

Sears, D. W. G., Ninagawa, K., and Singhvi, A. K. 2013. Luminescence Studies of Extraterrestrial Materials: Insights into their Recent Radiation and Thermal Histories and into their Metamorphic History. *Chemie der Erde* 73: 1–37. https://doi.org/10.1016/j.chemer.2012.12.001.

Shalgaonkar, C. S., and Narlikar, A. V. 1972. Review: A Review of the Recent Methods for Determining Trap Depth from Glow Curves. *Journal of Materials Science* 7: 1465–71. https://doi.org/10.1007/BF00574938.

Singhvi, A., Kaushal, R., and Parida, S. 2022. Luminescence Dating and Quaternary Geology: The Indian Narrative. *Journal of the Palaeontological Society of India* 67: 183–210.

Singhvi, A. K. 1981. A Possible Correlation between the Alpha Efficiency and the Anomalous Fading Characteristics. *Ancient TL* 14: 10.

Singhvi, A. K., and Aitken, M. J. 1978. Americium-241 for Alpha-Irradiations. *Ancient TL* 2: 2–9.

Smith, M. R., and Bandfield, J. L. 2012. Geology of Quartz and Hydrated Silica-Bearing Deposits near Antoniadi Crater, Mars. *Journal of Geophysical Research: Planets* 117: E06007.

Solomon, S. C., Aharonson, O., Aurnou, J. M., Banerdt, W. B., Carr, M. H., Dombard, A. J., Frey, H. V., et al. 2005. New Perspectives on Ancient Mars. *Science* 307: 1214–20. http://www.jstor.org/stable/3840200.

Spooner, N. A. 1987. The Effect of Light on the Thermoluminescence of Quartz.

Thomsen, K. J., Bøtter-Jensen, L., Denby, P. M., Moska, P., and Murray, A. S. 2006. Developments in Luminescence Measurement Techniques. *Radiation Measurements* 41: 768–773.

Tsukamoto, S., Duller, G. A. T., Wintle, A. G., and Muhs, D. 2011. Assessing the Potential for Luminescence Dating of Basalts. *Quaternary Geochronology* 6: 61–70. https://doi.org/10.1016/j.quageo.2010.04.002.

Velasco, F., Herrero, J. M., Suárez, S., Yusta, I., Alvaro, A., and Tornos, F. 2013. Supergene Features and Evolution of Gossans Capping Massive Sulphide Deposits in the Iberian Pyrite Belt. *Ore Geology Reviews* 53: 181–203. https://www.sciencedirect.com/science/article/pii/S016913681300019X.

Viñals, J., Roca, A., and Arranz, M. 2003. Autoclave Alkaline Decomposition and Cyanidation of Jarosite-Beudantite Phases from Rio Tinto Gossan Ores. *Canadian Metallurgical Quarterly* 42: 29–40. https://doi.org/10.1179/cmq.2003.42.1.29.

Viñals, J., Roca, A., Cruells, M., and Núñez, C. 1995. Characterization and Cyanidation of Rio Tinto Gossan Ores. *Canadian Metallurgical Quarterly* 34: 115–122. https://www.sciencedirect.com/science/article/pii/000844339400022C.

Wallinga, J., Murray, A., and Wintle, A. 2000. The Single-Aliquot Regenerative-Dose (SAR) Protocol Applied to Coarse-Grain Feldspar. *Radiation Measurements* 32: 529–533.

Wills, A. S., Harrison, A., Ritter, C., and Smith, R. I. 2000. Magnetic Properties of Pure and Diamagnetically Doped Jarosites: Model Kagomé Antiferromagnets With Variable Coverage of the Magnetic Lattice. *Physical Review B: Condensed Matter* 61: 6156.

Wintle, A. G. 1973. Anomalous Fading of Thermo-Luminescence in Mineral Samples. *Nature* 245: 143–44.

Wintle, A. G., and Murray, A. S. 2006. A Review of Quartz Optically Stimulated Luminescence Characteristics and their Relevance in Single-Aliquot Regeneration Dating Protocols. *Radiation Measurements* 41: 369–391.

Xu, H., Zhao, ˇ. Y., Vogel, ˇ. S. C., Hickmott, D. D., Daemen, ˇ. L. L., and Hartl, M. A. 2010. Thermal Expansion and Decomposition of Jarosite: A High-Temperature Neutron Diffraction Study. *Physics and Chemistry of Minerals* 37: 73–82.

Zhang, J., and Wang, L. 2020. Thermoluminescence Dating of Calcite – Alpha Effectiveness and Measurement Protocols. *Journal of Luminescence* 223: 117205. https://doi.org/10.1016/j.jlumin.2020.117205.

Zimmermans, D. W. 1972. Relative Thermoluminescence Effects of Alpha- and Beta- Radiation. *Radiation Effects* 14: 81–92.

SUPPORTING INFORMATION

Additional supporting information may be found in the online version of this article.

Data S1. Supplementary figures and tables.